ACCSCIENCE PUBLISHING

Advances in Radiotherapy & Nuclear Medicine

ISSN: 3060-8554 (Print)
ISSN: 2972-4392 (Online)
Volume 4 · Issue 1
March 2026

ACCSCIENCE PUBLISHING

Advances in Radiotherapy & Nuclear Medicine

Print ISSN: 3060-8554
Online ISSN: 2972-4392

Advances in Radiotherapy & Nuclear Medicine is a peer-reviewed and open-access journal that aims to publish and disseminate novel research in the breadth of radiation oncology, physics, and biology.

The journal aims to advance our understanding in the radiotherapy and provide a platform to oncologists and physicians to showcase their findings in original fundamental and clinical research as well as to present new ideas that highlight the changes in the radiation oncological clinical practice.

About the Publisher

AccScience Publishing is a publishing company based in Singapore. We publish a range of high-quality, open-access, peer-reviewed journals and books from a broad spectrum of disciplines.

Contact Us

Managing Editor
arnm.office@accscience.sg

AccScience Publishing
2 Venture Drive, #07-06 Vision Exchange,Singapore 608526.

Volume 4 • Issue 1 • March 2026
ISSN 3060-8554 (print) ISSN 2972-4392 (online)

Advances in Radiotherapy & Nuclear Medicine

ACCSCIENCE PUBLISHING

Access Science Without Barriers

ADVANCES IN RADIOTHERAPY & NUCLEAR MEDICINE

ISSN: 3060-8554 (print)
ISSN: 2972-4392 (online)

Editorial and Production Credits

Publisher: AccScience Publishing
Managing Editor: Freda Wang
Production Editor: Sharmila Velapasamy
Article Layout and Typeset: Sinjore Technologies (India)

For all advertising queries, contact arnm.office@accscience.sg.

Supplementary file

Supplementary files of articles can be obtained at https://accscience.com/journal/ARNM/4/1.

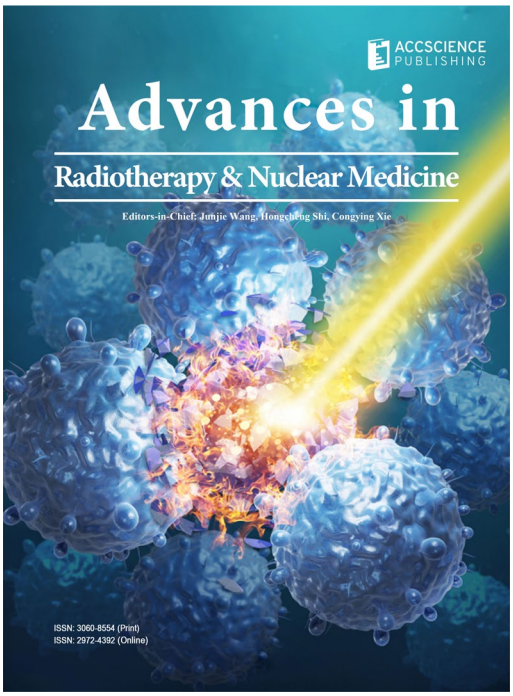

Advances in Radiotherapy & Nuclear Medicine

Editorial Board

Youth Editorial Board Members

*Editorial Board Members as of March 4, 2026

ACCSCIENCE PUBLISHING

Volume 4 | Issue 1 | March 2026 | Page 1 – 109 |

Advances in Radiotherapy & Nuclear Medicine

https://accscience.com/journal/ARNM

CONTENTS

ACCSCIENCE PUBLISHING

Advances in Radiotherapy & Nuclear Medicine

REVIEW ARTICLE

Incidental pituitary uptake on FDG PET/CT: Physiologic variants, pitfalls, and pathologic mimics

Marwah Abdulrahman[1†], Raghad M. Al-Houwari[1†], Manar W. Alomari[1], Rezhan Ali[1], Shahed Obeidat[1], and Akram Al-Ibraheem[1,2*]

[1]Department of Nuclear Medicine, King Hussein Cancer Center, Amman, Jordan

[2]Department of Radiology and Nuclear Medicine, School of Medicine, University of Jordan, Amman, Jordan

Abstract

Incidental pituitary uptake on ^{18}F-deoxy-glucose positron emission tomography combined with computed tomography (^{18}F-FDG PET/CT) is rare, occurring in <1% of scans, yet its identification carries significant clinical implications. Accurate interpretation requires a systematic diagnostic approach integrating metabolic, structural, and hormonal assessment. While the normal pituitary gland demonstrates low-level or background FDG activity, focal uptake may suggest pathology ranging from physiologic hyperplasia and benign adenomas to inflammatory conditions such as hypophysitis, or malignant etiologies including pituitary neuroendocrine tumors and metastatic disease. The intensity of uptake, quantified by the maximum standardized uptake value (SUV_{max}), serves as a critical diagnostic indicator; an SUV_{max} threshold above 4.1 has been proposed to differentiate benign from malignant lesions with high sensitivity and specificity. Complementary pituitary magnetic resonance imaging (MRI) offers essential anatomic correlation to define lesion morphology, extension, and contrast enhancement patterns, while endocrine evaluation helps establish functional activity and hormonal imbalance. Histopathologic confirmation remains reserved for cases with inconclusive imaging or atypical presentation. This review synthesizes available literature, emphasizing PET-based metabolic features and interpretive pitfalls, while acknowledging the role of computed tomography and MRI in comprehensive lesion characterization. Early recognition and appropriate follow-up are crucial to avoid misdiagnosis and to guide timely management of clinically significant pituitary lesions.

Keywords: Pituitary uptake; Incidentaloma; FDG PET/CT; Differential diagnosis

1. Introduction

The pituitary gland is a central endocrine organ that regulates the function of multiple peripheral endocrine glands through the secretion of a range of hormones. Anatomically, the gland lies within the sella turcica at the base of the skull and is covered by the dura mater.[1] Under normal physiological conditions, it is small and generally demonstrates only a low or background level of FDG uptake on ^{18}F-fluorodeoxyglucose (FDG) positron emission tomography/computed tomography (PET/CT).[2]

†These authors contributed equally to this work.

***Corresponding author:**
Akram Al-Ibraheem
(aibraheem@khcc.jo)

Citation: Abdulrahman M, Al-Houwari RM, Alomari MW, Ali R, Obeidat S, Al-Ibraheem A. Incidental pituitary uptake on FDG PET/CT: Physiologic variants, pitfalls, and pathologic mimics. *Adv Radiother Nucl Med*. 2026;4(1):1-15. doi: 10.36922/ARNM025390050

Received: September 24, 2025

Revised: October 26, 2025

Accepted: November 25, 2025

Published online: December 8, 2025

Incidental findings on ^{18}F-FDG PET/CT have been reported with rate ranges from 6.7% to 12%.[1] Among these, incidental pituitary uptake represents a relatively uncommon and diagnostically challenging subset. These pituitary incidentalomas are defined as asymptomatic lesions unexpectedly detected on head magnetic resonance imaging (MRI) or CT performed for unrelated indications, and their clinical significance remains incompletely understood.[3]

The most frequently reported cause of incidental pituitary uptake on routine whole-body ^{18}F-FDG PET/CT is primary pituitary tumors, most commonly pituitary neuroendocrine tumors (PitNETs), as classified by the World Health Organization (WHO), replacing the older terminology of pituitary adenomas.[4] Other less common differential diagnoses include metastatic pituitary lesions, Langerhans cell histiocytosis (LCH), and inflammatory conditions such as lymphocytic hypophysitis. However, physiologic uptake without a corresponding structural lesion may occasionally be observed as well.[5]

In the era of precision oncology and amid rising cancer incidence, ^{18}F-FDG PET/CT scans performed for evaluation frequently reveal unexpected areas of increased uptake, with 5–12% of scans showing findings suggestive of secondary or synchronous malignancies.[6] Focal FDG uptake within the pituitary gland with or without corresponding structural abnormalities on CT represents a finding of uncertain clinical significance that requires careful correlation with clinical history, endocrine profile, and dedicated MR imaging to distinguish physiologic variants and benign entities from true pituitary pathology. Despite the increasing utilization of PET/CT in oncologic practice, limited literature exists characterizing the prevalence and nature of incidental pituitary uptake, encompassing both malignant and non-malignant processes. This review aims to explore the differential diagnoses and underlying etiologies of incidental pituitary FDG uptake on ^{18}F-FDG PET/CT.

2. Methods

A literature search was performed to identify studies reporting incidental pituitary uptake on ^{18}F-FDG PET/CT and related imaging modalities. The search included PubMed, Scopus, and Google Scholar, covering publications up to September 2025. Search terms combined relevant keywords and MeSH terms, including "incidental pituitary uptake," "pituitary incidentaloma," "FDG PET/CT," "pituitary adenoma," "pituitary metastasis," "hypophysitis," and "pituitary neuroendocrine tumor." Boolean operators (AND/OR) were applied to refine results.

Eligible articles included original research studies, case reports, case series, and relevant review articles published in English, providing relevant PET/CT imaging data, with information on tracer uptake, lesion characteristics, and clinical correlation. Articles lacking full text, non-English publications, or studies without PET/CT data were excluded.

Data extraction focused on the following parameters: patient demographics, underlying pathology, imaging characteristics (including standardized uptake value [SUV_{max}], lesion size, localization, and tracer type), MRI or CT correlation, endocrine evaluation, and clinical outcomes. Where available, findings from alternative PET tracers beyond ^{18}F-FDG, such as ^{18}F-2-fluorodeoxysorbitol (^{18}F-FDS), ^{11}C-Methionine (^{11}C-MET), ^{68}Ga-PSMA, ^{68}Ga-DOTA-TATE, ^{18}F-choline, and ^{68}Ga-FAPI, were also recorded to provide comparative insights. No formal quality appraisal was performed, consistent with the narrative review design.

3. Discussion and literature review

The incidence of unexpected FDG-avid pituitary lesions is <1%, which is much lower than the incidence of FDG-avid incidentalomas in other endocrine organs such as the thyroid and adrenal glands.[3] Reported causes of pituitary uptake on ^{18}F-FDG PET/CT include a wide range of etiologies and can be systematically categorized according to the WHO classification, broadly including physiologic, inflammatory, and neoplastic processes[4] (Table 1).

3.1. Non-neoplastic lesions

3.1.1. Physiologic or normal variants

The pituitary gland, a small structure located in the sella turcica at the base of the skull, typically demonstrates FDG uptake that is similar to background activity, making it difficult to visualize on routine ^{18}F-FDG PET/CT. This limited detectability is primarily due to the partial volume effect along with the gland's small size.[2] True incidental physiological FDG uptake in the normal pituitary gland is uncommon, reported in fewer than 1% of cases.[3]

Comparative analysis[2] demonstrated that focal pituitary FDG uptake is more frequently detected with digital PET than with conventional PET. Quantitative assessment of pituitary gland uptake was performed using SUV measurements. Digital PET demonstrated higher pituitary SUV_{max} and SUV_{mean} as compared to conventional PET (3.63 ± 1.31 vs. 2.63 ± 0.51, p=0.0011; 2.47 ± 0.85 vs. 1.99 ± 0.46, p=0.012, respectively) and higher pituitary/background SUV_{max}, reflecting increased sensitivity for detecting pituitary uptake[2] (Figure 1). They also suggested that the level and intensity of pituitary uptake can help differentiate physiological from pathological activity, as

Table 1. Classification of pituitary uptake on PET/CT (aligned with WHO principles)

Category	Subcategory and pathologies (with examples from literature)
Non-neoplastic lesions	(A) Physiologic/Normal variants • Physiologic pituitary uptake (*e.g.*, correlation with TSH levels) • Pituitary stalk uptake (normal variant) • Pituitary gland hyperplasia (e.g., secondary to adrenal insufficiency) (B) Inflammatory/Systemic disease • Hypophysitis (lymphocytic, IgG4-related, immune checkpoint inhibitor–induced) • Neurosarcoidosis (*e.g.*, neurohypophysial involvement) • Erdheim–Chester disease • ANCA-associated vasculitis • LCH • Pituitary tuberculosis
Neoplastic lesions	(A) PitNETs • Functioning PitNETs: - ACTH-secreting (Cushing's disease) - GH-producing - Prolactinomas - TSH-secreting - Gonadotropin-secreting (often clinically non-functioning) - Non-functioning PitNETs (incidentalomas) - Pituitary carcinoma (B) Non-PitNETs • Epithelial cysts: Rathke's cleft cyst • Neural/Gial tumors: Pituicytoma • Mesenchymal tumors: Meningioma, leiomyosarcoma (metastasis) • Embryonal tumors: Craniopharyngioma (adamantinomatous/papillary)
Metastatic/ Secondary lesions	• Carcinoma metastases: Lung (non-small cell), breast cancer, colon cancer, *etc.* • NET metastases • Melanoma • Lymphoma: Primary or secondary • Sarcoma metastases (*e.g.*, leiomyosarcoma)
Complications/ Mimics	• Pituitary apoplexy (hemorrhage/infarction within a PitNET) • Post-treatment changes (*e.g.*, post-surgical recurrence/remnant) • Mass effect/Invasion from adjacent tumors (*e.g.*, parasellar meningioma, chondrosarcoma)

Abbreviations: ACTH: Adrenocorticotrophic hormone; ANCA: Anti-neutrophil cytoplasmic antibodies; CT: Computed tomography; GH: Growth hormone; LCH: Langerhans cell histiocytosis; NET: Neuroendocrine tumors; PET: Positron emission tomography; PitNETs: Pituitary neuroendocrine tumors; TSH: Thyroid stimulating hormone.

low-to-intermediate uptake is generally physiological with no corresponding MRI abnormality, whereas high uptake warrants further evaluation to exclude underlying pathology[2] (Figure 2).

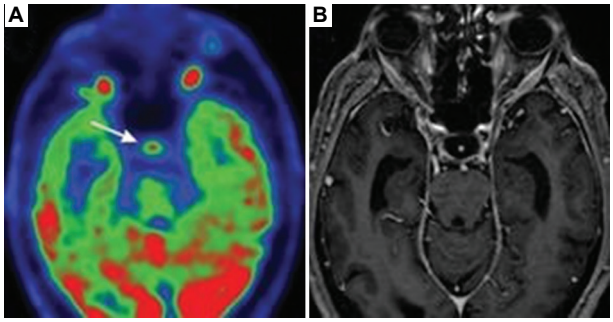

Figure 1. Physiological ^{18}F-FDG uptake in the pituitary gland on digital PET/CT in a 71-year-old male with acral melanoma. The fused PET/CT image (A) demonstrates focal physiological FDG uptake in the normal pituitary gland (white arrow), which corresponds to a normal appearance on MRI (B). This example illustrates the ability of digital PET to detect subtle variations in physiological pituitary uptake. This figure is adapted from Jain *et al.*,[2] available under a Creative Commons Attribution (CC BY 4.0) license.
Abbreviations: CT: Computed tomography; MRI: Magnetic resonance imaging; PET: Positron emission tomography.

An interesting case of metastatic lung adenocarcinoma in whom ^{18}F-FDG PET/CT revealed bilateral adrenal metastases along with unexpected focal pituitary uptake (SUV_{max} 3.9). Biochemical testing revealed elevated adrenocorticotropic hormone (ACTH) and low-normal cortisol, consistent with primary adrenal insufficiency. The hypermetabolic pituitary gland was thus attributed to secondary corticotrophic hyperplasia rather than a primary neoplasm.[7]

Ding *et al.*[8] retrospectively evaluated the level of pituitary FDG uptake in relation to serum thyroid-stimulating hormone (TSH) levels in 215 patients with differentiated thyroid cancer. They found that diffuse pituitary FDG activity in the setting of elevated TSH represents a physiologic response rather than pathology, with a significant positive correlation between SUV_{max} and TSH ($r = 0.479$, $p<0.05$). Uptake was notably higher in hypothyroid patients compared with both euthyroid patients and healthy controls, a physiologic response to hypothalamic–pituitary axis activation from loss of thyroid hormone feedback. This finding suggests measurement of TSH values before interpreting incidental pituitary uptake on FDG PET/CT in hypothyroid patients.[8]

3.1.2. Inflammatory or systemic disease

Incidental FDG uptake in the pituitary stalk may occasionally reflect underlying systemic inflammatory conditions, such as immunoglobulin G4-related disease, and its resolution with appropriate therapy often supports distinguishing these reversible inflammatory processes from true pituitary lesions.[9]

Autoimmune hypophysitis is a rare disorder characterized by lymphocytic infiltration of the pituitary

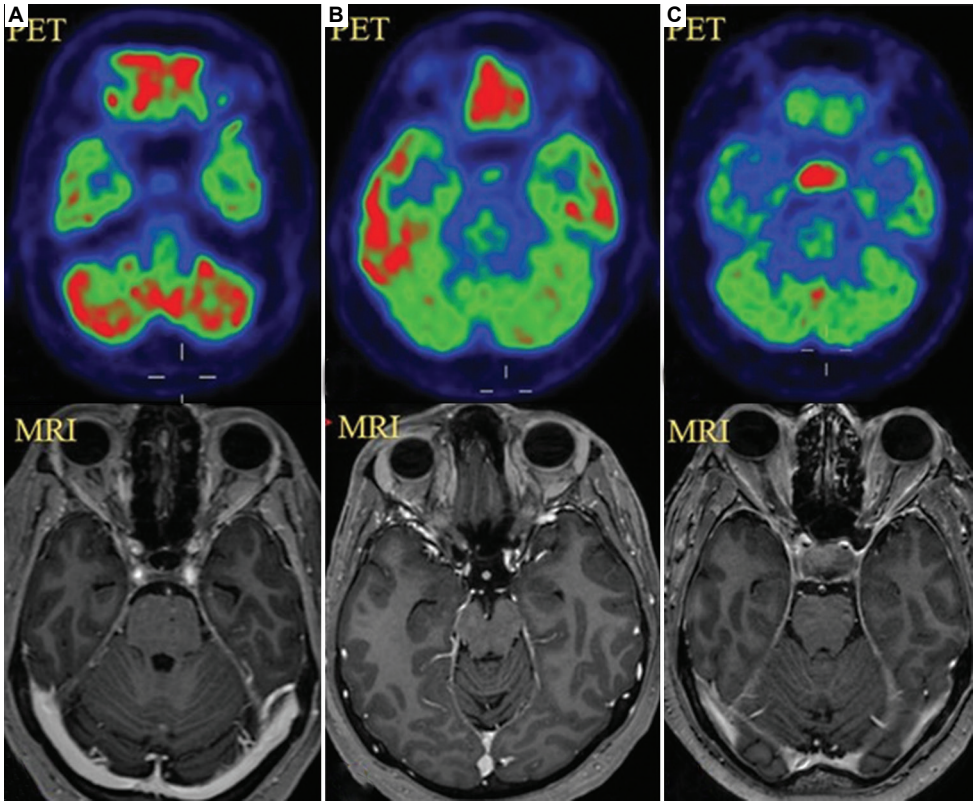

Figure 2. Grades of pituitary uptake ^{18}F-FDG PET/CT. (A) Low uptake in a 40-year-old female with breast cancer on hormonal therapy; PET/CT and MRI show a normal pituitary gland. (B) Intermediate uptake in a 35-year-old female with choriocarcinoma and lung metastases; PET/CT and MRI show a normal pituitary gland. (C) High uptake in a 64-year-old male with colon cancer; PET/CT shows increased pituitary activity, with MRI confirming a pituitary macroadenoma. This figure is adapted from Jain *et al.*,[2] available under a Creative Commons Attribution (CC BY 4.0) license.
Abbreviations: CT: Computed tomography; MRI: Magnetic resonance imaging; PET: Positron emission tomography.

gland, with an incidence of 0.24–0.87%.[10] ^{18}F-FDG PET/CT can demonstrate increased uptake in the pituitary stalk, aiding lesion localization and supporting diagnosis when MRI findings are equivocal. Although FDG uptake is not specific and cannot reliably distinguish autoimmune from neoplastic or infectious etiologies, it often normalizes following treatment, as mentioned earlier.[11] Emerging evidence suggests that FDS, a radiotracer primarily developed for bacterial infections, may also accumulate in autoimmune inflammation, raising the possibility of its use in differentiating sterile from infectious pituitary lesions[10] (Figure 3).

Similarly, immune-related hypophysitis, a therapy-induced form of pituitary inflammation, is reported in 8.5–14% of patients receiving combination immune checkpoint inhibition such as anti–CTLA-4/anti–PD-1 therapy, imposing a diagnostic challenge. It commonly manifests as pituitary enlargement on CT/MRI or increased metabolic features on ^{18}F-FDG PET/CT, reflecting inflammatory glandular changes that may precede overt clinical or biochemical abnormalities. These imaging findings are usually mild, transient, and without optic chiasm compression, but interpretation can be complicated by concurrent high-dose glucocorticoid therapy[12,13] (Figure 4).

Neurosarcoidosis, an atypical manifestation of systemic sarcoidosis, can involve the hypothalamic–pituitary axis with resultant granulomatous inflammation. This leads to focal hypermetabolism in the pituitary gland on the ^{18}F-FDG PET/CT, mimicking pituitary adenomas or other lesions. MRI may reveal contrast-enhancing pituitary or stalk lesions. Biopsy remains the definitive diagnostic tool, but is often impractical due to the gland's location.[14]

Pituitary involvement in antineutrophil cytoplasmic antibody (ANCA)–associated vasculitis (AAV) is rare and can occur at any stage of the disease. In a retrospective study of 150 AAV patients in 2020, 2% (3 patients) were found to have pituitary dysfunction. Two of them were ANCA-positive (one PR3-ANCA, one MPO-ANCA), and one was ANCA-negative but histologically confirmed to have granulomatous inflammation. Pituitary involvement

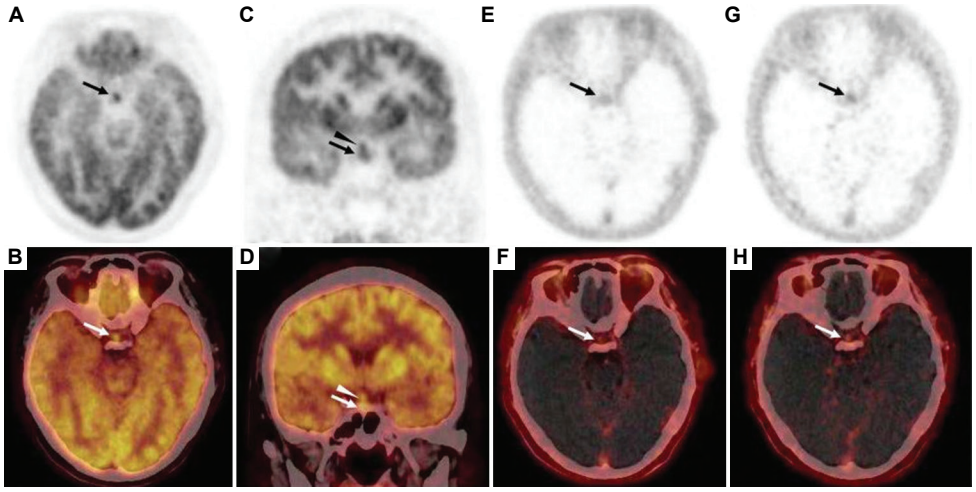

Figure 3. FDG (A-D) and FDS (E-H) PET/CT illustrating inflammatory pituitary uptake in autoimmune hypophysitis. (A-D) FDG and ^{18}F-2-fluorodeoxysorbitol (^{18}F-FDS) PET/CT of autoimmune hypophysitis. Both the pituitary gland (black and white arrows) and stalk lesions (black and white head arrows) show mild FDG uptake (SUV_{max} 5.5 at 40 min), aiding in lesion localization. The lesions also demonstrated FDS activity (SUV_{max} 1.1 at 30 min; 0.73 at 120 min), whereas (E-H) normal brain tissue showed minimal uptake, supporting the potential of FDG in detecting aseptic inflammation. This figure is adapted from Kong *et al.*,[10] available under a Creative Commons Attribution (CC BY 4.0) license.
Abbreviations: CT: Computed tomography; PET: Positron emission tomography; SUV: Standardized uptake value.

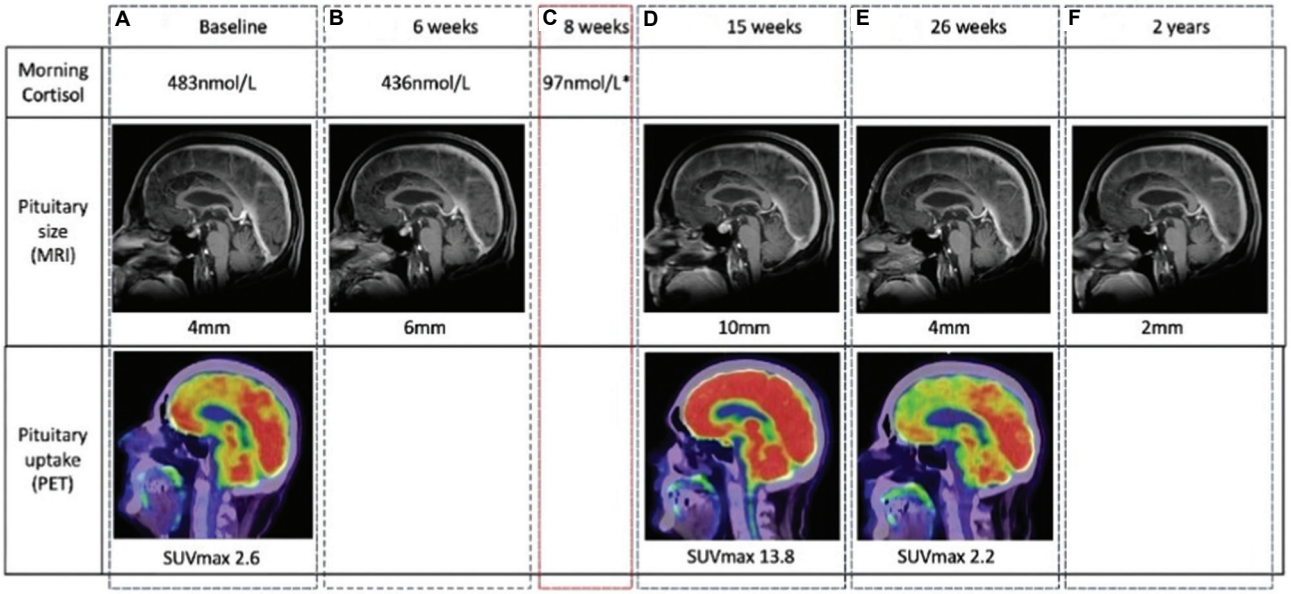

Figure 4. Temporal changes in pituitary size and FDG uptake in a patient with clinically diagnosed hypophysitis. The pituitary fossa is indicated by a dotted white circle. (A) Baseline imaging shows normal pituitary size and metabolic activity. (B) At 6 weeks, MRI for brain metastasis surveillance shows a slight (2 mm) increase in pituitary size, with normal morning cortisol. (C) At 8 weeks, the patient develops headache and lethargy; morning cortisol is subnormal, leading to a clinical diagnosis of hypophysitis. (D) Seven weeks after symptom onset, PET/CT shows marked increase in pituitary FDG uptake and size. (E and F) Follow-up imaging demonstrates gradual normalization of pituitary size and metabolic activity. This case highlights the dynamic changes in pituitary FDG uptake associated with inflammatory processes. This figure is adapted from Galligan *et al.*,[13] available under a Creative Commons Attribution (CC BY 4.0) license.
Abbreviations: CT: Computed tomography; PET: Positron emission tomography.

presented either as the initial manifestation or developed during the disease course, with symptoms including central diabetes insipidus, hypogonadism, polyuria, polydipsia, galactorrhea, and amenorrhea. MRI detected pituitary enlargement and thickening of the pituitary stalk in two patients, while one patient had a normal MRI but demonstrated FDG uptake in the pituitary fossa on ^{18}F-FDG PET-CT, emphasizing that even when MRI is

normal, PET-CT can facilitate diagnosis and monitoring of treatment response.[15]

Erdheim–Chester disease, a rare systemic non-LCH, is another etiological disease of inflammatory FDG uptake in the pituitary gland. A reported case with an unremarkable pituitary MRI, while ^{18}F-FDG PET/CT revealed increased uptake in the posterior pituitary, reflecting active involvement. Histopathology typically demonstrates foamy CD68^{+} histiocytes and Touton giant cells, supporting the diagnosis.[16]

A recent retrospective analysis of 15,085 ^{18}F-FDG PET/CT studies, abnormal pituitary uptake (SUV_{max} >2.5) was a rare finding, occurring in only 0.23% of patients (n = 36). The most common etiology was a primary pituitary tumor (58%), followed by inflammatory conditions such as tubercular and lymphocytic hypophysitis, as well as metastases. SUV_{max} values varied according to lesion type and metabolic activity, and ^{18}F-FDG PET/CT findings were generally concordant with MRI. Interestingly, among these, a case of disseminated tuberculosis demonstrated pituitary involvement, with ^{18}F-FDG PET/CT showing uptake (SUV_{max} 5.5). MRI revealed an enlarged pituitary gland with an enhancing sellar and suprasellar lesion involving the pituitary stalk, which resolved completely on follow-up imaging after treatment[17] (Figure 5A). Moreover, ^{18}F-FDG-PET/CT is highly effective in detecting residual or recurrent pituitary lesions post-surgery, particularly when MRI is limited by altered postoperative anatomy. When combined with biochemical and histopathological assessment, ^{18}F-FDG PET/CT provides a comprehensive approach for the diagnosis, characterization, and management of these lesions[17] (Figure 5B).

3.2. Neoplastic lesions

A large-cohort study of over 13,000 subjects established that incidental focal pituitary uptake on ^{18}F-FDG PET/CT with an SUVmax >4.1 is the optimal threshold for prompting further investigation, demonstrating high sensitivity (97%) and specificity (88%) for pathological uptake. The authors conclude that such findings warrant dedicated pituitary MRI and endocrine hormonal testing to exclude a functional adenoma or other pathology.[18]

3.2.1. PitNETs

PitNETs, previously known as pituitary adenomas, are typically benign tumors that originate in the pituitary

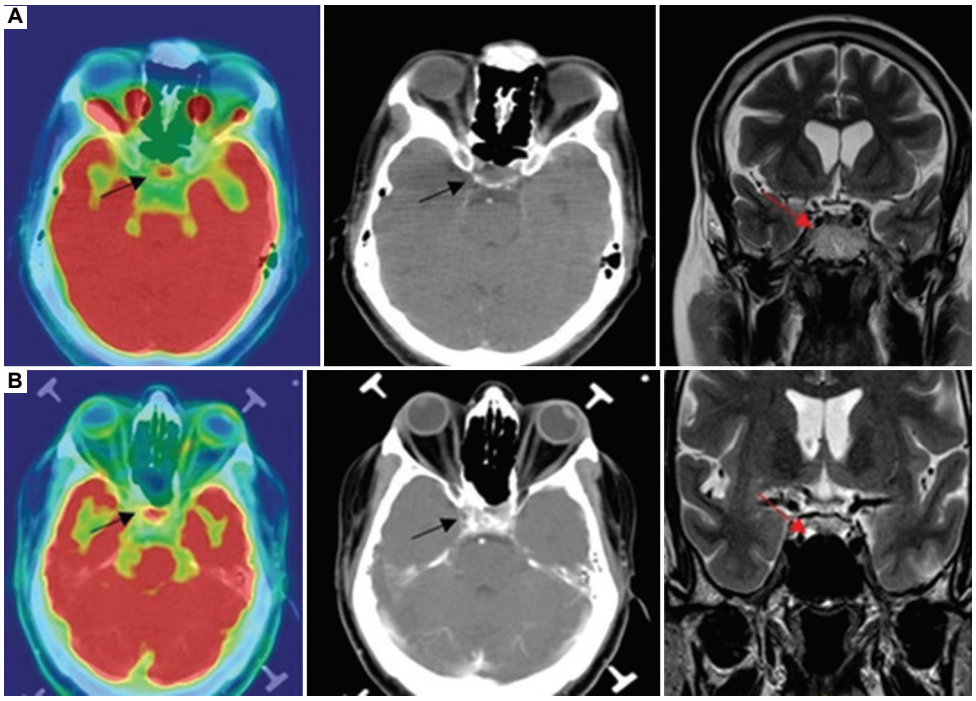

Figure 5. FDG PET/CT demonstrating pituitary inflammatory and neoplastic uptake across two clinical scenarios. (A) Pituitary FDG uptake (SUV 5.5) in a 52-year-old male with disseminated tuberculosis, showing pituitary and stalk enlargement on MRI. (B) ^{18}F-FDG PET/CT detection of recurrent pituitary adenoma (SUV_{max} 3.35) in a 51-year-old male following transsphenoidal excision, with MRI and histopathology confirming atypical growth hormone–secreting adenoma. This figure is reproduced/adapted from Stanly *et al.*,[17] available under the Creative Commons Attribution 4.0 International License (CC BY 4.0).
Abbreviations: CT: Computed tomography; MRI: Magnetic resonance imaging; PET: Positron emission tomography; SUV: Standardized uptake value.

gland. They can, however, develop outside of the sella turcica, a condition known as ectopic PitNET.[19]

Most pituitary lesions, over 90%, are pituitary adenomas. They are categorized based on their size and whether or not they secrete hormones. They are frequently discovered by chance on brain scans, MRI, and CT scans, a finding known as pituitary incidentalomas, appearing in 4–20% of these scans, and most of them are microadenomas. However, they are a much rarer finding on ^{18}F-FDG PET/CT scans, showing up in only 0.073–0.8% of cases.[20]

Early research demonstrated that the normal pituitary gland primarily uses non-esterified fatty acids for energy, with minimal glucose oxidation through the Krebs' cycle or pentose phosphate pathway.[21] However, ^{18}F-FDG-PET scans have indicated that pituitary adenomas may undergo a metabolic shift, similar to the Warburg effect seen in malignant tumors, where they become more reliant on glycolysis for their energy needs.[22] In addition, studies have shown that FDG uptake tends to be higher in larger PitNETs (macroadenomas) than in smaller ones, and interestingly, non-functioning PitNETs often show higher FDG uptake compared to functioning ones, even when their sizes are similar[23] (Figure 6).

Of 13,145 subjects undergoing ^{18}F-FDG PET/CT, incidental pituitary uptake was found in 0.8%. In cases with a final diagnosis, 40.8% were pathologic, predominantly pituitary adenomas. The degree of FDG accumulation was a key differentiator; using an SUV_{max} cutoff of 4.1 provided a sensitivity of 96.6% and specificity of 88.1% for identifying pathologic lesions, indicating that semi-quantitative analysis is highly useful for determining which incidental findings warrant further diagnostic evaluation.[18]

Similarly, based on a review of 24,007 scans, incidental pituitary hypermetabolism was found in 0.13% of the cases (SUV_{max} >4.1), with the most common causes being

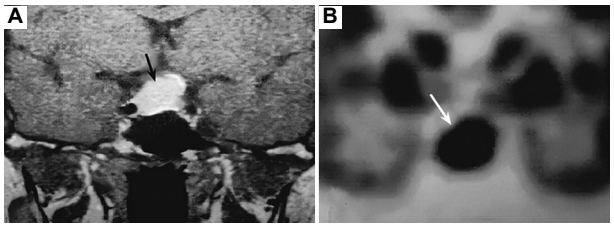

Figure 6. MRI and FDG PET/CT of a non-functioning pituitary adenoma (case 11). (A) MRI shows a 17 mm pituitary macroadenoma (black arrow). (B) ^{18}F-FDG PET/CT demonstrates corresponding increased uptake in the pituitary fossa (white arrow; SUV_{max} 13.1). This figure is adapted from Seok *et al.*,[23] available under a Creative Commons Attribution (CC BY 4.0) license.

Abbreviations: CT: Computed tomography; MRI: Magnetic resonance imaging; PET: Positron emission tomography; SUV: Standardized uptake value.

primary pituitary tumors, metastatic malignancy, and LCH[5] (Figures 7 and 8). However, benign physiologic uptake without a correlative lesion can also occur. An SUV_{max} threshold serves as a valuable quantitative parameter for distinguishing pathological entities, such as metastatic pituitary lesions, from benign physiologic variants. This highlights the importance of meticulous correlation with clinical context and complementary imaging findings to ensure accurate interpretation[5] (Figure 9).

Building on this overview of pituitary neoplastic lesions, including PitNETs and the general applications of FDG PET/CT, we will now explore several specific entities in greater detail:

A. Non-functioning adenomas

Miljić *et al.*[20] described a 70-year-old man with prior rectal and lung cancer in whom ^{18}F-FDG PET/CT incidentally detected a hypermetabolic pituitary lesion, initially suspected as metastasis. Further work-up confirmed a silent gonadotroph adenoma. Other reported cases of non-functional PitNETs include non-Hodgkin's lymphoma, lung and prostate cancers, highlighting that such findings can occur alongside other malignancies[24] (Figure 10).

B. Functioning adenomas

Cushing's disease (CD). CD results from ACTH-secreting pituitary tumors and often presents diagnostic challenges. Although MRI is the standard modality, it detects these lesions in only 50–90% of cases, leaving a significant proportion of tumors radiologically occult. This limitation highlights the potential complementary role of 18F-FDG PET in identifying pituitary abnormalities.[25]

One study investigated whether ovine-CRH (oCRH) stimulation could enhance the detection of corticotropinomas on 18F-FDG PET. oCRH significantly increased tumor SUV_{mean} without affecting normal pituitary uptake, improving detection rates from 44% to 55% with no false positives.[22] In contrast, Zhou *et al.*[26] retrospectively analyzed 47 patients and found that ^{18}F-FDG PET/CT had limited diagnostic value in CD, as pituitary and adrenal SUV_{max} did not differ significantly between cases with detectable lesions and those that remained occult.

On the other hand, a study by Kim *et al.*[27] explored whether dexamethasone (DEX) suppression could improve the use of ^{18}F-FDG PET/CT to locate ACTH-secreting pituitary adenomas in patients with CD. They found that DEX suppression did not significantly improve the localization of these tumors. While the SUV_{max} of adenomas increased compared to normal pituitary glands after DEX but the difference was not statistically significant. However, a correlation was noted between FDG uptake and cortisol levels

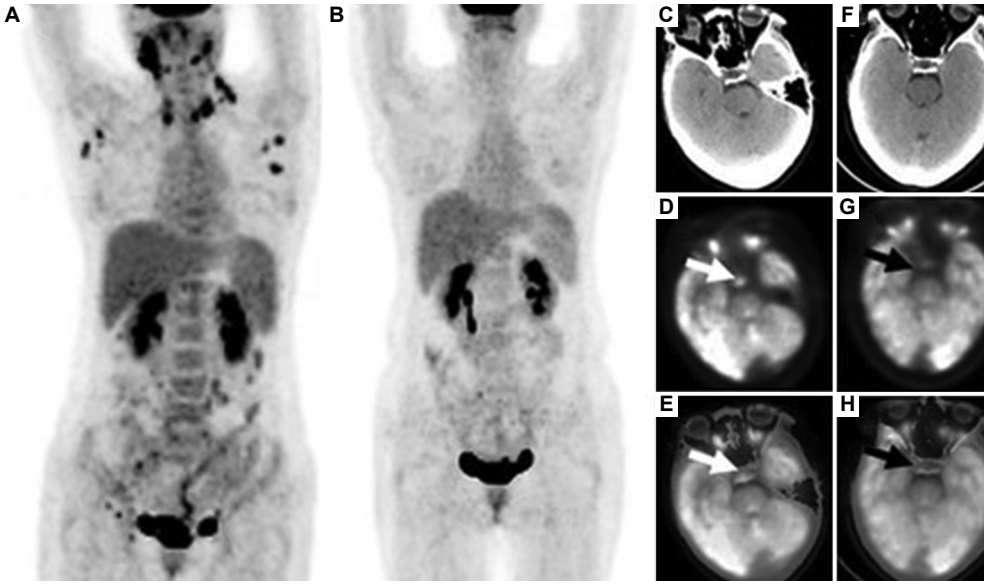

Figure 7. Whole-body PET (MIP) of a patient with Langerhans cell histiocytosis, demonstrating multiple hypermetabolic lymph nodes (SUV_{max} 4.4–13.2) before treatment (A) with resolution post-chemotherapy (B). Pituitary uptake is also visible on PET, CT, and fused PET/CT images (white arrows, SUV_{max} 6.0) before treatment, decreasing after chemotherapy (black arrows, SUV_{max} 3.6), highlighting therapy-related changes in metabolic activity. This figure is adapted from Ju *et al*.,[5] available under a Creative Commons Attribution (CC BY 3.0) license.
Abbreviations: CT: Computed tomography; MIP: Maximum intensity projection; PET: Positron emission tomography; SUV: Standardized uptake value.

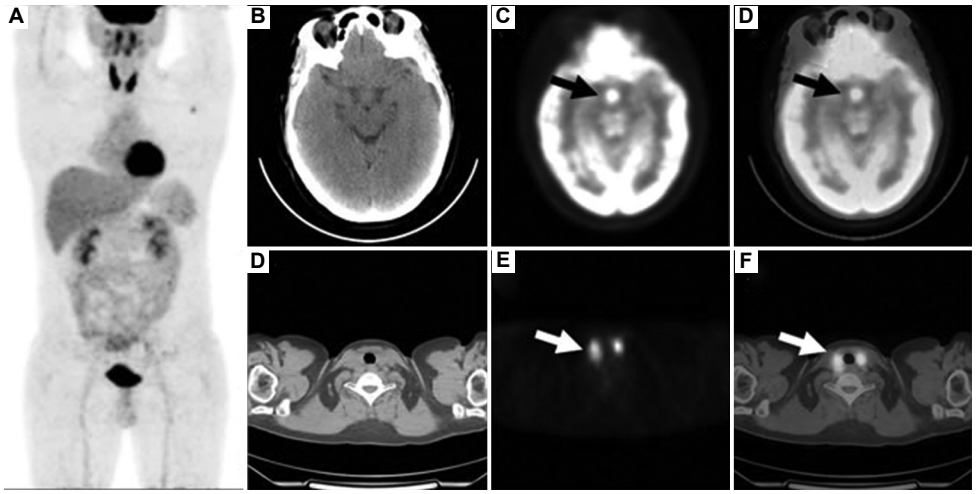

Figure 8. ^{18}F-FDG PET/CT findings in a patient with Langerhans cell histiocytosis demonstrating concurrent pituitary and diffuse thyroid hypermetabolism. (A) MIP image showing diffuse thyroid uptake and focal increased FDG activity in the pituitary region. (B) Axial CT of the brain demonstrating normal pituitary morphology. (C and D) PET and fused PET/CT images, respectively, of the brain, revealing markedly increased FDG uptake in the pituitary gland (black arrows, SUV_{max} = 12.9). (E) Axial CT of the neck showing residual thyroid tissue. (F and G) PET and fused PET/CT images, respectively, demonstrating diffuse thyroid hypermetabolism (white arrows, SUV_{max} = 11.3). These findings highlight that inflammatory or infiltrative disorders such as Langerhans cell histiocytosis may exhibit intense pituitary FDG uptake, potentially mimicking neoplastic lesions. This figure is adapted from Ju *et al*.,[5] available under a Creative Commons Attribution (CC BY 3.0) license.
Abbreviations: CT: Computed tomography; MIP: Maximum intensity projection; PET: Positron emission tomography; SUV: Standardized uptake value.

after DEX suppression. Tumors with higher FDG uptake showed a weaker response to the high-dose DEX suppression test, meaning their cortisol levels were less suppressed. This suggests that the metabolic activity shown by FDG uptake might be linked to the degree of cortisol suppression.[27]

C. Prolactinoma

Ginet *et al.*[28] reported drug-resistant epilepsy in a 63-year-old man with who underwent ^{18}F-FDG and ^{18}F-fluorodopa (^{18}F-FDOPA) PET scans. Both scans showed increased uptake in the sellar region, but the ^{18}F-FDOPA

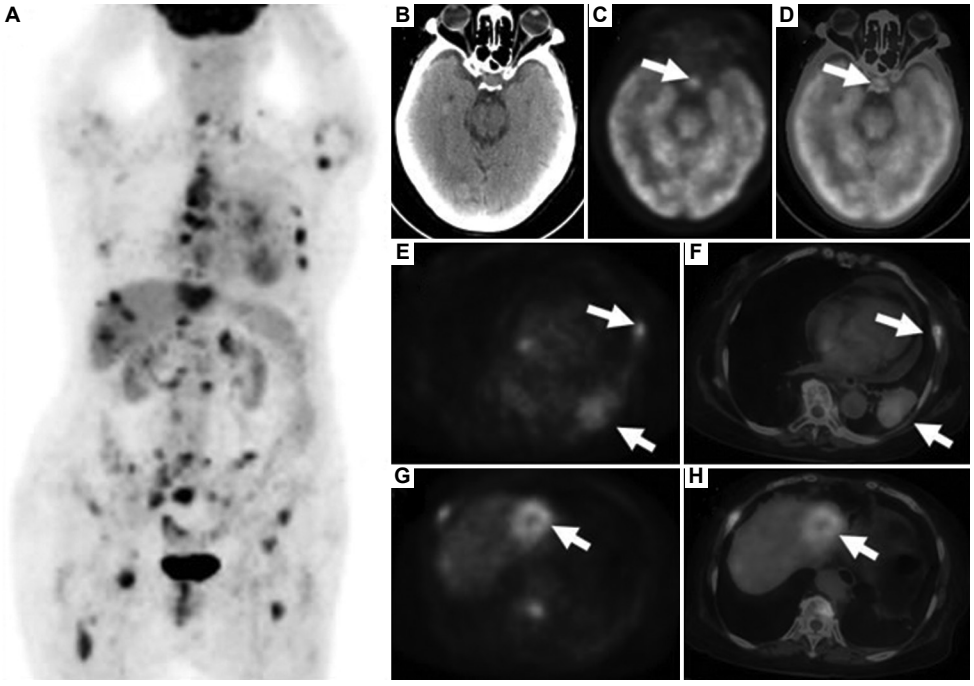

Figure 9. Whole-body ^{18}F-FDG PET/CT images of a patient with lung cancer and multiple systemic metastases demonstrating pituitary hypermetabolism. (A) MIP PET image shows multiple hypermetabolic lesions. (B-D) Brain CT, PET, and fused PET/CT images, respectively, reveal increased FDG uptake in the pituitary gland (white arrows), with an SUV_{max} of 7.3. (E and F) Cross-sectional PET and fused PET/CT images of the chest, respectively, demonstrate a hypermetabolic mass in the left lower lobe of the lung with adjacent rib destruction (white arrows). (G and H) Abdominal PET and fused PET/CT images show a hypermetabolic lesion in the left hepatic lobe suggestive of liver metastasis (white arrows). This figure is adapted from Ju *et al.*,[5] available under a Creative Commons Attribution (CC BY 3.0) license.
Abbreviations: CT: Computed tomography; MIP: Maximum intensity projection; PET: Positron emission tomography; SUV: Standardized uptake value.

uptake was significantly higher, with an SUV_{max} ratio of 2.8 relative to cortical regions compared to 1.3 for ^{18}F-FDG. This greater uptake with ^{18}F-FDOPA is likely due to the presence of amino acid receptors, particularly L-type, within a prolactinoma.[28]

3.2.2. Pituitary malignancies

Zhong *et al.*[29] reported a 30-year-old woman who was initially diagnosed with a non-functional pituitary macroadenoma invading the left cavernous sinus based on MRI. However, an intraoperative biopsy suggested malignancy, prompting a PET/CT scan that showed a high concentration of ^{18}F-FDG in the sellar region with an SUV_{max} of 6.73. Combining the biopsy results with the PET/CT findings, the patient was diagnosed with an atypical pituitary adenoma with a strong suspicion of malignancy.[29]

Moreover, a 33-year-old woman with progressive vision loss had an MRI revealing a pituitary lesion, initially suspected to be an abscess. To distinguish between malignancy and inflammation, both ^{18}F-FDG and ^{18}F-FDS were used in a PET/CT scan. While ^{18}F-FDS was expected to accumulate only in inflamed tissue, both scans showed considerable tracer uptake in the lesion with an SUV_{max} of 4.73 and 1.49 for FDG and ^{18}F-FDS, respectively. A biopsy ultimately confirmed the lesion to be a spindle cell carcinoma, subsequently concluding that ^{18}F-FDS can also accumulate in malignant tumours.[30]

3.2.3. Metastatic or secondary lesions

Metastatic involvement of the pituitary gland is rare, accounting for only 0.4% of intracranial metastases and approximately 1% of surgically treated pituitary lesions.[31] However, the most frequently encountered primary site is lung cancer in men (46%) and breast cancer in women (50%). Other less common sources include renal, prostate, and colon cancers (each 3–5%).[32,33]

Several case reports have documented pituitary metastases originating from various cancers such as non-small cell lung cancer,[34] squamous cell carcinoma of the tonsils[35] and melanoma,[36] which were incidentally detected on routine ^{18}F-FDG PET/CT exhibiting variable FDG uptake in the sellar region, with SUV_{max} values typically lower than those of systemic metastatic sites but higher than background brain activity.

Another recently reported case described leiomyosarcoma with biopsy-proven metastasis to the sellar

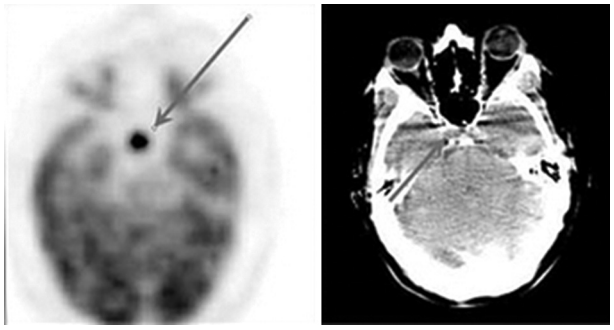

Figure 10. Whole-body and brain ^{18}F-FDG PET/CT images of a 49-year-old man with biopsy-proven small lymphocytic lymphoma demonstrating incidental pituitary uptake. The initial staging PET/CT revealed widespread hypermetabolic lymphadenopathy and bone marrow involvement, along with an intense focus of FDG uptake in the sellar region (SUV_{max} 16.6; white arrow), raising suspicion for pituitary involvement or a benign adenoma. Following chemotherapy, a repeat PET/CT showed complete metabolic response of all lymphoma lesions, while persistent intense pituitary hypermetabolism (SUV_{max} 18.6; white arrow) remained, consistent with a benign pituitary adenoma. Subsequent gadolinium-enhanced MRI confirmed a 7.5 × 5.5 mm well-defined pituitary lesion with lack of enhancement relative to the surrounding gland, characteristic of a non-functioning pituitary adenoma. This figure is adapted from Karapolat *et al.*,[24] available under a Creative Commons Attribution (CC BY 3.0) license.
Abbreviations: CT: Computed tomography; MRI: Magnetic resonance imaging; PET: Positron emission tomography; SUV: Standardized uptake value.

region, initially mimicking a pituitary macroadenoma. The lesion demonstrated rapid interval growth, suprasellar extension, cavernous sinus invasion, and bony erosion, with only faint FDG uptake on ^{18}F-FDG PET/CT, which complicated the distinction from a benign adenomatous process.[37]

However, FDG uptake is typically much higher in lymphoma, which is exceedingly rare in the pituitary gland, with non-Hodgkin lymphoma identified in the vast majority of cases. A reported case of nodular lymphocyte-predominant Hodgkin lymphoma presenting with hypopituitarism, in which ^{18}F-FDG PET/CT revealed pituitary lymphomatous infiltration.[38]

Pituitary lymphoma is extremely rare, classified as either primary pituitary lymphoma, confined to the pituitary and stalk, or secondary pituitary lymphoma, representing systemic spread. Notably, only 19 cases of primary pituitary lymphoma and 16 cases of secondary pituitary lymphoma were documented. Clinical manifestations often include hypopituitarism, diabetes insipidus, visual field defects, or headache, while laboratory tests may show elevated soluble interleukin-2 receptor levels. MRI typically demonstrates an isointense sellar mass on T1, iso- to hypointense signal on T2, and uniform contrast enhancement. ^{18}F-FDG PET/CT usually reveals hypermetabolic uptake in the pituitary, aiding in guiding biopsy, treatment decision, and interim/end-of-therapy evaluation. Early recognition of pituitary lymphoma is crucial in the differential diagnosis of pituitary lesions, since timely initiation of systemic chemotherapy can lead to long-term remission, as illustrated by reported cases of secondary pituitary lymphoma responding well to treatment.[39]

In a retrospective study of 10,347 ^{18}F-FDG PET/CT examinations aimed to analyze the incidence of pituitary metastasis in various cancers, Piciu *et al.*[40] identified four cases of pituitary metastases (0.038%) from breast carcinoma, lung adenocarcinoma, malignant melanoma, and colon adenocarcinoma. The mean SUV_{max} of metastatic lesions was 13.25 ± 4.9 (range, 8.6–21.5), significantly higher than the mean SUV_{max} of benign pituitary lesions reported in the literature (10.29 ± 4.5, range 4.7–29.3; p=0.0184). These findings suggest that increased FDG avidity may serve as a useful tool in distinguishing pituitary metastases from benign or physiological uptake, although overlap in values necessitates cautious interpretation.[40]

3.3. Complications or mimics

Abnormal pituitary uptake on ^{18}F-FDG PET/CT can represent a diagnostic pitfall, as it may mimic metastatic disease or other sellar lesions. Hemorrhagic or necrotic pituitary macroadenomas, particularly those with apoplexy, can exhibit intense heterogeneous FDG avidity, raising suspicion for metastasis despite being benign.[41] Papillary craniopharyngiomas also demonstrate high FDG uptake, often exceeding that of adenomatous subtypes, likely related to BRAFV600E-driven upregulation of glucose metabolism, and should be considered in the differential diagnosis of suprasellar FDG-avid lesion.[42] Similarly, pituicytomas, rare benign neoplasms of the posterior pituitary, may show mild FDG uptake and variable MRI characteristics, including T2 hypointensity, heterogeneous enhancement, and occasional invasive behavior, further complicating preoperative interpretation.[43] Finally, a case of a highly FDG-avid sphenoid sinus mass (SUV_{max} 16.1) closely abutting the sella turcica mimicked pituitary uptake.[19] These examples underscore the importance of correlating PET findings with MRI and clinical evaluation to accurately distinguish authentic pituitary uptake from other adjacent lesions, avoiding misdiagnosis and guiding appropriate management.

3.4. Other explored radiotracers beyond the conventional ^{18}F-FDG

While 18F-FDG remains the principal agent in oncologic imaging, its utility in the pituitary gland is often hindered by the high physiological glucose metabolism of the adjacent normal brain parenchyma, which creates significant

background noise and obscures subtle pathological findings, particularly microadenomas or residual disease post-surgery. Comparative studies explicitly highlight this FDG limitation, demonstrating the superior diagnostic yield of amino acid tracers like ^{11}C-MET. ^{11}C-MET uptake is mediated by the L-type amino acid transporter 1, resulting in a more favorable tumor-to-background ratio compared to FDG. This distinction is clinically significant in patients with functioning pituitary adenomas, where ^{11}C-MET PET/CT achieved an overall positive rate of 95% compared to only 67% for ^{18}F-FDG PET/CT. The difference is especially pronounced in the setting of recurrent microadenomas, where ^{11}C-MET demonstrated 100% detection against ^{18}F-FDG's 22% positive rate.[44]

While incidental pituitary uptake on FDG PET is rare, other tracers such as ^{68}Ga-PSMA can also demonstrate pituitary localization. A 76-year-old man with a history of prostate and lung cancer underwent restaging PET/CT. The pituitary gland showed intense uptake on ^{18}F-FDG PET/CT (SUV_{max} 13.9) but only mild uptake on ^{68}Ga-PSMA PET/CT (SUV_{max} 1.9). MRI confirmed a macroadenoma filling and expanding the sella.[45]

In addition, a case report has documented increased ^{18}F-choline PET/CT uptake (SUV_{max} = 5.3) in the same patient who also showed increased ^{18}F-FDG uptake (SUV_{max} = 16.2) in a non-functioning pituitary adenoma.[25] Similar case reports are also available in the literature.[46]

The diagnostic challenge of pituitary lesions persists, as the high physiological brain uptake on ^{18}F-FDG PET/CT often obscures pathological findings. The novel ^{68}Ga-FAPI tracer, which targets fibroblast activation protein, offers a promising solution. As demonstrated in the provided LCH study, FAPI PET provides exceptional tumor-to-background contrast in the skull base, leading to superior lesion delineation and diagnostic confidence for pituitary involvement compared to FDG PET. This enhanced detection capability can significantly impact clinical management by improving disease staging and guiding treatment decisions.[47] Furthermore, ^{68}Ga-FAPI PET/CT has demonstrated superior delineation of pituitary fibrosarcoma compared to ^{18}F-FDG PET/CT and MRI. In a reported case, FAPI PET clearly outlined tumor margins, detected clivus invasion, and offered high lesion-to-background contrast due to minimal physiological brain uptake, highlighting its potential for evaluating fibroblast-rich pituitary lesions and its theranostic applications.[48]

Pan *et al.*[49] reported a 63-year-old male with Waldenström macroglobulinemia (WM) who developed peripheral neuropathies and was diagnosed with Bing–Neel syndrome (Central Nervous System [CNS] involvement of WM). Brain MRI revealed a coexisting pituitary macroadenoma. In ^{18}F-FDG PET/CT, the macroadenoma was hypermetabolic (SUV_{max} 10.4), while ^{68}Ga-Pentixafor PET/CT, a CXCR4-targeted tracer, detected involvement in bone marrow, lymph nodes, thoracic/sacral nerve roots, and notably bilateral choroid plexus, lesions not visible on FDG PET or MRI. Following six cycles of chemotherapy, PET/CT demonstrated complete remission of WM and CNS lesions on both tracers; however, the pituitary macroadenoma remained FDG-avid. This case highlights the complementary roles of FDG and CXCR4-targeted PET in differentiating coexisting pituitary lesions from CNS involvement in WM, and underscores the potential of ^{68}Ga-Pentixafor PET/CT for detecting rare CNS infiltration sites such as the choroid plexus[49] (Figure 11).

Interestingly, the so-called double pituitary hot spot sign was described in a 55-year-old female with newly diagnosed carcinoid syndrome who underwent a ^{68}Ga-DOTA-TATE PET/CT for tumor localization. The scan successfully identified the primary tumor in her small bowel, but also revealed an incidental, intense focus of tracer uptake near her pituitary gland. Subsequent MRI confirmed this to be a skull base meningioma. The ability of ^{68}Ga-DOTA-TATE PET/CT to show high uptake in meningiomas can aid in differentiating them from other skull base tumors, such as craniopharyngiomas, which is crucial for clinical management and treatment planning, including for radiotherapy or peptide receptor radionuclide therapy.[50]

3.5. Emerging role of artificial intelligence (AI) and radiomics

The future landscape of incidental pituitary uptake evaluation is expected to be significantly shaped by AI, specifically the integration of machine learning (ML) models and radiomics. Radiomics involves the high-throughput extraction of numerous quantitative features—such as texture, shape, and intensity distribution—from medical images that are invisible to the human eye. This methodology has already shown promise in general ^{18}F-FDG PET/CT oncology, proving capable of distinguishing inflammatory processes from malignancies in other body regions based on metabolic heterogeneity.[51] Crucially, ML models informed by radiomics have also been successfully applied to dedicated pituitary imaging, notably MRI, to predict surgical outcomes, characterize tumor subtypes, and guide treatment planning for PitNETs.[52]

Moreover, a recently published systematic review comprehensively examined the contemporary clinical applications of radiomics in pituitary adenomas, with particular emphasis on diagnostic, predictive, and prognostic modeling. The authors concluded that

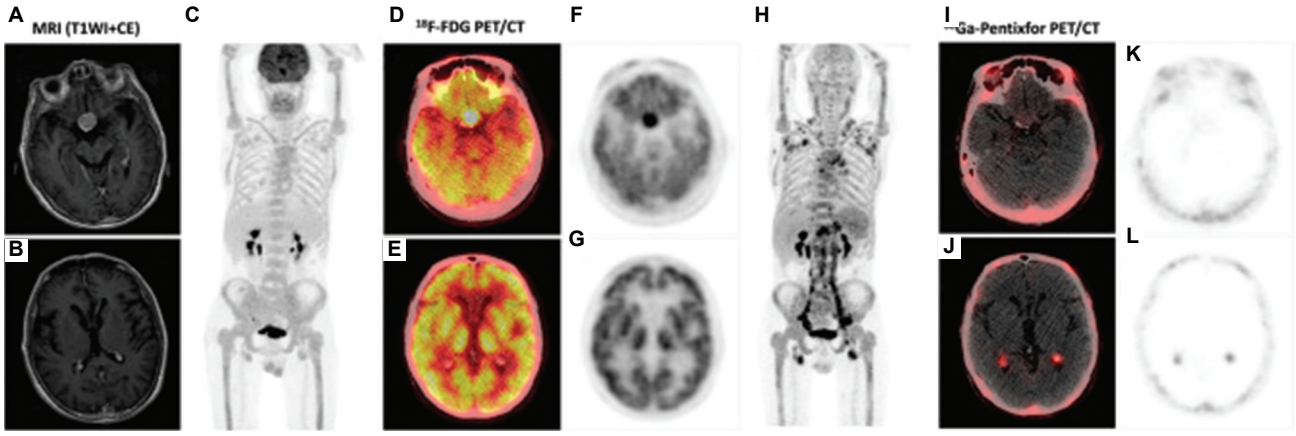

Figure 11. Baseline and comparative PET/CT evaluation in a 63-year-old man with Waldenström's macroglobulinemia and biopsy-confirmed Bing–Neel syndrome. (A and B) Axial contrast-enhanced T1-weighted MRI shows a pituitary macroadenoma without other intracranial abnormalities. (C and D) The MIP image of the ^{18}F-FDG PET shows diffuse homogeneous bone marrow uptake and multiple nodal involvements (C), while axial fusion and PET images reveals intense FDG uptake in the pituitary macroadenoma (SUV_{max} 10.4; white arrows) (D-G). (H-L) In contrast, ^{68}Ga-Pentixafor PET MIP demonstrates avid skeletal and nodal disease with additional tracer uptake in the bilateral choroid plexus (SUV_{max} 4.0; yellow arrows) (H), as confirmed by fusion and PET images (I-L). Notably, the pituitary macroadenoma exhibits no ^{68}Ga-Pentixafor uptake, indicating absent CXCR4 expression. This figure is adapted from Pan *et al.*,[49] available under a Creative Commons Attribution (CC BY 3.0) license.
Abbreviations: CT: Computed tomography; MIP: Maximum intensity projection; MRI: Magnetic resonance imaging; PET: Positron emission tomography; SUV: Standardized uptake value.

radiomics facilitates robust, noninvasive prediction of pituitary adenoma subtypes, tumor consistency, invasiveness, therapeutic response, and risk of recurrence.[53] The existing literature presents evidence supporting the application of AI and ML models in the field of head and neck cancer, encompassing key areas such as detection, differentiation from benign lesions, segmentation, staging, response assessment, and prognosis determination.[54] While these findings are currently preliminary and limited in their integration into routine clinical practice, future research and developmental efforts are expected to translate these perspectives into a standardized, comprehensive approach for the evaluation and stratification of head and neck malignancies, including those of the pituitary gland.

4. Conclusion

Incidental pituitary uptake on ^{18}F-FDG PET/CT is an uncommon but clinically significant finding that encompasses a broad spectrum of etiologies, ranging from physiologic variants and inflammatory disorders to benign and malignant neoplasms. Although rare, its detection necessitates careful interpretation, as focal pituitary hypermetabolism may mimic or mask underlying pathology. Correlation with endocrine function, MRI, and clinical context is essential to distinguish true lesions from benign or physiologic processes.

Looking ahead, novel molecular tracers such as ^{68}Ga-FAPI and ^{11}C-methionine are poised to enhance diagnostic accuracy, offering superior lesion-to-background contrast and greater sensitivity for small or metabolically distinct lesions. AI–driven semi-quantitative analysis and automated SUV assessment may further improve lesion characterization and reproducibility, particularly in borderline or equivocal cases. Insights from these emerging tools, combined with robust imaging–endocrine correlation, can inform future updates to pituitary incidentaloma management guidelines, ensuring more precise risk stratification and evidence-based follow-up strategies.

Acknowledgments

We would like to acknowledge the King Hussein Cancer Center (KHCC) for its invaluable institutional support. We also extend our gratitude to the authors of the previously published works from which figures were adapted for use in this manuscript.

Funding

None.

Conflict of interest

The authors declare they have no competing interests.

Author contributions

Conceptualization: Marwah Abdulrahman, Raghad M. Al-houwari, Akram Al-Ibraheem

Writing–original draft: Marwah Abdulrahman, Raghad M. Al-houwari

Writing–review & editing: Manar W. Alomari, Rezhan Ali, Shahed Obeidat, Akram Al-Ibraheem

Ethics approval and consent to participate

Not applicable.

Consent for publication

Not applicable.

Availability of data

Not applicable.

References

1. Pencharz D, Nathan M, Wagner TL. Evidence-based management of incidental focal uptake of fluorodeoxyglucose on PET-CT. *Br J Radiol*. 2018;91(1084):20170774.

   doi: 10.1259/bjr.20170774

2. Jain A, Usmani S, Al Riyami K, *et al*. High physiological 18 F-FDG uptake in normal pituitary gland on digital PET scanner. *World J Nucl Med*. 2024;23(3):161-167.

   doi: 10.1055/s-0044-1786733

3. Jeong SY, Lee SW, Lee HJ, *et al*. Incidental pituitary uptake on whole-body 18F-FDG PET/CT: A multicentre study. *Eur J Nucl Med Mol Imaging*. 2010;37(12):2334-2343.

   doi: 10.1007/s00259-010-1571-5

4. Asa SL, Ezzat S, Mete O. Clinical integration and application of the 2022 WHO pituitary tumor classification. *Neurooncol Adv*. 2025;7(Suppl 1):i10-i16.

   doi: 10.1093/noajnl/vdae145

5. Ju H, Zhou J, Pan Y, LV J, Zhang Y. Evaluation of pituitary uptake incidentally identified on 18F-FDG PET/CT scan. *Oncotarget*. 2017;8(33):55544-55549.

   doi: 10.18632/oncotarget.15417

6. Britt CJ, Maas AM, Kennedy TA, Hartig GK. Incidental findings on FDG PET/CT in head and neck cancer. *Otolaryngol--Head Neck Surg*. 2018;158(3):484-488.

   doi: 10.1177/0194599817742579

7. Weng JH, Lee JK, Wu MF, Shen CY, Kao PF. Pituitary FDG uptake in a patient of lung cancer with bilateral adrenal metastases causing adrenal cortical insufficiency. *Clin Nucl Med*. 2011;36(8):731-732.

   doi: 10.1097/RLU.0b013e31821a26bf

8. Ding Y, Wu S, Xu J, Wang H, Ma C. Pituitary 18F-FDG uptake correlates with serum TSH levels in thyroid cancer patients on 18F-FDG PET/CT. *Nucl Med Commun*. 2019;40(1):57-62.

   doi: 10.1097/MNM.0000000000000940

9. Hu G, Huo L, Li F, Luo Y. Renal involvement of immunoglobulin G4-related disease presenting as a solitary hypermetabolic mass mimicking renal tumor on 18 F-FDG PET/CT. *Clin Nucl Med*. 2023;48(8):e400-e402.

   doi: 10.1097/RLU.0000000000004721

10. Kong Z, Wang Y, Ma W, Cheng X. Role of 18F-fluorodeoxyglucose (FDG) and 18F-2-fluorodeoxy sorbitol (FDS) in autoimmune hypophysitis: A case report. *BMC Endocr Disord*. 2020;20(1):84.

    doi: 10.1186/s12902-020-00567-8

11. Kubo H, Ohtsubo H, Shiraoka A, Watanabe M, Kyoraku I, Okamoto K. [A case of suspected IgG4-related hypophysitis presented with panhypopituitarism and central diabetes insipidus]. *Rinsho Shinkeigaku*. 2024;64(6):398-402.

    doi: 10.5692/clinicalneurol.cn-001934

12. Van Der Hiel B, Blank CU, Haanen JBAG, Stokkel MPM. Detection of early onset of hypophysitis by (18)F-FDG PET-CT in a patient with advanced stage melanoma treated with ipilimumab. *Clin Nucl Med*. 2013;38(4):e182-e184.

    doi: 10.1097/RLU.0b013e3182639765

13. Galligan A, Iravani A, Lasocki A, *et al*. Imaging for assessment of cancer treatment response to immune checkpoint inhibitors can be complementary in identifying hypophysitis. *Front Endocrinol*. 2023;14:1295865.

    doi: 10.3389/fendo.2023.1295865

14. Berntsson SG, Elmgren A, Gudjonsson O, Grabowska A, Landtblom AM, Moraes-Fontes MF. A comprehensive diagnostic approach in suspected neurosarcoidosis. *Sci Rep*. 2023;13(1):6539.

    doi: 10.1038/s41598-023-33631-z

15. Li C, Zou Y, Lu X, Wang G, Shu X. Pituitary dysfunction in patients with ANCA associated vasculitis: Prevalence, presentation, and outcomes. *Ther Adv Chronic Dis*. 2020;11:2040622320930636.

    doi: 10.1177/2040622320930636

16. Ding H, Li Y, Ruan C, *et al*. Chinese Erdheim-Chester disease: Clinical-pathology-PET/CT updates. *Endocrinol Diabetes Metab Case Rep*. 2015;2015:150055.

    doi: 10.1530/EDM-15-0055

17. Stanly A, Sunny SS, Benjamin J, *et al*. Utility of F18-FDG PET/CT in the evaluation of pituitary uptake. *World J Nucl Med*. 2024;23(4):234-241.

    doi: 10.1055/s-0044-1787967

18. Hyun SH, Choi JY, Lee KH, Choe YS, Kim BT. Incidental focal 18F-FDG uptake in the pituitary gland: Clinical significance and differential diagnostic criteria. *J Nucl Med*. 2011;52(4):547-550.

    doi: 10.2967/jnumed.110.083733

19. Usui Y, Kurokawa R, Fukushima T, *et al*. Ectopic pituitary neuroendocrine tumor arising in the sphenoid sinus with

an avid 18F-fluorodeoxyglucose uptake masquerading as malignancy: A case report. *Radiol Case Rep*. 2023;18(9): 2943-2947.

doi: 10.1016/j.radcr.2023.05.063

20. Miljić D, Manojlović-Gačić E, Skender-Gazibara M, *et al*. All that glitters on PET is not cancer! 18F-deoxy-glucose avidity versus tumor biology: Pituitary incidentaloma in a survivor of two previous unrelated malignancies. *Endokrynol Pol*. 2017;68(3):352-359.

doi: 10.5603/EP.2017.0027

21. Viña JR, Page RB, Davis DW, Hawkins RA. Aerobic glycolysis by the pituitary gland *in vivo*. *J Neurochem*. 1984;42(5): 1479-1482.

doi: 10.1111/j.1471-4159.1984.tb02814.x

22. Boyle J, Patronas NJ, Smirniotopoulos J, *et al*. CRH stimulation improves 18F-FDG-PET detection of pituitary adenomas in Cushing's disease. *Endocrine*. 2019;65(1):155-165.

doi: 10.1007/s12020-019-01944-7

23. Seok H, Lee EY, Choe EY, *et al*. Analysis of 18F-fluorodeoxyglucose positron emission tomography findings in patients with pituitary lesions. *Korean J Intern Med*. 2013;28(1):81-88.

doi: 10.3904/kjim.2013.28.1.81

24. Karapolat I, Oncel G, Kumanlıoğlu K. Clinically occult pituitary adenoma can appear as a hypermetabolic lesion on whole body FDG PET imaging in a patient with lymphoma. *Mol Imaging Radionucl Ther*. 2013;22(1):18-20.

doi: 10.4274/Mirt.258

25. Albano D, Bosio G, Bertagna F. Incidental pituitary adenoma detected by 18F-FDG PET/CT and 18F-choline PET/CT in the same patient. *Rev Espanola Med Nucl E Imagen Mol*. 2018;37(4):250-252.

doi: 10.1016/j.remn.2017.07.002

26. Zhou J, Ju H, Zhu L, Pan Y, Lv J, Zhang Y. Value of fluorine-18-fluorodeoxyglucose PET/CT in localizing the primary lesion in adrenocorticotropic hormone-dependent Cushing syndrome. *Nucl Med Commun*. 2019;40(5):539-544.

doi: 10.1097/MNM.0000000000000989

27. Kim K, Kim DK, Moon JH, *et al*. Dexamethasone suppression for 18F-FDG PET/CT to localize ACTH-secreting pituitary tumors. *Cancer Imaging*. 2023;23(1):85.

doi: 10.1186/s40644-023-00600-8

28. Ginet M, Cuny T, Schmitt E, Marie PY, Verger A. 18F-FDOPA PET imaging in prolactinoma. *Clin Nucl Med*. 2017;42(8):e383-e384.

doi: 10.1097/RLU.0000000000001721

29. Zhong C, Yin S, Zhou P, Jiang S. Pituitary atypical adenoma or carcinoma sensitive to temozolomide combined with radiation therapy: A case report of early identification and management. *Turk Neurosurg*. 2014;24(6):963-966.

doi: 10.5137/1019-5149.JTN.9629-13.1

30. Cheng X, Zhu W, Cui R. Increased 18F-2-fluorodeoxysorbitol (18F-FDS) activity in a pituitary spindle cell carcinoma. *Clin Nucl Med*. 2016;41(12):953-955.

doi: 10.1097/RLU.0000000000001391

31. Habu M, Tokimura H, Hirano H, *et al*. Pituitary metastases: Current practice in Japan. *J Neurosurg*. 2015;123(4): 998-1007.

doi: 10.3171/2014.12.JNS14870

32. Komninos J, Vlassopoulou V, Protopapa D, *et al*. Tumors metastatic to the pituitary gland: Case report and literature review. *J Clin Endocrinol Metab*. 2004;89(2):574-580.

doi: 10.1210/jc.2003-030395

33. Marsh JC, Garg S, Wendt JA, Gielda BT, Turian JV, Herskovic AM. Intracranial metastatic disease rarely involves the pituitary: Retrospective analysis of 935 metastases in 155 patients and review of the literature. *Pituitary*. 2010;13(3):260-265.

doi: 10.1007/s11102-010-0229-4

34. Le Meur C, Campedel L, Kharroubi D, Amrane K. Pituitary metastasis of non-small cell lung cancer with high FDG uptake on PET/CT pituitary metastasis of non-small cell lung carcinoma. *Clin Nucl Med*. 2022;47(7):e506-e508.

doi: 10.1097/RLU.0000000000004179

35. Matejka M, Gellen JS, Kraus T, Griessenauer CJ, Ueberschaer MF. Transnasal endoscopic resection of a pituitary metastasis from a tonsillar squamous cell carcinoma (SCC): A case report and a review of the literature. *Cureus*. 2025;17(7):e88146.

doi: 10.7759/cureus.88146

36. Mormando M, Puliani G, Barnabei A, *et al*. A rare case of pituitary melanoma metastasis: A dramatic and prolonged response to Dabrafenib-Trametinib therapy. *Front Endocrinol*. 2020;11:471.

doi: 10.3389/fendo.2020.00471

37. Weber MD, Carlstrom LP, Vignolles-Jeong J, *et al*. Endoscopic endonasal approach for resection of sellar leiomyosarcoma metastasis: Illustrative case. *J Neurosurg Case Lessons*. 2024;8(11):CASE2435.

doi: 10.3171/CASE2435

38. Seymour M, Robertson T, Papacostas J, *et al*. A woman with visual loss, amenorrhoea and polyuria: The first reported case of nodular lymphocyte-predominant Hodgkin lymphoma presenting with hypopituitarism. *Endocrinol Diabetes Metab Case Rep*. 2021;2021:20-0100.

doi: 10.1530/EDM-20-0100

39. Koiso T, Akutsu H, Takano S, *et al*. Malignant lymphoma in the parasellar region. *Case Rep Med*. 2014;2014:747280.

doi: 10.1155/2014/747280

40. Piciu A, Mester A, Piciu D. Pituitary metastases discovered by 18F-FDG PET/CT during other cancers monitoring: Are there any differences of SUVs between benign and malignant diseases? *Clin Nucl Med*. 2021;46(1):e44-e46.

doi: 10.1097/RLU.0000000000003313

41. Dejust S, Decoudier B, Higel B, Litre CF, Morland D. Gonadotropin-secreting pituitary macroadenoma complicated with hemorrhagic apoplexy in 18F-FDG PET/CT. *Clin Nucl Med*. 2021;46(9):748-749.

doi: 10.1097/RLU.0000000000003710

42. Kaida H, Matsukubo Y, Im SW, Kashiwagi N, Ishii K. High 18F-FDG uptake in a papillary craniopharyngioma of the third ventricle. *Clin Nucl Med*. 2023;48(3):245-247.

doi: 10.1097/RLU.0000000000004562

43. Cheng ML, Zhao J, Lin Y, Qiu HS. Pituicytoma: Four cases with unusual imaging features and a literature review. *Neuro Endocrinol Lett*. 2021;42(7):425-432.

44. Feng Z, He D, Mao Z, *et al*. Utility of 11C-methionine and 18F-FDG PET/CT in patients with functioning pituitary adenomas. *Clin Nucl Med*. 2016;41(3):e130-e134.

doi: 10.1097/RLU.0000000000001085

45. Beyhan E, Erol Fenercioğlu Ö, Karagöz Y, Ergül N, Çermik TF. Mild 68Ga PSMA-11 uptake in incidental pituitary adenoma. *Mol Imaging Radionucl Ther*. 2022;31(3):244-245.

doi: 10.4274/mirt.galenos.2021.97752

46. Maffione AM, Mandoliti G, Pasini F, Colletti PM, Rubello D. Pituitary non-functioning adenoma disclosed at 18F-choline PET/CT to investigate a prostate cancer relapse. *Clin Nucl Med*. 2016;41(10):e460-461.

doi: 10.1097/RLU.0000000000001328

47. Zhang W, Wu Y, Guo L, Li X, Shen G. [68Ga]GaFAPI PET/CT in the evaluation of Langerhans cell histiocytosis: Comparison with [18]FFDG PET/CT. *Eur J Nucl Med Mol Imaging*. 2025;52(6):2187-2197.

doi: 10.1007/s00259-025-07097-2

48. Cai Y, Liu M, Zhang Y, Du H, Huo L, Jing H. The superiority of [68Ga]Ga-FAPI PET/CT over MRI and [18]FFDG PET/CT in delineating a rare case of pituitary fibrosarcoma. *Eur J Nucl Med Mol Imaging*. 2025.

doi: 10.1007/s00259-025-07467-w

49. Pan Q, Luo Y, Cao X, Li J, Feng J. Bing-neel syndrome and coexisting pituitary macroadenoma in a patient with waldenström macroglobulinemia revealed by 18F-FDG and 68Ga-pentixafor PET/CT. *Diagnostics (Basel)*. 2023;13(7):1334.

doi: 10.3390/diagnostics13071334

50. Law WP, Fiumara F, Fong W, Macfarlane DJ. The 'double pituitary hot spot' sign of skull base meningioma on gallium-68-labelled somatostatin analogue PET. *J Med Imaging Radiat Oncol*. 2013;57(6):680-683.

doi: 10.1111/1754-9485.12069

51. Manafi-Farid R, Askari E, Shiri I, *et al*. [18]FFDG-PET/CT radiomics and artificial intelligence in lung cancer: Technical aspects and potential clinical applications. *Semin Nucl Med*. 2022;52(6):759-780.

doi: 10.1053/j.semnuclmed.2022.04.004

52. Yang Q, Ke T, Wu J, *et al*. Preoperative prediction of pituitary neuroendocrine tumor invasion using multiparametric MRI radiomics. *Front Oncol*. 2025;14:1475950.

doi: 10.3389/fonc.2024.1475950

53. Banihashemian SS, Bayat M, Pirayesh E, Divband G, Abolhosseini A, Akbari ME. First experience of radionuclide therapy with 177Lu-FAPI-2286 in a patient with metastatic mediastinal sarcoma. *Clin Nucl Med*. 2024;49(7):e334-e337.

doi: 10.1097/RLU.0000000000005255

54. Sadaghiani MS, Rowe SP, Sheikhbahaei S. Applications of artificial intelligence in oncologic 18F-FDG PET/CT imaging: A systematic review. *Ann Transl Med*. 2021;9(9):823.

doi: 10.21037/atm-20-6162

ACCSCIENCE PUBLISHING

Advances in Radiotherapy & Nuclear Medicine

REVIEW ARTICLE

Breast cancer radiotherapy and the risk of lung injury: Advances and perspectives

Shubhankar Suman*

Department of Oncology, Lombardi Comprehensive Cancer Center, Georgetown University Medical Center, Georgetown University, Washington, District of Columbia, United States of America

Abstract

Breast cancer is the most prevalent malignancy among women worldwide, and radiotherapy (RT) plays a central role in reducing local recurrence and improving survival. Technological advances such as three-dimensional conformal RT (3D-CRT), intensity-modulated RT (IMRT), volumetric-modulated arc therapy (VMAT), and particle therapies have enhanced dose conformity and reduced exposure to surrounding healthy tissues, particularly the lungs. Nevertheless, radiation-induced lung injury (RILI) remains a clinically relevant concern because of the close anatomical relationship between the breast and lung. RILI is a biphasic process, comprising early radiation pneumonitis and late radiation-induced pulmonary fibrosis, with severity influenced by dose distribution and treatment modality. While 3D-CRT carries a moderate risk due to limited beam modulation, IMRT and VMAT improve target coverage but may increase low-dose exposure to larger lung volumes, potentially increasing the risks of subclinical injury and, in the long term, secondary malignancy. Adjunctive lung-sparing strategies, including deep inspiration breath-hold and image-guided techniques, further reduce pulmonary dose. Proton beam therapy, particularly pencil beam scanning, offers additional lung protection through Bragg peak–based dose deposition, minimizing exit dose and irradiation of non-target tissues. Early clinical data suggest a lower incidence of RILI with PBT, although long-term outcomes remain under investigation. Carbon ion RT remains investigational in breast cancer. This review summarizes current evidence on RILI risk across modern RT modalities. A deeper understanding of modality-specific risks is essential for guiding personalized treatment planning and implementing effective lung-sparing strategies.

Keywords: Breast cancer radiotherapy; Radiation-induced lung injury; Radiation pneumonitis; Radiation-induced lung fibrosis; Tamoxifen; Senotherapeutics

***Corresponding author:**
Shubhankar Suman
(ss2286@georgetown.edu)

Citation: Suman S. Breast cancer radiotherapy and the risk of lung injury: Advances and perspectives. *Adv Radiother Nucl Med*. 2026;4(1):16-32.
doi: 10.36922/ARNM025340041

Received: August 18, 2025

Revised: November 26, 2025

Accepted: December 19, 2025

Published online: January 21, 2026

1. Introduction

Breast cancer is the most frequently diagnosed malignancy among women worldwide, with an estimated 2.3 million new cases and over 670,000 deaths in 2022, making it the leading cause of cancer-related morbidity and mortality in women globally.[1,2] In the United States, the American Cancer Society projects 316,950 new cases of invasive breast cancer and 42,170 related deaths in 2025, positioning it as the second leading cause of cancer mortality among women, after lung cancer.[3,4] Advances in screening,

diagnosis, and treatment have led to steady improvements in breast cancer survival rates across most countries, with 5-year relative survival exceeding 80% in many regions.[5,6] Approximately 60% of patients with breast cancer are estimated to receive adjuvant radiotherapy (RT) as part of multidisciplinary management for early-stage and locally advanced disease, most commonly following breast-conserving surgery and in selected post-mastectomy cases.[7-9] Despite substantial advances in RT techniques ranging from three-dimensional conformal RT (3D-CRT) to more conformal modalities such as intensity-modulated RT (IMRT), volumetric modulated arc therapy (VMAT), and particle-based (proton or carbon-ion) beam therapy, radiation-induced lung injury (RILI) remains a clinically significant, dose-limiting toxicity that can adversely impact quality of life, pulmonary function, and long-term survival.[10] Its occurrence is influenced by multiple factors, including the irradiated lung volume, mean lung dose (MLD), fractionation schedule, concurrent systemic therapies (e.g., taxanes, trastuzumab, and immunotherapy), pre-existing pulmonary disease, smoking history, and individual radiosensitivity.[10,11]

Pathophysiologically, RILI occurs through two interconnected phases: (i) acute phase, commonly termed radiation pneumonitis (RP), which typically manifests within weeks to a few months after RT. RP may present as asymptomatic radiographic changes or as a symptomatic inflammatory response characterized by cough, dyspnea, low-grade fever, and, in severe cases, hypoxemia. Although RP is often self-limiting or responsive to corticosteroid therapy, it can predispose patients to subsequent chronic injury. (ii) Chronic phase, referred to as radiation-induced pulmonary fibrosis (RIPF; also termed radiation-induced lung fibrosis [RILF]), represents an irreversible stage characterized by permanent remodeling of lung architecture.[11] The process is driven by the activation and proliferation of myofibroblasts, excessive extracellular matrix (ECM) deposition, and distortion of alveolar structures.[12,13] Persistent low-grade inflammation, aberrant wound-healing responses, and ongoing oxidative stress contribute to the progressive loss of lung compliance and function. Beyond functional impairment, RIPF creates a pro-oncogenic microenvironment marked by chronic inflammation, cytokine dysregulation (e.g., elevated transforming growth factor-beta [TGF-β], interleukin 6 [IL-6]), and persistent DNA damage.[14-19] This milieu has been implicated in second primary lung cancer development, particularly in long-term survivors. While the absolute risk of lung cancer after breast RT is relatively low, it appears to be dose-dependent and synergistically amplified by coexisting carcinogenic exposures such as tobacco smoking.[20-22] The risk is greater in patients who received higher doses to larger lung volumes, those treated at younger ages, and those surviving many years after therapy. Radiation-associated lung malignancies may arise as primary lung cancers induced by mutagenic radiation injury, or present as pulmonary metastases from breast cancer (or less commonly, metastases from another primary). Given the growing number of breast cancer survivors worldwide,[5,6] it is critical to minimize the incidence of RIPF and subsequent lung malignancy. This review provides a comprehensive synthesis of current evidence on the incidence, pathophysiology, and clinical implications of RILI in breast cancer survivors, with an emphasis on modality-specific risks and emerging technologies aimed at reducing pulmonary toxicity.

2. RT modalities in breast cancer treatment and management

RT remains an essential component of multidisciplinary breast cancer management, offering proven reductions in local recurrence and improvements in disease-specific and overall survival across early-stage, locally advanced, and post-mastectomy settings. Over the past three decades, technical innovations have transformed breast RT from two-dimensional approaches to highly conformal, image-guided modalities capable of sculpting dose around complex target volumes while limiting irradiation to surrounding normal tissues, including the lungs.[23,24] 3D-CRT, historically the standard of care, uses forward-planned tangential fields shaped to the breast or chest wall, with or without regional nodal irradiation (RNI). While this technique achieves acceptable target coverage in many cases, its limited beam modulation capacity can result in suboptimal conformity around irregular anatomy, leading to incidental exposure of adjacent lung parenchyma, particularly when internal mammary nodes are included.[25,26] To address these limitations, IMRT and its rotational variant, VMAT, have been widely adopted.[27,28] Both employ inverse planning to modulate beam intensity across multiple angles, enabling superior target conformity, improved dose homogeneity, and better coverage of complex structures such as the chest wall with RNI.[27,29,30] However, the improved conformity often comes at the cost of a larger "low-dose bath" to surrounding tissues, increasing the volume of ipsilateral and contralateral lung receiving low radiation doses, which may have implications for subclinical RILI and, in long-term survivors, secondary malignancy risk.[27,31,32] Consequently, the integration of lung-sparing adjuncts, including deep inspiration breath-hold (DIBH), surface-guided RT, and image-guided RT, has become routine in many centers, particularly for left-sided breast cancer, to minimize cardiopulmonary exposure.[33-35]

In addition to ongoing developments in IMRT/VMAT, the advent of particle therapy has introduced new opportunities for further sparing of lung tissue.[36] Pencil beam scanning (PBS) proton radiation therapy (PRT), an advanced form of proton beam delivery, uses magnetically steered, narrow proton "pencils" to deposit dose spot-by-spot and layer-by-layer, creating highly conformal plans with minimal exit dose beyond the target. This is especially advantageous in scenarios involving internal mammary node irradiation, bilateral disease, or challenging thoracic anatomy, where the mean heart dose and ipsilateral lung V20 (percentage of lung volume receiving ≥20 Gy) can be significantly reduced compared to IMRT/VMAT.[28,37,38] Clinical series and early-phase trials have reported favorable dosimetric profiles and promising reductions in estimated normal tissue complication probabilities for cardiopulmonary endpoints, though robust, long-term outcome data are still awaited.[28,39-41] Carbon ion RT (CIRT) represents another advancement in particle therapy, delivering high linear energy transfer radiation with enhanced relative biological effectiveness (RBE) and sharp distal dose fall-off achieved through a spread-out Bragg peak. While CIRT offers theoretical advantages for local control and normal tissue sparing, its role in breast cancer remains largely investigational, with clinical application restricted to a small number of specialized centers in Japan, Germany, and other selected regions.[42-44]

Irrespective of the beam type (photon vs. particle beam) used in RT, the total prescribed dose is conventionally measured in Grays (Gy), which quantifies the physical energy deposited per unit mass of tissue. However, different types of radiation vary not only in physical dose delivery but also in their biological effectiveness, i.e., their capacity to induce cellular damage that mediates both tumor control and normal tissue injury.[45] This includes stochastic effects such as radiation-induced carcinogenesis, which can occur even at low doses, making biological dose considerations particularly relevant when evaluating long-term pulmonary and secondary cancer risks.[20,23,26,31] To account for RT modality-dependent biological impact, the concept of RBE is used. RBE is defined as the ratio of the dose of a reference radiation (typically photons) to the dose of the test radiation that produces the same biological effect. For conventional photon-based techniques such as IMRT, the RBE is standardized at 1.[46,47] PRT, which delivers charged particles with higher linear energy transfer than photons and induces denser ionization and more complex DNA damage, has a clinically adopted RBE of approximately 1.1.[47] Accordingly, proton doses are expressed as Gy(RBE), calculated by multiplying the physical dose by RBE, allowing meaningful comparison with photon doses.[9] CIRT, which exhibits substantially higher linear energy transfer than protons, is associated with a correspondingly higher RBE, typically ranging from 2 to 3 depending on tissue type and biological endpoint.[28,43] This adjustment ensures that the biological impact of PRT and CIRT is accurately represented and compared to photon doses in IMRT/VMAT (Table 1).

Beyond external-beam advancements, several technique-specific approaches also contribute to reducing pulmonary exposure. Accelerated partial-breast irradiation (APBI), delivered through either external-beam modalities or brachytherapy (e.g., interstitial or balloon-based techniques), limits the high-dose region to the lumpectomy cavity with steep dose fall-off, markedly reducing incidental lung dose compared with whole-breast or RNI.[7] Although APBI is applicable only to selected early-stage patients, its dosimetric profile supports a substantially lower risk of RILI relative to conventional whole-breast irradiation. Collectively, these modality-specific differences in dose distribution, conformity, temporal delivery characteristics, and normal tissue sparing underpin variations in the risk and presentation of RILI among breast cancer patients. Understanding the physical principles and clinical trade-offs of each technique is therefore critical in tailoring RT to individual patients, balancing local control with the minimization of pulmonary toxicity.

3. Pathophysiological hallmarks of RILI

RILI encompasses a spectrum of pathological changes ranging from acute inflammation to chronic fibrosis, and in rare cases, may contribute to an increased risk of neoplastic transformation.[48,49] These pathological states are marked by distinct histopathological and molecular signatures, reflecting complex interactions between irradiated lung parenchyma, resident cells, and the immune system.[50]

Radiation pneumonitis represents the early inflammatory response of the lung parenchyma to exposure to ionizing radiation (IR), typically occurring within 1–6 months after treatment. In breast cancer, the reported incidence of clinically significant RP generally ranges from ~1% to 13%, although higher or lower values have been described depending on study design, diagnostic criteria, era of treatment, and dosimetric characteristics.[51,52] Histopathologically, RP is characterized by acute injury and apoptosis of type I pneumocytes, which are essential for efficient gas exchange. In response, type II pneumocytes, responsible for surfactant production and epithelial repair, undergo compensatory hyperplasia and may display cellular atypia. Microvascular injury plays a pivotal role in RP pathogenesis. Increased endothelial permeability leads to interstitial and intra-alveolar edema, with fluid accumulation in alveolar septa and airspaces.

Table 1. A comparison of irradiation parameters commonly used in IMRT, PRT, and CIRT

Parameters	IMRT	PRT	CIRT
Total dose	40–60 Gy	40–60 Gy (RBE)[a]	40–70 Gy (RBE)[b]
Fraction dose	2–3 Gy per fraction	1.8–2.5 Gy (RBE) per fraction	3.0–4.0 Gy (RBE) per fraction
Hypofractionation	Widely standardized with robust evidence (40–42.5 Gy in 15 fractions)	Protocols vary (26–40 Gy (RBE) in 5–15 fractions); increasing interest in ultra-hypofractionation	48–64 Gy (RBE) in 12–16 fractions; Ultra-hypofractionated protocols 45–50 Gy (RBE) in 4–8 fractions
Dose conformity	High	Very high	Very high
Lung dose	Lower than 3D-CRT, but increased V5	Minimal	Minimal
Incidence of RP (%)	<5	<1	<1
Radiation fibrosis	Less extensive	Minimal	Minimal
Long-term lung function	Mild changes possible	Under investigation	Under investigation

Notes: [a]In PRT, dose is reported in Gy (RBE) (Gray relative biological effectiveness [RBE]) to account for the increased biological potency of protons compared to photons (average RBE~1.1). [b]In CIRT, dose is reported in Gy (RBE) to account for the increased biological potency of carbon-ions compared to photons (average RBE 2–3).
Abbreviations: CIRT: Carbon ion radiotherapy; CRT: Conformal radiotherapy; IMRT: Intensity-modulated radiotherapy; PRT: Pencil beam scanning proton therapy; RP: Radiation pneumonitis.

This is accompanied by a prominent inflammatory infiltrate composed predominantly of mononuclear cells (lymphocytes, monocytes, and macrophages), with neutrophils in early stages, resulting in alveolitis.[53] Severe cases show hyaline membrane formation, composed of eosinophilic proteinaceous material along alveolar ducts and spaces, indicating extensive epithelial barrier disruption. Vascular congestion, perivascular inflammatory cuffs, and endothelial apoptosis are frequently observed. At the molecular level, RP is orchestrated by an inflammatory cytokine cascade involving tumor necrosis factor-alpha (TNF-α), IL-1β, IL-6, and chemokines such as C–C motif ligand 2 (CCL2) and C–X–C motif ligand 8 (CXCL8), which mediate leukocyte recruitment and activation.[54] Activation of nuclear factor-kappa B (NF-κB) and oxidative stress pathways further amplifies tissue injury.

Radiation-induced pulmonary fibrosis represents the late, often progressive phase of RILI, typically manifesting 6–24-month post-irradiation. Its incidence in breast cancer varies from 1% to 40% of patients, largely depending on the type of study (retrospective vs. prospective), diagnostic criteria, follow-up duration, and radiation technique.[10,55,56] RIPF is driven by an aberrant wound-healing response, in which normal parenchyma is replaced by dense ECM rich in type I and III collagen, fibronectin, and proteoglycans. Specifically, RIPF is driven largely by epithelial-mesenchymal transition (EMT) triggered by IR. At the molecular level, IR generates reactive oxygen species (ROS), which activate the ROS/extracellular signal-regulated kinase pathway and promote Snail-G9a complex formation, leading to epigenetic suppression of E-cadherin via H3K9 methylation.[57] Heat shock protein 27, forkhead box protein M1, and various microRNAs further regulate EMT: suppression of miR-541-5p, miR-486-3p, and miR-155-5p, along with the activation of sphingosine 1-phosphate receptor 3/TGF-β1 signaling, enhances Snail/Slug expression and fibrosis progression.[58] Excess ROS also activates the NACHT, LRR, and PYD domains-containing protein 3 (NLRP3) inflammasome, increasing IL-1β and driving fibroblast-to-myofibroblast differentiation. Finally, radiation-induced lactate secretion by fibroblasts acidifies the extracellular milieu, activating TGF-β and perpetuating fibrosis. Immune modulation and the persistent activation and proliferation of fibroblasts and their differentiation into myofibroblasts play a central role in contributing to ECM overproduction and tissue contraction during fibrosis progression,[59,60] where regulatory T cells and M2-polarized macrophages produce pro-fibrotic cytokines (e.g., IL-4 and IL-13) and TGF-β, amplifying EMT and ECM deposition.[61] Additionally, cellular senescence in macrophages and type II alveolar cells promotes RIPF through the senescence-associated secretory phenotype (SASP), which releases TNF-α, IL-1α, and IL-13, further stimulating M2 macrophages.[62,63] TGF-β1 signaling is considered the master regulator of radiation-induced fibrogenesis, sustaining myofibroblast activation and *ECM* gene transcription long after the initial injury.[64,65] Additional contributors include connective tissue growth factor, platelet-derived growth factor (PDGF), and endothelin-1.[58,66] Architecturally, fibrosis leads to the loss of lung volume, mediastinal shift toward the irradiated side, hemidiaphragm elevation, and displacement of hilar structures. Traction bronchiectasis arises from fibrotic retraction of lung parenchyma. Thickening of alveolar walls and obliteration of capillary

beds result in impaired gas exchange and chronic hypoxia, perpetuating the fibrotic cycle (Figure 1). Most cases of RIPF following breast RT are subclinical or mild, detected only on follow-up imaging as focal scarring and volume loss within the irradiated field; however, in severe cases, restrictive lung disease and hypoxemia can occur.

4. RILI following breast cancer RT

Breast RT inevitably delivers some degree of incidental dose to the ipsilateral lung; however, modern RT techniques consistently report a low incidence of symptomatic RP, typically in the range of 1–5%. Residual variability across studies largely reflects differences in diagnostic criteria, patient selection, and the transition from older, less conformal approaches to contemporary planning and delivery techniques.[10,67] Asymptomatic radiological changes are more frequently observed than clinically significant symptoms. Irradiation of regional lymphatic nodes, particularly the internal mammary and supraclavicular nodes, has been linked to greater lung dose exposure and, consequently, an elevated risk of RILI.[10,68,69] A meta-analysis of breast cancer patients treated with 3D-CRT reported low-grade RP in 22–62% of cases, with a median frequency of ~42%.[70] Although IMRT may increase the volume of lung receiving low-dose radiation (potentially contributing to subclinical RILI),[71,72] the incidence of clinically significant RP is lower than with older techniques.[73] Most RP events are Grades 0–1, presenting as asymptomatic or mild symptoms without functional impairment. Grade 2 RP, requiring corticosteroid intervention, is infrequent, and severe RP (Grades 3–4) is exceptionally rare in breast cancer patients treated with IMRT. For example, in a prospective study (2010–2013) using multibeam IMRT in 113 patients, the median lung V5 was 100% and V20 was 29%.[74] Respiratory toxicity occurred in only 10.6% of patients (11/104), with a single Grade 3 RP event (0.96%). No significant changes were seen in pulmonary function tests or pneumonitis scores post-treatment. However, the median follow-up (~4.5 years) may not capture late-onset RILI.

Meanwhile, PRT, particularly with PBS techniques, is an emerging modality for early-stage and locally advanced breast cancer. Dosimetric and early clinical studies indicate that PRT can reduce both early and late lung toxicities.[75,76] Comparative planning studies consistently demonstrate superior target coverage and reduced doses to organs-at-risk compared with photon-based IMRT or VMAT.[77,78] Evidence from other thoracic malignancies suggests potential benefits. For example, randomized trials in non-small cell lung cancer did not show significant reductions in Grade ≥3 RP or local failure with protons versus IMRT, but did demonstrate improved cardiac sparing.[79] The particle therapy cooperative group consensus statement notes that, despite strong dosimetric advantages, current evidence does not yet provide Level 1 or 2 data demonstrating superior clinical outcomes for PRT over IMRT in breast cancer, including statistically significant reductions in symptomatic RP.[80] The consensus recognizes PRT's potential for enhanced normal tissue sparing, mainly in high-risk, anatomically complex scenarios (e.g., left-

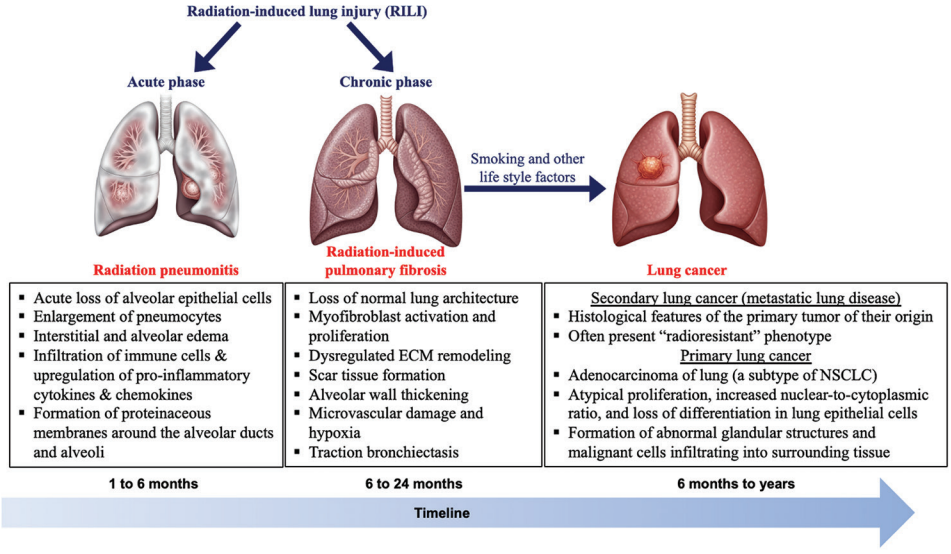

Figure 1. Illustration of pathological progression and associated histopathological hallmarks of radiation-induced lung injury and its potential progression to lung cancer. Initial lung image with pneumonitis, fibrosis, and lung cancers was created using Gemini (Google LLC) and subsequently edited, labeled, and annotated by the author using Adobe Illustrator and Microsoft PowerPoint.
Abbreviations: ECM: Extracellular matrix; NSCLC: Non-small cell lung cancer.

sided chest wall with nodal irradiation, bilateral disease, and re-irradiation). PRT is still evolving and moving toward robust, model-based, and trial-driven validation of PBT strategies, encouraging enrollment in trials, and harmonizing technical standards across centers to improve evidence quality. Ongoing randomized trials and extended follow-up are expected to clarify the long-term incidence of RILI and help identify breast cancer subgroups that may derive the greatest clinical benefit from PRT.[80]

5. Dosimetric predictors and clinical risk factors for RILI in breast cancer RT

Dosimetric parameters are pivotal in both predicting and mitigating the risk of RILI, particularly in modern breast cancer RT, where precision targeting and sparing of organs-at-risk are paramount. The most validated predictors of pulmonary toxicity are the MLD and the volume of lung receiving a given threshold dose (Vx Gy), with V20 being the most clinically relevant. An MLD <15 Gy and V20 < 30% are consistently associated with a lower likelihood of RILI, whereas V20 > 30% significantly increases the risk of clinically relevant pneumonitis and late fibrosis.[81,82] MLD values exceeding 20 Gy have been correlated with an approximately 20% incidence of symptomatic pneumonitis.[81] Notably, V5 > 50% increases the "low-dose bath" to the lungs after photon RT and has been linked to higher rates of radiographic lung changes and potential subclinical injury.[81,83] Conversely, DIBH, particularly in left-sided breast cancer, substantially reduces both lung and cardiac doses, thereby lowering RILI risk.[34,84] PRT, leveraging the Bragg peak to eliminate exit dose, has been shown to achieve the lowest integral lung dose among all modalities.[85] A meta-analysis by Gokula *et al.*[70] supports maintaining V20 < 30% to minimize pulmonary complications. Similarly, limiting MLD to <15 Gy is associated with a reduced risk of both RP and RIPF.[11,86]

Several clinical and treatment-related factors can exacerbate RILI risk. Hypofractionation (larger fraction sizes over fewer sessions) may increase toxicity compared with conventional fractionation.[11,87] RNI, especially when targeting the internal mammary or supraclavicular nodes, substantially elevates ipsilateral lung V20 and MLD, thus heightening RILI risk.[32,88] Patient-specific factors also play a crucial role. These include pre-existing pulmonary disease (e.g., chronic obstructive pulmonary disease and interstitial lung disease), advanced age (particularly >50 years), smoking history, higher tumor and nodal stage, and concurrent or recent chemotherapy.[89] Sequential chemoradiation after breast-conserving surgery usually results in only mild, transient pneumonitis (Grade ≤2). However, tamoxifen combined with the luteinizing hormone-releasing hormone (LHRH) analog goserelin has been associated with a notably increased risk of pneumonitis in breast cancer patients receiving chemoradiation.[90] Additional contributors, such as thoracic cage anatomical abnormalities, may predispose patients to higher lung doses during treatment (Table 2). Taken together, RILI risk is determined by an interplay between dosimetric thresholds, treatment technique, and individual patient factors. Optimal lung-sparing strategies require an integrated approach that accounts for both quantitative dose metrics and qualitative clinical considerations.

6. Subclinical RILI and cancer risk following breast cancer RT

Breast cancer RT can create a pro-inflammatory microenvironment in the lung, which theoretically could influence the initiation or promotion of secondary lung malignancies in breast cancer survivors. It is important to distinguish between second primary lung cancers (arising from native lung epithelial cells) and pulmonary metastases from breast cancer or other primaries. Pulmonary metastases retain the histologic and immunophenotypic features of the primary breast tumor; they are distinct from second primary lung cancers arising from native lung epithelium. The risk of second primary lung cancer after breast RT is generally low. However, it increases with time since treatment, higher irradiated lung volumes, and smoking history. A large Swedish population-based cohort study reported that at 20 years, the cumulative incidence of lung cancer was 3.0% in women treated with RT compared with 2.3% in those who did not receive RT, with excess risk

Table 2. Risk factors for RILI development after breast cancer radiotherapy

Parameters	Associated risk
V5 (percentage of lung volume receiving >5 Gy) ≤65%	Increased chronic lung injury
V20 (percentage of lung volume receiving >20 Gy) >35%	~7% risk of RILI
Mean lung dose >20 Gy	~20% risk of RILI
Age >50 years	Reduced pulmonary reserve, increased RILI risk
Smoking	Increased RILI risk
Pre-existing conditions (COPD or interstitial lung disease)	Predispose patients to RILI
Concurrent therapies (tamoxifen or chemotherapy)	May influence RILI progression
Anatomical deformities	An uneven radiation field increases lung exposure

Abbreviations: COPD: Chronic obstructive pulmonary disease; RILI: Radiation-induced lung injury.

becoming apparent after 5 years and increasing with longer follow-up.[49] Multiple studies have demonstrated a strong synergistic effect between RT and smoking, with absolute risks several-fold higher in smokers compared to never-smokers.[91-93] Subclinical RILI, detectable only on imaging or histopathology, may contribute to long-term carcinogenic risk by inducing persistent inflammation, oxidative stress, and genomic instability in lung tissue.[67,89] Radiation can cause DNA double-strand breaks, chromosomal rearrangements, and mutations in oncogenes (e.g., *EGFR* and *KRAS*) and tumor suppressors (e.g., *TP53*), all of which can promote malignant transformation.[89,94,95] Absolute long-term risks of modern breast cancer RT in the context of lung cancer incidence were approximately 4% for long-term continuing smokers versus 0.3% for nonsmokers.[89] IMRT and VMAT often increase the "low-dose bath" to the lung, which in modeling studies has been associated with higher excess absolute risk of lung malignancies compared with 3D-CRT.[96] However, large registry analyses have not consistently shown higher second cancer diagnoses with IMRT versus 3D-CRT over median follow-ups of 5–10 years.[97] PRT, particularly PBS, offers distinct dosimetric advantages by eliminating exit dose and reducing integral lung exposure. Cartechini *et al.*[98] demonstrated that PBS plans for breast cancer with RNI significantly reduced MLD and estimated absolute risk for secondary lung cancer compared with both VMAT and 3D-CRT. Paganetti *et al.*[99] modeled lifetime attributable risk using patient-specific plans and found that contralateral lung and breast second cancer risks could be markedly reduced with PBS compared to photon-based RT. These benefits are particularly relevant for younger patients with a long life expectancy, in whom even small absolute reductions in risk translate to greater long-term benefit. Overall, while the absolute incidence of second primary lung cancer after breast RT remains low, risk mitigation through lung dose reduction, smoking cessation, and the use of advanced modalities such as DIBH and PRT remains an important component of survivorship care.

7. Tamoxifen and RILI risk in breast cancer RT survivors

Tamoxifen, a selective estrogen receptor modulator, remains a key component of adjuvant endocrine therapy for hormone receptor-positive breast cancer, significantly lowering recurrence and mortality.[100,101] However, its concurrent use with RT has been associated with a heightened risk of RILI, particularly pulmonary fibrosis.[102-104] Clinical and translational studies suggest that tamoxifen may exacerbate fibrotic changes through the upregulation of TGF-β, a cytokine pivotal in promoting ECM deposition and fibrogenesis.[102,105,106] Several prospective and retrospective analyses have reported higher rates of clinically significant lung fibrosis when tamoxifen was administered during RT compared to RT alone.[10,107,108] While the timing of tamoxifen administration (sequential vs. concurrent) has been investigated, most evidence indicates that its impact is mediated via tissue remodeling pathways rather than acute injury, and temporal separation may not fully mitigate risk.

Nonetheless, several pragmatic clinical strategies have been proposed to reduce potential tamoxifen-associated pulmonary toxicity in patients undergoing RT, particularly those with elevated baseline lung dose metrics or pre-existing pulmonary compromise. These include (i) deferring tamoxifen until the completion of RT, while initiating temporary ovarian suppression (e.g., LHRH agonist) in premenopausal women to maintain systemic endocrine blockade during RT; (ii) starting adjuvant endocrine therapy with ovarian suppression ± an aromatase inhibitor during RT, followed by introducing tamoxifen after RT if clinically indicated; (iii) limiting the duration of tamoxifen (e.g., to the initial 2 years) before transitioning to an aromatase inhibitor in appropriate candidates; and (iv) using aromatase inhibitor upfront in postmenopausal women when appropriate, thereby avoiding potential tamoxifen-related enhancement of fibrotic pathways during RT.

These individualized approaches may be particularly relevant for patients at higher risk of RILI due to factors such as large RT volumes, RNI, and compromised baseline lung function. Breast cancer survivors treated with adjuvant RT have a modest but measurable long-term risk of developing a second primary lung cancer, particularly in the ipsilateral lung.[109] Importantly, population-based analyses have not demonstrated a significant increase in second primary lung cancer incidence attributable to tamoxifen. In fact, some reports suggest that patients who develop second primary lung cancer after receiving anti-estrogen therapy (predominantly tamoxifen) may experience improved lung cancer-specific survival, possibly reflecting systemic antitumor effects.[110] Overall, current evidence does not support tamoxifen as an independent risk factor for second primary lung cancer. However, its interaction with RT-related pulmonary effects remains an area of ongoing investigation.

Beyond endocrine therapy, the expanding use of targeted and immune-based systemic agents in breast cancer raises new considerations regarding their potential interaction with RT and the risk of RILI. Anti-human epidermal growth factor receptor 2 therapies such as trastuzumab are generally safe in combination with breast RT.[111] Immune checkpoint inhibitors, increasingly incorporated into

early-stage and metastatic triple-negative breast cancer, introduce an additional layer of complexity given their capacity to induce immune-mediated pneumonitis, which may overlap temporally and mechanistically with RILI.[112] As systemic therapy options continue to broaden, understanding and anticipating how these agents interact with thoracic irradiation will be increasingly important to personalize treatment sequencing, reduce pulmonary toxicity, and maintain optimal oncologic outcomes.

8. RILI assessment and emerging therapeutics

Early and accurate assessment of RILI remains a clinical challenge, as its manifestations often overlap with treatment-related pneumonitis, infectious etiologies, and cancer-related pulmonary complications. Diagnostic evaluation relies on a combination of morphologic, functional, and increasingly computational approaches.[113,114] Pulmonary function tests may demonstrate early restrictive changes, including reductions in lung volumes and diffusing capacity, which frequently precede overt radiographic findings.[114] While conventional chest radiographs may reveal volume loss or linear scarring within irradiated fields, high-resolution computed tomography (CT) (HRCT) is the gold standard for characterizing RILI across its inflammatory and fibrotic phases. Typical features include ground-glass opacities, patchy consolidation with air bronchograms, volume loss, traction bronchiectasis, and architectural distortion conforming to radiation dose distributions. Positron emission tomography-CT can support differential diagnosis by distinguishing metabolically quiescent radiation fibrosis from fluorodeoxyglucose-avid recurrent or second primary malignancy. Increasingly, imaging acquired during RT, particularly cone-beam CT (CBCT) used for image guidance, offers an opportunity to monitor early subclinical density changes that may signal evolving injury.

Beyond conventional imaging, advanced functional and computational tools are enhancing early detection and risk stratification. Functional imaging modalities, such as single photon emission CT/CT perfusion, dual-energy CT, and hyperpolarized gas magnetic resonance imaging, allow regional mapping of ventilation and perfusion, enabling the identification of high-value lung subunits that may be preferentially spared during treatment.[113,114] Parallel advances in radiomics and artificial intelligence (AI) now permit the extraction of high-dimensional quantitative features from baseline staging CT, serial HRCT, or even daily CBCT datasets. These radiomic and machine-learning models capture subtle texture, heterogeneity, and voxel-wise dose-response patterns that are not discernible to the human eye and have shown promise in predicting both acute pneumonitis and late fibrosis earlier and with greater accuracy than traditional dose–volume metrics. The integration of longitudinal "delta-radiomics," dose-coupled feature analysis, and functional-avoidance planning provides a foundation for future adaptive strategies in which treatment plans may be dynamically modified based on early imaging signatures of lung sensitivity.[115,116] Collectively, the convergence of morphologic imaging, functional assessment, and AI-driven predictive analytics is reshaping the clinical approach to RILI. As breast cancer treatment increasingly incorporates systemic agents with intrinsic lung disease risk and more advanced RT modalities, a refined and multimodal assessment framework will be essential for optimizing patient selection, tailoring dose distributions, and ultimately reducing the long-term pulmonary burden among breast cancer survivors.

Mild RP (Grades 1 and 2) is often managed conservatively with observation, cough suppressants, and bronchodilators. Systemic corticosteroids remain the mainstay for moderate to severe RP (Grade ≥2), with prednisone initiated at 0.5–1.0 mg/kg/day for 2–4 weeks, followed by a gradual taper over 6–12 weeks according to symptomatic and radiographic response. Inhaled corticosteroids, such as budesonide or fluticasone, may serve as adjunctive therapy, particularly for steroid-sensitive phenotypes or during tapering. In steroid-refractory cases, immunosuppressants, including mycophenolate mofetil, azathioprine, and cyclophosphamide, have been employed, though clinical trial data are limited. Optimal outcomes require multimodal strategies accounting for patient-specific factors, lung radiosensitivity, tissue turnover, and dosimetric parameters.[11,12,15]

Radiation-induced lung fibrosis is characterized by progressive respiratory impairment. Supportive measures, including long-term oxygen therapy, pulmonary rehabilitation, and bronchodilators, are critical for maintaining exercise tolerance and quality of life. Repurposing anti-fibrotic agents approved for idiopathic pulmonary fibrosis is under investigation. Pirfenidone, a TGF-β and TNF-α antagonist, and nintedanib, a tyrosine kinase inhibitor targeting vascular endothelial growth factor receptor, PDGF receptor, and fibroblast growth factor receptor pathways, have demonstrated anti-fibrotic efficacy in preclinical RILF models.[117] Radiation-modifying strategies can be classified as radioprotectors, mitigators, or therapeutic agents, each targeting distinct phases of tissue injury. Radioprotectors are administered pre-irradiation, mitigators during or immediately after exposure, and therapeutic agents post-toxicity to slow or reverse damage.[118] Amifostine, a thiol-based radioprotector, is clinically approved and has been associated with reduced

RP incidence in thoracic RT with a favorable safety profile.[119] Other agents, including porphyrins (AEOL 10113), cerium oxide nanoparticles, and BIO300 (genistein formulation), similarly attenuate oxidative stress, pro-fibrotic signaling, and vascular damage in animal models.[120-122] Pentoxifylline, a xanthine derivative, mitigates lung toxicity by enhancing microcirculation, reducing TNF-α, and decreasing vascular resistance by regulating cellular senescence.[123]

Additional evidence has also implicated cellular senescence in the pathogenesis of both RILI and secondary lung carcinogenesis.[124] Senescent cells, which accumulate after IR, secrete a SASP comprising pro-inflammatory, pro-fibrotic, and pro-tumorigenic factors such as TGF-β, IL-6, IL-1β, and matrix metalloproteinases. Persistent SASP signaling promotes chronic inflammation, fibrosis, and genomic instability,[125-129] creating a microenvironment conducive to cancer development.[130,131] Senotherapeutics, targeting these cells, offer a novel strategy to mitigate RILI and long-term malignancy risk.[132] Senotherapeutics fall into two categories: senolytics, which selectively induce apoptosis in senescent cells by targeting survival pathways, and senomorphics, which suppress SASP without eliminating the cells.[128,129,133] Preclinical models of thoracic irradiation have demonstrated that senolytic cocktails, such as dasatinib plus quercetin, reduce fibrosis and inflammation, preserve lung architecture, and improve survival. Senomorphic agents such as rapamycin, a mammalian target of rapamycin inhibitor, delay fibrosis progression.[128,129,133,134]

From a clinical perspective, these approaches could be therapeutically integrated to intervene in patients exhibiting early radiographic or functional signs of lung injury. Critical considerations for translation include optimal timing relative to RT, dose scheduling, potential interactions with systemic therapies (e.g., endocrine agents and targeted therapies), and long-term safety in a population already exposed to adjuvant or RNI. Early-phase clinical trials leveraging biomarkers of senescence (such as circulating SASP factors and imaging surrogates) could provide patient stratification tools, enabling precision mitigation of RILI. Overall, senotherapeutics represent a promising frontier for reducing both acute and chronic pulmonary toxicity after breast cancer RT, with the potential to improve long-term lung health and survivorship outcomes pending rigorous clinical validation.

9. Conclusion

RILI remains a pivotal consideration in the radiotherapeutic management of breast cancer, despite advances in treatment precision. A comprehensive understanding of RILI's biphasic trajectory from RP to RILF is essential for optimizing individualized treatment planning and mitigating toxicity. Beyond acute manifestations, long-term pulmonary consequences include persistent fibrosis, reduced pulmonary function, and an elevated risk of second primary lung cancer. These consequences are modulated by multiple factors, including latency periods, baseline lung function, prior smoking history, age at exposure, and interactions with systemic therapies such as tamoxifen. While evidence regarding tamoxifen's effect on second primary lung cancer remains inconclusive,[135] its concurrent use with RT has been associated with enhanced fibrotic potential via TGF-β–mediated pathways.[102,105,106] Given the potential for delayed complications, structured long-term follow-up is imperative. Subclinical RILI may be overlooked, which could lead clinicians to underestimate long-term secondary malignancy risk. Clinicians should maintain vigilance for new pulmonary symptoms and employ individualized screening strategies, guided by patient-specific risk factors. Surveillance protocols should integrate imaging modalities, ranging from chest radiography to HRCT scans for early detection, coupled with regular pulmonary function assessments. Risk stratification should consider both dosimetric parameters and clinical variables, including age, baseline lung function, smoking history, and concurrent systemic therapies. Emerging approaches, such as AI and predictive modeling, hold promise for refining risk assessment and identifying patients at a higher risk of RILI and secondary malignancies.[136-138] Technological advances in RT, including VMAT, have significantly improved dose conformity and reduced high-dose exposure to normal lung tissue. PRT and CIRT offer further potential for sparing healthy tissue and mitigating pulmonary toxicity, with early data suggesting favorable toxicity profiles. Investigational approaches, such as FLASH RT delivering ultra-high dose rates (≥40 Gy/s), are particularly compelling due to preclinical evidence of normal tissue sparing while maintaining tumoricidal efficacy.[139-141] The integration of these novel modalities with systemic therapies, including endocrine agents, immunotherapies, and targeted treatments, represents a critical frontier for future research.

Prospective, multi-institutional studies are urgently needed to clarify the long-term pulmonary outcomes associated with PRT, CIRT, and FLASH RT. In parallel, translational research into biomarkers of RILI, including circulating TGF-β, cytokine signatures, and senescence-associated markers, could enable early detection and preemptive intervention. Emerging therapeutics targeting fibrosis, oxidative stress, and cellular senescence—including senolytics and senomorphics—offer opportunities to mitigate RILF and reduce secondary malignancy risk.

Integration of these interventions with precision RT may redefine the therapeutic index, optimizing tumor control while preserving long-term pulmonary health. In conclusion, continued innovation in breast cancer RT must be paired with rigorous long-term monitoring and patient-centered care strategies. The central challenge is to achieve sustained oncologic control while minimizing pulmonary injury, thereby improving survival, functional outcomes, and quality of life for the growing population of breast cancer survivors. Future research must emphasize not only technological refinement but also mechanistic understanding, biomarker-guided risk stratification, and combinatorial therapeutic strategies to fully realize this goal.

Acknowledgments

None.

Funding

The author received funding from the National Institute of Allergy and Infectious Diseases (NIAID), NIH (Grant No. R21AI193883), and the U.S. Department of Defense, United States Army Medical Research Acquisition Activity (Grant No. HT9425-24-1-0450).

Conflict of interest

Shubhankar Suman is an Editorial Board Member of this journal but was not in any way involved in the editorial and peer-review process conducted for this paper, directly or indirectly. The author has no competing interests to declare.

Author contributions

This is a single-authored article.

Ethics approval and consent to participate

Not applicable.

Consent for publication

Not applicable.

Availability of data

Not applicable.

References

1. Guglielmi G. Breast cancer is on the rise: Data reveal drastic gap in survival rates. *Nature*. 2025;639(8053):16.

   doi: 10.1038/d41586-025-00265-2

2. Kim J, Harper A, McCormack V, *et al*. Global patterns and trends in breast cancer incidence and mortality across 185 countries. *Nat Med*. 2025;31(4):1154-1162.

   doi: 10.1038/s41591-025-03502-3

3. Siegel RL, Kratzer TB, Giaquinto AN, Sung H, Jemal A. Cancer statistics, 2025. *CA Cancer J Clin*. 2025;75(1):10-45.

   doi: 10.3322/caac.21871

4. Bennett LL. Effects of pharmacological dose of vitamin C on MDA-MB-231 cells. *Biomedicines*. 2025;13(3):640.

   doi: 10.3390/biomedicines13030640

5. Tang DD, Ye ZJ, Liu WW, *et al*. Survival feature and trend of female breast cancer: A comprehensive review of survival analysis from cancer registration data. *Breast*. 2025;79:103862.

   doi: 10.1016/j.breast.2024.103862

6. Peeters NJMCV, Meer DJVD, Kok M, *et al*. Five-year conditional relative survival up to 10 years post-diagnosis among adolescent and young adult breast cancer patients by age, stage, and receptor subtype. *J Natl Cancer Cent*. 2025;5(3):297-305.

   doi: 10.1016/j.jncc.2025.01.005

7. Kolářová I, Melichar B, Sirák I, *et al*. The role of adjuvant radiotherapy in the treatment of breast cancer. *Curr Oncol*. 2024;31(3):1207-1220.

   doi: 10.3390/curroncol31030090

8. Polgár C, Kahán Z, Ivanov O, *et al*. Radiotherapy of breast cancer-professional guideline 1st central-eastern european professional consensus statement on breast cancer. *Pathol Oncol Res*. 2022;28:1610378.

   doi: 10.3389/pore.2022.1610378

9. Qiao K, Wei Y, Tao C, Zhu J, Yuan S. Proton therapy for breast cancer: Reducing toxicity. *Thorac Cancer*. 2024;15(30):2156-2165.

   doi: 10.1111/1759-7714.15451

10. Gueiderikh A, Sarrade T, Kirova Y, *et al*. Radiation-induced lung injury after breast cancer treatment: Incidence in the CANTO-RT cohort and associated clinical and dosimetric risk factors. *Front Oncol*. 2023;13:1199043.

    doi: 10.3389/fonc.2023.1199043

11. Giuranno L, Ient J, De Ruysscher D, Vooijs MA. Radiation-induced lung injury (RILI). *Front Oncol*. 2019;9:877.

    doi: 10.3389/fonc.2019.00877

12. Jin H, Yoo Y, Kim Y, Kim Y, Cho J, Lee YS. Radiation-induced lung fibrosis: Preclinical animal models and therapeutic strategies. *Cancers (Basel)*. 2020;12(6):1561.

    doi: 10.3390/cancers12061561

13. Kong FM, Hayman JA, Griffith KA, *et al*. Final toxicity results of a radiation-dose escalation study in patients with non-small-cell lung cancer (NSCLC): Predictors for

radiation pneumonitis and fibrosis. *Int J Radiat Oncol Biol Phys*. 2006;65(4):1075-1086.

doi: 10.1016/j.ijrobp.2006.01.051

14. Chen K, Liu C, Li X, *et al*. Risk and prognosis of secondary lung cancer after radiation therapy for thoracic malignancies. *Clin Respir J*. 2024;18(5):e13760.

doi: 10.1111/crj.13760

15. Jarzebska N, Karetnikova ES, Markov AG, Kasper M, Rodionov RN, Spieth PM. Scarred lung. An update on radiation-induced pulmonary fibrosis. *Front Med (Lausanne)*. 2020;7:585756.

doi: 10.3389/fmed.2020.585756

16. Ang L, Ghosh P, Seow WJ. Association between previous lung diseases and lung cancer risk: A systematic review and meta-analysis. *Carcinogenesis*. 2021;42(12):1461-1474.

doi: 10.1093/carcin/bgab082

17. Schonfeld SJ, Curtis RE, Anderson WF, González ABD. The risk of a second primary lung cancer after a first invasive breast cancer according to estrogen receptor status. *Cancer Causes Control*. 2012;23(10):1721-1728.

doi: 10.1007/s10552-012-0054-3

18. Asaithamby A, Shay JW, Minna JD. Cellular senescence and lung cancer prognosis. *Transl Lung Cancer Res*. 2022;11(10):1982-1987.

doi: 10.21037/tlcr-22-678

19. Zhou L, Ruscetti M. Senescent macrophages: A new "old" player in lung cancer development. *Cancer Cell*. 2023;41(7):1201-1203.

doi: 10.1016/j.ccell.2023.05.008

20. Egawa H, Furukawa K, Preston D, *et al*. Radiation and smoking effects on lung cancer incidence by histological types among atomic bomb survivors. *Radiat Res*. 2012;178(3):191-201.

doi: 10.1667/rr2819.1

21. Vogelius IR, Bentzen SM. A literature-based meta-analysis of clinical risk factors for development of radiation induced pneumonitis. *Acta Oncol*. 2012;51(8):975-983.

doi: 10.3109/0284186X.2012.718093

22. Dracham CB, Shankar A, Madan R. Radiation induced secondary malignancies: A review article. *Radiat Oncol J*. 2018;36(2):85-94.

doi: 10.3857/roj.2018.00290

23. Corn BW, Galper S, David MB. The coming of age of breast radiotherapy. *Curr Oncol*. 2023;30(5):5179-5181.

doi: 10.3390/curroncol30050392

24. González-Sanchis A, Brualla-González L, Fuster-Diana C, *et al*. Surface-guided radiation therapy for breast cancer: More precise positioning. *Clin Transl Oncol*. 2021;23(10):2120-2126.

doi: 10.1007/s12094-021-02617-6

25. Adeneye S, Akpochafor M, Adegboyega B, *et al*. Evaluation of three-dimensional conformal radiotherapy and intensity modulated radiotherapy techniques for left breast post-mastectomy patients: Our experience in Nigerian sovereign investment authority-lagos university teaching hospital cancer center, South-West Nigeria. *Eur J Breast Health*. 2021;17(3):247-252.

doi: 10.4274/ejbh.galenos.2021.6357

26. Racka I, Majewska K, Winiecki J. Three-dimensional conformal radiotherapy (3D-CRT) vs. volumetric modulated arc therapy (VMAT) in deep inspiration breath-hold (DIBH) technique in left-sided breast cancer patients-comparative analysis of dose distribution and estimation of projected secondary cancer risk. *Strahlenther Onkol*. 2023;199(1):90-101.

doi: 10.1007/s00066-022-01979-2

27. Chang JS, Chang JH, Kim N, Kim YB, Shin KH, Kim K. Intensity modulated radiotherapy and volumetric modulated arc therapy in the treatment of breast cancer: An updated review. *J Breast Cancer*. 2022;25(5):349-365.

doi: 10.4048/jbc.2022.25.e37

28. Ruan H, Okamoto M, Ohno T, Li Y, Zhou Y. Particle radiotherapy for breast cancer. *Front Oncol*. 2023;13:1107703.

doi: 10.3389/fonc.2023.1107703

29. Kendall R, Robinson T, Reed V, *et al*. Why is volumetric modulated arc therapy not considered the standard of care for locoregional radiation therapy for breast cancer patients? *Adv Radiat Oncol*. 2025;10(5):101728.

doi: 10.1016/j.adro.2025.101728

30. Wang R, Shen J, Yan H, *et al*. Dosimetric comparison between intensity-modulated radiotherapy and volumetric-modulated arc therapy in patients of left-sided breast cancer treated with modified radical mastectomy: CONSORT. *Medicine (Baltimore)*. 2022;101(2):e28427.

doi: 10.1097/MD.0000000000028427

31. Li F, Liu H, Wu H, Liang S, Xu Y. Risk factors for radiation pneumonitis in lung cancer patients with subclinical interstitial lung disease after thoracic radiation therapy. *Radiat Oncol*. 2021;16(1):70.

doi: 10.1186/s13014-021-01798-2

32. Park SH, Lim JK, Kang MK, *et al*. Predictive factors for severe radiation-induced lung injury in patients with lung cancer and coexisting interstitial lung disease. *Radiother Oncol*. 2024;192:110053.

doi: 10.1016/j.radonc.2023.110053

33. Testolin A, Ciccarelli S, Vidano G, Avitabile R, Dusi F, Alongi F. Deep inspiration breath-hold intensity modulated

radiation therapy in a large clinical series of 239 left-sided breast cancer patients: A dosimetric analysis of organs at risk doses and clinical feasibility from a single center experience. *Br J Radiol*. 2019;92(1101):20190150.

doi: 10.1259/bjr.20190150

34. Bergom C, Currey A, Desai N, Tai A, Strauss JB. Deep inspiration breath hold: Techniques and advantages for cardiac sparing during breast cancer irradiation. *Front Oncol.* 2018;8:87.

doi: 10.3389/fonc.2018.00087

35. Aznar MC, Carrasco de Fez P, Corradini S, *et al*. ESTRO-ACROP guideline: Recommendations on implementation of breath-hold techniques in radiotherapy. *Radiother Oncol*. 2023;185:109734.

doi: 10.1016/j.radonc.2023.109734

36. Kang Y, Bues M, Halyard MY, *et al*. Dose delivery reproducibility for PBS proton treatment of breast cancer patients with and without mask immobilization. *Radiat Oncol*. 2023;18(1):157.

doi: 10.1186/s13014-023-02323-3

37. Durante M, Debus J, Loeffler JS. Physics and biomedical challenges of cancer therapy with accelerated heavy ions. *Nat Rev Phys.* 2021;3(12):777-790.

doi: 10.1038/s42254-021-00368-5

38. Jette D, Chen W. Creating a spread-out Bragg peak in proton beams. *Phys Med Biol.* 2011;56(11):N131-N138.

doi: 10.1088/0031-9155/56/11/N01

39. Luo W, Ali YF, Liu C, *et al*. Particle therapy for breast cancer: Benefits and challenges. *Front Oncol*. 2021;11:662826.

doi: 10.3389/fonc.2021.662826

40. Bradley JA, Dagan R, Ho MW, *et al*. Initial report of a prospective dosimetric and clinical feasibility trial demonstrates the potential of protons to increase the therapeutic ratio in breast cancer compared with photons. *Int J Radiat Oncol Biol Phys.* 2016;95(1):411-421.

doi: 10.1016/j.ijrobp.2015.09.018

41. Smith NL, Jethwa KR, Viehman JK, *et al*. Post-mastectomy intensity modulated proton therapy after immediate breast reconstruction: Initial report of reconstruction outcomes and predictors of complications. *Radiother Oncol*. 2019;140:76-83.

doi: 10.1016/j.radonc.2019.05.022

42. Malouff TD, Mahajan A, Krishnan S, Beltran C, Seneviratne DS, Trifiletti DM. Carbon ion therapy: A modern review of an emerging technology. *Front Oncol*. 2020;10:82.

doi: 10.3389/fonc.2020.00082

43. Yu B, Li KW, Fan Y, Pei X. Value of carbon-ion radiation therapy for breast cancer. *Int J Part Ther.* 2024;14:100629.

doi: 10.1016/j.ijpt.2024.100629

44. Karasawa K, Omatsu T, Shiba S, Irie D, Wakatsuki M, Fukuda S. A clinical study of curative partial breast irradiation for stage I breast cancer using carbon ion radiotherapy. *Radiat Oncol*. 2020;15(1):265.

doi: 10.1186/s13014-020-01713-1

45. Dale RG, Jones B. The assessment of RBE effects using the concept of biologically effective dose. *Int J Radiat Oncol Biol Phys.* 1999;43(3):639-645.

doi: 10.1016/s0360-3016(98)00364-2

46. Jones B. Proton radiobiology and its clinical implications. *Ecancermedicalscience*. 2017;11:777.

doi: 10.3332/ecancer.2017.777

47. Wedenberg M, Lind BK, Hårdemark B. A model for the relative biological effectiveness of protons: The tissue specific parameter α/β of photons is a predictor for the sensitivity to LET changes. *Acta Oncol.* 2013;52(3):580-588.

doi: 10.3109/0284186X.2012.705892

48. Beach TA, Finkelstein JN, Chang PY. Epithelial responses in radiation-induced lung injury (RILI) allow chronic inflammation and fibrogenesis. *Radiat Res.* 2023;199(5):439-451.

doi: 10.1667/rade-22-00130.1

49. Wennstig AK, Wadsten C, Garmo H, *et al*. Risk of primary lung cancer after adjuvant radiotherapy in breast cancer-a large population-based study. *NPJ Breast Cancer.* 2021;7(1):71.

doi: 10.1038/s41523-021-00280-2

50. Wang Y, Zhang J, Shao C. Cytological changes in radiation-induced lung injury. *Life Sci.* 2024;358:123188.

doi: 10.1016/j.lfs.2024.123188

51. Kawakami W, Takamatsu S, Taka M, *et al*. Factors associated with radiation pneumonitis in patients receiving electron boost radiation for breast-conserving therapy: A retrospective review. *Adv Radiat Oncol.* 2020;5(6):1141-1146.

doi: 10.1016/j.adro.2020.08.009

52. Lee JW, Chung MJ. Safety of hypofractionated volumetric modulated arc therapy for early breast cancer: A preliminary report. *Oncol Lett.* 2023;26(2):330.

doi: 10.3892/ol.2023.13916

53. Rahi MS, Parekh J, Pednekar P, *et al*. Radiation-induced lung injury-current perspectives and management. *Clin Pract*. 2021;11(3):410-429.

doi: 10.3390/clinpract11030056

54. Kasmann L, Deitrich A, Staab-Weijnitz C, *et al*. Radiation-induced lung toxicity - cellular and molecular mechanisms of pathogenesis, management, and literature review. *Radiat Oncol.* 2020;15(1):214.

doi: 10.1186/s13014-020-01654-9

55. Chirilă ME, Kraja F, Marta GN, *et al*. Organ-sparing techniques and dose-volume constrains used in breast cancer radiation therapy - results from European and Latin American surveys. *Clin Transl Radiat Oncol.* 2024;46:100752.

doi: 10.1016/j.ctro.2024.100752

56. Flores-Balcázar CH, Urías-Arce DM. Evaluation of tumor control and normal tissue complication probabilities in patients receiving comprehensive nodal irradiation for left-sided breast cancer. *Curr Oncol.* 2024;31(6):3189-3198.

doi: 10.3390/curroncol31060241

57. Nagaraja SS, Subramanian U, Nagarajan D. Radiation-induced H3K9 methylation on E-cadherin promoter mediated by ROS/Snail axis: Role of G9a signaling during lung epithelial-mesenchymal transition. *Toxicol in Vitro.* 2021;70:105037.

doi: 10.1016/j.tiv.2020.105037

58. Yu Z, Xu C, Song B, *et al*. Tissue fibrosis induced by radiotherapy: Current understanding of the molecular mechanisms, diagnosis and therapeutic advances. *J Transl Med.* 2023;21(1):708.

doi: 10.1186/s12967-023-04554-0

59. Kendall RT, Feghali-Bostwick CA. Fibroblasts in fibrosis: Novel roles and mediators. *Front Pharmacol*. 2014;5:123.

doi: 10.3389/fphar.2014.00123

60. Wang X, Sun X, Mu L, Chen W. Cancer-associated fibroblasts induce epithelial-mesenchymal transition in endometrial cancer cells by regulating pituitary tumor transforming gene. *Cancer Invest.* 2019;37(3):134-143.

doi: 10.1080/07357907.2019.1575969

61. Li Q, Cheng Y, Zhang Z, *et al*. Inhibition of ROCK ameliorates pulmonary fibrosis by suppressing M2 macrophage polarisation through phosphorylation of STAT3. *Clin Transl Med.* 2022;12(10):e1036.

doi: 10.1002/ctm2.1036

62. Mukherjee A, Epperly MW, Shields D, *et al*. Ionizing irradiation-induced Fgr in senescent cells mediates fibrosis. *Cell Death Discov.* 2021;7(1):349.

doi: 10.1038/s41420-021-00741-4

63. Chung EJ, Kwon S, Reedy JL, *et al*. IGF-1 receptor signaling regulates type II pneumocyte senescence and resulting macrophage polarization in lung fibrosis. *Int J Radiat Oncol Biol Phys.* 2021;110(2):526-538.

doi: 10.1016/j.ijrobp.2020.12.035

64. Kim KK, Sheppard D, Chapman HA. TGF-β1 signaling and tissue fibrosis. *Cold Spring Harb Perspect Biol.* 2018;10(4):a022293.

doi: 10.1101/cshperspect.a022293

65. Shi X, Young CD, Zhou H, Wang X. Transforming growth factor-β signaling in fibrotic diseases and cancer-associated fibroblasts. *Biomolecules*. 2020;10(12):1666.

doi: 10.3390/biom10121666

66. Fijardo M, Kwan JYY, Bissey PA, Citrin DE, Yip KW, Liu FF. The clinical manifestations and molecular pathogenesis of radiation fibrosis. *EBioMedicine*. 2024;103:105089.

doi: 10.1016/j.ebiom.2024.105089

67. Hanania AN, Mainwaring W, Ghebre YT, Hanania N, Ludwig M. Radiation-induced lung injury: Assessment and management. *Chest*. 2019;156(1):150-162.

doi: 10.1016/j.chest.2019.03.033

68. Whelan TJ, Olivotto IA, Parulekar WR, *et al*. Regional nodal irradiation in early-stage breast cancer. *N Engl J Med*. 2015;373(4):307-316.

doi: 10.1056/nejmoa1415340

69. Poortmans PM, Collette S, Kirkove C, *et al*. Internal mammary and medial supraclavicular irradiation in breast cancer. *N Engl J Med.* 2015;373(4):317-327.

doi: 10.1056/nejmoa1415369

70. Gokula K, Earnest A, Wong LC. Meta-analysis of incidence of early lung toxicity in 3-dimensional conformal irradiation of breast carcinomas. *Radiat Oncol.* 2013;8:268.

doi: 10.1186/1748-717X-8-268

71. Us SB, Bayrak G, Ballı E, Büyükakıllı B. Histological, immunohistochemical and electron-microscopic evaluation of different radiotherapy doses effects on rat's lung. *Tissue Cell.* 2025;95:102860.

doi: 10.1016/j.tice.2025.102860

72. Konkol M, Śniatała P, Milecki P. Radiation-induced lung injury - what do we know in the era of modern radiotherapy. *Rep Pract Oncol Radiother*. 2022;27(3):552-565.

doi: 10.5603/rpor.a2022.0046

73. Chao PJ, Lee HF, Lan JH, *et al*. Propensity-score-matched evaluation of the incidence of radiation pneumonitis and secondary cancer risk for breast cancer patients treated with IMRT/VMAT. *Sci Rep.* 2017;7(1):13771.

doi: 10.1038/s41598-017-14145-x

74. Ho AY, Ballangrud A, Li G, *et al*. Long-term pulmonary outcomes of a feasibility study of inverse-planned, multibeam intensity modulated radiation therapy in node-positive breast cancer patients receiving regional nodal irradiation. *Int J Radiat Oncol Biol Phy.* 2019;103(5):1100-1108.

doi: 10.1016/j.ijrobp.2018.11.045

75. Yu NY, DeWees TA, Voss MM, *et al*. Cardiopulmonary toxicity following intensity-modulated proton therapy (IMPT) versus intensity-modulated radiation therapy (IMRT) for stage III non-small cell lung cancer. *Clin Lung*

Cancer. 2022;23(8):e526-e535.

doi: 10.1016/j.cllc.2022.07.017

76. Zou Z, Bowen SR, Thomas HMT, Sasidharan BK, Rengan R, Zeng J. Scanning beam proton therapy versus photon IMRT for stage III lung cancer: Comparison of dosimetry, toxicity, and outcomes. *Adv Radiat Oncol*. 2020;5(3):434-443.

doi: 10.1016/j.adro.2020.03.001

77. Ger RB, Lentz JM, Niedzielski JS, *et al*. Dosimetric advantage of scanning beam proton therapy in gynecologic patients receiving adjuvant radiotherapy. *Cancers (Basel)*. 2025;17(12):2010.

doi: 10.3390/cancers17122010

78. Cui Y, Pan Y, Li Z, *et al*. Dosimetric analysis and biological evaluation between proton radiotherapy and photon radiotherapy for the long target of total esophageal squamous cell carcinoma. *Front Oncol.* 2022;12:954187.

doi: 10.3389/fonc.2022.954187

79. Liao Z, Lee JJ, Komaki R, *et al*. Bayesian adaptive randomization trial of passive scattering proton therapy and intensity-modulated photon radiotherapy for locally advanced non-small-cell lung cancer. *J Clin Oncol.* 2018;36(18):1813-1822.

doi: 10.1200/jco.2017.74.0720

80. Mutter RW, Choi JI, Jimenez RB, *et al*. Proton therapy for breast cancer: A consensus statement from the particle therapy cooperative group breast cancer subcommittee. *Int J Radiat Oncol Biol Phys.* 2021;111(2):337-359.

doi: 10.1016/j.ijrobp.2021.05.110

81. Yilmaz U, Koylu M, Savas R, Alanyali S. Imaging features of radiation-induced lung disease and its relationship with clinical and dosimetric factors in breast cancer patients. *J Cancer Res Ther*. 2023;19:S0.

doi: 10.4103/jcrt.jcrt_442_21

82. Wang W, Xu Y, Schipper M, *et al*. Effect of normal lung definition on lung dosimetry and lung toxicity prediction in radiation therapy treatment planning. *Int J Radiat Oncol Biol Phys.* 2013;86(5):956-963.

doi: 10.1016/j.ijrobp.2013.05.003

83. Prasun P, Kharade V, Pal V, Gupta M, Das S, Pasricha R. Dosimetric comparison of hypofractionated regimen in breast cancer using two different techniques: Intensity-modulated radiation therapy (IMRT) and volumetric-modulated arc therapy (VMAT). *Cureus.* 2023;15(4):e38045.

doi: 10.7759/cureus.38045

84. Hanczyk E, Piecuch D, Kopcial S, Jonska-Gmyrek J. Factors affecting the effectiveness of DIBH (Deep inspiratory breath hold) in patients with left breast cancer: A Narrative review. *Appl Sci.* 2024;14(16):7287.

doi: 10.3390/app14167287

85. Kong W, Huiskes M, Habraken SJM, *et al*. Reducing the lateral dose penumbra in IMPT by incorporating transmission pencil beams. *Radiother Oncol.* 2024;198:110388.

doi: 10.1016/j.radonc.2024.110388

86. Marks LB, Bentzen SM, Deasy JO, *et al*. Radiation dose-volume effects in the lung. *Int J Radiat Oncol Biol Phys.* 2010;76(3 Suppl):S70-S76.

doi: 10.1016/j.ijrobp.2009.06.091

87. Liu Y, Wang W, Shiue K, *et al*. Risk factors for symptomatic radiation pneumonitis after stereotactic body radiation therapy (SBRT) in patients with non-small cell lung cancer. *Radiother Oncol.* 2021;156:231-238.

doi: 10.1016/j.radonc.2020.10.015

88. Park SH, Kim JC. Regional nodal irradiation in pT1-2N1 breast cancer patients treated with breast-conserving surgery and whole breast irradiation. *Radiat Oncol J*. 2020;38(1):44-51.

doi: 10.3857/roj.2019.00647

89. Taylor C, Correa C, Duane FK, *et al.* Estimating the risks of breast cancer radiotherapy: Evidence from modern radiation doses to the lungs and heart and from previous randomized trials. *J Clin Oncol.* 2017;35(15):1641-1649.

doi: 10.1200/jco.2016.72.0722

90. Mangesius J, Minasch D, Fink K, *et al.* Systematic risk analysis of radiation pneumonitis in breast cancer: Role of cotreatment with chemo-, endocrine, and targeted therapy. *Strahlenther Onkol.* 2023;199(1):67-77.

doi: 10.1007/s00066-022-02032-y

91. Ford MB, Sigurdson AJ, Petrulis ES, *et al*. Effects of smoking and radiotherapy on lung carcinoma in breast carcinoma survivors. *Cancer.* 2003;98(7):1457-1464.

doi: 10.1002/cncr.11669

92. Prochazka M, Hall P, Gagliardi G, *et al*. Ionizing radiation and tobacco use increases the risk of a subsequent lung carcinoma in women with breast cancer: Case-only design. *J Clin Oncol.* 2005;23(30):7467-7474.

doi: 10.1200/jco.2005.01.7335

93. Kaufman EL, Jacobson JS, Hershman DL, Desai M, Neugut AI. Effect of breast cancer radiotherapy and cigarette smoking on risk of second primary lung cancer. *J Clin Oncol.* 2008;26(3):392-398.

doi: 10.1200/jco.2007.13.3033

94. Ding NH, Li JJ, Sun LQ. Molecular mechanisms and treatment of radiation-induced lung fibrosis. *Curr Drug Targets.* 2013;14(11):1347-1356.

doi: 10.2174/13894501113149990198

95. Gurtner K, Kryzmien Z, Koi L, *et al*. Radioresistance of KRAS/TP53-mutated lung cancer can be overcome by

radiation dose escalation or EGFR tyrosine kinase inhibition *in vivo*. *Int J Cancer.* 2020;147(2):472-477.

doi: 10.1002/ijc.32598

96. Abo-Madyan Y, Aziz MH, Aly MM, *et al*. Second cancer risk after 3D-CRT, IMRT and VMAT for breast cancer. *Radiother Oncol*. 2014;110(3):471-476.

doi: 10.1016/j.radonc.2013.12.002

97. Pithadia KJ, Advani PG, Citrin DE, *et al*. Comparing risk for second primary cancers after intensity-modulated vs 3-dimensional conformal radiation therapy for prostate cancer, 2002-2015. *JAMA Oncol.* 2023;9(8):1119-1123.

doi: 10.1001/jamaoncol.2023.1638

98. Cartechini G, Fracchiolla F, Menegotti L, *et al*. Proton pencil beam scanning reduces secondary cancer risk in breast cancer patients with internal mammary chain involvement compared to photon radiotherapy. *Radiat Oncol*. 2020;15(1):228.

doi: 10.1186/s13014-020-01671-8

99. Paganetti H, Depauw N, Johnson A, Forman RB, Lau J, Jimenez R. The risk for developing a secondary cancer after breast radiation therapy: Comparison of photon and proton techniques. *Radiother Oncol.* 2020;149:212-218.

doi: 10.1016/j.radonc.2020.05.035

100. Kadakia KC, Henry NL. Adjuvant endocrine therapy in premenopausal women with breast cancer. *Clin Adv Hematol Oncol.* 2015;13(10):663-672.

101. Uslu Y, Kocatepe V, Sezgin DS, Uras C. Adherence to adjuvant tamoxifen and associated factors in breast cancer survivors. *Support Care Cancer*. 2023;31(5):285.

doi: 10.1007/s00520-023-07742-2

102. Azria D, Gourgou S, Sozzi WJ, *et al*. Concomitant use of tamoxifen with radiotherapy enhances subcutaneous breast fibrosis in hypersensitive patients. *Br J Cancer*. 2004;91(7):1251-1260.

doi: 10.1038/sj.bjc.6602146

103. Harris EE, Christensen VJ, Hwang WT, Fox K, Solin LJ. Impact of concurrent versus sequential tamoxifen with radiation therapy in early-stage breast cancer patients undergoing breast conservation treatment. *J Clin Oncol.* 2005;23(1):11-16.

doi: 10.1200/jco.2005.09.056

104. McGee SF, Clemons M, Pond G, *et al.* A randomized trial comparing concurrent versus sequential radiation and endocrine therapy in early-stage, hormone-responsive breast cancer. *Curr Oncol.* 2024;31(8):4531-4545.

doi: 10.3390/curroncol31080338

105. Etori S, Nakano R, Kamada H, *et al*. Tamoxifen-induced lung injury. *Intern Med.* 2017;56(21):2903-2906.

doi: 10.2169/internalmedicine.8649-16

106. Zhao T, Sun Z, Lai X, *et al*. Tamoxifen exerts anti-peritoneal fibrosis effects by inhibiting H19-activated VEGFA transcription. *J Transl Med.* 2023;21(1):614.

doi: 10.1186/s12967-023-04470-3

107. Koc M, Polat P, Suma S. Effects of tamoxifen on pulmonary fibrosis after cobalt-60 radiotherapy in breast cancer patients. *Radiother Oncol*. 2002;64(2):171-175.

doi: 10.1016/s0167-8140(02)00136-6

108. Kuo SH, Tseng LM, Chen ST, *et al*. Radiotherapy versus low-dose tamoxifen following breast-conserving surgery for low-risk and estrogen receptor-positive breast ductal carcinoma *in situ*: An international open-label randomized non-inferiority trial (TBCC-ARO DCIS Trial). *BMC Cancer.* 2023;23(1):865.

doi: 10.1186/s12885-023-11291-6

109. Wong LY, Kapula N, He H, *et al*. Risk of developing subsequent primary lung cancer after receiving radiation for breast cancer. *JTCVS Open.* 2023;16:919-928.

doi: 10.1016/j.xjon.2023.10.031

110. Burns TF, Stabile LP. Targeting the estrogen pathway for the treatment and prevention of lung cancer. *Lung Cancer Manag.* 2014;3(1):43-52.

doi: 10.2217/lmt.13.67

111. Debbi K, Grellier N, Loganadane G, *et al*. Interaction between radiation therapy and targeted therapies in HER2-positive breast cancer: Literature review, levels of evidence for safety and recommendations for optimal treatment sequence. *Cancers*. 2023;15(8):2278.

doi: 10.3390/cancers15082278

112. Lin MX, Zang D, Liu CG, Han X, Chen J. Immune checkpoint inhibitor-related pneumonitis: Research advances in prediction and management. *Front Immunol.* 2024;15:1266850.

doi: 10.3389/fimmu.2024.1266850

113. Weller A, Dunlop A, Oxer A, *et al*. Spect perfusion imaging versus CT for predicting radiation injury to normal lung in lung cancer patients. *Br J Radiol.* 2019;92(1101):20190184.

doi: 10.1259/bjr.20190184

114. Zhang X, Zhang Z, Huang M, *et al*. Pathological mechanisms of radiation-induced lung injury and novel nano-drug delivery therapeutic strategies. *Int J Nanomedicine.* 2025;20:12431-12465.

doi: 10.2147/IJN.S551477

115. Qi YJ, Su GH, You C, *et al*. Radiomics in breast cancer: Current advances and future directions. *Cell Rep Med.* 2024;5(9):101719.

doi: 10.1016/j.xcrm.2024.101719

116. Nardone V, Reginelli A, Rubini D, *et al*. Delta radiomics: An updated systematic review. *Radiol Med*. 2024;129(8):1197-1214.

doi: 10.1007/s11547-024-01853-4

117. Ma M, Chu Z, Quan H, *et al*. Natural products for anti-fibrotic therapy in idiopathic pulmonary fibrosis: Marine and terrestrial insights. *Front Pharmacol.* 2025;16:1524654.

doi: 10.3389/fphar.2025.1524654

118. Suman S, Jain S, Chandna S. Recent patents in the field of radioprotector development: Opportunities and challenges. *Recent Pat Biotechnol.* 2013;7(3):219-227.

doi: 10.2174/18722083113076660012

119. Antonadou D, Throuvalas N, Petridis A, *et al*. Effect of amifostine on toxicities associated with radiochemotherapy in patients with locally advanced non-small-cell lung cancer. *Int J Radiat Oncol Biol Phys.* 2023;57(2):402-408.

doi: 10.1016/s0360-3016(03)00590-x

120. Rabbani ZN, Batinic-Haberle I, Anscher MS, *et al*. Long-term administration of a small molecular weight catalytic metalloporphyrin antioxidant, AEOL 10150, protects lungs from radiation-induced injury. *Int J Radiat Oncol Biol Phys*. 2007;67(2):573-580.

doi: 10.1016/j.ijrobp.2006.09.053

121. Kadivar F, Haddadi G, Mosleh-Shirazi MA, Khajeh F, Tavasoli A. Protection effect of cerium oxide nanoparticles against radiation-induced acute lung injuries in rats. *Rep Pract Oncol Radiother*. 2020;25(2):206-211.

doi: 10.1016/j.rpor.2019.12.023

122. Singh VK, Serebrenik AA, Fatanmi OO, *et al*. The radioprotectant, BIO 300, protects the lungs from total-body irradiation injury in C57L/J mice. *Radiat Res.* 2023;199(3):294-300.

doi: 10.1667/rade-22-00142.1

123. Lin Y, Xu Z, Zhou B, Ma K, Jiang M. Pentoxifylline inhibits pulmonary fibrosis by regulating cellular senescence in mice. *Front Pharmacol.* 2022;13:848263.

doi: 10.3389/fphar.2022.848263

124. Jha SK, De Rubis G, Devkota SR, *et al*. Cellular senescence in lung cancer: Molecular mechanisms and therapeutic interventions. *Ageing Res Rev.* 2024;97:102315.

doi: 10.1016/j.arr.2024.102315

125. Kumar K, Angdisen J, Ma J, Datta K, Fornace AJ, Suman S. Simulated galactic cosmic radiation exposure-induced mammary tumorigenesis in $Apc^{Min/+}$ mice coincides with activation of ERα-ERRα-SPP1 signaling axis. *Cancers (Basel)*. 2024;16(23):3954.

doi: 10.3390/cancers16233954

126. Feng T, Xie F, Lee LMY, *et al*. Cellular senescence in cancer: From mechanism paradoxes to precision therapeutics. *Mol Cancer*. 2025;24(1):213.

doi: 10.1186/s12943-025-02419-2

127. Klepacki H, Kowalczuk K, Łepkowska N, Hermanowicz JM. Molecular regulation of SASP in Cellular senescence: Therapeutic implications and translational challenges. *Cells*. 2025;14(13):942.

doi: 10.3390/cells14130942

128. Kumar K, Moon BH, Kumar S, *et al*. Senolytic agent ABT-263 mitigates low- and high-LET radiation-induced gastrointestinal cancer development in $Apc^{1638]N/+}$ mice. *Aging (Albany NY)*. 2025;17(1):97-115.

doi: 10.18632/aging.206183

129. Kumar K, Kumar S, Datta K, Fornace AJ, Suman S. High-LET-radiation-induced persistent DNA damage response signaling and gastrointestinal cancer development. *Curr Oncol*. 2023;30(6):5497-5514.

doi: 10.3390/curroncol30060416

130. Chen C, Chen J, Zhang Y, Zhang Q, Shi H. Senescence-associated secretory phenotype in lung cancer: Remodeling the tumor microenvironment for metastasis and immune suppression. *Front Oncol*. 2025;15:1605085.

doi: 10.3389/fonc.2025.1605085

131. Suman S. Integrative analysis of radiation-induced senescence-associated secretory phenotype factors in kidney cancer progression. *Genes (Basel)*. 2025;16(1):85.

doi: 10.3390/genes16010085

132. Pan J, Li D, Xu Y, *et al*. Inhibition of Bcl-2/xl With ABT-263 selectively kills senescent type II pneumocytes and reverses persistent pulmonary fibrosis induced by ionizing radiation in mice. *Int J Radiat Oncol Biol Phys.* 2017;99(2):353-361.

doi: 10.1016/j.ijrobp.2017.02.216

133. Suman S, Fornace AJ. Countermeasure development against space radiation-induced gastrointestinal carcinogenesis: Current and future perspectives. *Life Sci Space Res (Amst)*. 2022;35:53-59.

doi: 10.1016/j.lssr.2022.09.005

134. Justice JN, Nambiar AM, Tchkonia T, *et al*. Senolytics in idiopathic pulmonary fibrosis: Results from a first-in-human, open-label, pilot study. *EBioMedicine.* 2019;40:554-563.

doi: 10.1016/j.ebiom.2018.12.052

135. Rosell J, Nordenskjöld B, Bengtsson NO, *et al*. Long-term effects on the incidence of second primary cancers in a randomized trial of two and five years of adjuvant tamoxifen. *Acta Oncol.* 2017;56(4):614-617.

doi: 10.1080/0284186X.2016.1273547

136. Liang B, Tian Y, Chen X, *et al*. Prediction of radiation pneumonitis with dose distribution: A convolutional neural

network (CNN) based model. *Front Oncol*. 2020;9:1500.

doi: 10.3389/fonc.2019.01500

137. Hatamabadi Farahani E, Sadeghi H, Seif F, Marzabadi MA, Rezaee R. Analyzing secondary cancer risk: A machine learning approach. *Asian Pac J Cancer Prev*. 2025;26(1):239-248.

doi: 10.31557/apjcp.2025.26.1.239

138. Felici A, Peduzzi G, Pellungrini R, Campa D. Artificial intelligence to predict cancer risk, are we there yet? A comprehensive review across cancer types. *Eur J Cancer.* 2025;222:115440.

doi: 10.1016/j.ejca.2025.115440

139. Kim JS, Kim HJ. FLASH radiotherapy: Bridging revolutionary mechanisms and clinical frontiers in cancer treatment - a narrative review. *Ewha Med J.* 2024;47(4):e54.

doi: 10.12771/emj.2024.e54

140. Guo Y, Hao S, Huang Q, *et al.* Unraveling the dual nature of FLASH radiotherapy: From normal tissue sparing to tumor control. *Cancer Lett.* 2025;630:217895.

doi: 10.1016/j.canlet.2025.217895

141. Webster M, Podgorsak A, Li F, *et al.* New approaches in radiotherapy. *Cancers (Basel)*. 2025;17(12):1980.

doi: 10.3390/cancers17121980

ACCSCIENCE PUBLISHING

Advances in Radiotherapy & Nuclear Medicine

REVIEW ARTICLE

CXCR4-targeted theranostics in non-Hodgkin lymphoma: Present evidence and future directions

Marcus Yoakam[1], Uma A. Obalapuram[1], Kameron Hahn[1], and Samir Dalia[2]*

[1]Department of Medical Education, College of Osteopathic Medicine, Kansas City University, Joplin, Missouri, United States of America

[2]Department of Medical Oncology, Mercy Hospital, Joplin, Missouri, United States of America

Abstract

Non-Hodgkin lymphoma (NHL) is a biologically heterogeneous group of lymphoid malignancies with variable clinical outcomes despite advances in chemotherapy, immunotherapy, and cellular therapies. The C–X–C chemokine receptor 4 (CXCR4)/C–X–C motif chemokine ligand 12 (CXCL12) axis plays a central role in lymphocyte trafficking, survival, and tumor microenvironment interactions. It is frequently dysregulated in NHL, making it an attractive target for precision oncology. CXCR4-directed theranostics combines molecular imaging and targeted radionuclide therapy, enabling real-time assessment of receptor expression, patient stratification, and personalized treatment delivery. Diagnostic positron emission tomography imaging using ^{68}Ga-pentixafor reliably visualizes CXCR4-expressing disease, while therapeutic agents, such as ^{177}Lu- or ^{90}Y-pentixather and CXCR4-targeted antibody–drug conjugates demonstrate selective tumor targeting and potent cytotoxicity in preclinical and early clinical studies. Despite promising antitumor activity and manageable toxicity, several challenges remain, including heterogeneous and dynamically regulated CXCR4 expression, protective microenvironmental niches, hematologic toxicity, radiopharmaceutical limitations, and infrastructural requirements for widespread clinical implementation. Ongoing research is focused on optimizing dosing, refining patient selection, combining CXCR4-targeted therapies with other modalities, and expanding clinical trials to establish efficacy and safety. CXCR4 theranostics holds substantial potential to improve precision management of NHL by integrating diagnostic and therapeutic modalities into a unified, patient-tailored approach.

Keywords: Thernostics/Theragnostics; C–X–C chemokine receptor 4; Non-Hodgkin lymphoma; 68Ga-pentaxifor; 177Lu-pentixather; Radioligand therapy

***Corresponding author:**
Samir Dalia
(samir.dalia@mercy.net)

Citation: Yoakam M, Obalapuram UA, Hahn K, Dalia S. CXCR4-targeted theranostics in non-Hodgkin lymphoma: Present evidence and future directions. *Adv Radiother Nucl Med*. 2026;4(1):33-45. doi: 10.36922/ARNM025480061

Received: November 30, 2025

Revised: December 19, 2025

Accepted: January 9, 2026

Published online: January 27, 2026

1. Introduction

Non-Hodgkin lymphoma (NHL) is a heterogeneous group of lymphoid malignancies with diffuse large B-cell lymphoma (DLBCL) and follicular lymphoma comprising the most common subtypes.[1] NHL encompasses over 90 subtypes, primarily of B-cell origin, but can also include T-cell and rare natural-killer-cell lymphomas.[2] Standard first-line

therapy for DLBCL is rituximab, cyclophosphamide, doxorubicin, vincristine, and prednisone (R-CHOP), curing 60–70% of all patients.[3] Despite these successes, a substantial proportion of patients experience refractory or relapsed disease, highlighting the complexity and biological diversity of NHL. DLBCL, for example, consists of multiple molecular subgroups including: Germinal center B-cell–like (GCB), activated B-cell–like (ABC), and other genetically defined entities that differ in prognosis, patterns of progression, and response to therapy.[4,5] This heterogeneity complicates treatment selection and contributes to the persistent challenge of achieving durable remissions in all patient populations.[6] Advances in targeted therapies, such as Bruton tyrosine kinase inhibitors, phosphoinositide 3-kinase (PI3K) inhibitors, bispecific antibodies, and chimeric antigen receptor T-cell therapy (CAR T), have expanded the therapeutic landscape, particularly for relapsed or refractory disease.[7] However, challenges remain regarding optimal sequencing, accessibility, long-term toxicity, and management of treatment-related immune effects.[8] CAR T-cell therapy, while transformative for select patients, is limited by manufacturing time, toxicity profiles, and variable durability of response.[9] These gaps in current management continue to drive the pursuit of more precise and effective therapeutic approaches.

2. Methods

We conducted a targeted narrative review of the literature published between January 1995 and December 2025, focusing on C–X–C chemokine receptor 4 (CXCR4)-targeted diagnostics, therapeutics, and theranostic applications in NHL and other hematologic malignancies. A systematic search was performed across PubMed/MEDLINE, Embase, and ClinicalTrials.gov, supplemented by manual searches of reference lists from key publications and selected hematology, oncology, and nuclear medicine journals. Search strategies combined controlled keywords related to CXCR4 biology, molecular imaging, and radionuclide therapy. Key search terms included combinations of "CXCR4," "CXCR4 axis," "theranostics" or "theragnostics," "non-Hodgkin lymphoma" or "NHL," "hematologic malignancies," "68Ga-Pentixafor," "177Lu-Pentixather," "90Y-Pentixather," "CXCR4-directed imaging," "radionuclide therapy," and "receptor-targeted therapy." Additional searches incorporated terms, such as "PET imaging," "radioligand therapy (RLT)," and "targeted alpha or beta therapy" to capture evolving theranostic approaches. We included peer-reviewed clinical trials, observational studies, small patient cohorts, and translational or mechanistic preclinical studies that provided insights relevant to CXCR4-based diagnostic–therapeutic strategies. Case series and early clinical experiences were included when they informed feasibility, safety, dosimetry, or patient selection. Preclinical studies were considered if they elucidated CXCR4 expression patterns, ligand–receptor interactions, or biodistribution data with direct relevance to clinical theranostics. Exclusion criteria comprised single-patient case reports, conference abstracts lacking full methodological detail, and publications not available in English. Priority was given to studies addressing NHL subtypes and other hematologic malignancies with established or emerging CXCR4 expression, as well as investigations supporting integrated theranostic paradigms, including CXCR4-directed positron emission tomography (PET) imaging for patient selection and response assessment, followed by CXCR4-targeted radionuclide therapy.

3. The CXCR4/CXCL12 axis

The CXCR4/CXCL12 axis is one of the most biologically significant chemokine systems and plays a central role in hematopoiesis and lymphocyte positioning. CXCR4 expression is particularly high on B-lymphocyte precursors and is also found on early T-cell lineages.[10] Disruption of CXCR4 signaling or suppression of CXCL12 mobilizes hematopoietic progenitors into the peripheral blood, especially in response to cytokines, such as interleukin (IL)-3, granulocyte colony-stimulating factor, Fms-like tyrosine kinase 3 ligand, and stem cell factor.[10,11] Beyond the marrow, CXCR4 enables lymphocyte entry into secondary lymphoid organs through high endothelial venules, which express CXCL12, although CCR7 is also required for efficient homing.[12,13] Within lymph nodes, CXCL12 promotes B-cell migration and germinal center formation and supports T-cell survival by upregulating anti-apoptotic proteins, including B-cell lymphoma 2 (BCL-2) and BCL-extra large (xL).[14,15] Additional pathways engaged by CXCR4 include the PI3K/protein kinase B pathway (AKT), the rat sarcoma/mitogen-activated protein kinase/extracellular signal-regulated kinase pathway, the phospholipase C-mediated calcium signaling pathway, the mechanistic (mammalian) target of rapamycin pathway, and the nuclear factor kappa-light-chain-enhancer of activated B cells pathway, while overstimulation leads to β-arrestin–dependent internalization and desensitization.[16,17] Collectively, these pathways promote proliferation, migration, and survival properties that malignant cells frequently exploit.

Aberrant CXCR4 expression and signaling are well documented in hematologic cancers, including NHL. One study reported CXCR4 expression in 10 of 12 NHL cell lines and 18 of 19 primary samples, with significantly higher expression than normal lymphoid cells.[18] CXCR4 blockade decreased migration, proliferation, and tumor

growth both *in vitro* and *in vivo*. Furthermore, several large immunohistochemical and transcriptomic studies have demonstrated that approximately half to two-thirds of cases express CXCR4 at meaningful levels. A cohort analysis of 743 *de novo* DLBCL patients treated with R-CHOP showed that CXCR4 positivity correlated with more aggressive features, including bulky disease, high Ki-67 indices, and MYC or BCL2 dysregulation, and independently predicted inferior progression-free survival, particularly in the GCB subgroup.[19] Additional molecular studies suggest that CXCR4 expression is enriched within the ABC or non-GCB subtype, further linking CXCR4 signaling to clinically aggressive tumor biology.[20]

Outside of DLBCL, CXCR4 expression is also observed in a range of indolent and aggressive lymphomas. In early imaging cohorts using ^{68}Ga-pentixafor PET/computed tomography (CT) (a noninvasive radiolabel that selectively binds CXCR4), multiple subtypes, including follicular lymphoma, mantle cell lymphoma (MCL), marginal zone lymphoma (MZL), lymphoplasmacytic lymphoma, Waldenström macroglobulinemia, and some T-cell lymphomas, have demonstrated CXCR4-targetable uptake.[21] MZL, in particular, appears to display consistently high receptor expression, and recent head-to-head work in untreated MZL showed that ^{68}Ga-pentixafor PET/CT outperformed ^{18}F-fluorodeoxyglucose (^{18}F-FDG) for lesion detection and staging, suggesting that CXCR4 biology may be especially relevant in indolent subtypes.[22] The biologic role of CXCR4 extends beyond simple cell-surface expression; experimental models indicate that CXCR4 signaling promotes dissemination and microenvironmental homing. In DLBCL xenograft systems, high CXCR4 expression increased metastatic spread, whereas pharmacologic blockade reduced dissemination and improved survival.[23] Additional *in vitro* work suggests that CXCR4 upregulation may contribute to therapeutic resistance by impairing antibody-dependent cytotoxicity, as CXCR4 inhibition enhances rituximab-mediated killing in DLBCL cell lines.[24] In summary, the expression landscape of CXCR4 across NHL subtypes provides a strong biological foundation for theranostic strategies, offering both prognostic information and a therapeutically actionable target.

4. Theranostics

Theranostics, also spelled theragnostics, is an emerging paradigm in precision oncology in which diagnostic imaging and targeted therapy are integrated into a single, continuous strategy. Rather than treating diagnosis and therapy as separate processes, theranostics uses molecularly matched radiopharmaceuticals to visualize tumor biology, select appropriate candidates for treatment, deliver targeted radionuclide therapy, and monitor therapeutic response in real time. This approach enables clinicians to personalize cancer care at the molecular level, improving both treatment accuracy and clinical outcomes.[25] The foundational concept of theranostics relies on the pairing of a diagnostic radiotracer, typically labeled with a positron-emitting isotope for PET imaging, allowing precise localization and quantification of target expression, and a therapeutic agent. If the target is suitably expressed, the patient can then receive a therapeutic version of the same ligand, labeled instead with a β- or α-emitting radionuclide that delivers cytotoxic radiation directly to malignant cells.[26] Because the same molecular target is used for both imaging and therapy, patient selection becomes more biologically informed, reducing unnecessary toxicity and increasing the likelihood of response.

Over the past decade, theranostics has gained prominence through the success of established radiopharmaceuticals, such as ^{177}Lu-dotatate for neuroendocrine tumors and ^{177}Lu-PSMA-617 for metastatic castration-resistant prostate cancer. These therapies have demonstrated meaningful improvements in survival, quality of life, and disease control, validating the clinical utility of molecularly targeted radionuclide therapy.[25,27,28] The rationale for extending the theranostic paradigm to hematologic malignancies stems from the unique biological and clinical characteristics of these diseases. Hematologic cancers often exhibit highly specific lineage markers, surface antigens, and microenvironmental features that can be leveraged for molecular targeting.[26,27] Many of these targets, such as cluster of differentiation (CD)20, CD38, CD123, and CXCR4, are already well characterized through decades of immunophenotyping and therapeutic antibody development, creating a strong translational foundation for radioligand innovation.

The systemic nature of leukemias, lymphomas, and myelomas makes them particularly suitable for radiopharmaceutical approaches, as circulating or disseminated malignant cells may be more uniformly exposed to targeted radiation than deep or hypoxic solid-tumor regions.[29,30] Integration of theranostics in hematologic cancers also has the potential to transform current treatment algorithms. Molecular imaging enables quantitative, whole-body assessment of antigen expression, improving patient selection, anticipating resistance, and allowing real-time adaptation of therapy. Early-phase studies continue to explore radiolabeled antibodies, small molecules, and peptides targeting hematologic antigens, with preclinical models demonstrating potent eradication of malignant clones and minimal off-target toxicity. Together, these efforts highlight a growing consensus

that theranostics could meaningfully enhance precision treatment options for lymphoma, leukemia, and plasma-cell disorders, extending the reach of molecularly targeted radionuclide therapy beyond solid tumors.[31,32]

4.1. ^{68}Ga-pentixafor PET/CT as a diagnostic agent

^{68}Ga-pentixafor is a PET radiotracer labeled with the positron-emitting isotope gallium-68 that binds with high affinity and selectivity to CXCR, enabling reliable visualization of receptor-positive tumor tissues.[33,34] Prior investigations have demonstrated that ^{68}Ga-pentixafor demonstrates consistently high uptake in hematologic malignancies, with tracer accumulation closely correlating to underlying CXCR4 expression.[35] Because tracer intensity reflects the *in vivo* distribution of CXCR4, ^{68}Ga-pentixafor provides sensitive detection of disease sites with high lesion-to-background contrast. The clinical implications of this imaging capability are significant, as delineation of areas with elevated CXCR4 expression may enable rapid identification of patients most likely to benefit from CXCR4-directed therapeutic strategies. Evidence from hematologic cancers, including multiple myeloma and MCL, shows that ^{68}Ga-pentixafor PET produces high tracer uptake and excellent image contrast across diverse disease presentations. Notably, more than 500 of approximately 700 published clinical PET scans using this agent have demonstrated clear and reproducible tracer accumulation at known disease sites, highlighting its robustness and diagnostic reliability.[35]

Recent meta-analytic data reinforce these findings. A pooled analysis of CXCR4-targeted PET in hematologic malignancies reported a detection rate of 99.4% for B-cell lymphomas, indicating extremely high sensitivity across multiple NHL subtypes.[36] Additional studies have shown that ^{68}Ga-pentixafor outperforms ^{18}F-FDG in specific contexts, including in multiple myeloma, where pentixafor demonstrated higher sensitivity (77.8% vs. 65.0%), and in MCL, where it achieved superior detection rates and higher standardized uptake values relative to FDG.[37,38] In newly diagnosed NHL, ^{68}Ga-pentixafor uptake has been observed across a wide array of subtypes, including lymphoplasmacytic lymphoma, MZL, DLBCL, follicular lymphoma, MCL, and several indolent B-cell lymphomas, as well as selected T-cell lymphomas. In certain entities, such as lymphoplasmacytic and MZL, ^{68}Ga-pentixafor PET/CT has demonstrated broader disease detection and higher lesion signal intensity than ^{18}F-FDG, supporting its utility in settings where FDG uptake is variable or low.[39] Prospective data in MCL have further shown that CXCR4-directed PET/magnetic resonance imaging (MRI) can reach sensitivities approaching 100%, significantly surpassing FDG-PET performance and offering improved assessment of bone marrow and splenic involvement.[38]

Beyond initial diagnosis, ^{68}Ga-pentixafor may also serve as a valuable tool for treatment response assessment. Longitudinal imaging studies in MCL have reported that end-of-therapy complete remission is more frequently detected on ^{68}Ga-pentixafor PET than on conventional MRI, highlighting potential relevance for response-adapted strategies.[37] These findings support the concept that functional CXCR4 imaging may reveal disease biology not captured by purely morphologic criteria. The greatest clinical utility of ^{68}Ga-pentixafor, however, may lie in its role as the diagnostic component of CXCR4-targeted theranostic platforms approaches in which both imaging and therapy are integrated using structurally related molecular agents.[35,36] Because ^{68}Ga-pentixafor effectively maps CXCR4 expression *in vivo*, it enables patient selection for subsequent CXCR4-directed radionuclide therapy, including treatments using therapeutic isotopes, such as ^{177}Lu- or ^{90}Y-labeled pentixather. This theranostic workflow is particularly advantageous in hematologic cancers, where accurate detection of disease burden and receptor expression is closely linked to treatment decisions and therapeutic outcomes. Collectively, the existing body of evidence, including its demonstrated specificity, reproducible uptake patterns, and established role in CXCR4-directed theranostics, underscores the considerable promise of ^{68}Ga-pentixafor as a targeted imaging modality for CXCR4-expressing NHL. These findings highlight the importance of continued, NHL-focused investigation to clarify its diagnostic value, prognostic implications, and integration within personalized treatment paradigms.

4.2. ^{177}Lu-pentixather as a therapeutic agent

^{177}Lu-pentixather is a radiolabeled CXCR4 antagonist that has shown significant therapeutic value as the treatment counterpart to ^{68}Ga-pentixafor imaging, particularly in hematologic malignancies, such as lymphoma, multiple myeloma, and acute myeloid leukemia (AML).[35,40] Preclinical studies have demonstrated that ^{177}Lu-pentixather binds with high affinity, specificity, and selectivity to CXCR4, ensuring targeted uptake into CXCR4-expressing tumor tissues.[41] Once internalized, ^{177}Lu-pentixather emits β-particles capable of producing both direct DNA double-strand breaks and indirect oxidative damage within malignant cells, and the absorbed dose delivered to the tumor microenvironment is sufficient to drive substantial cytotoxicity while limiting off-target exposure.[38,41]

In xenograft mouse models of acute lymphoblastic leukemia (ALL) and AML, CXCR4-targeted endoradiotherapy using ^{177}Lu-pentixather effectively localized to regions of leukemic infiltration, reduced

leukemic burden in affected organs, and induced alterations in the leukemia-supportive microenvironment. Notably, mesenchymal stem cells exposed to therapeutic radiation preserved viability and physiological function *ex vivo*, suggesting that ^{177}Lu-pentixather may selectively disrupt malignant architectures without fully compromising normal stromal support systems.[42] Translational relevance is supported by early clinical evidence: In three patients with heavily pretreated, refractory AML who received ^{177}Lu-pentixather before a second stem cell transplantation, therapy was associated with measurable leukemia reduction, successful execution of a subsequent transplant, and hematopoietic engraftment, demonstrating feasibility and potential therapeutic benefit.[43] Complementary studies have further highlighted the favorable biodistribution and organ dosimetry profile of ^{177}Lu-pentixather, particularly its high marrow-targeting capacity, supporting its clinical potential as a CXCR4-directed therapeutic.[38,44] These findings provide a compelling rationale for expanding the investigation of ^{177}Lu-pentixather into NHL. In particular, future work may pursue increasingly personalized theranostic strategies that integrate ^{68}Ga-pentixafor PET imaging with ^{177}Lu-pentixather therapy, establishing a unified diagnostic–therapeutic workflow centered on quantifying and exploiting CXCR4 expression. Another promising direction involves evaluating ^{177}Lu-pentixather in combination with established modalities, such as chemotherapy, immunotherapy, and targeted agents, to enhance treatment efficacy through synergistic mechanisms.

Additional studies could also optimize dosing and fractionation strategies to improve the therapeutic index or extend its application beyond NHL by exploring roles in broader hematologic malignancies.[33,40] Finally, because CXCR4 mediates multiple oncogenic pathways, future research may examine whether ^{177}Lu-pentixather can be leveraged to modulate signaling networks beyond CXCR4 alone, further broadening its relevance. The demonstrated receptor specificity, selective *in vivo* uptake, and capacity to induce meaningful therapeutic responses all support continued preclinical and clinical investigation of ^{177}Lu-pentixather as a potential therapeutic agent for CXCR4-expressing NHL.

4.3. Comparative value of CXCR4 PET vs. fluorodeoxyglucose PET

Fluorodeoxyglucose PET and CXCR4 PET differ in molecular targets, clinical application, and diagnostic performance. FDG PET visualizes increased glucose metabolism, a hallmark of many aggressive cancers, whereas CXCR4 PET images tumor expression of the CXCR4 receptor, a pathway central to the biology of numerous hematologic malignancies. As noted, ^{68}Ga-pentixafor PET has demonstrated higher lesion detection rates and improved contrast in several lymphoma subtypes compared with FDG PET.[22] These advantages stem from the frequent overexpression of CXCR4 in hematologic malignancies, making CXCR4 PET particularly useful for precise disease characterization in this setting.

Fluorodeoxyglucose PET remains the most reliable modality for solid tumors. A single-center, prospective study published in 2025 demonstrated that patients with locally advanced non-small-cell lung carcinoma who underwent ^{18}F-FDG PET/CT-based radiotherapy planning exhibited a significantly higher incidence of changes to planning target volumes (PTV) compared to conventional CT-based planning. Modifications to the primary tumor PTV were observed in 23/30 (76.6%) cases and nodal PTV changes in 19/30 (63.3%) cases, demonstrating that ^{18}F-FDG PET/CT significantly improves radiotherapy planning by more precisely defining tumor and nodal volumes, identifying undetected lesions, and guiding dose adaptation, although larger long-term studies are required to confirm potential locoregional control and survival improvements.[45] In contrast, CXCR4 uptake in solid tumors is variable and often low, restricting its diagnostic utility in these settings.[35,36] As a glucose analog, FDG retains broad applicability across diverse malignant diseases and remains the standard tool for staging and response assessment in solid tumor oncology. Altogether, the modalities are complementary; CXCR4 PET offers superior performance in many hematologic cancers, while FDG PET maintains broad diagnostic relevance and sensitivity in solid tumors.

4.4. Dosimetry and practical implementation of CXCR4-directed RLT

Dosimetric analysis is central to the clinical deployment of CXCR4 RLT, as physiological CXCR4 expression in hematopoietic stem and progenitor cells introduces unique considerations. Organ-level dosimetry has consistently identified the kidneys as a major dose-limiting structure, with reported kidney dose coefficients of roughly 1.4 Gy/GBq and corresponding bone-marrow dose coefficients around 0.4 Gy/GBq in early human series.[46] These values fall within acceptable ranges for many therapeutic settings but become critical when RLT is deployed in heavily pretreated patients or in combination with stem cell-toxic regimens. Bone marrow toxicity is expected, as the CXCR4–CXCL12 axis is fundamental to marrow homing; thus, profound cytopenias are not only likely but may be therapeutically desired when using CXCR4 RLT as part of myeloablative conditioning before autologous or allogeneic stem cell transplant. In contrast, when RLT is contemplated outside the transplant context,

more conservative dosing or individualized dosimetry is required to avoid prolonged marrow aplasia.[46,47] In practical terms, the theranostic workflow begins with ^{68}Ga-pentixafor PET/CT to confirm sufficient target expression and guide dosimetry planning. Patients who demonstrate robust uptake undergo a low-dose ^{177}Lu-Pentixather "tracer" study, followed by serial SPECT/CT or planar imaging over several days to construct patient-specific time–activity curves for tumor and critical organs.[47] These curves inform absorbed-dose calculations, enabling personalized activity selection that balances therapeutic intensity with organ safety. Patients receiving high-dose therapy, especially those with marrow involvement, often require stem cell rescue, which is a well-established component of CXCR4 RLT protocols in hematologic diseases, such as AML. The overall feasibility demonstrated in these early experiences provides a framework for extending CXCR4 RLT into NHL, where many patients with relapsed or refractory disease may benefit from a personalized, receptor-directed radiopharmaceutical approach.

5. Present landscape and future directions

Early clinical studies have begun to evaluate how CXCR4-targeted diagnostics compare with standard staging procedures, which patients may benefit from CXCR4-directed RLT, and the safety and efficacy of CXCR4-targeted therapeutic approaches. Present guidelines for MZL staging typically include CT imaging, esophagogastroduodenoscopy, and bone marrow biopsy. A recent study directly compared these standard modalities with CXCR4-targeted PET using ^{68}Ga-pentixafor.[48] Relative to CT-based staging,^{68}Ga-pentixafor PET led to upstaging in a meaningful proportion of patients, resulting in changes to oncologic management through either escalation or de-escalation of treatment. For assessment of gastrointestinal involvement and bone marrow infiltration, CXCR4 PET demonstrated accuracies of 94% and 76.8%, respectively, when benchmarked against esophagogastroduodenoscopy and biopsy. Based on quantitative PET parameters, 18% of patients were considered eligible for CXCR4-targeted RLT. Collectively, these findings suggest that ^{68}Ga-Pentixafor PET may serve as a valuable primary diagnostic tool to augment and, in some cases, replace traditional staging procedures in MZL while also helping identify patients who may benefit from downstream RLT. Early therapeutic studies have also explored CXCR4-directed RLT in aggressive lymphomas. In a small cohort of six previously treated patients with refractory DLBCL, RLT was administered following confirmation of CXCR4 expression on ^{68}Ga-pentixafor PET.[49] Pre-therapeutic dosimetry was used to individualize radioligand dose based on tumor uptake and normal-organ constraints. Estimated achievable tumor doses were up to 5.5 Gy/GBq for ^{177}Lu-pentixather and 16.7 Gy/GBq for ^{90}Y-pentixather; kidney tolerance emerged as the primary limiting factor. Due to its more favorable clearance profile, including a reduction to approximately 750 mGy in the bone marrow by day 14, ^{90}Y-pentixather was selected over ^{177}Lu-pentixather for treatment. Administered activities ranged from 2.8 to 6.4 GBq. All patients experienced complete myeloablation within 8–23 days without acute treatment-related adverse events, and two patients achieved partial antitumor responses. A larger follow-up study of 21 previously treated lymphoma patients receiving ^{90}Y-pentixather RLT reported significant myeloablation, including a mean leukocyte decline of 24.5% from day 0 to day 2 and 79.4% from day 0 to pre-transplant conditioning, along with substantial reductions in LDH as a marker of antitumor activity.[50] Safety evaluation revealed no cases of tumor lysis syndrome and only 2 grade 3–4 adverse events out of 25 events reported, with no grade 5 toxicities. These results support CXCR4-targeted RLT as a feasible approach with meaningful antitumor activity and manageable toxicity and suggest it may serve as an alternative or adjunct conditioning strategy for hematopoietic stem cell transplantation.

As data accumulate on β-emitting CXCR4 radioligands, interest has expanded toward next-generation therapeutic platforms that may overcome limitations of current agents. One promising area involves α-emitting CXCR4 radioligands, particularly ^{225}Ac-based constructs.[51] Alpha particles deliver extremely high linear-energy transfer radiation over a range of only a few cell diameters, producing dense double-strand DNA breaks while minimizing off-target exposure. This mechanism is particularly attractive for infiltrative marrow-based malignancies, such as many NHL subtypes, where β-particle crossfire may be either insufficiently potent or excessively marrow-toxic. Preliminary technical work supports the feasibility of α-emitter CXCR4 constructs, including new methods for quantifying intracellular retention and daughter-nuclide redistribution using direct α-spectroscopy. Despite their promise, α-emitters introduce challenges, such as radionuclide recoil, unpredictable microdosimetry, and complex safety considerations, mandating rigorous preclinical validation before broader clinical use.[51] Nonetheless, if these hurdles are addressed, α-emitters may offer more potent therapy with fewer cycles or lower cumulative doses, expanding the therapeutic window of CXCR4-based strategies.

In addition, advances in CXCR4-targeted therapeutics have expanded beyond radiopharmaceuticals to include

small molecules, peptides, monoclonal antibodies, antibody–drug conjugates (ADCs), and combination regimens. Small-molecule and peptide inhibitors represent an important class within this landscape. Mavorixafor (Xolremdi), an oral CXCR4 antagonist, has been shown to sensitize lymphoma cells to chemotherapy, improving the activity of cytotoxic agents. Motixafortide (BL-8040) has demonstrated inhibition of lymphoma cell proliferation in both *in vitro* and *in vivo* models, supporting its suitability for combination therapy in NHL.[52,53] Monoclonal antibodies and ADCs provide additional receptor-targeted strategies. PF-06747143 and ulocuplumab exhibit strong antitumor activity in preclinical NHL models, particularly when paired with standard treatments.[54] Anti-CXCR4 ADCs have also shown selective cytotoxicity toward CXCR4-expressing lymphoma cells while sparing normal tissues, further supporting receptor-specific targeting for enhanced therapeutic precision.[55] Several combination-based approaches demonstrate synergistic potential. CXCR4 antagonists, combined with anti-CD20 or anti-CD19 antibodies, enhance apoptosis and antibody-dependent cytotoxicity in NHL.[52] A next-generation CXCR4 inverse agonist (IQS-01.01RS), combined with bromodomain inhibitors, such as CPI203, downregulates MYC and AKT signaling, promoting apoptosis and tumor regression in DLBCL.[56] CXCR4 blockade has also been shown to restore sensitivity to immune checkpoint inhibitors, indicating a potential role in combination immunotherapy. Next-generation CXCR4 ligands, including small molecules, peptides, monoclonal antibodies, and ADCs, remain in development for NHL.

Combination strategies also represent an important frontier. Preclinical studies have shown that pharmacologic inhibition of CXCR4 enhances the cytotoxic effects of anti-CD20 antibodies, improving rituximab-mediated killing in DLBCL models and suggesting that CXCR4 blockade modulates microenvironmental resistance mechanisms.[24] Additionally, CXCR4-directed RLT may achieve synergistic effects when combined with myeloablative regimens used before stem cell transplantation, as demonstrated in AML patients receiving high-dose ^{177}Lu-pentixather with stem cell rescue.[46] Early work in solid tumors further suggests that pairing CXCR4-targeted RLT with radiosensitizing agents can augment tumor cell death, offering a theoretical rationale for similar strategies in NHL.[57] Finally, although not yet evaluated in clinical lymphoma studies, CXCR4-directed agents could be combined with immunotherapies, such as CAR-T cells or bispecific antibodies by reducing tumor burden, altering the stromal microenvironment, or facilitating immune-cell trafficking. Such combinations represent promising, albeit still speculative, directions for future clinical trials.

Comprehensive care for cancer patients extends beyond diagnosis and treatment to include intensive monitoring for changes and the need for adjustments in care. Recently, technological developments in the medical field have progressed rapidly and continuously evolved. Among these transformative developments was the introduction of the Internet of Things (IoT) within medical practice, which described the use of Internet-based devices, tools, and applications capable of consuming, producing, processing, and communicating data.[58] Although it has not been addressed in NHL specifically, the use of wearable devices as an application of IoT in cancer patients undergoing treatment serves as a promising tool for monitoring symptoms, tracking adverse effects, and ensuring quality of life. This technology supports the broader goal of comprehensive cancer care that aligns with the principles of theranostics.[59]

In summary, the collective data support a growing role for CXCR4-targeted strategies in staging, response assessment, and therapy across multiple NHL subtypes. For clarity and completeness, Table 1 provides a consolidated summary of CXCR4-targeted diagnostic studies in lymphoma, and Table 2 provides a consolidated summary of CXCR4-targeted therapeutic studies in lymphoma.

6. Limitations

Despite the promise of this emerging form of precision oncology, several key hurdles remain in developing a broadly effective CXCR4-directed theranostic strategy for NHL. First, CXCR4 expression exhibits substantial heterogeneity across tumors and even within individual patients, which can undermine the reliability of imaging for candidate selection and limit therapeutic efficacy.[40,60] This variability is compounded by dynamic regulation of CXCR4 on malignant cells, as antigen downregulation and microenvironment-mediated modulation can occur in response to therapy or disease progression, further reducing the consistency of target expression and complicating real-time imaging–therapy matching.[32,61] In addition, the protective CXCR4/CXCL12 niche, common among AML, ALL, and multiple myeloma, can shield malignant cells from achieving uniform radioligand exposure, limiting the cytotoxic potential of targeted radionuclide delivery.[42,50] Stromal interactions, chemokine gradients, and microenvironmental retention all contribute to therapeutic resistance and may necessitate combination strategies to disrupt niche-mediated protection. Because CXCR4 is physiologically expressed on normal hematopoietic stem and progenitor

Table 1. CXCR4-targeted diagnostic studies in lymphoma

Study/Year	Cancer type	CXCR4 modality	Patients enrolled	Purpose/Key findings	Limitations
Duell *et al*., 2023[48]	MZL	^{68}Ga-pentixafor PET	100	Compared CXCR4 PET with standard staging; PET upstaged some cases; 94% accuracy for GI involvement, 76.8% for marrow; 18% eligible for RLT	Single-center; modest cohort; lacked long-term outcomes; not validated in multicenter trials
Habringer *et al*., 2018[43]	ALL, AML	^{68}Ga-pentixafor PET/^{177}Lu-pentixather	3 refractory AML patients, used cell line-based xenograft ALL mouse models (no human ALL trial patients)	PET imaging with ^{68}Ga-Pentixafor visualized CXCR4^{+}leukemic burden in xenografts; ^{177}Lu-Pentixather reduced leukemia burden in mice; in the 3 AML patients, CXCR4 ERT enabled leukemia clearance and successful second alloSCT	Small clinical sample; preclinical models heavily predominate; no randomized or controlled clinical efficacy data; limited range of cancer types; ALL human data lacking; AML and ALL populations; applicability to NHL extrapolated
Zhang *et al*., 2022[20]	DLBCL, ABC, and non-GCB	CXCR4 expression (immunohistochemistry, mRNA analysis); *in vitro* functional assays using DLBCL cell lines, genomic profiling	N/A, gene expression profiles were obtained from TCGA and GEO databases	CXCR4 was significantly upregulated in DLBCL, particularly in ABC/non-GCB subtypes, and higher CXCR4 expression correlated with adverse clinicopathological features and poorer overall survival; CXCR4 inhibition reduced cell viability *in vitro*	No CXCR4 PET imaging performed; no assessment of CXCR4 mutations; data are on cell viability and requires human validation. Applicability to NHL is extrapolated.
Schottelius *et al*., 2017[41]	B-NHL, AML, and MM	^{177}Lu-pentixather PET	N/A, cell lines	First-in-human CXCR4 imaging; high specificity and favorable dosimetry	Early feasibility; limited subgroup representation

Abbreviations: ABC: Activated B-cell-like lymphoma; ALL: Acute lymphoblastic leukemia; AML: Acute myeloid leukemia; B-NHL: B-cell non-Hodgkin lymphoma; DLBCL: Diffuse large B-cell lymphoma; GEO: Gene expression omnibus; GI: Gastrointestinal; MM: Multiple myeloma; Non-GCB: Nongerminal center B-cell lymphoma; PET: Positron emission tomography; RLT: Radioligand therapy; TCGA: The Cancer Genome Atlas.

Table 2. CXCR4-targeted therapeutic studies in lymphoma

Study/Year	Cancer type	CXCR4 modality/agent	Patients enrolled	Purpose/Key findings	Limitations
Lapa *et al*., 2019[49]	Refractory DLBCL	^{177}Lu-/^{90}Y-pentixather RLT	6	Demonstrated feasibility of CXCR4-targeted RLT; tumor doses up to 5.5 (Lu) and 16.7 (Y) Gy/GBq; complete myeloablation; 2/6 partial responses	Very small sample size; heterogeneous prior treatments; short follow-up
Dreher *et al*., 2024[50]	Relapsed/refractory lymphomas	^{90}Y-pentixather RLT	21	Significant myeloablation and metabolic response; LDH decline; low severe toxicity	Primarily a conditioning study; lacked a randomized comparator; mixed histologies
Braitsch *et al*., 2025[46]	AML (conditioning trial)	High-dose ^{177}Lu-pentixather	7, Not lymphoma patients	Effective tumor debulking; feasible transplant-conditioning approach; supports NHL strategies	AML population; applicability to NHL extrapolated
Farasat *et al*., 2025[51]	Preclinical lymphoma models	225Ac CXCR4 α-therapy	Preclinical	Demonstrated feasibility of α-radionuclide CXCR4 ligands; characterized microdosimetry and recoil	Preclinical only; unknown clinical safety; radionuclide handling challenges
Beider *et al*., 2013[52]	DLBCL, FL (preclinical)	Motixafortide (CXCR4 inhibitor)	N/A, cell lines *in vitro* and *in vivo*	CXCR4 blockade inhibited proliferation; synergized with chemotherapy and anti-CD20 antibodies	Preclinical; clinical dosing/toxicity unknown
Martino *et al*., 2024[53]	Translational lymphoma cohorts	Motixafortide	Not specified, overview of early phase cohort, preclinical	Enhanced sensitivity to cytotoxic and immune therapies; supports combination strategies	Early-phase; limited lymphoma-specific clinical endpoints

(Cont'd...)

Table 2. ***(Continued)***

Study/Year	Cancer type	CXCR4 modality/agent	Patients enrolled	Purpose/Key findings	Limitations
Cancilla *et al*., 2020[54]	NHL models	Anti-CXCR4 monoclonal antibodies	Preclinical	Strong single-agent activity; improved ADCC with standard therapies	Preclinical; antibody pharmacokinetics not assessed clinically
Costa *et al*., 2019[55]	Lymphoma xenografts	CXCR4-targeted ADCs	Preclinical	Selective killing of CXCR4+lymphoma cells; low off-target toxicity	Preclinical; safety, dosing, immunogenicity unknown
Recasens-Zorzo *et al*., 2019[56]	MYC-high DLBCL	CXCR4 inverse agonist+BET inhibitor	Preclinical	Combination suppressed MYC/AKT signaling; induced apoptosis and tumor regression	Pre-clinical; requires human validation
Reinholdt *et al*., 2016[24]	DLBCL	CXCR4 blockade+ rituximab	Preclinical	CXCR4 inhibition enhanced rituximab-mediated killing; reduced microenvironmental resistance	Mechanistic; no clinical translation
Fath *et al*., 2024[57]	Solid-tumor models	CXCR4-targeted RLT+ radiosensitizers	Preclinical	Radiosensitizer-enhanced RLT potency; theoretical NHL applicability	Not lymphoma; requires hematologic validation

Abbreviations: ADCC: Antibody-dependent cellular cytotoxicity; AML: Acute myeloid leukemia; BET: Bromodomain; CD: Cluster of differentiation; DLBCL: Diffuse large B-cell lymphoma; FL: Follicular lymphoma; LDH: Lactate dehydrogenase; NHL: Non-Hodgkin lymphoma; RLT: Radioligand therapy.

cells, targeted RLT also presents a substantial risk of hematologic toxicity. Profound myelosuppression, leukopenia, and prolonged marrow aplasia have been documented across early clinical experiences, with several studies highlighting the need for stem cell support or transplantation rescue due to dose-limiting marrow injury.[50,62] Pharmacokinetic and radiochemical limitations further constrain theranostic performance. CXCR4-targeting radioligands may exhibit rapid systemic clearance, radiolabel instability, insufficient tumor penetration, or off-target uptake, all of which compromise therapeutic index and make individualized dosimetry challenging.[63,64] Finally, widespread clinical adoption of CXCR4 theranostics requires specialized radiopharmacy infrastructure, harmonized manufacturing processes, and integration with transplant and supportive-care pathways. Long-term toxicity data remain incomplete, and robust biomarkers for patient selection and response prediction are still evolving.[40,64]

7. Conclusion

The CXCR4/CXCL12 axis represents a critical regulator of lymphocyte trafficking, survival, and tumor microenvironment interactions in NHL, making it an attractive target for precision oncology. Theranostic strategies that exploit CXCR4 allow simultaneous molecular imaging and targeted radionuclide therapy, enabling real-time assessment of receptor expression, patient stratification, and personalized treatment delivery. Preclinical and early clinical studies, including the use of ^{177}Lu-pentixather and CXCR4-targeted ADCs, have demonstrated selective tumor targeting, potent antitumor efficacy, and favorable tolerability, supporting the feasibility of this approach in both disseminated and nodal disease. By integrating diagnostic and therapeutic modalities, CXCR4-directed theranostics has the potential to refine current NHL management, complementing chemotherapy, stem cell transplantation, and immunotherapy while minimizing off-target toxicity. Despite these promising results, translation into routine clinical practice remains limited by the small size of early studies and the lack of large-scale, randomized trials. Future research should focus on well-powered clinical trials to validate efficacy, optimize dosing and imaging protocols, and assess long-term safety. Moreover, integration into standard-of-care pathways will require harmonization with existing therapies, development of patient selection criteria, and exploration of combination strategies to fully realize the potential of CXCR4 theranostics as a precision medicine tool in NHL.

Acknowledgments

None.

Funding

None.

Conflict of interest

The authors declare that they have no competing interests.

Author contributions

Conceptualization: Marcus Yoakam, Samir Dalia
Writing – original draft: Marcus Yoakam, Uma A. Obalapuram, Kameron Hahn
Writing – review & editing: All authors

Ethics approval and consent to participate

Not applicable.

Consent for publication

Not applicable.

Availability of data

Not applicable.

References

1. Armitage JO, Gascoyne RD, Lunning MA, Cavalli F. Non-Hodgkin lymphoma. *Lancet*. 2017;390(10091):298-310.
doi: 10.1016/S0140-6736(16)32407-2
2. Lewis WD, Lilly S, Jones KL. Lymphoma: Diagnosis and treatment. *Am Fam Physician*. 2020;101(1):34-41.
3. Stegemann M, Denker S, Schmitt CA. DLBCL 1L-what to expect beyond R-CHOP? *Cancers (Basel)*. 2022;14(6):1453.
doi: 10.3390/cancers14061453
4. Susanibar-Adaniya S, Barta SK. 2021 Update on Diffuse large B cell lymphoma: A review of current data and potential applications on risk stratification and management. *Am J Hematol*. 2021;96(5):617-629.
doi: 10.1002/ajh.26151
5. Crombie JL, Jun MP, Wang T, *et al*. Real-world outcomes with novel therapies in R/R DLBCL. *J Clin Oncol*. 2023;41(16_suppl):7552.
doi: 10.1200/JCO.2023.41.16_suppl.7552
6. Silkenstedt E, Salles G, Campo E, Dreyling M. B-cell non-Hodgkin lymphomas. *Lancet*. 2024;403(10438):1791-1807.
doi: 10.1016/S0140-6736(23)02705-8
7. Rivero A, Mozas P, Magnano L, López-Guillermo A. Novel targeted drugs for follicular and marginal zone lymphoma: A comprehensive review. *Front Oncol*. 2023;13:1170394.
doi: 10.3389/fonc.2023.1170394
8. Pytlik R, Polgarova K, Karolova J, Klener P. Current immunotherapy approaches in Non-Hodgkin lymphomas. *Vaccines (Basel)*. 2020;8(4):708.
doi: 10.3390/vaccines8040708
9. Huang J, Huang X, Huang J. CAR-T cell therapy for hematological malignancies: Limitations and optimization strategies. *Front Immunol*. 2022;13:1019115.
doi: 10.3389/fimmu.2022.1019115
10. Aiuti A, Webb IJ, Bleul C, Springer T, Gutierrez-Ramos JC. The chemokine SDF-1 Is a chemoattractant for human CD34+ hematopoietic progenitor cells and provides a new mechanism to explain the mobilization of CD34+ progenitors to peripheral blood. *J Exp Med*. 1997;185(1):111-120.
doi: 10.1084/jem.185.1.111
11. Christopher MJ, Liu F, Hilton MJ, Long F, Link DC. Suppression of CXCL12 production by bone marrow osteoblasts is a common and critical pathway for cytokine-induced mobilization. *Blood*. 2009;114(7):1331-1339.
doi: 10.1182/blood-2008-10-184754
12. Bai Z, Hayasaka H, Kobayashi M, *et al*. CXC chemokine ligand 12 promotes CCR7-dependent naive T cell trafficking to lymph nodes and Peyer's patches. *J Immunol*. 2009;182(3):1287-1295.
doi: 10.4049/jimmunol.182.3.1287
13. Okada T, Ngo VN, Ekland EH, *et al*. Chemokine requirements for b cell entry to lymph nodes and Peyer's patches. *J Exp Med*. 2002;196(1):65-75.
doi: 10.1084/jem.20020201
14. Allen CDC, Ansel KM, Low C, *et al*. Germinal center dark and light zone organization is mediated by CXCR4 and CXCR5. *Nat Immunol*. 2004;5(9):943-952.
doi: 10.1038/ni1100
15. Vitiello L, Ferraro E, De Simone S, *et al*. CXCL12 prolongs naive CD4+ T lymphocytes survival via activation of PKA, CREB and Bcl2 and BclXl up-regulation. *Int J Cardiol*. 2016;224:206-212.
doi: 10.1016/j.ijcard.2016.09.007
16. Ganju RK, Brubaker SA, Meyer J, *et al*. The alpha-chemokine, stromal cell-derived factor-1alpha, binds to the transmembrane G-protein-coupled CXCR-4 receptor and activates multiple signal transduction pathways. *J Biol Chem*. 1998;273(36):23169-23175.
doi: 10.1074/jbc.273.36.23169
17. Teixidó J, Martínez-Moreno M, Díaz-Martínez M, Sevilla-Movilla S. The good and bad faces of the CXCR4 chemokine receptor. *Int J Biochem Cell Biol*. 2018;95:121-131.
doi: 10.1016/j.biocel.2017.12.018
18. Bertolini F, Dell'Agnola C, Mancuso P, *et al*. CXCR4 neutralization, a novel therapeutic approach for Non-Hodgkin's lymphoma1. *Cancer Res*. 2002;62(11):3106-3112.
19. Chen J, Xu-Monette ZY, Deng L, *et al*. Dysregulated CXCR4 expression promotes lymphoma cell survival and independently predicts disease progression in germinal center B-cell-like diffuse large B-cell lymphoma. *Oncotarget*. 2015;6(8):5597-5614.

doi: 10.18632/oncotarget.3343

20. Zhang YA, Yang X, Yao J, Ren Y, Liu P. Identification of CXCR4 upregulation in diffuse large B-cell lymphoma associated with prognostic significance and clinicopathological characteristics. *Dis Markers*. 2022;2022:3276925.

doi: 10.1155/2022/3276925

21. Pan Q, Luo Y, Zhang Y, *et al*. Preliminary evidence of imaging of chemokine receptor-4-targeted PET/CT with [68Ga]pentixafor in non-Hodgkin lymphoma: Comparison to [18F]FDG. *EJNMMI Res*. 2020;10(1):89.

doi: 10.1186/s13550-020-00681-7

22. Kosmala A, Duell J, Schneid S, *et al*. Chemokine receptor-targeted PET/CT provides superior diagnostic performance in newly diagnosed marginal zone lymphoma patients: A head-to-head comparison with [18F]FDG. *Eur J Nucl Med Mol Imaging*. 2024;51(3):749-755.

doi: 10.1007/s00259-023-06489-6

23. Moreno MJ, Bosch R, Dieguez-Gonzalez R, *et al*. CXCR4 expression enhances diffuse large B cell lymphoma dissemination and decreases patient survival. *J Pathol*. 2015;235(3):445-455.

doi: 10.1002/path.4446

24. Reinholdt L, Laursen MB, Schmitz A, *et al*. The CXCR4 antagonist plerixafor enhances the effect of rituximab in diffuse large B-cell lymphoma cell lines. *Biomark Res*. 2016;4:12.

doi: 10.1186/s40364-016-0067-2

25. Langbein T, Weber WA, Eiber M. Future of theranostics: An outlook on precision oncology in nuclear medicine. *J Nucl Med*. 2019;60(Suppl 2):13S-19S.

doi: 10.2967/jnumed.118.220566

26. Ayalew BD, Abdullah, Khan SM, *et al*. Role of emerging theranostic technologies in precision oncology: Revolutionizing cancer diagnosis and treatment. *Oncologie*. 2025;27(2):229-238.

doi: 10.1515/oncologie-2024-0543

27. Hameed MY, Gul M, Chaudhry A, *et al*. From oncogenesis to theranostics: The transformative role of PSMA in prostate cancer. *Cancers (Basel)*. 2024;16(17):3039.

doi: 10.3390/cancers16173039

28. Iravani A, Violet J, Azad A, Hofman MS. Lutetium-177 prostate-specific membrane antigen (PSMA) theranostics: Practical nuances and intricacies. *Prostate Cancer Prostatic Dis*. 2020;23(1):38-52.

doi: 10.1038/s41391-019-0174-x

29. Sellmyer MA, Lee IK, Mankoff DA. Building the bridge: Molecular imaging biomarkers for 21st century cancer therapies. *J Nucl Med*. 2021;62(12):1672-1676.

doi: 10.2967/jnumed.121.262484

30. Zhang S, Wang X, Gao X, *et al*. Radiopharmaceuticals and their applications in medicine. *Sig Transduct Target Ther*. 2025;10(1):1.

doi: 10.1038/s41392-024-02041-6

31. Bogdanovic B, Hugonnet F, Montemagno C. Theranostics in hematological malignancies: Cutting-edge advances in diagnosis and targeted therapy. *Cancers (Basel)*. 2025;17(7):1247.

doi: 10.3390/cancers17071247

32. Parakh S, Lee ST, Gan HK, Scott AM. Radiolabeled antibodies for cancer imaging and therapy. *Cancers (Basel)*. 2022;14(6):1454.

doi: 10.3390/cancers14061454

33. Chen Z, Xue Q, Yao S. Nuclear medicine application of pentixafor/pentixather targeting CXCR4for imaging and therapy in related disease. *Mini Rev Med Chem*. 2023;23(7):787-803.

doi: 10.2174/1389557523666221216095821

34. Lindenberg L, Ahlman M, Lin F, Mena E, Choyke P. Advances in PET imaging of the CXCR4 receptor: [68Ga] Ga-PentixaFor. *Semin Nucl Med*. 2024;54(1):163-170.

doi: 10.1053/j.semnuclmed.2023.09.002

35. Buck AK, Haug A, Dreher N, *et al*. Imaging of C-X-C motif chemokine receptor 4 expression in 690 patients with solid or hematologic neoplasms using 68Ga-pentixafor PET. *J Nucl Med*. 2022;63(11):1687-1692.

doi: 10.2967/jnumed.121.263693

36. Chavoshi M, Mirshahvalad SA, Kohan A, *et al*. CXCR4-targeted PET imaging in hematologic malignancies: A systematic review and meta-analysis. *Clin Nucl Med*. 2025;50(1):e7-e16.

doi: 10.1097/RLU.0000000000005426

37. Mayerhoefer ME, Raderer M, Weber M, *et al*. 68Ga-pentixafor PET/MRI for treatment response assessment in mantle cell lymphoma: Comparison between changes in lesion CXCR4 expression on PET and lesion size and diffusivity on MRI. *Clin Nucl Med*. 2023;48(7):557-562.

doi: 10.1097/RLU.0000000000004638

38. Wang W, Huang M, Tian R, Shen G. Head-to-head comparison of 68Ga-PentixaFor PET/CT and FDG PET/CT for detecting hematologic and solid cancers: A systematic review and meta-analysis. *AJR Am J Roentgenol*. 2025;225(2):e2532708.

doi: 10.2214/AJR.25.32708

39. Albano D, Dondi F, Bertagna F, Treglia G. The role of [68Ga]Ga-Pentixafor PET/CT or PET/MRI in lymphoma: A systematic review. *Cancers (Basel)*. 2022;14(15):3814.

doi: 10.3390/cancers14153814

40. Buck AK, Serfling SE, Kraus S, *et al*. Theranostics in hematooncology. *J Nucl Med*. 2023;64(7):1009-1016.

doi: 10.2967/jnumed.122.265199

41. Schottelius M, Osl T, Poschenrieder A, *et al*. [177Lu] pentixather: Comprehensive preclinical characterization of a first CXCR4-directed endoradiotherapeutic agent. *Theranostics*. 2017;7(9):2350-2362.

doi: 10.7150/thno.19119

42. Rahimian S, Najafi H, Doroudian M. CXCR4-targeted theranostics in acute leukemia: Disrupting leukemic cell-microenvironment interactions with pentixafor and pentixather. *Med Oncol*. 2025;42(9):402.

doi: 10.1007/s12032-025-02924-w

43. Habringer S, Lapa C, Herhaus P, *et al*. Dual targeting of acute leukemia and supporting niche by CXCR4-directed theranostics. *Theranostics*. 2018;8(2):369-383.

doi: 10.7150/thno.21397

44. Hänscheid H, Schirbel A, Hartrampf P, *et al*. Biokinetics and dosimetry of [177Lu]Lu-pentixather. *J Nucl Med*. 2022;63:754-760.

doi: 10.2967/jnumed.121.262295

45. Mulita A, Valsamaki P, Bekou E, *et al*. Benefits from 18F-FDG PET-CT-based radiotherapy planning in stage III non-small-cell lung cancer: A prospective single-center study. *Cancers (Basel)*. 2025;17(12):1969.

doi: 10.3390/cancers17121969

46. Braitsch K, Lorenzini T, Hefter M, *et al*. CXCR4-directed endoradiotherapy with [177Lu]Pentixather added to total body irradiation for myeloablative conditioning in patients with relapsed/refractory acute myeloid leukemia. *Theranostics*. 2025;15(1):19-29.

doi: 10.7150/thno.101215

47. Buck AK, Serfling SE, Lindner T, *et al*. CXCR4-targeted theranostics in oncology. *Eur J Nucl Med Mol Imaging*. 2022;49(12):4133-4144.

doi: 10.1007/s00259-022-05849-y

48. Duell J, Buck AK, Hartrampf PE, *et al*. Chemokine receptor PET/CT provides relevant staging and management changes in marginal zone lymphoma. *J Nucl Med*. 2023;64(12):1889-1894.

doi: 10.2967/jnumed.123.266074

49. Lapa C, Hänscheid H, Kircher M, *et al*. Feasibility of CXCR4-directed radioligand therapy in advanced diffuse large B-cell lymphoma. *J Nucl Med*. 2019;60(1):60-64.

doi: 10.2967/jnumed.118.210997

50. Dreher N, Dörrler AL, Kraus S, *et al*. C-X-C motif chemokine receptor 4-targeted radioligand therapy in hematological malignancies-myeloablative effects, antilymphoma activity, and safety profile. *Clin Nucl Med*. 2024;49(2):146-151.

doi: 10.1097/RLU.0000000000004974

51. Farasat M, Saeedi B, Wharton L, *et al*. Novel Direct Alpha Spectroscopy Technique for ^{225}Ac Radiopharmaceutical Detection in Cancer Cells. *arXiv*. Preprint Posted Online; 2025.

doi: 10.48550/ARXIV.2501.10608

52. Beider K, Ribakovsky E, Abraham M, *et al*. Targeting the CD20 and CXCR4 pathways in non-hodgkin lymphoma with rituximab and high-affinity CXCR4 antagonist BKT140. *Clin Cancer Res*. 2013;19(13):3495-3507.

doi: 10.1158/1078-0432.CCR-12-3015

53. Martino EA, Bruzzese A, Labanca C, *et al*. Investigational CXCR4 inhibitors in early phase development for the treatment of hematological malignancies. *Expert Opin Investig Drugs*. 2024;33(9):915-924.

doi: 10.1080/13543784.2024.2388567

54. Cancilla D, Rettig MP, DiPersio JF. Targeting CXCR4 in AML and ALL. *Front Oncol*. 2020;10:1672.

doi: 10.3389/fonc.2020.01672

55. Costa MJ, Kudaravalli J, Ma JT, *et al*. Optimal design, anti-tumour efficacy and tolerability of anti-CXCR4 antibody drug conjugates. *Sci Rep*. 2019;9(1):2443.

doi: 10.1038/s41598-019-38745-x

56. Recasens-Zorzo C, Cardesa-Salzmann T, Petazzi P, *et al*. Pharmacological modulation of CXCR4 cooperates with BET bromodomain inhibition in diffuse large B-cell lymphoma. *Haematologica*. 2019;104(4):778-788.

doi: 10.3324/haematol.2017.180505

57. Fath MA, Liu D, Ewald JT, *et al*. Chemokine receptor CXCR4 radioligand targeted therapy using 177Lutetium-pentixather for pulmonary neuroendocrine cancers. *Radiat Res*. 2024;201(1):35-47.

doi: 10.1667/RADE-23-00064.1

58. Mulita F, Verras GI, Anagnostopoulos CN, Kotis K. A smarter health through the internet of surgical things. *Sensors (Basel)*. 2022;22(12):4577.

doi: 10.3390/s22124577

59. Albino de Queiroz D, André da Costa C, Aparecida Isquierdo Fonseca de Queiroz E, Folchini da Silveira E, da Rosa Righi R. Internet of things in active cancer treatment: A systematic review. *J Biomed Inform*. 2021;118:103814.

doi: 10.1016/j.jbi.2021.103814

60. Martin M, Mayer IA, Walenkamp AME, Lapa C, Andreeff M, Bobirca A. At the bedside: Profiling and treating patients with CXCR4-expressing cancers. *J Leukoc Biol*. 2021;109(5):953-967.

doi: 10.1002/JLB.5BT1219-714R

61. Etrych T, Braunova A, Zogala D, Lambert L, Renesova N, Klener P. Targeted drug delivery and theranostic strategies in malignant lymphomas. *Cancers (Basel)*. 2022;14(3):626.

doi: 10.3390/cancers14030626

62. Maurer S, Herhaus P, Lippenmeyer R, *et al.* Side effects of CXC-chemokine receptor 4-directed endoradiotherapy with pentixather before hematopoietic stem cell transplantation. *J Nucl Med*. 2019;60(10):1399-1405.

doi: 10.2967/jnumed.118.223420

63. Yang T, Shi D, Lin Q, *et al*. Synthesis, screening, and evaluation of theranostic molecular CPCR4-based probe targeting CXCR4. *Mol Pharmaceutics*. 2024;21(5):2415-2424.

doi: 10.1021/acs.molpharmaceut.3c01221

64. Buck AK, Stolzenburg A, Hänscheid H, *et al*. Chemokine receptor – Directed imaging and therapy. *Methods*. 2017;130:63-71.

doi: 10.1016/j.ymeth.2017.09.002

ACCSCIENCE PUBLISHING

Advances in Radiotherapy & Nuclear Medicine

ORIGINAL RESEARCH ARTICLE

Utilization of teleradiology services for healthcare delivery in Saudi Arabia

Sonal Arjuna[1], Neetika Mathur[2]*, Muktha Rawath[2], and Arjun Kalyanpur[1]

[1]Department of Clinical Radiology, Teleradiology Solutions, Ardmore, Pennsylvania, United States of America

[2]Department of Clinical Research, Teleradiology Solutions, Bengaluru, Karnataka, India

Abstract

Teleradiology, an innovative and disruptive technology, has demonstrated a track record in enhancing remote healthcare delivery in multiple clinical and healthcare settings. With the aim of understanding the impact of teleradiology on healthcare delivery in Saudi Arabia, a retrospective descriptive study was carried out between January 2014 and January 2024. Over the 10 years, 103,730 scans were transmitted for interpretation, thus providing consistent remote healthcare delivery in the Kingdom of Saudi Arabia (KSA). The highest category of scans was computed tomography (45.96%), followed by radiographs (40.27%), magnetic resonance imaging (9.06%), mammograms (4.17%), ultrasound (0.53%), and nuclear medicine (NM) (0.01%). For the study, global turnaround time (TAT) was calculated as the interval between submission of examination to the time report available online, and/or verbal confirmation of results, with a mean time of 19.48 h (95% confidence interval: 19.39–19.56), which is seminal under teleradiology in KSA. The outcomes reflect the use of teleradiology across different clinical locations and the criticality of care, whereas TAT was within accepted local and global standards. Previously published value-addition of teleradiology includes after-hours coverage and use during the COVID-19 pandemic. In the context of KSA, teleradiology using public–private partnership model supports equitable access to underserved areas while maintaining TAT, aligned with KSA Vision 2030 healthcare goals. The current study postulates that teleradiology connectivity may help complement on-site radiologists, optimize and enhance workflow, provide on-demand staffing solutions for ever-growing radiology examinations, while incremental use of round-the-clock subspecialists can help in second opinions, and address quality assurance, such as peer review, all aiding improved healthcare outcomes in KSA hospitals.

Keywords: Teleradiology; Radiology; Healthcare; Global turnaround time; Saudi Arabia; KSA Vision 2030

***Corresponding author:**
Neetika Mathur
(neetika.mathur@imagecorelab.com)

Citation: Arjuna S, Mathur N, Rawath M, Kalyanpur A, 2025, Utilization of teleradiology services for healthcare delivery in Saudi Arabia. *Adv Radiother Nucl Med*. 2026;4(1):46-56.
doi: 10.36922/ARNM025270033

Received: July 1, 2025

Revised: October 30, 2025

Accepted: November 18, 2025

Published online: December 4, 2025

1. Introduction

Telehealth is a leading-edge concept, utilizing information with telecommunication technologies in the realm of clinical services, to provide support for patients, physicians, and other healthcare professionals remotely. Teleradiology, a domain of telehealth services, involves the acquisition, transmission, and interpretation of diagnostic images

by a radiologist from a distant location. The implementation of teleradiology is primarily aimed at improving access to radiological diagnostics and reporting, especially in remote and underserved areas, thus enhancing overall healthcare delivery.[1] Teleradiology, with its unique, innovative, and disruptive technology, has demonstrated a track record that enhances overall healthcare delivery. It permits radiologists to render services remotely to the patient's location, aiding in seamless and efficient healthcare delivery. Studies have shown the pivotal role played by teleradiology globally in improving accessibility, accuracy, and efficiency, and delivering high-quality healthcare in remote geographical settings.[2-7] There has been an increase in volume of radiology examinations year-on-year,[8] including those performed after-hours, along with the rising demand for subspecialty radiology interpretations. Some of these factors have revolutionized radiology into a round-the-clock service, calling for expert radiologists to be available besides their regular working hours or after hours, including nights, weekends, and holidays. This continuous demand can put a substantial load on conventional on-site radiology services. Teleradiology has arisen as a vital solution, allowing seamless conveyance of diagnostic services over time zones and geographies, addressing these issues. Various studies have outlined the manifold merits of teleradiology with its inceptive role of "nighthawk" or after-hours reporting.[9,10] One of the most important benefits lies in enhanced turnaround times (TATs), assuring that emergency departments and urgent inpatient services receive rapid, high-quality imaging assessments, thereby facilitating timely patient management.[11,12]

Through teleradiology services, health establishments can gain consultations from radiologists with core competencies in neuroradiology, musculoskeletal imaging, thoracic imaging, and other subspecialties that may be inaccessible on-site, specifically in resource-constrained environments. This access improves diagnostic accuracy and certainty in treatment decision-making. Further dimension value of teleradiology lies in the provision for second opinions and collaborative reporting, which enrich clinical discussions and aid in complicated case management.

Furthermore, teleradiology offers to diminish radiologist burnout issues by streamlining workflows, optimizing the radiologist workforce, and balancing workloads across centers. It allows radiologists to adjust their work shifts to accommodate home responsibilities, such as child or elderly care, improving their quality of life.[8,13,14]

The most recent COVID-19 pandemic also served as an impetus for integrating teleradiology services for improved and efficient health care delivery in multiple clinical locations in the world. Multiple studies reported a rise in workload and work-related stress among healthcare professionals during the COVID-19 pandemic. With travel restrictions, social distancing norms, and an overwhelmed healthcare system, there was an urgent requirement for remote diagnostic solutions. Teleradiology appeared as a pivotal tool, permitting radiologists to interpret medical images and deliver timely reports to remote locations. This ensured uninterrupted diagnostic support, lowered TATs, and minimized exposure risks for both healthcare workers and patients.[15,16]. In the Middle East, multiple nations, including Iraq, Yemen, Syria, and Egypt, have been known to implement pertinent IT technologies, policies, and guidelines to promote the use of telemedicine programs. However, the progress of telemedicine is limited and slow, in part due to the complexity and diversity of societal and cultural backgrounds in the Middle East region. A study by Al-Samarraie *et al.*[17] reported that a number of technological, organizational, legal, cultural, traditional beliefs, literacy-related, linguistic, financial, individual, and regulatory barriers impede the full application of telemedicine and provision of the entire spectrum of medical services. For example, Arabi *et al.*[18] published the use of emails and social media applications, instead of traditional teleradiology methods, by a teleradiology group to deliver radiology services to Syrian patients, due to the absence of Picture Archiving and Communication Systems (PACSs). Clinicians and radiologists leverage Internet connectivity to conduct consultations and interpret reports directly, enabling timely and efficient patient care. However, the suboptimal quality of images due to weak technique and lack of contrast presented a significant challenge. The introduction of teleradiology services to underserved areas, particularly rural regions with low human resources, in the United Arab Emirates, Kingdom of Saudi Arabia (KSA), Jordan, and Lebanon in 1994 was met with mixed results due to the uneven distribution of radiologists with higher concentration in major cities.[19] In the context of KSA, which is the largest country in the Middle East, yet with a dispersed population, equitable access to basic and advanced radiology services is difficult to achieve in all segments. Moreover, KSA too faces a shortage of radiologists, with only 3255 radiologists for its population of 34 million, resembling the shortages elsewhere in the world.[20-23] KSA Vision 2030 seeks to diversify and privatize various sectors to transform the national economy. Within the healthcare sector, radiology has emerged as a strategic area of public–private partnership (PPP)–based modernization, in particular areas of digital health and specialized imaging networks.[24]

These challenges can be addressed through teleradiology, which leverages disruptive technology and board-certified

radiologists—including trained subspecialists—to effectively deliver quality reports across diverse healthcare settings. This includes underserved areas, emergency room (ER) services, and both inpatient and outpatient settings, for imaging studies of both acute and non-acute criticality, all in alignment with healthcare goals of KSA Vision 2030. Such a practice can address the shortage of radiologists and enable the provision of remote, round-the-clock, seamless healthcare by teleradiologists.

Over the last 10 years, the advancements in digital healthcare and the necessity to deliver prompt and accurate diagnostic services, especially in rural and underserved areas, have led to the tremendous growth in utilization of teleradiology services in Saudi Arabia. The Ministry of Health (MOH) is responsible for regulating the healthcare system and providing healthcare services across the country. Saudi Arabia allocates a significant amount of its budgetary expenditure to the healthcare and social development sectors, which amounted to US$45.5 billion in 2020, putting these sectors in the top spending categories.[25] The KSA Vision 2030 Plan aims to increase efficiency and invest over $65 billion to develop the country's healthcare infrastructure, reorganize and privatize health services and insurance, launch 21 "health clusters" across the country, and expand the provision of e-health services.[26] According to a study by Alahmad *et al.*,[27] 2024, teleradiology services are widely utilized in a variety of healthcare settings, including the MOH, non-MOH governmental hospitals, and private healthcare providers. In 2022, there were approximately 1800 radiologists working under the MOH in the Kingdom of Saudi Arabia. In addition to the MOH, 686 and 1700 radiologists worked in other government-funded and private institutions, respectively. Overall, there were a total of 3804 radiologists in the country, across all sectors.[28]

Despite its growing adoption, the utilization of teleradiology faces several challenges. A study by Khalifa *et al.*[29] revealed that the use of Electronic Medical Records and Health Information Systems has proven beneficial in medical and healthcare practices; however, healthcare professionals opposed the implementation of these systems. Despite the effectiveness and affordability of teleradiology, the primary barrier to its implementation in many Middle East and Northern Africa countries is the high cost of the software and hardware tools required to transmit radiological images.[30-32] Further, radiologists have expressed concerns about the quality and security of digital imaging, the need for robust IT infrastructure, and the potential for reduced diagnostic accuracy compared to in-person evaluations. There are also concerns about legal and regulatory issues, including patient confidentiality and data protection, which have also been reported elsewhere in the world.[33] A study by Zarei and Sharifat[34] in Iran indicated the lack of PACS and economic constraints as major challenges to the implementation of teleradiology. They suggested that the provision of financial incentives by the government and the development of telecommunication infrastructure, along with increased awareness of the benefits of teleradiology, such as physicians' recommendations, could contribute to the development of this technology in hospitals.[34] Moreover, inter-professional collaborations between the stakeholders, namely radiographers, on-site physicians, and radiologists, and a teleradiology service provider that offers guidance and training, may further enhance patient care.[35,36]

Within the last few years, the utilization of teleradiology by hospitals and diagnostic centers in Saudi Arabia has seen a dramatic rise, with improved telecommunications connectivity across the country. In a survey conducted to assess the perceptions of teleradiology among radiologists in Saudi Arabia, around 74% of participants perceived teleradiology to be beneficial for geographic, after-hour, and subspecialty coverage. Teleradiology was also perceived to help reduce the TAT of radiology interpretations.[27] Another survey concluded teleradiology to be a cost-effective solution, while enhancing accessibility, TAT, and quality reporting to remote locations.[37] Benefits of teleradiology for patients in the Middle East have been documented by several recent studies.[27,37-40] The current study aims to demonstrate the utilization of teleradiology practice in healthcare delivery in Saudi Arabia.

2. Materials and methods

With the aim of understanding the impact of teleradiology services on healthcare delivery in Saudi Arabia, a retrospective descriptive study was carried out between January 2014 and January 2024. The study involved the analysis of images originating from the Saudi Arabia–based healthcare system by a teleradiology service provider, founded in the USA. Over a period of 10 years, teleradiology services were consistently offered to different locations in KSA. The imaging modalities evaluated included computed tomography (CT), magnetic resonance imaging (MRI), ultrasonography (US), radiography (XR/CR), and mammogram (MG).

The telereporting workflow platform "RADspa," essentially incorporating a cloud-based Radiology Information System (RIS)/Picture Archival and Communication System (PACS) system, was utilized to transmit the DICOM images of the scans over a high-speed internet connection. The images were accessed

and interpreted by a pool of Western board-certified radiologists, including subspecialists in different body regions and modalities, and the medical reports were uploaded onto the same telereporting platform. The details related to the patient demographics, such as age and gender, previous reports and imaging, along with the details of the patient's presenting clinical signs and symptoms, and relevant medical history, were also uploaded into the RIS to allow for seamless reporting by the radiologist.

A descriptive analysis of the age, gender, and total number of patients/scans was performed. An analysis of the number of studies for different modalities and body regions was conducted. The patient location-based categorization of studies was listed as ER, outpatient, and inpatient locations from the dataset, whereas the criticality of the study was labeled as acute and non-acute, as pre-defined on the image requisition form from the hospital. Subsequently, the mean global turnaround time (gTAT) was calculated. For the purpose of the study, gTAT is defined as the time interval between the study being submitted for reporting from the hospital site to the time at which the report was available online or the results were confirmed through verbal communication. Therefore, it encompasses all aspects of the processes, including radiological as well as operational and technical. Some of which include, but are not limited to, lack of prior images and/or reports at time of reporting, incomplete set of diagnostic images, which have to be re-sent, complex cases requiring additional time to review and report, and occasionally extended waiting time for verbal confirmation of results to the healthcare providers. The gTAT had been previously agreed to be within 24 h for acute cases (including 2 h initial report time for all acute cases) and 48 h for routine cases, following mutual agreement between the healthcare entity and the teleradiology provider.

A retrospective analysis of radiology reports was performed to list the common acute findings in different body regions and across different modalities of radiology examinations. The peer review process was performed daily by technicians with experience of over 3 years and subspecialist radiologists for specialized examinations, and data spanning 2 years were reviewed for this study.

An approval was obtained from the institutional review board for this retrospective descriptive study. The ethical approval was not required as no patient information was involved in our analyses.

3. Results

Over a period of 10 years, a total of 103,730 scans were transmitted to the teleradiology service provider for interpretation. Among these, 97,524 scans were from a hospital at location A (smaller city) and 6206 scans were from location B (bigger city). The mean age of the patients was 47.39 years (95% confidence interval [CI]: 47.26–47.51). The median age of the patient was 50 years. The majority of the patients (37.7%) were aged in the range of 41–60 years. 51.30% (29,457) were males, whereas 48.70% (27,964) were females. There was a total of 57,421 patients from both hospitals, with 63% of the patients who had undergone single imaging and the remainder (37%) who had undergone concurrent multiple imaging studies or follow-up imaging.

Table 1 summarizes that CT scans accounted for 47,669 studies (45.96%) of all imaging examinations. Radiographs (computed radiography/direct digital radiography [CR/DX]) were the next most common modality, with 41,776 studies (40.27%), followed by MRI with 9397 studies (9.06%). Mammograms (MG) comprised 4326 studies (4.17%), ultrasounds 551 scans (0.53%), and NM 11 studies (0.01%).

Table 2 analyzes the distribution of studies among various body regions and across different modalities of radiological imaging. Within CT studies, cranial CTs (31%) were the most frequently requested examinations, followed by CT abdomen and pelvis (21%) and CT chest studies (17%). Under radiographs, the highest number of studies were of chest radiographs (34%), followed by lower (31%) and upper (15%) extremity radiographs.

The data analysis of the patient location for which teleradiology services were provided revealed that 65.81% studies were from the outpatient setting, whereas 26.13% of studies were ordered from the emergency setting, and inpatient studies amounted to 8.07% of the total (Figure 1).

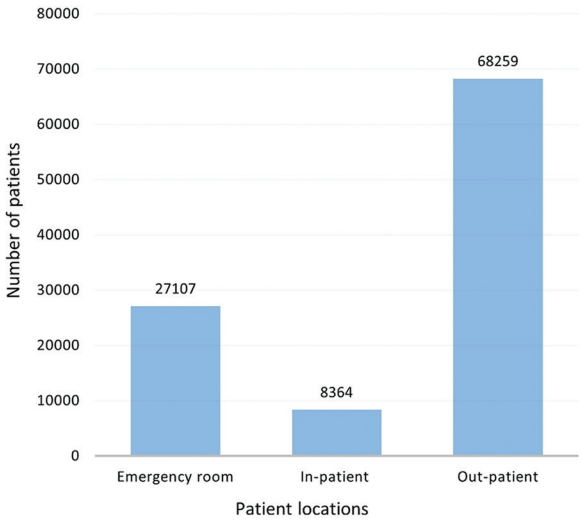

Figure 1. Distribution of cases based on patient location

Table 1. Distribution of imaging modalities across different descriptive metrics, including age, sex, and geographic region within the country

Descriptive metrics	Modality					
	CR/DX	CT	MG	MRI	US	NM
Total number of studies (*n*=1,03,730), (%)	41,776 (40.27)	47,669 (45.96)	4,326 (4.17)	9,397 (9.06)	551 (0.53)	11 (0.01)
Age (mean±standard deviation) (overall mean age=47)	41.17±0.09	52.1±0.09	50.95±0.11	50.06±0.18	37.66±0.93	50.18±8.05
Sex, (%)						
Male (*n*=50,642) (48.82%)	21,896 (43.24)	23,950 (47.30)	1 (0.00)	4,622 (9.12)	170 (0.34)	3 (0.00)
Female (*n*=53,088) (51.18%)	19,880 (37.4%)	23,719 (44.68)	4,325 (8.15)	4,775 (9)	381 (0.71)	8 (0.01)
Region, (%)						
Location A	41,776 (100)	43,694 (91.66)	4,326 (100)	7,202 (76.64)	515 (93.47)	11 (100)
Location B	-	3,975 (8.34)	-	2,195 (23.36)	36 (6.53)	-

Abbreviations: CR/DX: Computed radiography/Direct digital radiography; CT: Computed tomography; MG: Mammogram; MRI: Magnetic resonance imaging; US: Ultrasonography; NM: Nuclear medicine.

Table 2. Modality and body region distribution

Body region	Modality						
	NM	CT	Radiographs	MRI	US	MG	Total
Chest/lung	4	8,058	14,451	18	2	-	22,533
Brain/head/skull	3	14,840	426	2,891	29	-	18,189
Lower extremities	-	1,291	12,982	1,782	220	-	16,275
Abdomen and pelvis	-	11,176	966	390	206	-	12,738
Spine	-	3,728	5,553	3,156	-	-	12,437
Upper extremities	-	545	6,213	886	9	-	7,653
Cytogram/urogram/KUB	1	4,403	101	78	78	-	4,661
Breast	-	5	38	6	3	4,326	4,378
Facial bones/maxillo facial	-	2,718	837	99	-	-	3,654
Neck	-	905	79	91	4	-	1,079
Bone survey	3	-	130	-	-	-	133
Total	11	47,669	41,776	9,397	551	4,326	10,3730

Abbreviations: CT: Computed tomography; KBB: Kidneys, Ureters, and Bladder; MG: Mammogram; MRI: Magnetic resonance imaging; NM: Nuclear medicine; US: Ultrasonography.

The criticality-based categorization of cases revealed a higher representation of acute cases (53%) as compared to non-acute cases (including all regular and routine cases) (47%) (Figure 2). The mean gTAT was 19.48 h (95% CI: 19.39–19.56), consistent with the agreed 24 h and 48 h gTAT mentioned earlier. The gTAT values varied with the modalities interpreted (Figure 3). The mean gTAT for CT studies was 14.87 h (95% CI: 14.76–14.98), MRI studies 25.45 h (95% CI: 25.09–25.82), NM studies 25.10 h (95% CI: 13.05–37.16), US studies 14.33 h (95% CI: 13.19–15.48), and X-rays 21.15 h (95% CI: 21.04–21.26). Moreover, MG studies were 41.80 h (95% CI: 41.42– 42.17). To the best of our knowledge, there are no data available to compare

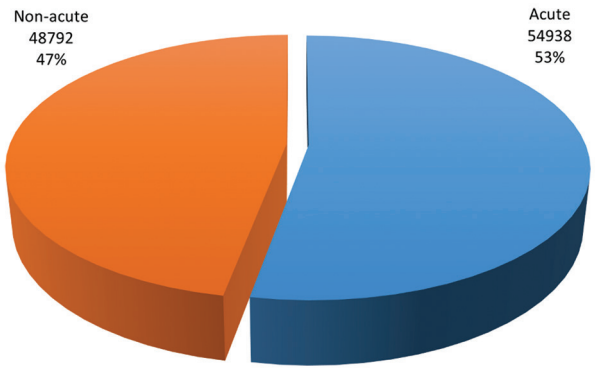

Figure 2. Criticality-based categorization of cases

gTAT in the general Gulf Cooperation Council countries, rendering these results of seminal significance in terms of publication on teleradiology and TATs in the KSA region. It was noted that while achieving gTAT, some qualitative challenges that hindered gTAT included the lack of pertinent prior images, slow image transmission, an unexpected surge of cases, complex studies with multiple findings necessitating more interpretation time, errors in the order entry that needed to be corrected, delayed order entry, and calls that were put on hold from the hospital during verbal communication.

The peer review process was performed daily by technicians with over 3 years of experience and subspecialist radiologists for specialized examinations, and data spanning 2 years were reviewed for this study. It was noted that peer review was conducted in nearly 25% of all performed examinations in 2022 and 2023, whereas the reported accuracy showed a marginal change of <2% during the investigation time.

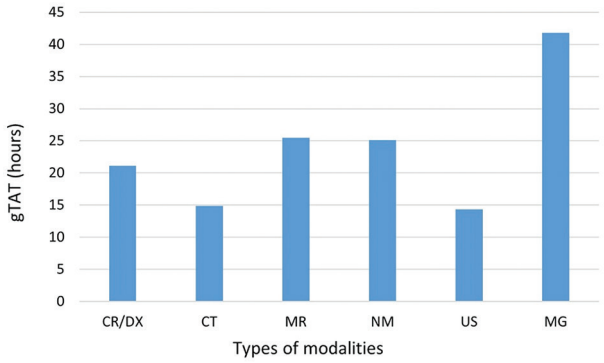

Figure 3. Distribution of global turnaround time across different modalities

The distribution of CT studies according to body region is shown in Figure 4. Teleradiology reports were provided for multiple clinical situations. Upon analyzing the common acute findings in different body regions and across different imaging modalities, the following results were obtained: Among acute intracranial processes, hemorrhage (367 cases) and infarct (106 cases) dominated. Occlusion/thrombosis (568 cases) was the highest reported acute vascular finding, followed by aneurysm (119 cases) and dense middle cerebral artery (48 cases) (Figure 5).

Regarding acute thoracic findings, opacity/consolidation/pneumonia was the most commonly reported thoracic finding, followed by pleural effusion, emphysema, pericardial effusion, pulmonary edema, lung collapse, and pneumothorax (Figure 6). Among non-acute thoracic findings, the maximum cases were reported for atelectasis (7,617 cases), followed by nodule (7588 cases), cardiomegaly (2287 cases), and fibrosis (713 cases).

Figure 7 illustrates the distribution of acute abdominal findings, with 45% of bowel obstruction, 19% of appendicitis, 21% of cholelithiasis/cholecystitis, and 8% of diverticulitis. It can be extrapolated that the results mentioned may help in evaluating incidence and prevalence to help shape the public health programs. Besides these, other prominent acute abdominal findings included pyelonephritis, perforation, pneumatosis, anastomotic leak, and ovarian torsion. A total of 4159 fracture cases were also reported.

4. Discussion

Teleradiology is a disruptive service, which leverages technology to provide multiple benefits, including amplifying providers' productivity and speeding up the

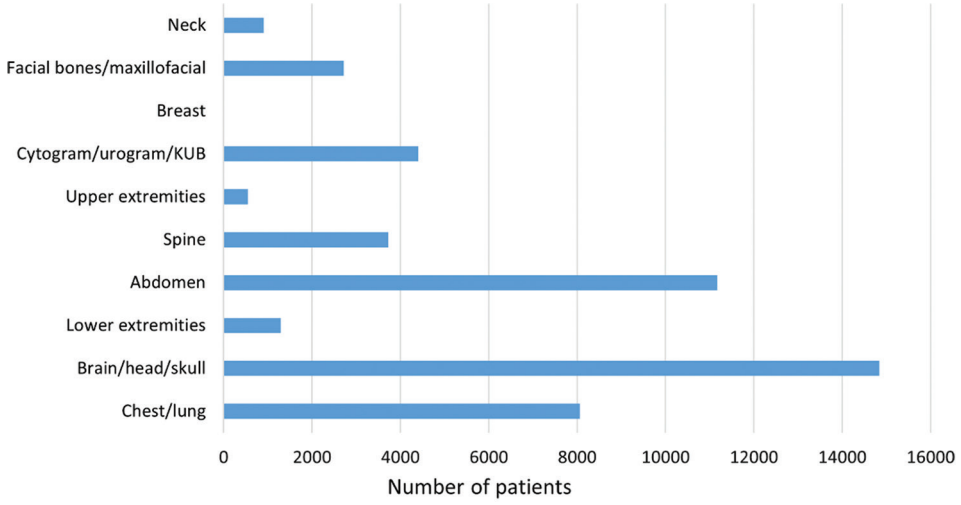

Figure 4. Number of computed tomography studies according to body region

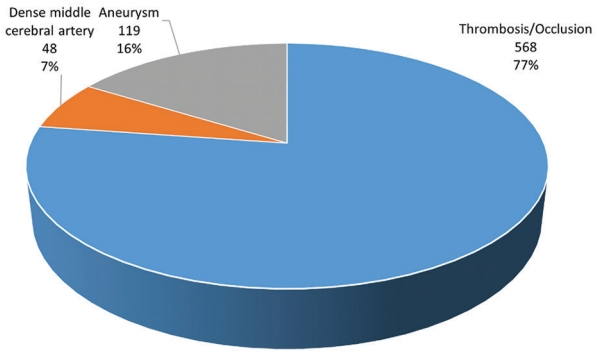

Figure 5. Distribution of acute vascular findings

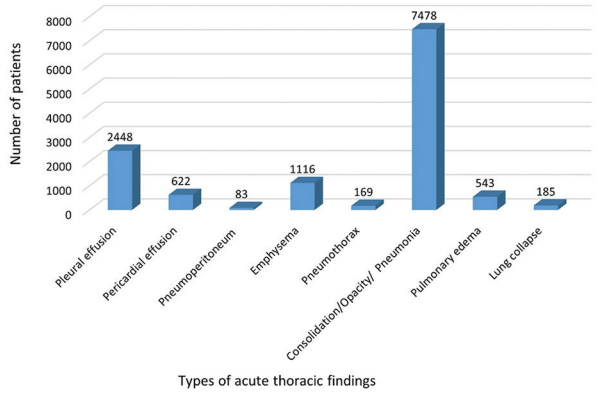

Figure 6. Distribution of acute thoracic findings

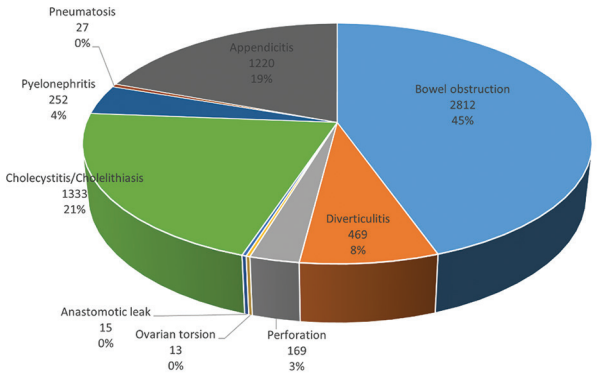

Figure 7. Distribution of acute abdominal findings

image analysis process to enhance patient outcomes.[13] The findings presented in this study reflect that the utilization of teleradiology can be an effective mechanism of high-quality healthcare delivery in Saudi Arabia.

Gender distribution is relatively balanced, with males slightly outnumbering females (51.18% vs. 48.82%). The majority of patients who had received imaging assessments were aged in the range of 41–60 years (37.70%), followed by those in the 21–40 years range (28.27%). This trend is in line with the highest utilization of radiology scans under the same age group in other studies.[2,41]

The majority of the studies reported were sent from a smaller city, possibly indicating a higher utilization rate of teleradiology services to ensure equitable health care delivery. High-quality diagnostic imaging enhances diagnostic accuracy and plays a critical role in guiding clinical decision-making and patient management.[42] CT is generally a front-line imaging modality for identifying and characterizing infections, tumors, traumatic injuries, skeletal disorders, and vascular conditions.[43] In this study, the most common modality requested was CT imaging (45.96% of all imaging modalities), followed by radiographs (CR/DX; 40.27%), magnetic resonance imaging (MRI; 9.06%), mammograms (MG; 4.17%), ultrasound (0.53%), and NM (0.01%). Compared to X-ray and nuclear imaging, CT offers accuracy and clarity advantages in detecting many but not all abnormalities, which represent the value-added of the modality in the context of teleradiology.[44,45]

Cranial CTs (31%) were the most frequently requested examinations, followed by abdomen and pelvis CT (21%) and chest CT studies (17%). The data interpretation in our study is aligned with the research conducted by Storjohann *et al.*[46] that reported cranial CTs as the most frequently requested examinations, followed by head/neck and abdominal studies.

The most commonly performed CT imaging by region was head as well as abdomen and pelvis, while the most frequent MRI examinations were of the spine and brain. These results reflect those of Rao *et al.*[12] Among radiographs, chest radiographs (34%) were the most prominent imaging performed. Similar results have been obtained in another research publication by our institution.[41] Teleradiology provides affordable, uninterrupted, round-the-clock access to diagnostic imaging for smaller hospitals by capitalizing on the 24/7 presence of radiologists through remote access and providing reports in an efficient manner. Further, teleradiology has proven its potential to provide healthcare services in multiple clinical settings, including ER, inpatient, and outpatient settings.[39,46-48] In our study, the data analysis of the patient location revealed that the teleradiology services were provided under multiple clinical settings, including outpatient (65.81%), emergency (26.13%), and inpatient (8.07%) settings.

According to a previous study, 41% of Saudi Arabian radiologists had opined that teleradiology has enhanced the quality of radiology reports during the COVID-19 pandemic, while 69.6% of participants believed that teleradiology is a helpful tool for imaging interpretation.[39] Our results corroborate these assumptions and indicate

that teleradiology services have the ability to enhance the quality of life for patients by promptly interpreting and offering guidance on acute and non-acute findings observed through imaging, across all clinical settings. Multiple studies reveal that teleradiology significantly reduces report TATs, especially in emergency and after-hour scenarios, ensuring faster clinical decision-making.[49,50]

The mean gTAT for the reporting studies was 19.48 h (95% CI: 19.39–19.56). The gTAT times listed in this study are seminal for those used in KSA's teleradiology settings. Various reasons were observed for the relative delay in turnaround, which have been discussed in the results section. Aligned with the growing utilization of teleradiology services worldwide, including the USA, Europe, New Zealand, and Australia,[11,51-54] our study projects increased teleradiology utilization in KSA. This expansion will help address radiologist shortages and manage the ever-increasing volume of radiology examinations.

5. Conclusion

The present study demonstrates the use of teleradiology utilization in healthcare delivery in the context of KSA in different locations, including ER, inpatient, and outpatient settings. In addition, teleradiology is used across different criticalities of care, including acute and non-acute patient care, and finally, the TAT of teleradiology reports was within the accepted local and global standards. Some limitations impacting teleradiology examinations include a lack of oversight on image quality and imaging protocols from a remote location, in addition to a lack of access to medical records, and occasional delay in receiving any pertinent prior imaging and or reports for the most recent examination reported by teleradiologists. Moreover, from the clinicians' end-user perspective, while all acute and urgent cases were relayed back to the physicians, and a telephone callback number was provided for all reported examinations for any follow-up, no quantitative data analysis was performed to measure any time difference in communication between the in-house radiology team and teleradiology providers, to gauge any statistical difference. The perceived security risks were mitigated using advanced IT solutions and a cybersecurity system. As mentioned previously, peer review data collection and report quality analysis were conducted during the study period (2 years); however, volume of data on peer review for subsequent years may provide an opportunity to empirically validate the findings, via questionnaire or other statistical methodology—an aspect which is currently out of the scope of the current study.

The value addition of teleradiology reported elsewhere includes, but is not limited to, after-hour reporting with improved TATs, the benefit of subspeciality and second consultations from a pool of teleradiologists with core competency in multiple subspecialities, enhanced radiology workflow, and high-quality reports. In the context of the KSA Vision 2030 plan, leveraging the PPP model, teleradiology can aid in digital health integration, providing equitable access to remote and underserved locations in KSA. The current study corroborates this principle with higher utilization of teleradiology services in location A (a smaller city) over the center-based based in a larger city. Teleradiology can also potentially complement on-site radiologists and optimize the workflow. It can help balance the ever-growing radiology case load by providing after-hours coverage for both acute and non-acute requests of medical imaging, providing back-up to accommodate any surge in cases, and offering coverage during vacation and/or illnesses of on-site radiologists, thereby facilitating staffing and optimization of workflow via teleradiology. A major advantage of an established teleradiology practice is the pool of radiologists, including trained subspecialists, who can offer tailored solutions for niche areas of radiology in a round-the-clock manner, on the basis of 24/7 coverage enabled through teleradiology. Further, integrating with artificial intelligence, teleradiology can improve health care.

These factors may contribute to the increased reporting of specific organs or conditions by subspecialist radiologists, thereby improving healthcare access and delivery in both remote and underserved areas and enhancing healthcare outcomes. In addition, the use of second opinions in the past has helped in patient care and management, which could be used by clinical departments, including radiology. Moreover, another perceived use of teleradiology aiding improved health care outcomes is quality assurance, which involves peer reviews of imaging studies from the hospital to the teleradiology service provider. Several factors have hindered the widespread acceptance of teleradiology in the past, including perceived risk of breach of security, patient confidentiality, along with financial budgetary constraints, and regulatory and licensing compliance. In light of advancements in technology, robust IT solutions and advanced cybersecurity systems can be provided to ensure patient confidentiality, while affordability, regulation, and licensing of teleradiology could be addressed by partnerships in private and public sectors in KSA. The outcomes of our investigation reflect that teleradiology provides an effective solution for rapid and good-quality interpretation of examinations in multiple clinical settings and across different criticalities of patient care performed in Saudi Arabia. The TAT for teleradiology

reports was within accepted local and global standards. Finally, it can be inferred that the benefits of teleradiology can both complement and advance healthcare delivery in different clinical locations and across the criticality of care. Establishing teleradiology connectivity with an established service provider, with documented high-quality diagnostic interpretations and quick TATs, may enhance the efficiency of patient care management across Saudi Arabian hospitals, consistent with the aspiration of the KSA Vision 2030 healthcare plan.

Acknowledgments

None.

Funding

None.

Conflict of interest

The authors declare they have no competing interests.

Author contributions

Conceptualization: Arjun Kalyanpur, Sonal Arjuna
Methodology: Neetika Mathur, Muktha Rawath
Investigation: Arjun Kalyanpur, Sonal Arjuna
Supervision: Arjun Kalyanpur
Visualization: Arjun Kalyanpur, Sonal Arjuna
Writing–original draft: Sonal Arjuna, Neetika Mathur
Writing–review & editing: Arjun Kalyanpur, Sonal Arjuna

Ethics approval and consent to participate

Not applicable.

Consent for publication

Not applicable.

Availability of data

The datasets generated and/or analyzed during the current study are not publicly available due to medical privacy laws, but are available from the corresponding author on reasonable request.

References

1. Chandramohan A, Krothapalli V, Augustin A, *et al*. Teleradiology and technology innovations in radiology: Status in India and its role in increasing access to primary health care. *Lancet Reg Health Southeast Asia*. 2024;23:100195.

   doi: 10.1016/j.lansea.2023.100195

2. Rudisill KE, Mathur N, Kalyanpur A. A teleradiology network for the improvement of healthcare and patient management in the developing countries of the African continent. *Clin Imaging*. 2024;111:110188.

   doi: 10.1016/j.clinimag.2024.110188

3. Kalyanpur A, Meka S, Joshi K, Somashekaran Nair HT, Mathur N. Teleradiology in Tripura: Effectiveness of a telehealth model for the rural health sector. *IJHTI*. 2022;1(02):7-12.

   doi: 10.60142/ijhti.v1i02.36

4. Kalyanpur A, Sudhindra RR, Rao P. The role of mobile van mammography supported by teleradiology in the early diagnosis of breast cancer: An innovative approach to a growing public health problem. *Int J Health Technol Innov*. 2022;1(03):2-8.

   doi: 10.60142/ijhti.v1i03.30

5. Bashshur RL, Krupinski EA, Thrall JH, Bashshur N. The empirical foundations of teleradiology and related applications: A review of the evidence. *Telemed J E Health*. 2016;22(11):868-898.

   doi: 10.1089/tmj.2016.0149

6. Jacobs JJWM, Ekkelboom R, Jacobs JPAM, Van Der Molen T, Sanderman R. Patient satisfaction with a teleradiology service in general practice. *BMC Fam Pract*. 2016;17(1):17.

   doi: 10.1186/s12875-016-0418-y

7. Henes FO, Stappenbeck P, Tahir E, *et al*. Implementation of a 24-hour teleradiology service for cruise ships: A pilot study. *Am J Roentgenol*. 2020;214(4):754-760.

   doi: 10.2214/AJR.19.21794

8. Peng YC, Lee WJ, Chang YC, Chan WP, Chen SJ. Radiologist burnout: Trends in medical imaging utilization under the national health insurance system with the universal code bundling strategy in an academic tertiary medical centre. *Eur J Radiol*. 2022;157:110596.

   doi: 10.1016/j.ejrad.2022.110596

9. Bradley WG. Offshore teleradiology. *J Am Coll Radiol*. 2004;1(4):244-248.

   doi: 10.1016/j.jacr.2003.12.043

10. Kalyanpur A, Neklesa VP, Pham DT, Forman HP, Stein ST, Brink JA. Implementation of an international teleradiology staffing model. *Radiology*. 2004;232(2):415-419.

    doi: 10.1148/radiol.2322021555

11. Agrawal A. Emergency teleradiology-past, present, and, is there a future? *Front Radiol*. 2022;2:866643.

    doi: 10.3389/fradi.2022.866643

12. Rao P, Mathur N, Kalyanpur A. Utilization of teleradiology by intensive care units: A cohort study. *Indian J Crit Care Med*. 2024;28(1):20-25.

    doi: 10.5005/jp-journals-10071- 24593

13. *Beating Burnout and Backlogs in Radiology - Ensuring a*

Sustainable Teleradiology Solution; 2025. Available from: https://www.hsj.co.uk/workforce/beating/burnout/and/backlogs/in/radiology/ensuring/sustainable/teleradiology/solution/7038861.article [Last accessed on 2025 Nov 25].

14. Kalyanpur A, Mathur N. Offshore reporting of radiologic examinations supplementing healthcare delivery worthy of Medicare reimbursement. *Imaging Radiat Res*. 2024;6(1):6404.

    doi: 10.24294/irr.v6i1.6404

15. Mc Fadden S, Flood T, Shepherd P, Gilleece T. Impact of COVID-19 on service delivery in radiology and radiotherapy. *Radiography (Lond)*. 2022;28:S16-S26.

    doi: 10.1016/j.radi.2022.03.009

16. Elshami W, Akudjedu TN, Abuzaid M, *et al*. The radiology workforce's response to the COVID-19 pandemic in the Middle East, North Africa and India. *Radiography (Lond)*. 2021;27(2):360-368.

    doi: 10.1016/j.radi.2020.09.016

17. Al-Samarraie H, Ghazal S, Alzahrani AI, Moody L. Telemedicine in Middle Eastern countries: Progress, barriers, and policy recommendations. *Int J Med Inform*. 2020;141:104232.

    doi: 10.1016/j.ijmedinf.2020.104232

18. Arabi M, Mamoun I, Masrani A, Alsayid M, Haroun N. Practice of teleradiology in crisis zones: The unique case of Syria. *Lancet Glob Health*. 2017;5(4):e399-e400.

    doi: 10.1016/S2214-109X(17)30083-9

19. Haddad MC, Loutfi SI, Tamraz JC, Al-Kutoubi AO. The status of radiology in the Arab world. First world report. *J Med Liban*. 2007;55(2):94-98.

20. AlSafran ZA, Arabi M, Alsafran FS, Ashour MA, Justaniah AI. Current and future needs for interventional radiologists in Saudi Arabia: Position statement by the Saudi interventional radiology society. *Arab J Intervent Radiol*. 2023;07(01):044-048.

    doi: 10.1055/s-0043-57042

21. Radiological Society of North America. *Radiology Facing a Global Shortage*. Available from: https://www.rsna.org/news/2022/may/global/radiologist-shortage [Last accessed on 2024 Sep 20].

22. Goh CXY, Ho FCH. The growing problem of radiologist shortages: Perspectives from Singapore. *Korean J Radiol*. 2023;24(12):1176-1178.

    doi: 10.3348/kjr.2023.0966

23. Kalidindi S, Gandhi S. Workforce crisis in radiology in the UK and the strategies to deal with it: Is artificial intelligence the saviour? *Cureus*. 2023;15(8):e43866.

    doi: 10.7759/cureus.43866

24. Available from: https://www.ncp.gov.sa/en/pages/default.aspx [Last accessed on 2025 Nov 25].

25. Al-Nozha OM. Key aspects of the Saudi healthcare system reform and the potential impact on the main stakeholders: A qualitative study. *J Taibah Univ Med Sci*. 2024;19(3):598-610.

    doi: 10.1016/j.jtumed.2024.04.007

26. Available from: https://www.trade.gov/country-commercial-guides/saudi-arabia-healthcare [Last accessed on 2025 Nov 25].

27. Alahmad H, Almanaa M, Abanomy A, *et al*. Navigating challenges in teleradiology implementation: A case study from Saudi Arabia's healthcare system. *J Multidiscip Healthc*. 2024;17:2083-2092.

    doi: 10.2147/JMDH.S460547

28. Saleh S. *Number of Radiologists in Saudi Arabia in 2022, by Sector*; 2024. Available from: https://www.statista.com/statistics/608546/number-of-radiologists-in-saudi-arabia-bysector [Last accessed on 2025 Nov 25].

29. Khalifa M. Barriers to health information systems and electronic medical records implementation. A field study of Saudi Arabian hospitals. *Proced Comput Sci*. 2013;21:335-342.

    doi: 10.1016/j.procs.2013.09.044

30. Abouzid MR, Elshafei SM, Elkhawas I, Elbana MK. Applications of telemedicine in the middle east and North Africa region: Benefits gained and challenges faced. *Cureus*. 2022;14:e26611

    doi: 10.7759/cureus.26611

31. Ryu S. Telemedicine: Opportunities and developments in member States: Report on the second global survey on eHealth 2009 (global observatory for eHealth series, Volume 2). *Healthc Inform Res*. 2012;18(2):153.

    doi: 10.4258/hir.2012.18.2.153

32. Crawford I, McBeth PB, Mitchelson M, Ferguson J, Tiruta C, Kirkpatrick AW. How to set up a low cost tele-ultrasound capable videoconferencing system with wide applicability. *Crit Ultrasound J*. 2012;4(1):13.

    doi: 10.1186/2036-7902-4-13

33. Fuentes A. Remote interpretation of ultrasound images. *Clin Obstet Gynecol*. 2003;46(4):878-881.

    doi: 10.1097/00003081-200312000-00019

34. Zarei J, Sharifat Z. A survey on teleradiology infrastructure in selected hospitals in Ahvaz, 2014. *J Healthc Manag J Health Syst Winter*. 2016;6(4):7-18.

35. Essop H, Kekana M. The need for improved telecommunication and collaborative practice among teleradiology end users in a rural district of South Africa. *J Radiol Nurs*. 2019;38(4):281-285.

    doi: 10.1016/j.jradnu.2019.07.006

36. Mozhgan K, Panahi Soh GS, Malekeh M, Mehdi K. The

survey of residents and radiologists' attitudes about access to patient information in teleradiology in Iran. *J Eng Appl Sci*. 2012;7(2):155-158.

doi: 10.3923/jeasci.2012.155.158

37. Alruwaili AR, Alshammari AA, Alsalhi FM, Aldamen SA, Alamri HS. Teleradiology in Saudi Arabia: A national survey and retrospective review of associated MRI reports. *BMC Health Serv Res*. 2024;24(1):1327.

doi: 10.1186/s12913-024-11706-5

38. Sadoughi F, Erfannia L, Sancholi M, Salmani F, Sarsarshahi A. Teleradiology in Southeast Iran: Evaluating the views of senior executives and radiologists. *Health Care Manag (Frederick)*. 2017;36(3):301-307.

doi: 10.1097/HCM.0000000000000162

39. Al-Dahery ST, Alsharif WM, Alamri FH, *et al*. The role of teleradiology during COVID-19 outbreak: Saudi radiologists' perspectives. *Saudi Med J*. 2023;44(2):202-210.

doi: 10.15537/smj.2023.44.2.20220793

40. Alshamrani K, Alkenawi A. Teleradiology public-private partnerships in Saudi Arabia: A review. *Int J Med Dev Countr*. 2021;5:1096-1099.

doi: 10.24911/IJMDC.51-1614155864

41. Kalyanpur A, Mathur N. The role of teleradiology in interpretation of ultrasounds performed in the emergency setting. *Digit Diagn*. 2024;5:231-242.

doi: 10.17816/DD624586

42. Crumley I, Halton J, Greig J, *et al*. The impact of computed radiography and teleradiology on patients' diagnosis and treatment in Mweso, the democratic republic of Congo. *PLoS One*. 2020;15(1):e0227773.

doi: 10.1371/journal.pone.0227773

43. Hermena S, Young M. *CT-Scan Image Production Procedures*. In: StatPearls. Treasure Island, FL: StatPearls Publishing; 2024. Available from: https://www.ncbi.nlm.nih.gov/books/nbk574548 [Last accessed on 2025 Nov 25].

44. Patel PR, De Jesus O. *CT Scan*. In: StatPearls. Treasure Island, FL: StatPearls Publishing; 2025. Available from: https://www.ncbi.nlm.nih.gov/books/nbk567796 [Last accessed on 2025 Nov 25].

45. Jukema RA, Dahdal J, Kooijman EM, *et al*. Diagnostic accuracy of non-invasive cardiac imaging modalities in patients with a history of coronary artery disease: A meta-analysis. *Heart*. 2024;111(1):4-10.

doi: 10.1136/heartjnl-2024-324248

46. Storjohann S, Kirsch M, Rosenberg B, *et al*. The accuracy of on-call CT reporting in teleradiology networks in comparison to in-house reporting. *Healthcare (Basel)*. 2021;9(4):405.

doi: 10.3390/healthcare9040405

47. Kalyanpur A, Mathur N. A teleradiology system for early ischemic and hemorrhagic stroke evaluation and management. *J Clin Interv Radiol ISVIR*. 2023;7(3):183-189.

doi: 10.1055/s-0043-1771379

48. Char A, Kalyanpur A, Puttanna Gowda VN, Bharathi A, Singh J. Teleradiology in an inaccessible area of Northern India. *J Telemed Telecare*. 2010;16(3):110-113.

doi: 10.1258/jtt.2009.009007

49. Hasan J, Shekhqader T, Al-Kabban FM, Najm G, Rathore SS. Bridging the gap: Opportunities, challenges, and future directions for teleradiology in rural healthcare. *Int J Community Med Public Health*. 2024;11(12):5017-5024.

doi: 10.18203/2394- 6040.ijcmph20243423

50. Nigatu AM, Yilma TM, Gezie LD, *et al*. Effect of teleradiology on patient waiting time and service satisfaction in public hospitals, Northwest Ethiopia: A quasi-experimental study. *BMC Health Serv Res*. 2025;25(1):603.

doi: 10.1186/s12913-025-12545-8

51. *Staffing Pressures Persist in Radiology: Can Teleradiology Bridge the Ever-Widening Gap*? Open MedScience; 2025. Available from: https://openmedscience.com/staffing/pressures-persist-in/radiology-can-teleradiology/bridge-the-ever-widening-gap [Last accessed on 2025 Nov 25].

52. Ranschaert ER, Binkhuysen FHB. European teleradiology now and in the future: Results of an online survey. *Insights Imaging*. 2013;4(1):93-102.

doi: 10.1007/s13244-012-0210-z

53. Jones DN, O'Donnell C, Stuckey J. 1998 Australian radiology workforce report. *Australas Radiol*. 2000;44(1):41-52.

doi: 10.1046/j.1440-1673.2000.00780.x

54. *2020 Clinical Radiology Workforce Census Report: New Zealand*. Available from: https://www.ranzcr.com/college/document-library/clinical-radiology-workforce-census-report-nz?searchword=ranzcr%20grievance%20policy [Last accessed on 2025 Nov 25].

ACCSCIENCE PUBLISHING

Advances in Radiotherapy & Nuclear Medicine

ORIGINAL RESEARCH ARTICLE

CXCR6 expression as a predictive biomarker for immunotherapy responsiveness in nasopharyngeal carcinoma

Zhen-Chong Yang[1,2]*, Ying-He Li[1,2], and Xi Zou[1,2]

[1]State Key Laboratory of Oncology in South China, Collaborative Innovation Center for Cancer Medicine, Guangdong Key Laboratory of Nasopharyngeal Carcinoma Diagnosis and Therapy, Sun Yat-Sen University Cancer Center, Guangzhou, Guangdong, China

[2]Department of Nuclear Medicine, Sun Yat-Sen University Cancer Center, Guangzhou, Guangdong, China

Abstract

Immunotherapy breakthroughs have revolutionized the treatment of nasopharyngeal carcinoma (NPC). The addition of toripalimab to gemcitabine–cisplatin (GP) chemotherapy as a first-line treatment for patients with NPC resulted in a manageable safety profile and superior progression-free survival compared with GP alone. However, the treatment benefited only a subset of patients. Therefore, we evaluated response patterns in patients with NPC who were treated with programmed cell death protein 1 (PD-1) inhibitors to assess the influence of the tumor immune microenvironment on the efficacy of immunotherapies. Fifty NPC patients treated with PD-1 inhibitors at the Sun Yat-sen University Cancer Center were identified, and 50 and 28 samples were collected before and during treatment, respectively. mRNA expression levels of 289 tumor-immune-related genes were analyzed using the NanoString nCounter. Immune infiltration and correlations between clinical characteristics and the expression of immune-related genes were assessed. Tumors that responded to immunotherapy had significantly lower T helper 1 cell infiltration and higher chemokine signature scores compared with non-responding tumors. Notably, anti-PD-1 immunotherapy-responsive tumors had higher *CXCR6* expression levels, suggesting that *CXCR6* may be involved in the immune surveillance of NPC and in shaping the tumor microenvironment (TME). In addition, significant differences in the TME were observed between pre-treatment and treatment samples. Overall, *CXCR6* expression was identified as a predictive biomarker for response to immunotherapy in NPC.

Keywords: *CXCR6*; Immunotherapy; Tumor immune microenvironment; Toripalimab; Nasopharyngeal carcinoma; Programmed cell death protein 1 inhibitors

***Corresponding author:**
Zhen-Chong Yang
(yangzc@sysucc.org.cn)

Citation: Yang Z, Li Y, Zou X. *CXCR6* expression as a predictive biomarker for immunotherapy responsiveness in nasopharyngeal carcinoma. *Adv Radiother Nucl Med*. 2026;4(1):57-68. doi: 10.36922/ARNM025390049

Received: September 23, 2025

Revised: November 12, 2025

Accepted: November 18, 2025

Published online: January 13, 2026

1. Introduction

Nasopharyngeal carcinoma (NPC) is a malignant tumor of the head and neck that originates from the nasopharyngeal epithelium and exhibits distinct biological behavior, including regional, ethnic, and familial aggregation. The global annual incidence of NPC is approximately 130,000 cases, with China accounting for 38.29% of all cases and

40.14% of related deaths.[1] Notably, NPC is considered to be driven predominantly by ecological and environmental factors rather than by hereditary genetic predisposition.[2] The occurrence of NPC is associated with environmental and genetic factors as well as Epstein–Barr virus (EBV) infection.[3] Treatment options for NPC include radiation therapy, chemotherapy, molecularly targeted therapy, and immunotherapy. Platinum-based concurrent chemotherapy remains a key treatment backbone for locally advanced NPC. Gemcitabine–cisplatin (GP) chemotherapy, the standard first-line treatment for NPC, has demonstrated superior progression-free survival (PFS) compared with earlier platinum-based regimens. Although a high percentage of patients with NPC initially respond to chemotherapy, the duration of response is typically short, with a median PFS of 7.0 months and a median overall survival (OS) of 22.1 months.[4,5]

Studies have revealed that 89–95% of patients with NPC express programmed death-ligand 1 (PD-L1), which can lead to T cell exhaustion.[6,7] The expression levels of PD-L1 are associated with recurrence, metastasis, and clinical progression of NPC.[6-8] *CTLA4* gene polymorphisms are associated with susceptibility to NPC.[9,10] Therefore, programmed cell death protein 1 (PD-1)/PD-L1 and cytotoxic T-lymphocyte–associated protein 4 inhibitors can be used to treat NPC. Moreover, PD-1/PD-L1 inhibitors have shown good clinical outcomes in phase I/II clinical trials. JUPITER-02[11] was a multicenter, randomized, phase III study that provided head-to-head comparisons of immune checkpoint inhibitors (ICI) plus GP versus standard first-line GP chemotherapy in patients with recurrent or metastatic NPC. The JUPITER-02 trial demonstrated that combining toripalimab with GP chemotherapy resulted in significantly longer median PFS compared with the placebo (11.7 vs. 8.0 months, p=0.0003).

The tumor microenvironment (TME) has emerged as a promising focus of research, and previous works have suggested immune gene signatures as biomarkers for prognosis and responses to ICIs.[12,13] High levels of tumor-infiltrating lymphocytes (TILs) containing $CD3^+$, $CD4^+$, and $CD8^+$ cells have been associated with improved PFS in patients with non-small cell lung carcinoma.[12,13] The NanoString gene expression panel contains 289 genes that function in different pathways, including those associated with tumor, TME, and immune responses.[14-16] A total of 289 genes related to the tumor immune microenvironment (TIME) have been curated, and various techniques have been used to analyze the TME. TIME-based gene expression signatures can help predict the efficacy of immunotherapy, enabling the identification of patients most likely to benefit. Hence, TIME analysis can elucidate the cell types, genes, and pathways involved in immune activation and suppression, facilitating the development of more effective ICI therapies for metastatic NPC. However, there is currently no biomarker to determine the efficacy of NPC immunotherapy through TME expression profiling.

Abnormal expression of chemokines (cysteine-X-chemokine [CXC]) is considered an important mechanism of tumor metastasis. CXC receptor 6 (CXCR6) is a receptor for CXC chemokine ligand 16 (CXCL16).[17] CXCL16 is expressed in $CD8^+$ T cells, T helper (Th) cells, natural killer (NK) T cells, and macrophages, whereas its receptor CXCR6 is primarily expressed in undifferentiated $CD8^+$ T cells, NK T cells, $CD8^+$ T cells, and $CD4^+$ T cells. Recent studies have shown that *CXCR6* is highly expressed in various malignant tumor cells and is associated with tumor proliferation, metastasis, invasion, and prognosis, suggesting that *CXCR6* expression may play a crucial role in tumorigenesis.[18,19] Hong *et al.*[20] found that enhanced *CXCR6* expression was associated with poorer survival outcomes in ovarian cancer cells. Adamski *et al.*[21] reported that enhanced *CXCR6* expression promoted the migration of melanoma and glioblastoma cells. Gillard *et al.*[22] found that *CXCR6* expression in NK cells was significantly upregulated in non-small cell lung cancer, suggesting that *CXCR6* may be involved in the immune surveillance of lung cancer and the formation of the TME. Parsonage *et al.*[23] found that NPC tumor cells express high levels of CXCL16 and attract $CXCR6^+$ T cells, including infiltrating $CD4^+$ T cells and regulatory T cells (Tregs), thereby promoting antitumor immune responses.[23] When CXCR6 binds to CXCL16, the Gi protein activates the phosphoinositide 3-kinase/protein kinase B pathway, initiating the phosphorylation of mammalian target of rapamycin, nuclear factor kappa B, and other pathway proteins, which in turn regulate cell proliferation, migration, DNA damage repair, protein synthesis, and apoptosis.[24] In addition, the CXCL16/*CXCR6* pair is involved in the formation of the TME in pancreatic, liver, and lung cancers, although its specific mechanism has not been elucidated. At present, *CXCR6* has not been reported as a biomarker predictive of response to NPC immunotherapy in NPC.

To understand the complex characteristics of the TME in patients with NPC, we used the NanoString platform to evaluate immune cell enrichment, immune cell infiltration scores, and immune signatures in patients with NPC. We identified *CXCR6* expression as a predictive biomarker of response to immunotherapy and demonstrated dynamic changes in the TME before and during immunotherapy.

2. Methods

2.1. Patients

This study included 50 patients who participated in the JUPITER-02 clinical trial (NCT03581786) at the Sun Yat-sen University Cancer Control Center. The study was approved by the Institutional Review Board of Sun Yat-sen University Cancer Control Centre, and informed consent was collected before enrollment. The JUPITER-02 clinical trial is an international multicenter, randomized, double-blind, placebo-controlled phase III clinical study of immunotherapy combined with standard chemotherapy for the first-line treatment of recurrent/metastatic NPC. The clinical trial included 289 patients who were randomized into a troripalimab plus GP group and a placebo plus GP group. The median PFS of patients in the placebo plus GP group was 9 months based on the JUPITER-02 study. Thus, we classified patients with PFS > 9 months as responders and those with PFS ≤ 9 months as non-responders. We collected 50 pre-treatment samples and 28 on-treatment samples.

2.2. NanoString gene expression profiling of 289 immune-related genes

Gene expression was measured using the nCounter platform (NanoString Technologies, United States), and transcriptomic analysis was conducted based on the 289-immune-related-gene NanoString panel. Positive and content normalization factors were calculated, and samples that passed quality control were included in subsequent analyses.

2.3. Estimation of TIME cell infiltration

Marker genes of 14 immune cell populations, including B cells, dendritic cells, macrophages, exhausted $CD8^+$ T cells, $CD8^+$ T cells, neutrophils, mast cells, cytotoxic cells, Tregs, NK $CD56^{dim}$ cells, NK cells, $CD45^+$ cells, and Th1 cells, were retrieved using a previously reported method.[25-27] Macrophages were classified as either M1 or M2, as previously reported.[27,29] M1 macrophages secrete pro-inflammatory cytokines and chemokines, present antigens, participate in antitumor immune responses, and act as immune sentinels. M2 macrophages reduce inflammation, promote tumor growth, and participate in immunosuppression. All TIME cell infiltration scores were calculated as the arithmetic mean of the expression levels of the constituent genes.

2.4. TIME signatures

We constructed gene sets comprising genes associated with several biological processes, including cytotoxic T lymphocyte levels, cytolytic activity (CYT) scores, chemokines, T-cell markers, total TIL scores, T-effector scores, an interferon-gamma signature, and an overall immune signature. The CYT score for each sample was calculated as the geometric mean of *PRF1* and *GZMA* expression. The remaining TIME signatures were calculated as the arithmetic mean expression of the corresponding genes.[30-32]

2.5. Analysis of differentially expressed genes (DEGs)

The NanoStringDiff package was used to identify DEGs between various groups. A $p<0.05$ and a fold change of ≥2 or ≤2 were considered to indicate statistically differential expression.

2.6. Gene set enrichment and pathway analysis

Gene ontology (GO) enrichment analysis was performed using the R package "clusterProfiler." The Benjamini–Hochberg method was used to adjust *p*-values for multiple comparisons, with a cutoff of 0.05.

2.7. Statistical analysis

The *t*-test was used to estimate immune cell types and immune signature scores of responding and non-responding tumors. A paired *t*-test was used to compare estimated immune cell types and immune signature scores between pre- and post-treatment samples. Survival analyses were performed using Kaplan–Meier curves and the log-rank test. Univariable and multivariable Cox proportional hazard regression models were constructed to adjust for confounding variables, including age, sex, smoking history, and body mass index. A logistic regression model was used to test correlations between the variables and responsiveness to anti-PD-1 agents. All statistical analyses were performed using R statistical software (version 4.1.3). Statistical tests were two-tailed, and $p<0.05$ was considered statistically significant.

3. Results

3.1. Patient characteristics

A total of 50 patients (37 males and 13 females) were enrolled. All patients had non-keratinizing squamous cell carcinoma. There were 39 patients (78%) with an Eastern Cooperative Oncology Group (ECOG) performance status score of 0 and 11 patients (22%) with an ECOG performance status score of 1. Additional baseline data are presented in Table S1. All patients were administered toripalimab plus GP as first-line treatment. Based on the median PFS of 9 months, we classified patients with a PFS > 9 months as the responding group and those with a PFS ≤ 9 months as the non-responding group. We collected

50 samples before treatment (pre-treatment samples) and 28 samples during treatment (on-treatment samples), all of which were paired (Table 1).

3.2. Characteristics of the TME in patients with NPC

We calculated enrichment scores for 16 immune cell types: B cells, dendritic cells (DCs), $CD4^{5+}$ cells, macrophages, exhausted CD^{8+} T cells, T cells, T regs, CD^{8+} T cells, neutrophils, mast cells, cytotoxic cells, NK $CD56^{dim}$ cells, NK cells, Th1 cells, M1 macrophages, and M2 macrophages (Figure 1A). The results indicated that a large number of immune cells infiltrated the TME in NPC, and responding tumors had higher levels of immune cell enrichment than non-responding tumors. Furthermore, we analyzed individual immune cell type scores (Figure 1B) and found that responding tumors had significantly lower Th1 cell infiltration than non-responding tumors. Analysis of eight immune signature scores revealed that only the chemokine signature score was significantly higher in the responding group (Figure 1C). These results suggest that Th1 cells and chemokine-related signatures may serve as biomarkers of the NPC TME. However, further research is required to confirm these observations.

Table 1. Summary of patient group information

Treatment type	Type of patient group	Pre-treatment	Post-treatment
Placebo+ gemcitabine–cisplatin	Responding	11	7
	Non-responding	12	4
Toripalimab+ gemcitabine–cisplatin	Responding	19	14
	Non-responding	8	3
Total		50	28

3.3. Comparison of immune-related gene expression in patients with NPC

In total, 21 DEGs were identified (Figure 2A). *BRCA1*, *BRIP1*, *CCL5*, *HAVCR2*, *MAGEA1*, and *CXCR6* were associated with the TIME in NPC. We found that *CXCR6* was more highly expressed in responding tumors than in non-responding tumors (Figure 2B). We then conducted

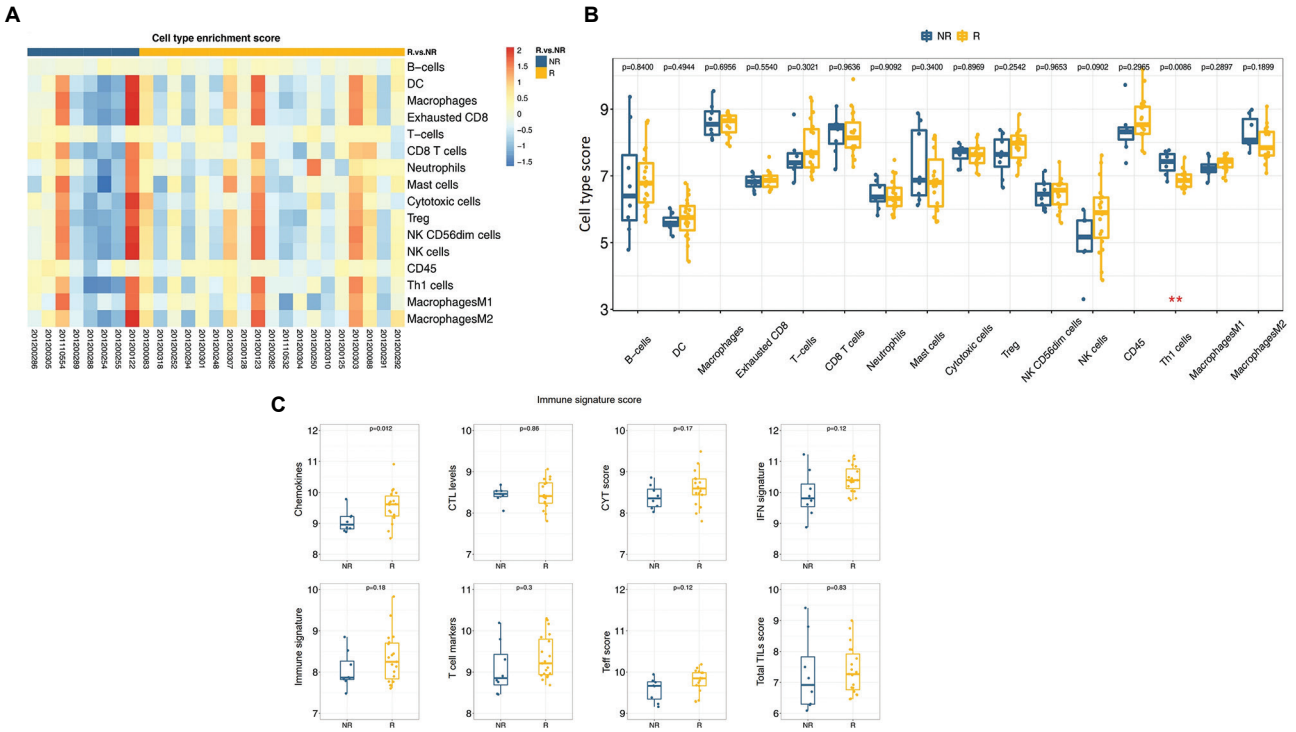

Figure 1. Comparison of cell type scores in immunotherapy-responsive (R) and non-responsive (NR) tumors. (A) Cell type enrichment scores in responding and non-responding tumors. Red indicates an increase in cell type scores, and blue indicates a decrease in cell type scores. (B) Cell type scores in responding and non-responding tumors. (C) Immune signature scores in responding and non-responding tumors.
Abbreviations: CTL: Cytotoxic T lymphocyte; CYT: Cytolytic activity; DC: Dendritic cell; IFN: Interferon; NK: Natural killer; Teff: T effector; TIL: Tumor-infiltrating lymphocytes.

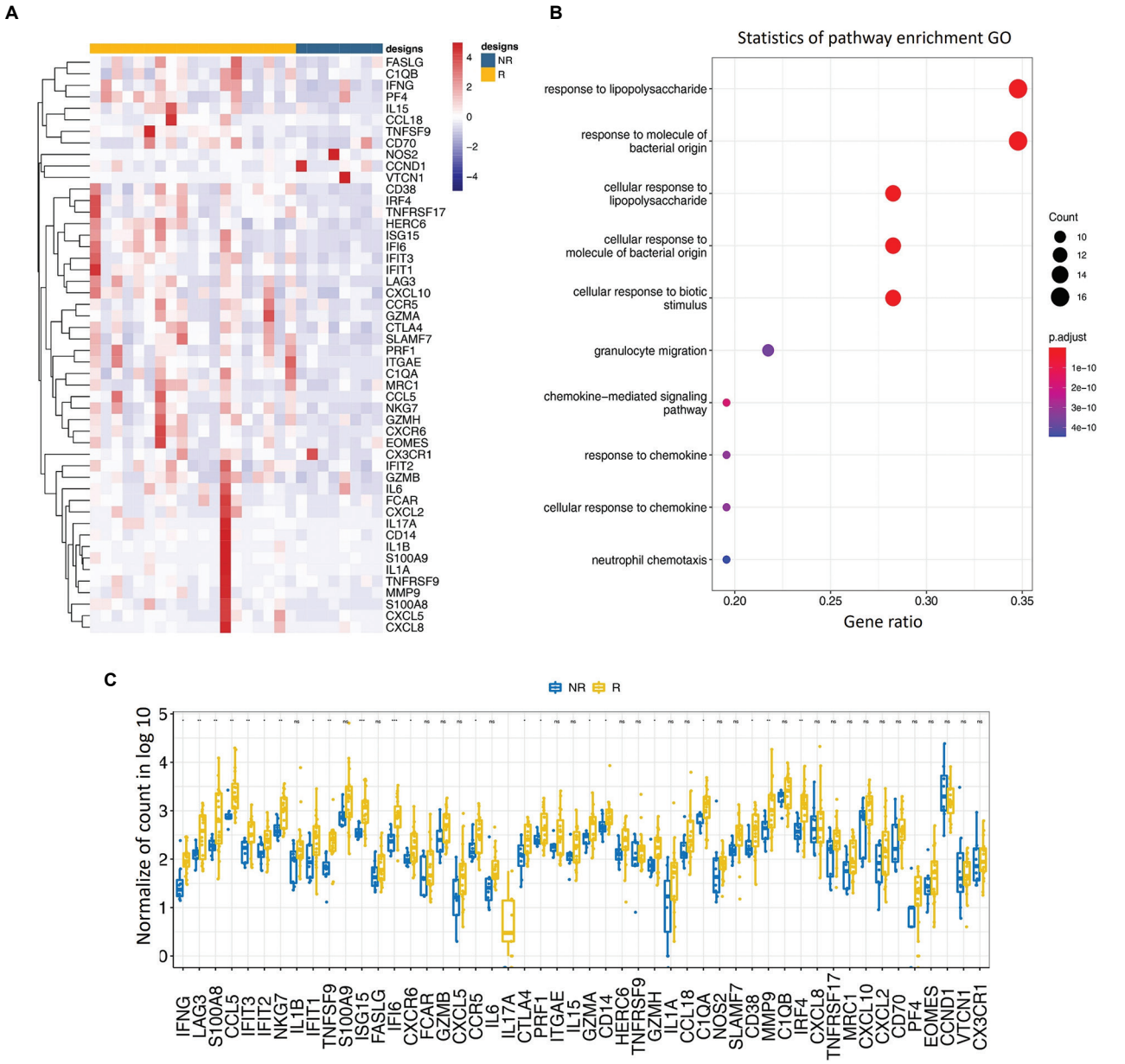

Figure 2. Analysis of genes that were differentially expressed between immunotherapy-responsive (R) and non-responsive (NR) tumors. (A) Heatmap of differentially expressed genes (DEGs). (B) Box plot of DEGs. (C) Gene ontology (GO) analysis.

GO analysis of genes that were differentially expressed in responding and non-responding tumors to determine their associated biological functions. GO analysis showed that upregulated genes were primarily enriched in chemokine-mediated signaling pathways, leukocyte adhesion, T-cell differentiation, and T-cell proliferation (Figure 2C). These findings suggest that *CXCR6* may be involved in immune surveillance in NPC and may help shape the TME.

3.4. Verification of *CXCR6* expression as a predictive biomarker associated with the response to immunotherapy in patients with NPC

Preliminary analysis of the TME revealed that *CXCR6* may be associated with the response to NPC immunotherapy. We used univariate analyses to determine whether *CXCR6* was a prognostic factor for NPC and found that several factors, including sex, ECOG, alcohol consumption, EBV, and PD-L1, were not associated with PFS under

immunotherapy (Table 2). However, *CXCR6* was associated with immunotherapy PFS (hazard ratio [HR] = 4.86; 95% confidence interval [CI]: 1.52–15.6; p=0.014) (Figure 3). The association between *CXCR6* and PFS remained significant (HR = 5.13; 95% CI: 1.40–18.8; p=0.014) in the multivariable Cox proportional hazards regression model including age, sex, PD-L1 expression, and EBV. Other factors, such as age, smoking status, and body mass index, were also associated with PFS during anti–PD-1 immunotherapy (Table 2).

Subsequently, we analyzed the TME characteristics in different *CXCR6* expression groups. We found that the two groups had different cell type enrichment scores (Figure 4A), immune cell type scores (Figure 4B), and immune signature scores (Figure 4C). The high *CXCR6* expression group had a higher degree of immune cell enrichment (Figure 4A). Immune cell infiltration was significantly higher in B cells, DCs, T cells, NK $CD56^{dim}$ cells, $CD45^{+}$ cells, and M1 macrophages (Figure 4B). Compared with the low *CXCR6* expression group, the high CXCR6 expression group had significantly higher immune signature scores, including CYT scores, immune scores, T-cell marker signatures, and total TILs (Figure 4C). Subsequently, we analyzed DEGs between high and low *CXCR6* expression groups (Figure 4D). The expression levels of *TNFSF18*, *CCND1*, *CD70*, *EGFR*, *NRC1*, and *TNFSF9* were higher in the high *CXCR6* group than in the low *CXCR6* group (Figure 4E). Downregulated genes were predominantly enriched in pathways such as the tumor necrosis factor response and T cell proliferation, whereas upregulated genes were predominantly enriched in pathways including leukocyte adhesion, monocyte proliferation, and lymphocyte proliferation (Figure 4F). Overall, our results suggest that *CXCR6* expression may serve as a predictive biomarker for response to immunotherapy in patients with NPC.

3.5. Changes in the TIME before and during treatment

To explore the changes in the TME following anti-PD-1 immunotherapy, mRNA data were generated from paired tissue samples collected from 17 patients before and during treatment. Enrichment scores of 16 cell types, B cells, DCs, macrophages, exhausted CD^{8+} T cells, T cells, CD^{8+} T cells, neutrophils, mast cells, cytotoxic cells, Tregs, NK $CD56^{dim}$ cells, NK cells, CD45 cells, Th1 cells, M1 macrophages, and M2 macrophages, were analyzed. The results showed that TIME profiles differed between pre-treatment and on-treatment samples (Figure 5A). Immune cell infiltration levels of T cells, mast cells, and $CD45^{+}$ cells increased during treatment (Figure 5B). In addition, we analyzed eight immune signature scores and found that T-cell marker and total TIL scores increased during treatment, whereas T-effector and CYT scores decreased (Figure 5C).

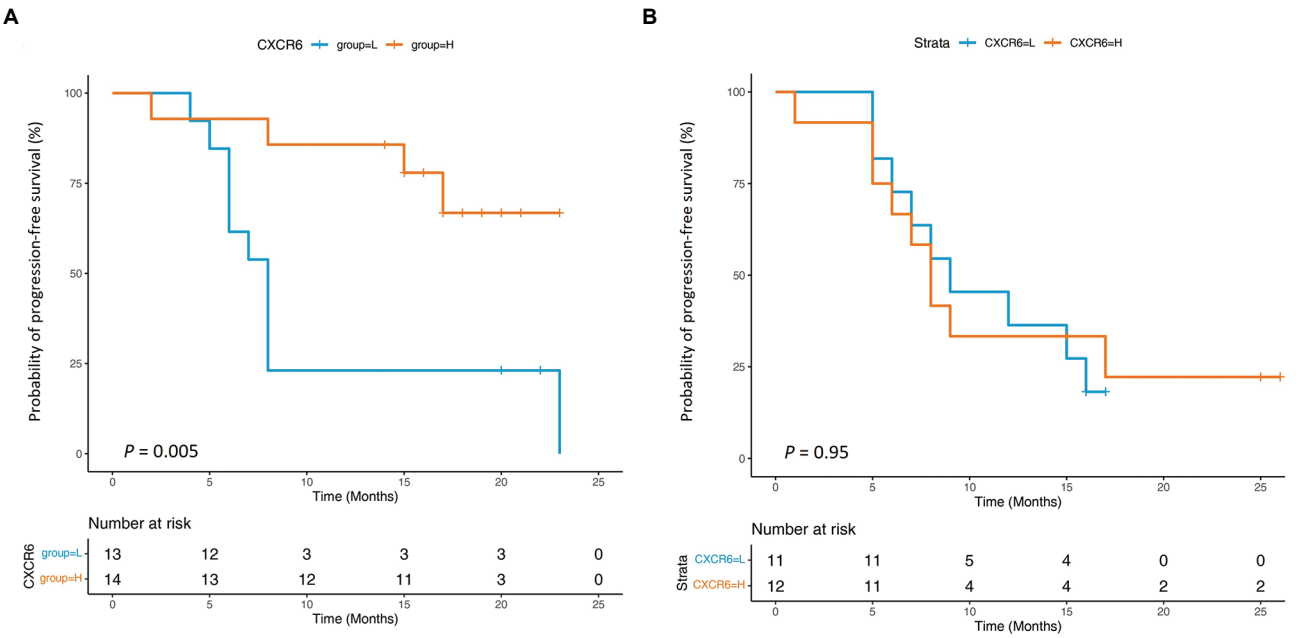

Figure 3. High *CXCR6* expression is associated with better response to anti-PD-1 immunotherapy in nasopharyngeal carcinoma. Red indicates increased cell type scores, and blue indicates decreased cell type scores. (A) Kaplan–Meier curves of progression-free survival (PFS) in the Toripalimab group. (B) Kaplan–Meier curves of PFS in the placebo group.

Table 2. Univariable and multivariable Cox regression analysis of clinical factors

Characteristic	[a]*n*	Univariable			Multivariable		
		HR	95% CI	*p*	HR	95% CI	*p*
Sex	27						
Female		-	-		-	-	
Male		0.40	0.13–1.20	0.10	3.12	0.58–16.9	0.2
Age (years)							
≤50		-	-		-	-	
>50		2.50	0.83–7.52	0.10	7.08	1.82–27.6	0.005
Eastern Cooperative Oncology Group performance score							
0		-	-				
1		1.13	0.31–4.13	0.8			
Smoking status							
No		-	-		-	-	
Yes		0.36	0.11–1.15	0.083	0.16	0.03–0.83	0.029
Alcohol use							
No		-	-				
Yes		0.46	0.10–2.06	0.3			
Body mass index (kg/m^2)							
18.5–22.9		-	-		-	-	
≥ 23		0.26	0.06–1.18	0.080	0.15	0.02–0.92	0.040
< 18.5		0.69	0.15–3.17	0.6	0.73	0.12–4.39	0.7
Epstein–Barr virus DNA (copies/mL)							
< 500		-	-				
≥ 500		1.60	0.21–12.3	0.7			
< 2,000		-	-				
≥ 2,000		0.94	0.29–3.00	>0.9			
CXCR6 expression							
High		-	-		-	-	
Low		4.86	1.52–15.6	0.008	5.13	1.40–18.8	0.014
PD-L1 expression	23						
TC <1%		-	-				
TC ≥1%		0.57	0.18–1.84	0.3			
TC <5%		-	-				
TC ≥5%		0.72	0.22–2.29	0.6			
IC <1%		-	-				
IC ≥1%		0.74	0.24–2.29	0.6			
IC <5%		-	-				
IC ≥5%		1.01	0.27–3.83	>0.9			
TC <1% and IC <1%		-	-				
TC ≥1% or IC ≥1%		0.71	0.21–2.41	0.6			
TC <5% and IC <5%		-	-				
TC ≥5% or IC ≥%		0.71	0.21, 2.41	0.6			

Note: [a]27 refers to the treatment group, 23 refers to the placebo group.
Abbreviations: CI: Confidence interval; HR: Hazard ratio; IC: Immune cell; PD-L1: Programmed death-ligand 1; TC: Tumor cell.

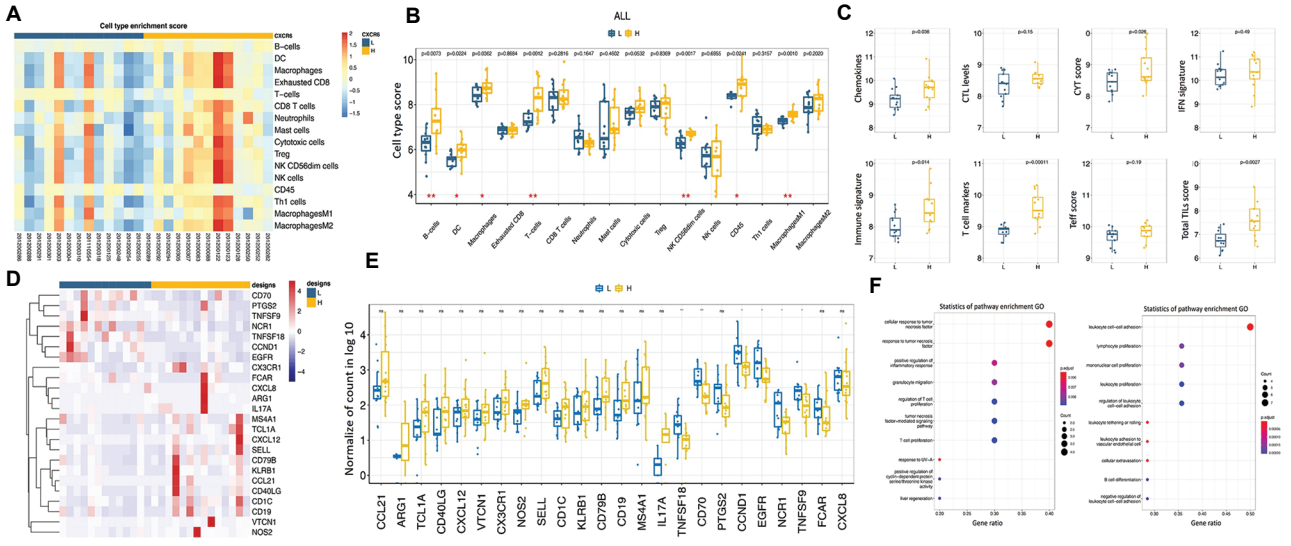

Figure 4. Cell type scores and differential gene expression in high (H) and low (L) *CXCR6* expression groups. (A) Cell type enrichment scores in the high and low *CXCR6* expression groups. Red indicates increased cell type scores, and blue indicates decreased cell type scores. (B) Cell type scores in high and low *CXCR6* expression groups. (C) Immune signature scores of high and low *CXCR6* expression groups. (D) Heatmap of differentially expressed genes (DEGs). (E) Box plot of DEGs. (F) Gene ontology (GO) analysis.

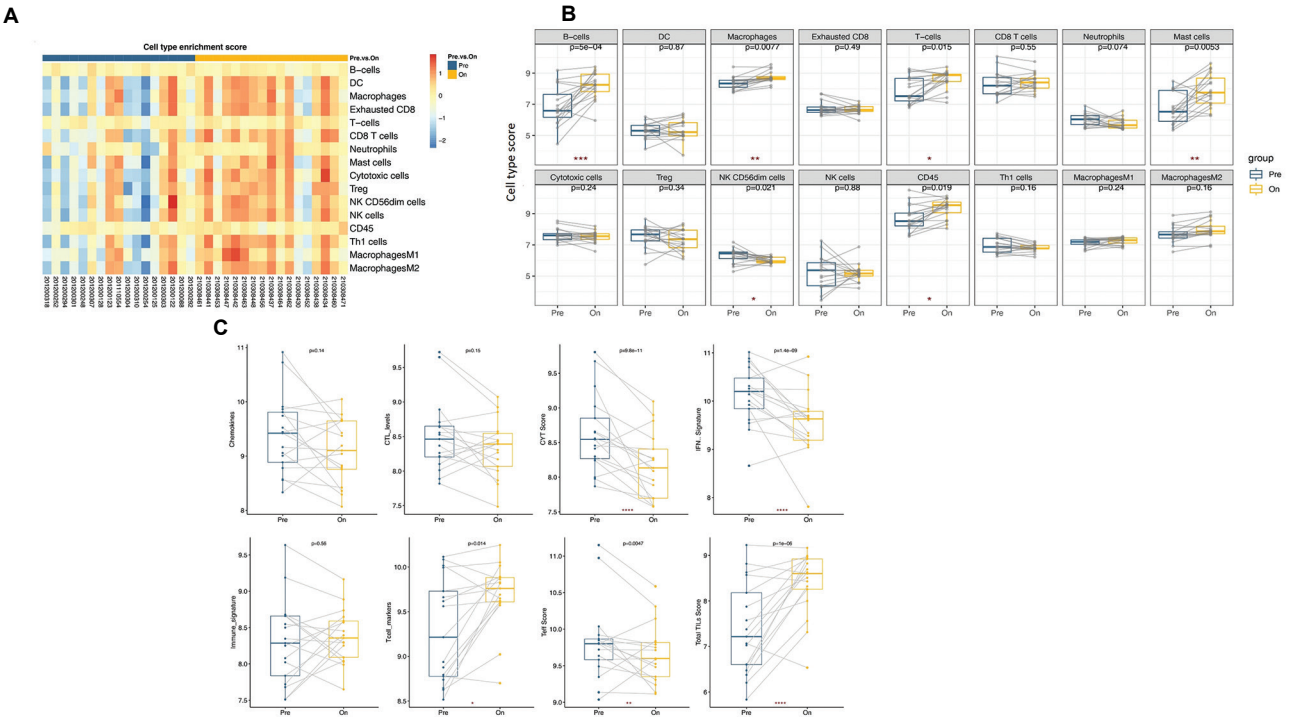

Figure 5. Tumor immune microenvironment changes before and during treatment. (A) Changes in cell type enrichment scores before and during treatment. Red indicates an increase, and blue indicates a decrease in the scores. (B) Changes in cell type scores before and during treatment. (C) Changes in immune signature scores before and during treatment.

4. Discussion

In this study, we aimed to understand the TME of NPC to identify biomarkers that can predict patients' response to anti-PD-1 immunotherapy. Anti-PD-1 immunotherapy-responsive tumors exhibited high *CXCR6* expression levels, suggesting that *CXCR6* may be involved in immune surveillance of NPC and in shaping the TIME. We also found that TIME profiles differed between pre-treatment

and on-treatment samples. Overall, *CXCR6* expression appears to be a predictive biomarker of response to immunotherapy in NPC.

Tumor cell generation is determined by gene mutations, whereas tumor progression is regulated by the TME and immune responses, and tumor occurrence and clinical prognosis correlate with the distribution and infiltration of immune cells in the TME.[33,34] Law *et al.*[35] found that a large number of immune cells were distributed within the tumor stroma, playing an important role in tumor development, invasion, metastasis, and drug sensitivity. In NPC, many lymphocytes infiltrate the microenvironment surrounding the tumor cells, and various immune cells and immune signatures contribute to NPC development,[36] which is consistent with our results. We also observed high cell infiltration scores for responding tumors, including $CD8^+$ T cells, neutrophils, cytotoxic cells, Treg cells, and M1 macrophages, although these differences were not statistically significant. However, previous studies have reported high infiltration levels of immune cells in NPC, including M0 macrophages, M1 macrophages, γδ T cells, activated $CD4^+$ T memory cells, and $CD8^+$ T cells, with differences that were also not statistically significant.[37] Non-responding tumors exhibited significantly higher scores for Th1 immune cell infiltration than responding tumors. Under normal immune function, Th1 and Th2 cells maintain a dynamic balance, supporting normal cellular immunity. However, upon exposure to tumor antigens, Th cell precursors selectively differentiate into Th1 or Th2 cells. Peripheral blood from NPC patients showed higher levels of Th2-derived cytokines than Th1-derived cytokines, which may contribute to tumor immune escape.[38] We found that the levels of Th1 cells were lower in responding tumors than in non-responding tumors. In addition, responding tumors exhibited higher chemokine signature scores than non-responding tumors. Moreover, Su *et al.*[39] reported the expression of chemokine-encoding genes in NK cells in the NPC microenvironment, and our results support their role as positive regulators of the immune response. The PD-1 pathways function broadly to regulate the immune network through both direct and indirect mechanisms.[40] Therefore, we consider that elevated chemokine signatures in responding tumors enhance the efficacy of immunotherapy.

Many studies on CXCL16/CXCR6 have focused on their roles in chemotaxis and recruitment of immune cells, thereby exerting antitumor immunity. CXCL16 can directly bind to the CXCR6 receptor expressed by tumor cells, inducing or inhibiting tumor cell growth through a series of intracellular signal transduction pathways and negatively regulating tumor progression. CXCL16/CXCR6 also regulates tumor immunity.[41] Parsonage *et al.*[23] found that NPC tumor cells express high levels of CXCL16 and attract $CXCR6^+$ T cells, including infiltrating $CD4^+$ T cells and Th cells, leading to an antitumor immune response. We found that, compared with the low *CXCR6* expression group, the high *CXCR6* expression group had significantly higher immune scores for B cells, DCs, T cells, NK $CD56^{dim}$ cells, $CD45^+$ cells, and M1 macrophages and higher immune signature scores, including CYT scores, T-cell marker signature, and total TIL scores. *CXCR6* may recruit immune cells and mediate the infiltration of immune cells such as T cells and NK cells, leading to antitumor immune responses. Thus, we postulate that *CXCR6* is overexpressed within the TIME, enhancing the response to immunotherapy.

We used NanoString to analyze the TIME in patients with NPC before and during immunotherapy. The results showed that the immune cell infiltration scores and immune signatures of the patients varied before and during treatment. In particular, T-cell marker and total TIL scores significantly increased, suggesting that the TME of NPC can affect immunotherapy response. However, further studies are required to confirm these observations. The changes that occur in the microenvironment following immunotherapy are complex and crucial. Tertiary lymphoid structures (TLSs) can improve antigen presentation and increase cytokine-mediated signaling.[37] We propose that the increase in tertiary lymphoid structures is associated with notable tumor responses. NPC tumor tissues contain abundant TILs, and their distinctive TME may confer heightened sensitivity to immunotherapy.[41] Gene expression typically represents a consequence of cancer progression rather than a causative factor.[42] Accordingly, we suggest that the overall TIL score increases following treatment, contributing to improved immunotherapy responses. However, our results require further analysis.

5. Conclusion

The TME in patients with NPC is complex. In this study, we analyzed molecules associated with immunotherapy efficacy to investigate how the TIME influences patient responses. Immunotherapy-responsive tumors exhibited higher immune cell enrichment and higher immune cell infiltration scores compared to non-responsive tumors. The TME in patients with NPC varied before and during immunotherapy. Hence, we conclude that *CXCR6* may serve as a predictive biomarker for response to immunotherapy in NPC. However, this study had some limitations. First, this was a retrospective analysis of a real-world study, and not all confounders could be controlled for. Moreover, the number of samples analyzed here was

small and may have led to potential selection bias. The results require external validation through a multicenter study. Therefore, clinical trials with larger sample sizes are necessary to assess the predictive value of *CXCR6*. In addition, the immune cell scores were not validated by immunohistochemistry. Finally, the function of *CXCR6* should be validated through *in vitro* studies.

Acknowledgments

The authors would like to thank the Xian Sheng company for their assistance with the NanoString technology.

Funding

None.

Conflict of interest

The authors declare that they have no competing interests.

Author contributions

Conceptualization: Zhen-Chong Yang
Formal analysis: Xi Zhou, Zhen-Chong Yang
Investigation: Ying-He Li
Methodology: Xi Zhou
Writing–original draft: Ying-He Li, Zhen-Chong Yang
Writing–review & editing: Zhen-Chong Yang

Ethics approval and consent to participate

The study was approved by the Hospital Institutional Review Board of Sun Yat-sen University Cancer Control Centre (2018-XY-007), and all patients provided written informed consent before enrollment.

Consent for publication

All patients provided written informed consent before enrollment.

Availability of data

The data that support the findings of this study are available from the corresponding author upon reasonable request.

References

1. Zhang Y, Chen L, Hu GQ, *et al*. Gemcitabine and cisplatin induction chemotherapy in nasopharyngeal carcinoma. *N Engl J Med*. 2019;381:1124-1135.

   doi: 10.1056/nejmoa1905287

2. Luo W. Nasopharyngeal carcinoma ecology theory: Cancer as multidimensional spatiotemporal "unity of ecology and evolution" pathological ecosystem. *Theranostics*. 2023;13(5):1607-1631.

   doi: 10.7150/thno.82690

3. Chen YP, Chan ATC, Le QT, Blanchard P, Sun Y, Ma J. Nasopharyngeal carcinoma. *Lancet*. 2019;394:64-80.

   doi: 10.1016/S0140-6736(19)30956-0

4. Zhang L, Huang Y, Hong S, *et al*. Gemcitabine plus cisplatin versus fluorouracil plus cisplatin in recurrent or metastatic nasopharyngeal carcinoma: A multicentre, randomised, open-label, phase 3 trial. *Lancet*. 2016;388:1883-1892.

   doi: 10.1016/S0140-6736(16)31388-5

5. Hsu C, Lee SH, Ejadi S, *et al*. Safety and antitumor activity of pembrolizumab in patients with programmed death-ligand 1-positive nasopharyngeal carcinoma: Results of the KEYNOTE-028 study. *J Clin Oncol*. 2017;35:4050-4056.

   doi: 10.1200/JCO.2017.73.3675

6. Fang W, Zhang J, Hong S, *et al*. EBV-driven LMP1 and IFN-γ up-regulate PD-L1 in nasopharyngeal carcinoma: Implications for oncotargeted therapy. *Oncotarget*. 2014;5:12189-12202.

   doi: 10.18632/oncotarget.2608

7. Hsu MC, Hsiao JR, Chang KC, *et al*. Increase of programmed death-1-expressing intratumoral CD8 T cells predicts a poor prognosis for nasopharyngeal carcinoma. *Mod Pathol*. 2010;23:1393-1403.

   doi: 10.1038/modpathol.2010.130

8. Xiao M, Qi F, Chen X, *et al*. Functional polymorphism of cytotoxic T-lymphocyte antigen 4 and nasopharyngeal carcinoma susceptibility in a Chinese population. *Int J Immunogenet*. 2010;37:27-32.

   doi: 10.1111/j.1744-313X.2009.00888.x

9. Andrei G, Trompet E, Snoeck R. Novel therapeutics for Epstein-Barr virus. *Molecules*. 2019;24:997.

   doi: 10.3390/molecules24050997

10. Yang Y, Qu S, Li J, *et al*. Camrelizumab versus placebo in combination with gemcitabine and cisplatin as first-line treatment for recurrent or metastatic nasopharyngeal carcinoma (CAPTAIN-1st): A multicentre, randomised, double-blind, phase 3 trial. *Lancet Oncol*. 2021;22:1162-1174.

    doi: 10.1016/S1470-2045(21)00302-8

11. Xu R, Mai H, Chen Q, *et al*. JUPITER-02: Randomized, double-blind, phase III study of toripalimab or placebo plus gemcitabine and cisplatin as first-line treatment for recurrent or metastatic nasopharyngeal carcinoma (NPC). *J Clin Oncol*. 2021;39:LBA2.

    doi: 10.1200/jco.2021.39.15_suppl.lba2

12. Fehrenbacher L, Spira A, Ballinger M, *et al*. Atezolizumab versus docetaxel for patients with previously treated non-small-cell lung cancer (Poplar): A multicentre, open-label, phase 2 randomised controlled trial. *Lancet*. 2016;387:1837-1846.

doi: 10.1016/S0140-6736(16)00587-0

13. Ayers M, Lunceford J, Nebozhyn M, *et al*. IFN-γ-related mRNA profile predicts clinical response to PD-1 blockade. *J Clin Invest*. 2017;127:2930-2940.

    doi: 10.1172/jci91190

14. Vitiello GA, Bowler TG, Liu M, *et al*. Differential immune profiles distinguish the mutational subtypes of gastrointestinal stromal tumor. *J Clin Invest*. 2019;129: 1863-1877.

    doi: 10.1172/jci124108

15. Danaher p, Warren s, Dennis L, *et al*. Gene expression markers of tumor infiltrating leukocytes. *J Immunother Cancer*. 2017;5:18.

    doi: 10.1186/s40425-017-0215-8

16. Jiang P, Gu S, Pan D, *et al*. Signatures of T cell dysfunction and exclusion predict cancer immunotherapy response. *Nat Med*. 2018;24:1550-1558.

    doi: 10.1038/s41591-018-0136-1

17. Groblewska M, Litman-Zawadzka A, Mroczko B. The role of selected chemokines and their receptors in the development of gliomas. *Int J Mol Sci*. 2020;21:3704.

    doi: 10.3390/ijms21103704

18. Ikeda T, Nishita M, Hoshi K, Honda T, Kakeji Y, Minami Y. Mesenchymal stem cell-derived CXCL16 promotes progression of gastric cancer cells by STAT3-mediated expression of Ror1. *Cancer Sci*. 2020;111:1254-1265.

    doi: 10.1111/cas.14339

19. Mir H, Kaur G, Kapur N, *et al*. Higher CXCL16 exodomain is associated with aggressive ovarian cancer and promotes the disease by CXCR6 activation and MMP modulation. *Sci Rep*. 2019;9:1-12.

    doi: 10.1038/s41598-019-38766-6

20. Hong L, Wang S, Li W, Wu D, Chen W. Tumor-associated macrophages promote the metastasis of ovarian carcinoma cells by enhancing CXCL16/CXCR6 expression. *Pathol Res Pract*. 2018;214:1345-1351.

    doi: 10.1016/j.prp.2018.07.009

21. Adamski V, Mentlein R, Lucius R, Synowitz M, Held-Feindt J, Hattermann K. The chemokine receptor CXCR6 evokes reverse signaling via the transmembrane chemokine CXCL16. *Int J Mol Sci*. 2017;18:1468.

    doi: 10.3390/ijms18071468

22. Gillard-Bocquet M, Caer C, Cagnard N, Crozet L, *et al*. Lung tumor microenvironment induces specific gene expression signature in intratumoral NK cells. *Front Immunol*. 2013;4:19.

    doi: 10.3389/fimmu.2013.00019

23. Parsonage G, Machado LR, Hui JW, *et al*. CXCR6 and CCR5 localize T lymphocyte subsets in nasopharyngeal carcinoma. *Am J Pathol*. 2012;180:1215-1222.

    doi: 10.1016/j.ajpath.2011.11.032

24. Borst O, Abed M, Alesutan I, *et al*. Dynamic adhesion of eryptotic erythrocytes to endothelial cells via CXCL16/ SR-PSOX. *Am J Physiol Cell Physiol*. 2012;302:C644-C651.

    doi: 10.1152/ajpcell.00340.2011

25. Newman AM, Liu CL, Green MR, *et al*. Robust enumeration of cell subsets from tissue expression profiles. *Nat Methods*. 2015;12:453-457.

    doi: 10.1038/nmeth.3337

26. Germano G, Frapolli R, Belgiovine C, *et al*. Role of macrophage targeting in the antitumor activity of trabectedin. *Cancer Cell*. 2013;23:249-262.

    doi: 10.1016/j.ccr.2013.01.008

27. Mosser DM, Edwards JP. Exploring the full spectrum of macrophage activation. *Nat Rev Immunol*. 2009;8:958-969.

    doi: 10.1038/nri2448

28. Damotte D, Warren S, Arrondeau J, *et al*. The tumor inflammation signature (TIS) is associated with anti-PD-1 treatment benefit in the CERTIM pan-cancer cohort. *J Transl Med*. 2019;17:357.

    doi: 10.1186/s12967-019-2100-3

29. Wherry EJ, Kurachi M. Molecular and cellular insights into T cell exhaustion. *Nat Rev Immunol*. 2015;15:486-499.

    doi: 10.1038/nri3862

30. Ritchie ME, Phipson B, Wu D, *et al*. Limma powers differential expression analyses for RNA-sequencing and microarray studies. *Nucleic Acids Res*. 2015;43:e47.

    doi: 10.1093/nar/gkv007

31. Foong RE, Shaw NC, Berry LJ, Hart PH, Gorman S, Zosky GR. Vitamin D deficiency causes airway hyperresponsiveness, increases airway smooth muscle mass, and reduces TGF-β expression in the lungs of female BALB/c mice. *Physiol Rep*. 2014;2:e00276.

    doi: 10.1002/phy2.276

32. Eisenhauer EA, Therasse P, Bogaerts J, *et al*. New response evaluation criteria in solid tumours: Revised RECIST guideline (version 1.1). *Eur J Cancer*. 2009;45:228-247.

    doi: 10.1016/j.ejca.2008.10.026

33. Hou P, Kapoor A, Zhang Q, *et al*. Tumor microenvironment remodeling enables bypass of oncogenic KRAS dependency in pancreatic cancer TME. *Cancer Discov*. 2020;10: 1058-1077.

    doi: 10.1158/2159-8290.cd-19-0597

34. Bi G, Chen Z, Yang X, *et al*. Identification and validation of tumor environment phenotypes in lung adenocarcinoma

by integrative genome-scale analysis. *Cancer Immunol Immunother*. 2020;69:1293-1305.

doi: 10.1007/s00262-020-02546-3

35. Law AMK, Lim E, Ormandy CJ, Gallego-Ortega D. The innate and adaptive infiltrating immune systems as targets for breast cancer immunotherapy. *Endocr Relat Cancer*. 2017;24:R123-R144.

doi: 10.1530/erc-16-0404

36. Chen YP, Yin JH, Li WF, *et al*. Single-cell transcriptomics reveals regulators underlying immune cell diversity and immune subtypes associated with prognosis in nasopharyngeal carcinoma. *Cell Res*. 2020;30:1024-142.

doi: 10.1038/s41422-020-0374-x

37. Cabrita R, Lauss M, Sanna A, *et al*. Tertiary lymphoid structures improve immunotherapy and survival in melanoma. *Nature*. 2020;577:561-565.

doi: 10.1038/s41586-019-1914-8

38. Derynck R, Turley SJ, Akhurst RJ. TGFβ biology in cancer progression and immunotherapy. *Nat Rev Clin Oncol*. 2021;18:9-34.

doi: 10.1038/s41571-020-0403-1

39. Su ZY, Siak PY, Leong CO, Cheah SC. Nasopharyngeal carcinoma and its microenvironment: Past, current, and future perspectives. *Front Oncol*. 2022;12:840467.

doi: 10.3389/fonc.2022.840467

40. Hamilton PT, Anholt BR, Nelson BH. Tumour immunotherapy: Lessons from predator-prey theory. *Nat Rev Immunol*. 2022;22(12):765-775.

doi: 10.1038/s41577-022-00719-y

41. Xu JY, Wei XL, Wang YQ, *et al*. Current status and advances of immunotherapy in nasopharyngeal carcinoma. *Ther Adv Med Oncol*. 2022;14.

doi: 10.1177/17588359221096214

42. Cui YY. Book review: Rethinking cancer: A new paradigm for the postgenomics era. Rethinking our path in the fight against cancer. *Curr Cancer Rep*. 2025;7:286-289.

doi: 10.25082/ccr.2025.01.004

ACCSCIENCE PUBLISHING

Advances in Radiotherapy & Nuclear Medicine

ORIGINAL RESEARCH ARTICLE

Evaluation of inter-fractional tumor target volume changes in ViewRay MRIdian LINAC adaptive radiotherapy using similarity metrics

Merve Konuk[1], Görkem Güngör[2], Banu Atalar[2], Serhat Aras[3]*, and Orhan İçelli[1]

[1]Department of Physics, Faculty of Arts and Sciences, Yildiz Technical University, Istanbul, Türkiye

[2]Department of Radiation Oncology, Faculty of Medicine, Acıbadem Mehmet Ali Aydınlar University, Istanbul, Türkiye

[3]Department of Radiation Oncology, Haydarpasa Numune Training and Research Hospital, University of Health Sciences, Istanbul, Türkiye

Abstract

Tumor geometry can change during radiotherapy, and interfractional anatomical variations may compromise target coverage and dose conformity if not properly addressed. Magnetic resonance–guided adaptive radiotherapy (MRgART) enables ongoing visualization of tumor morphology and provides a framework for individualized treatment adaptation. This study quantitatively evaluated interfractional gross tumor volume (GTV) changes in patients treated with a ViewRay MRIdian LINAC system and investigated which similarity metric most reliably characterizes these variations. Retrospective MR images from 37 patients were analyzed and grouped by anatomical region into the pelvis, abdomen, and thorax. Baseline GTV (GTV_0) was compared with GTVs from five consecutive fractions (GTV_1–GTV_5). Geometric agreement was assessed using four similarity metrics: Dice similarity coefficient (DSC), Jaccard similarity coefficient (JSC), Tanimoto similarity coefficient (TSC), and Ochiai similarity coefficient (OSC). Interfractional stability was evaluated using mean similarity values and standard deviations across fractions. The abdominal region exhibited the greatest interfractional variability, with marked volume changes observed particularly in pancreatic cancer patients. Pelvic and thoracic tumors demonstrated relatively greater geometric stability, with lung tumors showing comparatively consistent agreement across fractions. Across all anatomical regions, OSC showed the highest mean similarity values and the lowest variability, indicating greater robustness than the other metrics. Statistical analysis confirmed that OSC performed significantly better than DSC, JSC, and TSC in the pelvis and abdomen ($p<0.05$), while showing comparable behavior to DSC in the thorax. These findings indicate that OSC is a reliable metric for monitoring interfractional tumor geometry in MR-guided adaptive radiotherapy and may support more precise and efficient adaptive treatment strategies.

Keywords: Magnetic resonance imaging-guided linear accelerator; Adaptive radiotherapy; Gross target volume; Similarity coefficients; Magnetic resonance imaging-guided radiotherapy

***Corresponding author:**
Serhat Aras
(serhat.aras@sbu.edu.tr)

Citation: Konuk M, Güngör G, Atalar B, Aras S, İçelli O. Evaluation of inter-fractional tumor target volume changes in ViewRay MRIdian LINAC adaptive radiotherapy using similarity metrics. *Adv Radiother Nucl Med*. 2026;4(1):69-79. doi: 10.36922/ARNM025410055

Received: October 9, 2025

1st revised: November 11, 2025

2nd revised: December 10, 2025

Accepted: January 9, 2026

Published online: January 29, 2026

1. Introduction

Image-guided radiation therapy techniques are typically based on the assumption that no significant gross tumor volume (GTV) changes occur during the treatment course. However, anatomical changes such as postural changes, volume changes in the bladder, rectum, weight loss, and tumor regression clearly change the volume of the GTV and organs at risk (OARs) significantly. Accounting for target and OAR changes is important for the accurate delivery of dose to the tumor and the protection of OARs.[1,2] These changes are patient-specific events and depend on the prescription dose.[3-6] The magnitude of anatomical and volumetric changes during radiotherapy may vary among patients depending on the prescribed dose and fractionation schedule, potentially leading to clinically important dosimetric changes.[7,8]

Bhide *et al.*[9] conducted a comprehensive investigation into target volumes delineated using computed tomography (CT) in patients with head and neck cancer, with a particular focus on the temporal evolution of both tumor volume and OARs throughout the treatment course. Their findings demonstrated that measurable and clinically relevant volumetric alterations begin to manifest as early as the 2nd week of radiotherapy, highlighting the dynamic nature of anatomical structures in this region and underscoring the limitations of static, pre-treatment planning. In a similar context, Ramsey *et al.*[10] examined the feasibility and potential clinical value of adaptive radiotherapy (ART) in lung cancer patients by systematically assessing GTV changes captured through CT-based imaging during treatment. Their analysis revealed notable inter-fractional variations in GTV, largely influenced by respiratory motion and tumor regression, thereby supporting the need for adaptive radiation strategies in thoracic malignancies.

Collectively, these studies emphasize the importance of repeated imaging and adaptive planning to account for anatomical variability and to maintain optimal dose delivery throughout the radiotherapy course. They further indicate that this challenge cannot be adequately addressed by pre-treatment imaging alone (e.g., CT simulation). One of the most important recent innovations addressing this limitation is magnetic resonance imaging (MRI)-based radiotherapy systems. As MR images do not use ionizing radiation, they pose no additional radiation risk compared to CT-based imaging, which provides an advantage for weekly, daily, or continuous imaging during radiotherapy treatment. In addition, unlike other CT-based devices, patients can be treated with a new plan by replanning within minutes while remaining on the treatment table, in response to tumor volume changes, OAR motion, and tissue displacement.[11] Another feature of MRI-based systems is their real-time tracking capability.[4,12-20]

The ViewRay MRIdian LINAC contains a 0.35 T split superconducting magnet integrated with a linear accelerator.[21,22] Numerous studies have been conducted using retrospective MRI images of patients treated with this device.[23-33] Nierer *et al.*[34] investigated the dosimetric benefit of online ART on the MRI-guided linear accelerator (MR-LINAC). The MR-LINAC has demonstrated advantages in protecting OARs in liver, lung, abdominal, and prostate treatments. This technology appears to play a key role in treatment individualization through the integration of MRI and ART. For example, Rachi *et al.*,[35] in their study on head and neck ART, quantified volumetric change using the DSC.

The aim of this study was to systematically assess inter-fractional GTV variations across three anatomically distinct regions—pelvis, abdomen, and thorax—by utilizing an MRI-guided ART workflow. In addition, the study sought to identify which of four commonly used similarity coefficients—Dice similarity coefficient [DSC], Jaccard similarity coefficient (JSC), Tanimoto similarity coefficient (TSC), and Ochiai similarity coefficient (OSC)—provides the most reliable and sensitive quantitative measure of tumor volume changes throughout the treatment course, thereby establishing the most appropriate metric for guiding ART decision-making.

2. Materials and methods

This study was conducted at the Acıbadem Mehmet Ali Aydınlar University Health Sciences Institute and was based on the retrospective evaluation of MRI images obtained from 37 patients treated with the ViewRay MRIdian LINAC system. Inter-fractional variations in GTV were systematically analyzed across three major anatomical regions: The pelvis (19 patients), abdomen (13 patients), and thorax (5 patients) (Table 1).

The pelvic cohort consisted exclusively of prostate cancer patients, providing a relatively homogeneous group for assessing volumetric stability and treatment-related anatomical changes. In contrast, the abdominal cohort represented a more heterogeneous population, including patients diagnosed with pancreatic, gastric, and colorectal cancers, as well as those with abdominal metastases originating from lung, testicular, and ovarian malignancies. This diversity allowed for a broader evaluation of tumor behavior and volume variability within an anatomically and physiologically dynamic region. The thoracic cohort comprised patients with primary lung and breast cancers, along with rectal and cervical cancers, presenting with metastatic involvement of the lungs. The inclusion of both primary and metastatic thoracic tumors enabled the examination of inter-fractional GTV changes in a region

Table 1. Radiotherapy dose ranges and fractionation schedules by cancer type and anatomical region

Anatomical region	Cancer types	Dose range (Gy)	Number of fractions	Total dose range (Gy)
Pelvis	Prostate	7.25	5	36.25
Abdomen	Pancreatic	6.00–15.00	3–5	24–50
	Gastric			
	Colorectal			
	Lung (abdomen metastasis)			
	Testicular (abdomen metastasis)			
	Ovarian (abdomen metastasis)			
Thorax	Lung	7.00–12.00	3–5	24–50
	Breast			
	Rectal (lung metastasis)			
	Cervical (lung metastasis)			

significantly influenced by respiratory motion and thoracic organ dynamics. This detailed anatomical classification provided a robust framework for investigating how tumor type, regional organ mobility, and treatment-related factors contribute to inter-fractional GTV variations, thereby enhancing the study's capacity to identify clinically relevant patterns across different tumor locations.

Due to the distinct anatomical configurations and region-specific tumor motion characteristics, each anatomical site was evaluated independently to allow for a more accurate assessment of inter-fractional GTV variations and to better understand the clinical necessity for implementing ART. Pelvic structures, abdominal organs, and thoracic tissues exhibit markedly different patterns of physiological motion—such as bladder and rectal filling in the pelvis, gastrointestinal and diaphragmatic motion in the abdomen, and respiratory-driven displacement in the thorax—which can uniquely influence tumor position, shape, and volume throughout the treatment course. Therefore, a region-specific analytical approach was essential to capture these biological and mechanical differences and to determine whether ART would provide a measurable benefit in each anatomical setting.

In this study, four widely used volumetric similarity metrics—DSC, JSC, TSC, and OSC—were employed to quantitatively characterize the degree of agreement between GTV contours across treatment fractions. These metrics provided complementary perspectives on tumor volume changes by comparing overlap ratios, intersection-to-union relationships, and similarity indices derived from set theory and statistical classification. By applying these coefficients systematically, the study aimed to establish a robust and objective framework for evaluating inter-fractional anatomical variations and determining which metric most sensitively and reliably reflects clinically relevant changes that could influence ART decision-making.

2.1. Similarity coefficient calculations

First, the DSC[36] was used to measure the level of agreement between two segmentations. A and B represent the target regions for DSC calculation. The similarity criterion between target regions is calculated using Equation (1).

$$DSC(A,B)=\frac{2(A\cap B)}{(A+B)} \quad (1)$$

Here, $(A\cap B)$ represents the intersection of both image segments. $(A + B)$ is the sum of both image segments.

Second, the JSC[37] represents the intersection of the two sets divided by their union. JSC can be calculated using Equation (2).

$$JSC(A,B)=\frac{(A\cap B)}{(A\cup B)}=\frac{(A\cap B)}{(A)+(B)-(A\cap B)} \quad (2)$$

Third, the TSC[38] is formulated using statistical decision theory measures of true positive (TP), true negative (TN), false positive (FP), and false negative (FN) (Equation [3]).[39]

$$TSC(A,B)=\frac{TP}{TP+FP+FN}=\frac{|A\cap B|}{|A-B|+|B-A|+|A\cap B|} \quad (3)$$

Unlike the JSC, TSC includes the sum of the differences between sets A and B in the denominator part.

Finally, the OSC (also known as the Ochiai–Otsuka similarity coefficient) can be calculated using Equation (4):

$$OSC(A,B)=\frac{|A\cap B|}{\sqrt{|A|.|B|}} \quad (4)$$

Here, $|A\cap B|$ represents the intersection of the two sets, and $\sqrt{|A|.|B|}$ represents the square root of the product of the two sets.[40] DSC, JSC, TSC, and OSC values range between 0 and 1. When the value is close to 0, it indicates low similarity, whereas values close to 1 indicate high similarity.

The DSC, JSC, TSC, and OSC formulae (Equations [1]–[4]) were used in the study as follows. Firstly, the GTV0 volume was drawn and recorded in the ViewRay MRIdian treatment planning system (TPS) before treatment. Then, the volumes of GTV1 in the first

fraction, GTV2 in the second fraction, GTV3 in the third fraction, GTV4 in the fourth fraction, and GTV5 in the fifth fraction were contoured (delineated) for each patient and recorded in the system (Figure 1).

For the purpose of applying the four similarity coefficient formulas, intersection volumes were generated between the baseline contour (GTV0) and each subsequent fraction. Specifically, the intersection sets GTV0∩GTV1, GTV0∩GTV2, GTV0∩GTV3, GTV0∩GTV4, and GTV0∩GTV5 were computed to quantify the degree of overlap between the initial GTV and the corresponding GTV in each treatment fraction. These intersection volumes provided the fundamental geometric inputs required for calculating the similarity metrics.

In addition, for every patient, the GTV (cm^3), the intersection volumes, and the union volumes were extracted directly from the TPS. These values were subsequently incorporated into the DSC, JSC, TSC, and OSC calculations to derive the quantitative similarity scores (Table 2). This systematic workflow ensured that each similarity coefficient was calculated using consistent and anatomically meaningful volumetric inputs. Through this structured approach, inter-fractional GTV variations in the pelvic, abdominal, and thoracic regions were comprehensively evaluated based on the similarity coefficient outputs. This allowed for a robust comparison of volumetric consistency across fractions and enabled the identification of region-specific patterns in tumor volume changes during the course of MRI-guided ART.

In this study, the inter-fractional stability of similarity metrics was quantitatively defined as the degree of consistency of metric values across treatment fractions when comparing the GTV0 with subsequent fraction contours (GTV1–GTV5). Stability was evaluated using two complementary descriptive statistical parameters: the mean (M) and the standard deviation (SD) values of each similarity coefficient calculated across all fractions. The M similarity value was used to represent the overall level of geometric agreement between GTV0 and the inter-fractional GTVs, with higher mean values (ideally close to 1) indicating greater average volumetric overlap. The SD was used as a measure of inter-fractional variability, where lower SD values (ideally close to 0) indicate reduced fluctuation of the similarity coefficient across fractions and, therefore, higher metric stability. Accordingly, a similarity coefficient was considered more stable if it demonstrated both a high M similarity value (close to 1) and a low SD (close to 0) within the same anatomical region. This approach allows for differentiation between metrics that exhibit consistent behavior across fractions and those that are more sensitive to inter-fractional anatomical variations.

The similarity values obtained from all four metrics were subjected to a comprehensive ANOVA analysis using SPSS Statistics 26.0 (IBM, USA) to identify which

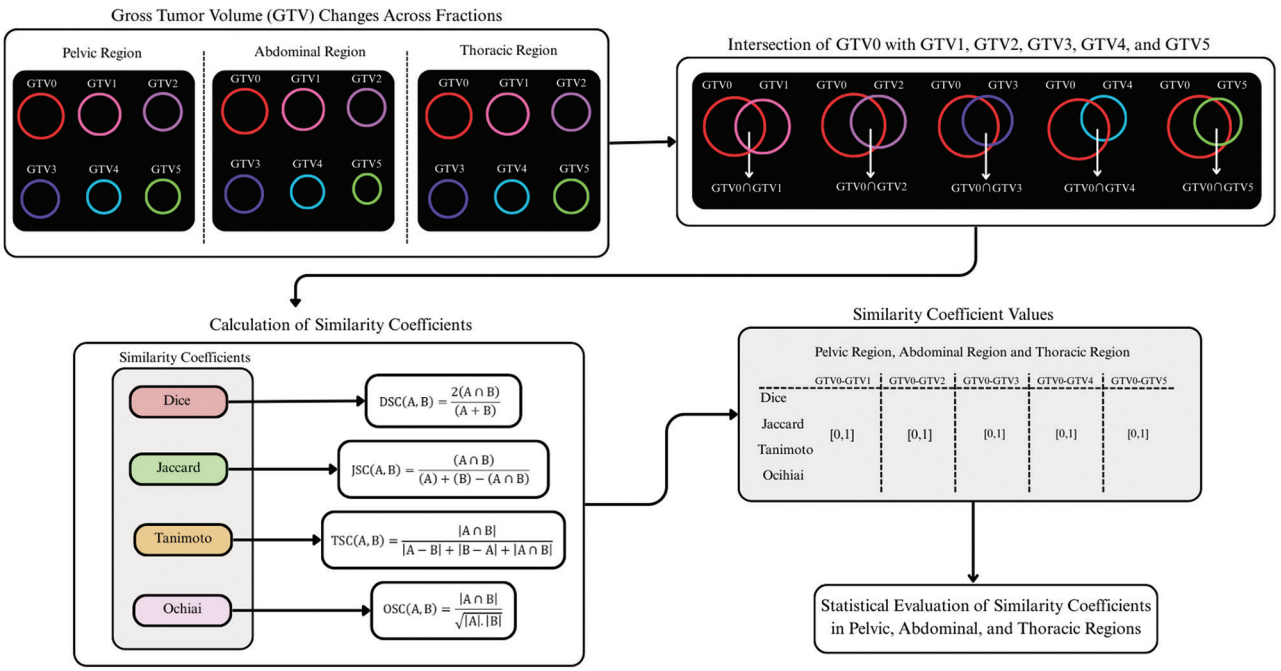

Figure 1. Different similarity coefficients and changes in GTVs during radiotherapy
Abbreviation: GTVs: Gross tumor volumes.

similarity coefficient demonstrated the most prominent, consistent, and statistically significant performance across the different tumor regions. This statistical evaluation aimed to compare the behavior of the coefficients in the pelvic, abdominal, and thoracic groups, thereby determining which metric most effectively captured inter-fractional GTV variations. Through this analysis, the study sought to establish the coefficient that provides the most reliable quantitative distinction among anatomical regions, supporting its potential use as a preferred metric in ART decision-making.

3. Results

The stability of similarity metrics was evaluated based on their M ± SD values across fractions, with lower variability (SD) interpreted as greater inter-fractional stability. During the analysis, it was observed that OSC values in the pelvic, abdominal, and thoracic regions were significantly higher than those of other similarity coefficients. In addition, in some regions, DSC and OSC values were found to be similar, suggesting that the performance of similarity measures varies across different anatomical sites.

To further investigate these variations, an ANOVA test was conducted to examine the statistical differences between the similarity measures for each region. According to the ANOVA analysis, significant differences were observed among the similarity coefficients in all three anatomical regions ($p<0.05$). The Friedman test confirmed that OSC differed significantly from the other coefficients in the pelvis and abdomen ($p<0.001$).

Table 2. Summary of gross tumor volume changes (cm^3) in pelvic, abdominal, and thoracic regions

Anatomical region	GTV	Minimum (cm^3)	Maximum (cm^3)	Mean (cm^3)	Standard deviation (cm^3)
Pelvis	GTV0	29.8	109.0	61.61	21.81
	GTV1	29.2	107.9	60.75	21.07
	GTV2	29.6	109.4	61.29	20.98
	GTV3	29.6	109.4	61.89	20.60
	GTV4	29.1	111.8	62.38	21.59
	GTV5	28.9	112.3	62.20	20.86
Abdomen	GTV0	1.6	81.1	16.58	19.27
	GTV1	1.9	68.3	15.76	16.70
	GTV2	2.1	67.3	15.78	16.43
	GTV3	2.3	65.4	15.55	16.05
	GTV4	7.3	65.2	19.27	18.37
	GTV5	7.3	60.4	19.07	16.98
Thorax	GTV0	0.7	49.8	9.680	16.50
	GTV1	0.7	49.8	9.740	16.47
	GTV2	0.7	49.1	9.710	16.21
	GTV3	0.7	50.6	9.940	16.73
	GTV4	0.7	6.70	3.200	2.650
	GTV5	0.7	4.60	1.830	1.870

Abbreviation: GTV: Gross tumor volume.

3.1. GTV changes for the pelvic region

Table 3 presents the DSC, JSC, TSC, and OSC similarity coefficients for the pelvic region during the fourth and fifth fractions. The results obtained were 0.88 ± 0.09, 0.88 ± 0.09, 0.88 ± 0.09, and 0.93 ± 0.05, respectively. These findings suggest a decrease in GTV volume similarity between the fourth and fifth fractions in the pelvic region compared to other fractions. Moreover, Figure 2 illustrates

Table 3. Ratio values of the Dice, Jaccard, Tanimoto, and Ochiai similarity coefficients for the pelvic, abdominal, and thoracic regions across treatment fractions

Similarity coefficients	Pelvic region		Abdominal region		Thoracic region	
	Mean	SD	Mean	SD	Mean	SD
DSC_1	0.95	0.05	0.93	0.05	0.95	0.06
DSC_2	0.91	0.07	0.92	0.06	0.94	0.08
DSC_3	0.90	0.08	0.89	0.08	0.93	0.09
DSC_4	0.88	0.09	0.89	0.06	0.93	0.09
DSC_5	0.88	0.09	0.85	0.08	0.92	0.11
DSC_ALL	0.91	0.06	0.91	0.06	0.93	0.09
JSC_1	0.95	0.05	0.87	0.09	0.91	0.10
JSC_2	0.91	0.07	0.85	0.11	0.89	0.14
JSC_3	0.90	0.08	0.81	0.13	0.88	0.15
JSC_4	0.88	0.09	0.80	0.11	0.88	0.15
JSC_5	0.88	0.10	0.75	0.13	0.87	0.18
JSC_ALL	0.91	0.06	0.84	0.10	0.89	0.15
TSC_1	0.95	0.05	0.87	0.09	0.91	0.10
TSC_2	0.91	0.07	0.85	0.11	0.89	0.14
TSC_3	0.90	0.08	0.81	0.13	0.88	0.15
TSC_4	0.88	0.09	0.80	0.11	0.88	0.15
TSC_5	0.88	0.10	0.75	0.13	0.87	0.18
TSC_ALL	0.91	0.06	0.84	0.10	0.89	0.15
OSC_1	0.97	0.03	0.93	0.05	0.95	0.05
OSC_2	0.95	0.04	0.92	0.06	0.94	0.08
OSC_3	0.94	0.04	0.89	0.08	0.93	0.09
OSC_4	0.93	0.05	0.89	0.06	0.93	0.09
OSC_5	0.93	0.06	0.86	0.08	0.92	0.11
OSC_ALL	0.95	0.03	0.91	0.05	0.94	0.08

Abbreviations: DSC: Dice similarity coefficients; JSC: Jaccard similarity coefficients; OSC: Ochiai similarity coefficients; SD: Standard deviation; TSC: Tanimoto similarity coefficients.

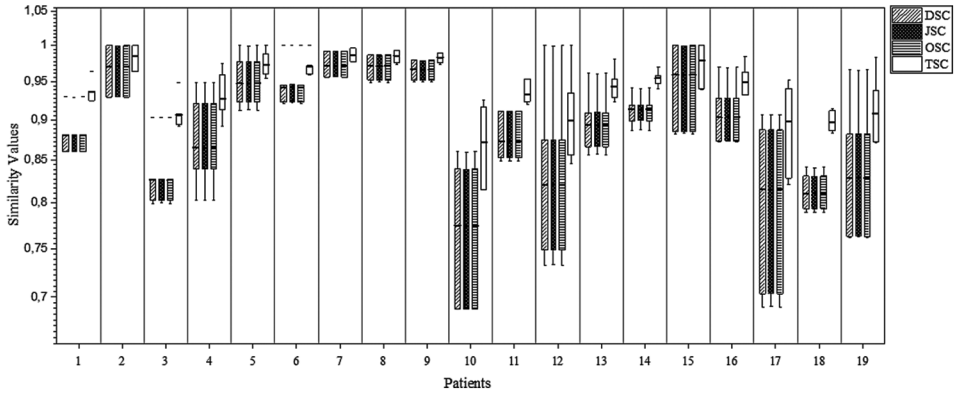

Figure 2. Box plot of the four similarity coefficient values for the pelvic region
Abbreviations: DSC: Dice similarity coefficient; JSC: Jaccard similarity coefficient; OSC: Ochiai similarity coefficient; TSC: Tanimoto similarity coefficient.

that the differences in GTV volume between fractions were not negligible in 4 out of 23 patients.

When similarity measurements in the pelvic region were evaluated pairwise using the Friedman test, a highly significant difference was found between OSC values and other metrics (DSC, JSC, and TSC) (p=0.000), while no significant difference was observed among DSC, JSC, and TSC values (p=1.000).

3.2. GTV changes for the abdominal region

The abdominal region exhibited the lowest similarity values among the three anatomical sites, particularly in the later fractions (fourth and fifth). For the fourth fraction, the similarity coefficients were 0.85 ± 0.08 (DSC), 0.75 ± 0.13 (JSC), 0.75 ± 0.13 (TSC), and 0.86 ± 0.08 (OSC), suggesting greater inter-fractional GTV variations compared to the pelvic and thoracic regions. Figure 3 presents the box plot of similarity coefficients, demonstrating a significant decline in JSC and TSC values relative to the pelvic region. The lowest similarity scores were observed in the fourth and fifth fractions, indicating significant inter-fractional tumor volume changes (Table 3).

According to the Friedman test (paired comparisons) results of the similarity measurements obtained for the abdominal region, there was no statistically significant difference between the JSC and TSC values (p=1.000), while there was a significant difference among the other similarity coefficient values (p=0.000).

3.3. GTV changes for the thoracic region

For the thoracic region, the similarity coefficients were 0.92 ± 0.11 (DSC), 0.87 ± 0.18 (JSC), 0.87 ± 0.18 (TSC), and 0.92 ± 0.11 (OSC), with the most pronounced changes occurring in the fifth fraction. While the lowest similarity coefficient in the thoracic region was higher than in the abdominal region, it remained comparable to values observed in the pelvic region. As shown in Figure 4, the box plot of similarity coefficients indicates relatively stable similarity values across fractions. Compared to the pelvic and abdominal regions, the thoracic region exhibited less inter-fractional variation (Table 3).

Friedman test results for similarity measurements in the thoracic region showed that there were no statistically significant differences between JSC and TSC (p=1.000) and DSC and OSC (p=0.298).

4. Discussion

Changes in target volume during radiotherapy are critical for ensuring accurate and precise dose delivery while minimizing radiation exposure to surrounding tissues. This study analyzed inter-fractional GTV variations in the pelvic, abdominal, and thoracic regions using the MR-LINAC imaging technique to assess their impact on radiotherapy planning. These findings highlight the importance of ART, especially in improving treatment efficacy.

Our findings emphasize the importance of frequent imaging and ART adjustments for abdominal tumors, particularly in high-precision dose administration. Furthermore, the findings show that abdominal tumors undergo greater volumetric changes than those in the pelvic and thoracic regions, necessitating region-specific ART strategies. Notably, the two patients with the lowest similarity scores and the most pronounced volume variations were receiving radiotherapy for pancreatic cancer, suggesting that pancreatic tumors exhibit substantial inter-fractional changes. These

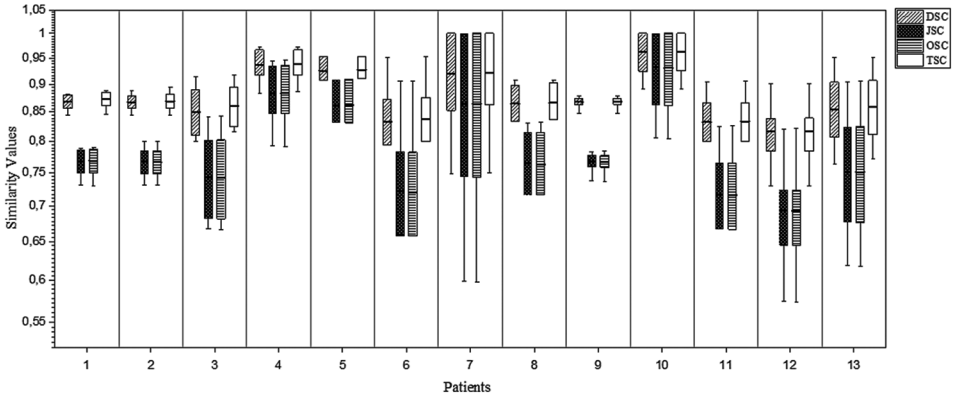

Figure 3. Box plot of the four similarity coefficient values for the abdominal region
Abbreviations: DSC: Dice similarity coefficient; JSC: Jaccard similarity coefficient; OSC: Ochiai similarity coefficient; TSC: Tanimoto similarity coefficient.

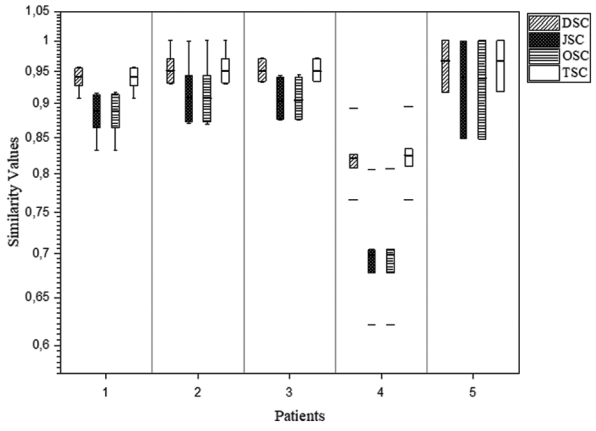

Figure 4. Box plot of the four similarity coefficient values for the thoracic region
Abbreviations: DSC: Dice similarity coefficient; JSC: Jaccard similarity coefficient; OSC: Ochiai similarity coefficient; TSC: Tanimoto similarity coefficient.

results reinforce the need for ART in pancreatic cancer treatment to accommodate dynamic tumor volume fluctuations.

These findings suggest that while ART may be necessary for selected thoracic cases, standard fractionation protocols could be sufficient in many patients. The presence of relatively higher OSC values across fractions suggests that this coefficient may be more resistant to respiratory motion artifacts. In addition, patients with the highest degree of GTV change were undergoing lung cancer radiotherapy, where both intra- and inter-fractional respiratory motion likely contributed to volume variations. These results highlight the necessity of considering all sources of tumor motion in lung cancer treatment planning to optimize dose delivery and tumor control.

These findings highlight the critical role of similarity coefficients in ART planning, as they provide a systematic approach to assessing inter-fractional tumor volume variations. Among the evaluated metrics, the superiority of JSC in distinguishing differences in small tumor volumes with high sensitivity was observed. This finding is supported by both the results of the present study and previous publications reporting the high sensitivity of the JSC metric in detecting minor volumetric variations. In addition, since JSC and TSC showed no significant differences, the TSC can also be used as an alternative metric in clinical assessments. The integration of both JSC and TSC into clinical workflows may assist radiation oncologists and medical physicists in making more precise and adaptive ART decisions.

Given the observed inter-fractional variations, our findings suggest that for pelvic and abdominal tumors, ART protocols should include more frequent imaging-based assessments to ensure optimal treatment delivery. Implementing similarity coefficient analysis in clinical practice can enhance decision-making in ART, helping clinicians identify patients who require adaptive interventions while minimizing unnecessary plan modifications.

This study provides valuable insights into the role of ART in managing inter-fractional tumor volume variations. However, further research is needed to evaluate intra-fractional variations in thoracic tumors and to determine how similarity coefficients can be effectively integrated into clinical workflows. Future studies should focus on prospective analyses with larger patient cohorts and explore the incorporation of similarity coefficients into TPS software. These developments could enhance ART by making it more precise, adaptive, and clinically efficient. In addition, investigating the correlation between similarity

coefficients and clinical outcomes such as local tumor control and treatment toxicity could further strengthen their role in personalized ART decision-making in the future.

The study's unique value lies in its examination of changes in target volume (GTV) through the use of three-dimensional MRI and similarity coefficient analyses. This analysis provides crucial contributions to radiotherapy treatment planning and implementation by highlighting the differences between segments and emphasizing the necessity of adaptive treatment approaches. A significant distinction was found between the fractions of tumors in the pelvis and abdomen according to the study's outcomes. Moreover, the statistical variations among the various similarity metrics were reviewed, and JSC stands out for its effectiveness in evaluating small tumor volume changes between fractions. As a result, the study presents innovative research for treatment response and enhancing treatment strategies. In addition, machine learning methods can be employed for calculating similarity coefficients and for examining statistical differences among these coefficients through classification or clustering techniques. The results obtained in this study facilitate deep learning and encourage further development of machine learning models in future research.

Inter-fractional GTV changes observed during MRI-guided radiotherapy may have direct clinical implications by affecting target coverage and dose distribution. Quantitative similarity analysis can aid in identifying patients who require adaptive replanning to preserve treatment efficacy while minimizing OAR exposure. Incorporating such metrics into ART workflows could enhance the objectivity and efficiency of adaptive decision-making in MR-LINAC–based radiotherapy. This research contributes to the optimization of ART workflows by identifying the most effective similarity-based segmentation approach. By improving tumor volume tracking accuracy, these findings may enhance patient-specific ART planning, support more precise dose adaptation strategies, and ultimately contribute to better clinical decision-making in MRI-guided radiotherapy. However, the limitations of this study include the lack of a larger patient population, the absence of intra-fractional change evaluation, the exclusion of long-course treatments, the lack of analysis on the clinical impact of ART, and the insufficient detail on the integration of similarity coefficients into clinical decision-making processes.

In the present study, the concept of similarity metric "stability" refers to the consistency of metric values across treatment fractions rather than sensitivity to small volumetric changes. Stability was quantitatively assessed using the standard deviation of similarity coefficients across fractions, as lower variability indicates greater robustness to inter-fractional anatomical fluctuations. Among the evaluated metrics, the OSC consistently demonstrated lower standard deviation values while maintaining high mean similarity scores, particularly in the pelvic and abdominal regions. This finding suggests that OSC is less affected by inter-fractional anatomical changes and provides more reproducible similarity estimates over the course of treatment. Such robustness is particularly advantageous in ART workflows, where excessive metric variability may trigger unnecessary plan adaptations.

In contrast, the JSC and TSC exhibited higher variability across fractions, especially in regions with pronounced anatomical motion or heterogeneous tumor behavior. While this increased variability reduces their stability, it may reflect higher sensitivity to small volumetric or geometric changes. Therefore, JSC and TSC should not be interpreted as inferior metrics, but rather as complementary tools that may be useful when the detection of subtle inter-fractional changes is clinically relevant. These findings highlight that metric stability and metric sensitivity represent distinct analytical properties, and the choice of similarity coefficient should be guided by the specific clinical objective. When reproducibility and robustness across fractions are prioritized—such as in routine MRI-guided ART—OSC appears to be a more suitable metric. Conversely, when the detection of small geometric deviations is of interest, JSC and TSC may provide additional value.

The main limitations of this study include the relatively small and heterogeneous patient cohort and the limited number of analyzed fractions. Tumor-specific anatomical and biological variations should be considered when interpreting the results. Future studies involving larger patient populations, longer follow-up, and prospective designs are required to validate the clinical applicability and reproducibility of the proposed similarity coefficient–based approach.

5. Conclusion

This study analyzed inter-fraction GTV changes in the pelvic, abdominal, and thoracic regions during MRI-guided ART. In our analysis, OSC was favored because it showed greater inter-fractional stability (higher mean values) with lower variability (lower SD) than the other metrics, particularly in the pelvic and abdominal regions. In the thoracic region, OSC and DSC behaved similarly. Therefore, OSC (and DSC for thoracic tumors) is appropriate when stability is the primary consideration, whereas JSC and TSC remain useful when greater sensitivity to small

volumetric changes is required. Our findings support the adoption of MR-based ART strategies in clinical routines and the importance of these technologies in improving treatment planning processes.

Acknowledgments

None.

Funding

None.

Conflict of interest

The authors declare that they have no competing interests.

Author contributions

Conceptualization: Orhan İçelli
Data curation: Merve Konuk
Formal analysis: Merve Konuk, Serhat Aras
Investigation: Serhat Aras, Banu Atalar
Methodology: Merve Konuk, Görkem Güngör
Supervision: Orhan İçelli
Visualization: Merve Konuk, Serhat Aras
Writing-original draft: Merve Konuk, Serhat Aras
Writing-review & editing: Merve Konuk, Serhat Aras

Ethics approval and consent to participate

This study was conducted retrospectively using only anonymized MR imaging data for a deep learning–based analysis. No patient intervention, additional data collection, or identifiable personal information was involved; therefore, ethical approval was not required under the relevant institutional and national regulations. All imaging data were obtained as part of routine clinical practice, and no procedures were performed specifically for research purposes.

Consent for publication

No patient intervention, additional data collection, or identifiable personal information was involved.

Availability of data

The data used/provided in this study are explicitly stated in the manuscript and are available from the corresponding author on reasonable request.

Further disclosure

During the preparation of this manuscript, the ChatGPT 5.1 language model developed by OpenAI was used solely to support English grammar correction, improve clarity and coherence of scientific expression, and assist in the translation of the text into English. All data analysis, scientific interpretation, and content generation were conducted exclusively by the author(s).

References

1. Van Timmeren JE, Chamberlain M, Bogowicz M, *et al*. MR-guided adaptive radiotherapy for head and neck cancer: Prospective evaluation of migration and anatomical changes of the major salivary glands. *Cancers (Basel)*. 2021;13(21):5404.

   doi: 10.3390/cancers13215404

2. Hirotaki K, Moriya S, Tachibana H, Sakae T. Detection of anatomical changes using two-dimensional x-ray images for head and neck adaptive radiotherapy. *Med Phys*. 2022;49(5):3288-3297.

   doi: 10.1002/mp.15587

3. Brock KK. Adaptive radiotherapy: Moving into the future. *Semin Radiat Oncol*. 2019;29(3):181-184.

   doi: 10.1016/j.semradonc.2019.02.011

4. Green OL, Henke LE, Hugo GD. Practical clinical workflows for online and offline adaptive radiation therapy. *Semin Radiat Oncol*. 2019;29(3):219-227.

   doi: 10.1016/j.semradonc.2019.02.004

5. Sonke JJ, Aznar M, Rasch C. Adaptive radiotherapy for anatomical changes. *Semin Radiat Oncol*. 2019;29(3):245-257.

   doi: 10.1016/j.semradonc.2019.02.007

6. Zhao JZ, Zheng H, Li LY, Zhang LY, Zhao Y, Jiang N. Predictors for weight loss in head and neck cancer patients undergoing radiotherapy: A systematic review. *Cancer Nurs*. 2015;38(6):245-257.

   doi: 10.1097/ncc.0000000000000231

7. Ding S, Liu B, Zheng S, *et al*. An exploratory analysis of MR-guided fractionated stereotactic radiotherapy in patients with brain metastases. *Clin Transl Radiat Oncol*. 2023;40:100602.

   doi: 10.1016/j.ctro.2023.100602

8. Mannerberg A, Persson E, Jonsson J, *et al*. Dosimetric effects of adaptive prostate cancer radiotherapy in an MR-linac workflow. *Radiat Oncol*. 2020;15(1):168.

   doi: 10.1186/s13014-020-01604-5

9. Bhide SA, Davies M, Burke K, *et al*. Weekly volume and dosimetric changes during chemoradiotherapy with intensity-modulated radiation therapy for head and neck cancer: A prospective observational study. *Int J Radiat Oncol Biol Phys*. 2010;76(5):1360.

   doi: 10.1016/j.ijrobp.2009.04.005

10. Ramsey CR, Langen KM, Kupelian PA, *et al*. A technique for adaptive image-guided helical tomotherapy for lung cancer.

Int J Radiat Oncol Biol Phys. 2006;64(4):12.

doi: 10.1016/j.ijrobp.2005.11.012

11. McDonald BA, Zachiu C, Christodouleas J, *et al*. Dose accumulation for MR-guided adaptive radiotherapy: From practical considerations to state-of-the-art clinical implementation. *Front Oncol*. 2023;12:1086258.

doi: 10.3389/fonc.2022.1086258

12. Fischer-Valuck BW, Henke L, Green O, *et al*. Two-and-a-half-year clinical experience with the world's first magnetic resonance image guided radiation therapy system. *Adv Radiat Oncol*. 2017;2(3):485-493.

doi: 10.1016/j.adro.2017.05.006

13. Kishan AU, Lee P. MRI-guided radiotherapy: Opening our eyes to the future. *Integr Cancer Sci Ther*. 2016;3(2):420-427.

doi: 10.15761/icst.1000181

14. Noel CE, Parikh PJ, Spencer CR, *et al*. Comparison of onboard low-field magnetic resonance imaging versus onboard computed tomography for anatomy visualization in radiotherapy. *Acta Oncol (Madr)*. 2015;54(9):1474-1482.

doi: 10.3109/0284186X.2015.1062541

15. Pollard JM, Wen Z, Sadagopan R, Wang J, Ibbott GS. The future of image-guided radiotherapy will be MR guided. *Br J Radiol*. 2017;90(1073):20160667.

doi: 10.1259/bjr.20160667

16. Klüter S, Katayama S, Spindeldreier CK, *et al*. First prospective clinical evaluation of feasibility and patient acceptance of magnetic resonance-guided radiotherapy in Germany. *Strahlentherapie Onkol*. 2020;196(8):691-698.

doi: 10.1007/s00066-020-01578-z

17. Redler G, Stevens T, Cammin J, *et al*. Dosimetric feasibility of utilizing the ViewRay magnetic resonance guided linac system for image-guided spine stereotactic body radiation therapy. *Cureus*. 2019;11:e6364.

doi: 10.7759/cureus.6364

18. Gani C, Boldrini L, Valentini V. Online MR guided radiotherapy for rectal cancer. New opportunities. *Clin Transl Radiat Oncol*. 2019;18:66-67.

doi: 10.1016/j.ctro.2019.04.005

19. Henke L, Kashani R, Robinson C, *et al*. Phase I trial of stereotactic MR-guided online adaptive radiation therapy (SMART) for the treatment of oligometastatic or unresectable primary malignancies of the abdomen. *Radiother Oncol*. 2018;126(3):519-526.

doi: 10.1016/j.radonc.2017.11.032

20. Murgić J, Gregov M, Mrčela I, *et al*. MRI-guided radiotherapy for prostate cancer: A new paradigm. *Acta Clin Croat*. 2022;61:65-70.

doi: 10.20471/acc.2022.61.S3.9

21. Klüter S. Technical design and concept of a 0.35 T MR-Linac. *Clin Transl Radiat Oncol*. 2019;18:98-101.

doi: 10.1016/j.ctro.2019.04.007

22. Wen N, Kim J, Doemer A, *et al*. Evaluation of a magnetic resonance guided linear accelerator for stereotactic radiosurgery treatment. *Radiother Oncol*. 2018;127(3):460-466.

doi: 10.1016/j.radonc.2018.04.034

23. Ericsson-Szecsenyi R, Zhang G, Redler G, *et al*. Robustness assessment of images from a 0.35T scanner of an integrated MRI-linac: Characterization of radiomics features in phantom and patient data. *Technol Cancer Res Treat*. 2022;21:15330338221099113.

doi: 10.1177/15330338221099113

24. Han Z, Sudhyadhom A, Hsu S, *et al*. Comparison of MR-soft tissue based versus biliary stent based alignment for image guidance in pancreatic SBRT. *J Appl Clin Med Phys*. 2023;24:e13965.

doi: 10.1002/acm2.13965

25. Kim JI, Park JM, Choi CH, An HJ, Kim YJ, Kim JH. Retrospective study comparing MR-guided radiation therapy (MRgRT) setup strategies for prostate treatment: Repositioning vs. replanning. *Radiat Oncol*. 2019;14(1):139.

doi: 10.1186/s13014-019-1349-2

26. Nousiainen K, Santurio GV, Lundahl N, Cronholm R, Siversson C, Edmund JM. Evaluation of MRI-only based online adaptive radiotherapy of abdominal region on MR-linac. *J Appl Clin Med Phys*. 2023;24(3):e13838.

doi: 10.1002/acm2.13838

27. Thorwarth D, Low DA. Technical challenges of real-time adaptive MR-guided radiotherapy. *Front Oncol*. 2021;11:634507.

doi: 10.3389/fonc.2021.634507

28. Boldrini L, Romano A, Chiloiro G, *et al*. Magnetic resonance guided SBRT reirradiation in locally recurrent prostate cancer: A multicentric retrospective analysis. *Radiat Oncol*. 2023;18(1):84.

doi: 10.1186/s13014-023-02271-y

29. Park JM, Wu HG, Kim HJ, Choi CH, Kim JI. Comparison of treatment plans between IMRT with MR-linac and VMAT for lung SABR. *Radiat Oncol*. 2019;14(1):105.

doi: 10.1186/s13014-019-1314-0

30. Maziero D, Straza MW, Ford JC, *et al*. MR-guided radiotherapy for brain and spine tumors. *Front Oncol*. 2021;11:626100.

doi: 10.3389/fonc.2021.626100

31. Sahin B, Zoto Mustafayev T, Gungor G, *et al*. First 500 fractions delivered with a magnetic resonance-guided radiotherapy system: Initial experience. *Cureus*.

2019;11:e6457.

doi: 10.7759/cureus.6457

32. Anderson P, Dogan N, Ford JC, *et al*. Repeatability, reproducibility, and the effects of radiotherapy on radiomic features of lowfield MR-LINAC images of the prostate. *Front Oncol*. 2024;14:1408752.

doi: 10.3389/fonc.2024.1408752

33. Turkkan G, Bilici N, Sertel H, *et al*. Clinical utility of a 1.5 T magnetic resonance imaging-guided linear accelerator during conventionally fractionated and hypofractionated prostate cancer radiotherapy. *Front Oncol*. 2022;12:909402.

doi: 10.3389/fonc.2022.909402

34. Nierer L, Eze C, Da Silva Mendes V, *et al*. Dosimetric benefit of MR-guided online adaptive radiotherapy in different tumor entities: Liver, lung, abdominal lymph nodes, pancreas and prostate. *Radiat Oncol*. 2022;17(1):53.

doi: 10.1186/s13014-022-02021-6

35. Rachi T, Ariji T, Takahashi S. Development of machine-learning prediction programs for delivering adaptive radiation therapy with tumor geometry and body shape changes in head and neck volumetric modulated arc therapy. *Adv Radiat Oncol*. 2023;8(4):101172.

doi: 10.1016/j.adro.2023.101172

36. Dice LR. Measures of the amount of ecologic association between species. *Ecology*. 1945;26(3):297-302.

doi: 10.2307/1932409

37. Jaccard P. The distribution of the flora in the alpine zone. *New Phytol*. 1912;11(2):37-50.

doi: 10.1111/j.1469-8137.1912.tb05611.x

38. Tanimoto TT. An Elementary Mathematical Theory of Classification and Prediction. In: *Proceedings IBM Internal Report*; 1958.

39. Taha AA, Hanbury A. Metrics for evaluating 3D medical image segmentation: Analysis, selection, and tool. *BMC Med Imaging*. 2015;15(1):29.

doi: 10.1186/s12880-015-0068-x

40. Romesburg HC. *Cluster Analysis for Researchers*. United States: Lulu Press; 1984.

ACCSCIENCE PUBLISHING

Advances in Radiotherapy & Nuclear Medicine

ORIGINAL RESEARCH ARTICLE

Real-world outcomes of radiation therapy-based multimodal therapy in thymic epithelial tumors: A single-center retrospective analysis

Sorun Shishak[1], Tejinder Kataria[1], Subham Pal[1], Susovan Banerjee[1], Deepak Gupta[1], Kushal Narang[1], Mayur Mayank[1], Shikha Goyal[2], Shina Goyal[3], Sameer Rastogi[4], Bosky Jain[5], Sasmita Priyadarshini Sahoo[6], Gargi Sharma[1], Sabyasachi Sarkar[1], and Shyam Singh Bisht[1]*

[1]Division of Radiation Oncology, Medanta The Medicity, Gurugram, Haryana, India

[2]Department of Radiation Oncology, Post Graduate Institute of Medical Education and Research, Chandigarh, India

[3]Department of Medical Oncology, Max Super Specialty Hospital, Dwarka, New Delhi, India

[4]Department of Medical Oncology, All India Institute of Medical Sciences, New Delhi, India

[5]Department of Radiology, Medanta The Medicity, Gurugram, Haryana, India

[6]Department of Radiation Oncology, Bagchi Sri Shankara Cancer Centre and Research Institute, Bhubaneswar, Odisha, India

Abstract

Thymic epithelial tumors (TETs) are rare malignancies with diverse histologic subtypes and complex clinical behavior, necessitating a multidisciplinary approach to care. We conducted a retrospective analysis of 52 patients with TETs treated at a tertiary cancer center, including 41 with thymoma and 11 with thymic carcinoma. The median age was 50 years for thymoma and 56 years for thymic carcinoma. Paraneoplastic syndromes, particularly myasthenia gravis, were more frequent in thymoma (46.3%) than in thymic carcinoma (9.1%). Most patients presented with advanced-stage disease (stage IIIA or higher accounted for 75.7% of thymoma cases and 72.8% of thymic carcinoma cases). Neoadjuvant chemotherapy was administered to 26.8% of thymoma cases and 27.3% of thymic carcinoma cases. Surgical resection was performed in 90.2% of thymoma and 63.6% of thymic carcinoma patients, with complete resection (R0) achieved in 83.8% and 71.4%, respectively. Post-operative radiotherapy (RT) was widely utilized, delivered via volumetric-modulated arc therapy or tomotherapy. Four patients with stage IVA thymoma received hyperthermic intrathoracic chemotherapy after cytoreductive surgery. At a median follow-up of 6 years, the 5-year overall survival for thymoma and thymic carcinoma was 70.0% and 30.7%, respectively, while the 5-year progression-free survival for thymoma and thymic carcinoma was 85.1% and 26%, respectively. Relapse occurred in 17.1% of thymoma and 63.6% of thymic carcinoma patients. Despite the predominance of advanced-stage disease and large tumor burden at presentation, an aggressive, multimodal treatment approach—including high rates of R0 resection, advanced RT techniques (e.g., volumetric modulated arc therapy, tomotherapy), multiline systemic therapy, and selective hyperthermic intrathoracic chemotherapy—demonstrates potential to improve treatment outcomes. Recurrence is the strongest predictor of mortality in both thymoma and thymic carcinoma.

Keywords: Thymoma; Thymic carcinoma; Thymic epithelial tumors; Myasthenia gravis; Multidisciplinary; Radiation; Post-operative radiotherapy

***Corresponding author:**
Shyam Singh Bisht
(shyam.bisht@medanta.org)

Citation: Shishak S, Kataria T, Pal S, *et al*. Real-world outcomes of radiation therapy-based multimodal therapy in thymic epithelial tumors: A single-center retrospective analysis. *Adv Radiother Nucl Med*. 2026;4(1):80-92.
doi: 10.36922/ARNM025360043

Received: September 1, 2025

Revised: November 25, 2025

Accepted: December 19, 2025

Published online: February 11, 2026

1. Introduction

Thymic epithelial tumors (TETs) comprise a rare and heterogeneous group of neoplasms arising from the epithelial cells of the thymus, primarily located in the anterior mediastinum.[1] Although they account for <1% of all malignancies, TETs represent up to 30% of anterior mediastinal tumors in adults.[2] The estimated incidence of thymomas ranges from 0.13 to 0.32 cases per 100,000 population annually,[3] whereas thymic carcinomas occur less frequently, with reported rates between 0.07 and 0.38/100,000 population per year.[4] Thymomas typically present in individuals between 40 and 70 years old, while thymic carcinomas present at a median age of 54–65 years.[5]

According to the 5th edition of the World Health Organization (WHO) classification of thoracic tumors, TETs are broadly classified into thymomas, thymic carcinomas, and thymic neuroendocrine tumors, based on architectural, cytological, and immunophenotypic features. Thymomas are further subdivided into types A, AB, B1, B2, and B3, as well as rarer variants, such as micronodular thymomas with lymphoid stroma and metaplastic thymomas.[6] Thymomas account for approximately 75–80% of all TETs, whereas thymic carcinomas and thymic neuroendocrine tumors comprise the remaining 10–15% and 5–10%, respectively.[7]

Biologically, thymomas tend to follow an indolent clinical course, with a propensity for local invasion and relatively favorable outcomes.[2] Thymic carcinomas, on the other hand, exhibit a more aggressive phenotype, characterized by a higher likelihood of lymphatic and hematogenous dissemination, therapeutic resistance, and poor prognosis.[5] One of the hallmark features distinguishing thymomas from other mediastinal tumors is their strong association with paraneoplastic syndromes, particularly myasthenia gravis (MG). Up to 30–50% of thymoma patients develop thymoma-associated MG, and approximately 20% of patients with MG are found to harbor an underlying thymoma.[8]

Given their rarity, histologic diversity, and complex clinical presentation, the optimal management of TETs necessitates a coordinated, multidisciplinary approach, involving pathologists, radiologists, neurologists, thoracic surgeons, radiation oncologists, and medical oncologists.

In this study, we present a retrospective analysis of patients with TETs managed at our tertiary care center, using data derived from an institutional database. Our objective is to evaluate the real-world application of multidisciplinary care and to describe treatment patterns and clinical outcomes of thymomas and thymic carcinomas.

2. Materials and methods

2.1. Study population

This retrospective study was conducted using an institutional database of patients diagnosed with thymoma or thymic carcinoma between January 2012 and April 2025. All patients with histologically confirmed thymoma or thymic carcinoma during this period were considered eligible, provided complete clinical, radiologic, and treatment data were available. Patients were excluded if: (i) Histopathology reports were incomplete or unavailable upon review, (ii) the diagnosis could not be confirmed, or (iii) essential clinical data required for analysis were missing.

2.2. Data collection

Clinical data were systematically recorded using a pre-designed case-report form derived from the electronic health information system. The dataset included detailed demographic information, such as age and sex, Eastern Cooperative Oncology Group Performance Status (ECOG PS), comorbidities; presenting symptoms, tumor characteristics, including size, Masaoka-Koga stage, and the WHO histological subtype, presence of paraneoplastic syndromes, and treatment modalities, comprising surgery, radiotherapy (RT), and chemotherapy. Additional data collected included treatment-related toxicity, graded according to standard criteria, and clinical outcomes categorized as alive and disease-free, alive with disease, or deceased due to disease or other causes, along with the date of past follow-up.

2.3. Baseline staging and pre-treatment evaluation

Baseline staging was performed for all patients using either contrast-enhanced computed tomography of the thorax and abdomen or fluorodeoxyglucose positron emission tomography-computed tomography. Pulmonary function tests were routinely conducted prior to treatment initiation. All collected data were compiled in Microsoft Excel.

2.4. Surgical management

Surgical management consisted of total thymectomy with resection of adjacent structures as required. Patients with pericardial involvement underwent pericardial resection followed by reconstruction, whereas those presenting with pleural disease underwent pleural resection. For patients with lung metastases or tumor adherence to the lung, either lobectomy of the involved lobe or wedge resection was performed. Unilateral phrenic nerve resection was performed in cases where the tumor was closely adherent to the nerve. Surgical clips were placed intraoperatively to facilitate radiation target volume delineation.

In patients with stage IVA disease and pleural dissemination, hyperthermic intrathoracic chemotherapy (HITHOC) was employed as an adjunct to cytoreductive surgery. In HITHOC, after macroscopic resection of all visible pleural disease, cisplatin-based chemotherapy was circulated within the thoracic cavity at 41–43°C for 60–90 min.

Lymph nodal dissection was not performed for thymomas; however, for thymic carcinoma, systematic lymph node dissection was performed, including sampling of anterior perithymic (N1) and deep intrathoracic/cervical (N2) nodes.

2.5. Post-operative RT

The decision to administer post-operative RT (PORT) in thymoma was guided by a combination of Masaoka-Koga stage, the WHO histologic subtype, and surgical margin status. Patients with early-stage disease (stage I–II) with the WHO type B2 or higher histology, all patients with stage III–IVA disease, and any patient with microscopic residual disease (R1) or macroscopic residual disease (R2) resection margins (irrespective of stage) were considered for PORT.

For RT planning, patients were immobilized in the supine position using a Vac-Lok or thoracic cast, and RT planning scans were acquired at 3-mm slice thickness. Target volumes were delineated by fusing baseline imaging studies and reconstructing the pre-resection gross tumor volume to define regions of prior tumor involvement. The post-operative tumor bed was subsequently identified and contoured across multiple respiratory phases, including free-breathing, end-expiratory, and end-inspiratory.

The post-operative bed incorporated surgical clip locations, areas of prior tumor contact with adjacent structures (e.g., pleura, pericardium, and mediastinum), and regions suspicious for residual or microscopic disease. An internal target volume was generated by integrating post-operative bed delineations across respiratory phases to account for tumor motion and anatomical variations. A clinical target volume (CTV) margin of 1 cm was added to the internal target volume to encompass potential microscopic disease spread. The planning target volume (PTV) was generated by applying a 5 mm isotropic expansion to the CTV. In regions adjacent to the heart, a reduced margin of 3 mm was applied to minimize cardiac exposure. Target volume delineation was performed collaboratively with the operating thoracic surgeon to ensure accurate coverage of at-risk areas. RT was delivered using tomotherapy or volumetric-modulated arc therapy (VMAT) with 6 MV photons.

2.6. Response assessment

Response assessment was conducted using contrast-enhanced computed tomography of the thorax at 3 months post-treatment, according to response evaluation criteria in solid tumors version 1.1, followed by six-monthly intervals for 5 years, and annual imaging thereafter. Metabolic response using positron emission tomography-computed tomography was recorded when available.

2.7. Statistical analysis

Statistical analysis was performed using the IBM Statistical Package for the Social Sciences Statistics for Windows, Version 20.0 (IBM, USA). Descriptive statistics, including means and medians, summarized qualitative variables. Overall survival (OS) and progression-free survival (PFS) were estimated using the Kaplan-Meier method. OS was calculated from the date of diagnosis to death from any cause or past follow-up, while PFS was calculated from treatment initiation to radiologic progression or death from any cause, whichever occurred first. Acute and late toxicities were graded according to the National Cancer Institute Common Terminology Criteria for adverse events version 5.

2.8. Ethical considerations

This study was conducted in accordance with the ethical principles outlined in the Declaration of Helsinki, Good Clinical Practice guidelines, and the Indian Council of Medical Research guidelines. Institutional ethics committee approval was obtained before study initiation (MICR: 1532/2023).

3. Results

This study included a total of 52 patients: 41 with thymoma (26 males, 15 females) and 11 with thymic carcinoma (6 males, 5 females). The median age was 50 years (range = 28–79 years) for thymoma and 54 years (range = 26–90 years) for thymic carcinoma. Among thymoma patients, ECOG PS was 0 in 25 (61%) and 1 in 16 (39%) patients, while thymic carcinoma patients had ECOG PS 1 in 5 (45.5%) and 2 in 6 (54.5%) patients. Comorbidities were present in 14 (34.1%) thymoma patients and 7 (63.6%).

Paraneoplastic syndromes were more frequent in thymoma, affecting 19 (46.3%) patients, including 17 (41.5%) with MG, 1 (2.4%) with pure red cell aplasia, and 1 (2.4%) with polycythemia vera, whereas only 1 (9.1%) thymic carcinoma patient had MG. The histopathology of this patient did not reveal thymoma components.

Common presenting symptoms in thymoma included fatigue (n = 14, 34.1%), ptosis (n = 10, 24.4%), cough

(*n* = 9, 22%), shortness of breath (*n* = 8, 19.5%), and chest pain (*n* = 5, 12.2%). In thymic carcinoma, fatigue was reported in one (9.1%) patient, chest pain in four (36.4%), dysphagia in two (18.2%), shortness of breath in three (27.3%), and cough in two (18.2%) patients. The average maximal tumor diameter was 97.5 mm (range = 28–160 mm) in thymoma and 77.5 mm (range = 50–90 mm) in thymic carcinoma.

The Masaoka-Koga stage distribution for thymoma was as follows: Stage I (*n* = 3, 7.3%), IIA (*n* = 6, 14.6%), IIB (*n* = 1, 2.4%), IIIA (*n* = 4, 9.8%), IIIB (*n* = 7, 17.1%), IVA (*n* = 17, 41.5%), and IVB (*n* = 3, 7.3%). For thymic carcinoma, stages included IIB (*n* = 3, 27.3%), IIIA (*n* = 1, 9.1%), IIIB (*n* = 2, 18.2%), IVA (*n* = 1, 9.1%), and IVB (*n* = 4, 36.4%).

Among thymoma patients with distant metastases, metastatic involvement was observed in the skeleton (*n* = 1) and bilateral lungs (*n* = 2). In thymic carcinoma, metastatic sites included the liver and lung (*n* = 1), brain, liver, and skeletal sites (*n* = 1), bilateral lungs (*n* = 1), and non-regional lymph nodes (*n* = 1). WHO histological classification for thymoma showed subtype B2 as the most common (*n* = 19, 46.3%), followed by B3 (*n* = 13, 31.7%), B1 (*n* = 4, 9.8%), A (*n* = 3, 7.3%), and AB (*n* = 2, 4.9%). Patient demographic and clinicopathological details are summarized in Table 1.

Treatment details are presented in Tables 2 and 3. Among patients with thymoma (*n* = 41), 11 patients (26.8%) received neoadjuvant chemotherapy (NACT), primarily consisting of six cycles of the CAP regimen (cyclophosphamide [CAP], doxorubicin, and cisplatin). A total of 37 patients (90.2%) underwent surgical resection (Table 2). Among these, complete (R0) resection was achieved in 31 patients (83.8%), R1 in 2 patients (5.4%), and R2 in 4 patients (10.8%).

Four patients with stage IVA disease received HITHOC with cisplatin following cytoreductive surgery. Adjuvant chemotherapy was administered to eight patients (30.8%). PORT was delivered to all 37 surgically treated patients, with doses ranging from 45 to 60 Gy delivered in 25–30 fractions at 1.8–2 Gy per fraction.

Three patients with stage I disease received adjuvant RT. The indications included WHO type B3 histology in one patient, uncertain resection margins with capsular breach in another, and tumor adherence to the phrenic nerve with associated pleural thickening in the third, raising concern for microscopic residual disease. One patient was deemed unfit for surgery due to multiple comorbidities and was treated with definitive RT. Three patients with stage IVB disease and distant metastases were managed with palliative chemotherapy and palliative radiation.

Among the 11 patients with thymic carcinoma, three patients (27.3%) received NACT with paclitaxel and

Table 1. Patient characteristics

Characteristics	Thymoma (*n*=41; 78.8%)	Thymic carcinoma (*n*=11; 21.2%)
Age (years)		
Median	50	54
Range	28–79	26–90
Sex		
Male	26 (63.4)	6 (54.5)
Female	15 (36.6)	5 (45.5)
ECOG PS		
0	25 (61)	-
1	16 (39)	5 (45.5)
2	-	6 (54.5)
Comorbid conditions		
Yes	14 (34.1)	7 (63.6)
No	27 (65.9)	4 (36.3)
Paraneoplastic syndrome (yes/no)	Yes: 19 (46.3); No: 22 (53.7)	Yes: 1 (9.1); No: 10 (90.9)
Myasthenia gravis	17 (41.5)	1 (9.1)
Pure red cell aplasia	1 (2.4)	-
Polycythemia vera	1 (2.4)	-
Presenting symptoms		
Fatigue	14 (34.1)	1 (9.1)
Ptosis	10 (24.4)	-
Cough	9 (22)	2 (18.2)
Dyspnea	8 (19.5)	3 (27.3)
Chest pain	5 (12.2)	4 (36.4)
Hoarseness	3 (7.3)	1 (9.1
Dysphagia	-	2 (18.2)
Size of tumor (mm)		
Average maximal diameter (median)	97.5	77.5
Range	28–160	50–90
Masaoka-Koga stage		
I	3 (7.3)	-
IIA	6 (14.6)	-
IIB	1 (2.4)	3 (27.3)
IIIA	4 (9.8)	1 (9.1)
IIIB	7 (17.1)	2 (18.2)
IVA	17 (41.5)	1 (9.1)
IVB	3 (7.3)	4 (36.4)
Sites of metastasis		
Skeletal	1	-
Bilateral lung	2	1
Lung and liver	-	1
Brain, liver, and skeletal	-	1
Non-regional lymph nodes	-	1

(Cont'd...)

Table 1. ***(Continued)***

Characteristics	Thymoma (*n*=41; 78.8%)	Thymic carcinoma (*n*=11; 21.2%)
WHO subtype		
A	3 (7.3)	-
AB	2 (4.9)	-
B1	4 (9.8)	-
B2	19 (46.3)	-
B3	13 (31.7)	-
Thymic carcinoma histology		
Squamous cell carcinoma	-	6 (54.5)
Undifferentiated carcinoma, NOS	-	5 (45.5)

Abbreviations: ECOG PS: Eastern cooperative oncology group performance status; NOS: Not otherwise specified; WHO: World Health Organization.

Table 2. Treatment details (various modalities)

Treatment details	Thymoma (*n*=41) (%)	Thymic carcinoma (*n*=11) (%)
Surgery		
Yes	37 (90.2)	7 (63.6)
No	4 (9.8)	4 (36.4)
Resection status		
R0	31 (83.8)	-
R1	2 (5.4)	-
R2	4 (10.8)	-
Radiation		
Post-operative	37 (90.2)	7 (63.6)
Definitive	1 (2.4)	-
Palliative radiotherapy	3 (7.3)	4 (36.4)
Dose (median)	45 Gy	-
Dose (range)	45–64 Gy	-
Chemotherapy		
NACT	11 (26.8)	3 (27.3)
Adjuvant	8 (30.8)	-
HITHOC	4 (15.4)	-
Palliative	3 (11.5)	4 (36.7)

Abbreviation: HITHOC: Hyperthermic intrathoracic chemotherapy; NACT: Neoadjuvant chemotherapy; R0: Complete resection; R1: Microscopic residual disease; R2: Macroscopic residual disease.

carboplatin. Surgical resection was performed in seven patients (63.6%), of whom five (71.4%) achieved R0 resection, while two (28.6%) patients had R2 resection. All surgically treated patients received PORT. Four patients (36.4%) with metastatic disease were treated with palliative chemotherapy: Two received paclitaxel and carboplatin,

Table 3. Treatment details (stage-wise)

Treatment details	Stage	Thymoma (*n*)	Thymic carcinoma (*n*)
Surgery followed by PORT	Total	26	4
	I	3	-
	IIA	6	-
	IIB	1	3
	IIIA	4	-
	IIIB	3	1
	IVA	9	-
NACT followed by surgery, PORT, and adjuvant chemotherapy	Total	5	-
	IIIB	2	-
	IVA	3	-
NACT followed by surgery with HITHOC, PORT, and adjuvant chemotherapy	Total	2	-
	IIB	1	-
	IVA	1	-
NACT followed by surgery and PORT	Total	2	3
	IIIA	-	1
	IIIB	-	1
	IVA	2	1
NACT followed by surgery with HITHOC and PORT	Total	1	-
	IVA	1	-
NACT followed by definitive RT	Total	1	-
	IIIB	1	-
Surgery with HITHOC followed by PORT and adjuvant chemotherapy	Total	1	-
	IVA	1	-
Palliative chemotherapy and palliative RT	Total	3	4
	IVB	3	4

Abbreviations: HITHOC: Hyperthermic intrathoracic chemotherapy; NACT: Neoadjuvant chemotherapy; PORT: Post-operative radiotherapy; RT: Radiotherapy.

while the other two were treated with cisplatin and etoposide. RT was delivered using tomotherapy in 16 patients (30.8%) and VMAT in the remaining 36 patients (69.2%).

Among thymoma patients, seven (17.1%) experienced disease relapse (Table 4), with a median time to relapse of 14 months (range = 2–26 months). Among these, five patients developed bilateral pleural or pulmonary metastases (out-of-field recurrence), while one patient each developed brain and liver metastases. 6 out of 7 (85.7%) relapsed patients died from disease progression within 6 months of recurrence.

Overall, 10 patients (24.4%) with thymoma died during the study period. The causes of death included disease relapse in six patients, myasthenic crisis in two patients, grade 3 chemotherapy-induced thrombocytopenia in one

Table 4. Relapse pattern for thymoma and thymic carcinoma

Relapse pattern	Thymoma (*n*)	Thymic carcinoma (*n*)
Lung and pleura (out of field)	5	1
Brain	1	2
Liver	1	3
Kidney	-	1
Non-regional lymph nodes	-	2
Skeletal	-	2

patient, and a metastatic second primary breast malignancy in one patient.

Among patients with thymic carcinoma, 7 out of 11 (63.6%) experienced disease relapse. Sites of recurrence included liver and pararectal deposits (n = 1), multiple skeletal metastases with renal involvement (n = 1), leptomeningeal dissemination (n = 1), supraclavicular fossa and skeletal metastases (n = 1), isolated liver metastasis (n = 1), combined liver and brain involvement (n = 1), and pulmonary, supraclavicular fossa, and hilar lymph node metastases (n = 1). A total of 8 out of 11 patients (72.7%) with thymic carcinoma died during the study period. This included all seven patients who experienced disease relapse and one additional patient who died from a pulmonary thromboembolism unrelated to disease progression.

At a median follow-up of 6 years, the 5-year OS rates were 70.0% for thymoma and 30.7% for thymic carcinoma (Figure 1). The 5-year PFS for thymoma and thymic carcinoma were 85.1% and 26%, respectively (Figure 2). At the past follow-up, 26 thymoma patients (63.4%) were alive without disease. Seven patients (17.0%) developed grade 2 pneumonitis as late toxicity.

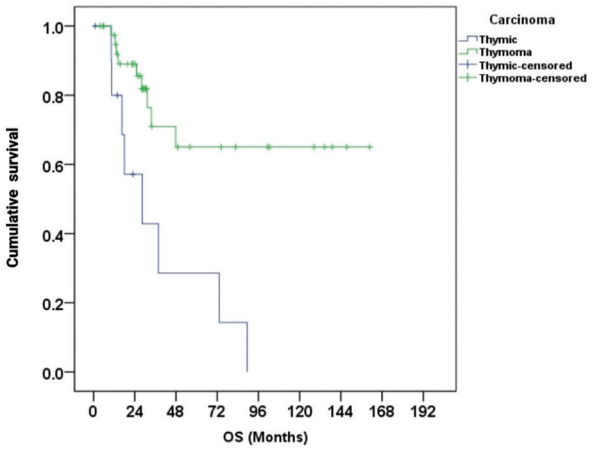

Figure 1. Five-year overall survival of thymoma and thymic carcinoma

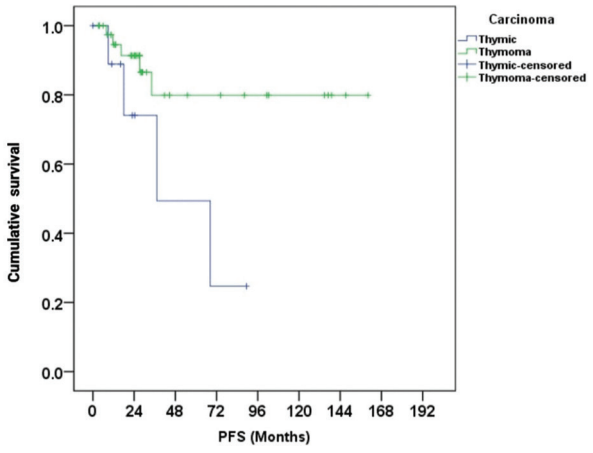

Figure 2. Five-year progression-free survival of thymoma and thymic carcinoma

4. Discussion

TETs display distinct biological behaviors, and this fundamental difference is reflected in their clinical presentation, stage at diagnosis, and overall prognosis.

In the present study, the median age of patients with thymoma was 50 years, approximately a decade younger than Western series reporting a median age of 60 years.[1] This younger age reflects the demographic profile of India, as supported by Rathod *et al.*[9] (median age of 51.5 years) and Chowdhary *et al.*[10] (median age of 52.1 years). The median age for thymic carcinoma in the present study was 54 years, within the range reported in the literature (54–65.5 years),[5] suggesting a tendency for thymic carcinoma to present in slightly older individuals.

Gender distribution also varied between the subtypes. While thymomas generally have no consistent gender predilection, some reports indicate a female preponderance in types A, AB, and B1, and male predominance in more aggressive subtypes.[11] In our cohort, 63.4% of thymoma patients were male, whereas thymic carcinoma also showed a slight male preponderance, consistent with prior reports.[5]

Considering the central role of the thymus in immune tolerance and T-cell maturation, thymomas are frequently associated with paraneoplastic autoimmune disorders, most commonly MG. Other neuromuscular, hematological, collagen, endocrine, and dermatological autoimmune disorders have also been reported in thymoma, reflecting the broad immunologic dysregulation induced by these tumors.[8] In contrast, thymic carcinomas are rarely associated with MG. In our cohort, 41.5% of thymoma patients had MG, which aligns with the known global incidence of 30–50%. These patients typically

presented with symptoms, such as ptosis, hoarseness, and dyspnea, or were diagnosed during a workup for worsening MG symptoms. In contrast, patients without MG most commonly presented with cough or chest pain. In our study, 9% of thymic carcinoma patients had MG, consistent with the literature.[12]

A recent analysis of the Surveillance, Epidemiology, and End Results database involving 3,857 patients, comprising 2,688 with thymoma and 1,169 with thymic carcinoma, identified tumor size as an independent prognostic factor for both cancer-specific survival and OS.[13] Tumors measuring ≤6.5 cm were significantly associated with improved outcomes in both histologic subtypes. Among patients with thymoma, those with tumors ≤6.5 cm who received RT or chemotherapy demonstrated significantly improved OS.

Similarly, patients with thymic carcinoma ≤6.5 cm experienced greater benefit from systemic and RT. In our cohort, the median tumor sizes for thymoma and thymic carcinoma were 97.5 mm and 77.5 mm, respectively, exceeding the 6.5-cm threshold and suggesting a potentially higher-risk population. Thymoma sizes were larger in our cohort compared to other Indian studies,[9] whereas thymic carcinoma sizes were comparable to existing literature (5.4–8.7 cm).

In our study, Masaoka-Koga stages IIIB, IVA, and IVB constituted 65.9% of the thymoma patient population, with IVA being the most common stage (41.5%), consistent with the findings of Kumar *et al.*[14] but contrary to Rathod *et al.*[9] and Chowdhary *et al.*,[10] where stages I–II (57% and 44.3%, respectively) were most prevalent. The sites of metastases in our cohort included the pleura and lung in one patient and the skeleton in another. Pleural/lung and lymph nodes have previously been reported to be the most common sites of metastases, with liver and brain involvement being less frequent.[15,16] Advanced disease at presentation is a hallmark of thymic carcinoma—a 2020 study from the National Cancer Database reported that 68% of patients presented with regional or distant disease.[5] In the present study, among thymic carcinoma patients, the majority (36.4%) had metastases with the most common sites being the liver, lung, and non-regional lymph nodes, consistent with existing literature.

In addition, nodal metastases and distant spread were more frequent in thymic carcinoma. Higher ECOG PS scores and a greater burden of comorbid conditions were observed among thymic carcinoma patients in our cohort.

The International Thymic Malignancy Group worldwide database of 4,221 thymomas reported type B2 thymoma as the most common (28%) and type A as the least common (12%) histotype, and noted a higher incidence of types AB and B3 and lower incidences of A and B2 in Asians.[17] In contrast, a large retrospective study on histotyping of Indian thymomas identified B2 as the most common histology.[18] In the present study, B2 was the most prevalent subtype, and together, B2 and B3 subtypes constituted 78.0% of our patient population.

Surgical resection remains the cornerstone of curative-intent treatment for TETs. For most resectable tumors, the primary oncologic goal is the complete excision of the lesion through total thymectomy, along with removal of any contiguous or non-contiguous disease when feasible.[19] R0 resection is one of the most significant prognostic factors for long-term survival in patients with thymic malignancies. Achieving a complete resection may necessitate en bloc removal of adjacent structures that are directly invaded by the tumor.

Commonly resected structures include the pericardium, phrenic nerve, pleura, lung parenchyma, and, in select cases, major vascular structures, such as the innominate vein or superior vena cava. While unilateral phrenic nerve resection may be necessary for oncologic clearance, bilateral phrenic nerve sacrifice is generally avoided due to the high risk of post-operative respiratory compromise. During surgery, systematic inspection of the pleural surfaces is recommended, as pleural metastases may not be readily apparent on pre-operative imaging. In some patients, removal of pleural implants may be required to achieve a complete gross resection.

In the present study, 83.8% of thymoma patients underwent R0 resection, which is comparable to the literature.[20] In thymic carcinoma, systematic lymph node dissection, including sampling of both anterior and deep mediastinal nodes, is recommended due to higher rates of nodal involvement.[21] In contrast, nodal dissection is not recommended for thymoma, given the low incidence of nodal metastasis, and may only be considered if clinically or radiologically suspicious lymphadenopathy is present. In patients with stage IVA disease and pleural dissemination, HITHOC was utilized at our institution as an adjunct to cytoreductive surgery, consistent with recommended treatment strategies for select cases of TETs.[22]

Radiation therapy plays a key adjunctive role in the management of TETs, particularly in the post-operative setting.[23-26] Adjuvant RT is indicated for patients with R1 or R2 resections, capsular invasion, and advanced-stage disease (stage II or higher), especially in the context of high-risk histology, such as type B3 thymoma or thymic carcinoma. Definitive RT is reserved for unresectable tumors or cases where surgery is contraindicated.

The indications for PORT in TETs depend on several factors, including the Masaoka-Koga stage, resection status, and WHO histologic subtype.[2,8,27] According to the National Comprehensive Cancer Network guidelines, adjuvant RT is recommended for patients with R1 or R2 after surgery, for those with R0 but capsular invasion, and for stages II through IV disease.[2] The European Society for Medical Oncology guidelines similarly recommend adjuvant RT for R1 and R2 resections at any stage, R0 resections in stage IIA with type B3 histology or stage IIB with B2-B3 histology, and stages III-IVA irrespective of resection status or WHO subtype.[8]

Definitive RT combined with concurrent chemotherapy is reserved for unresectable cases. Recommended PORT doses range from 45 to 50 Gy for R0 resections and 50 to 54 Gy for R1 resections, while definitive treatment doses range from 60 to 70 Gy. However, doses above 64 Gy are often difficult to deliver safely due to the proximity of critical adjacent organs, such as the heart and lungs. Guidelines for optimal CTV delineation underscore the value of a multidisciplinary approach, and studies have demonstrated that collaborative delineation with thoracic surgeons assisting radiation oncologists results in smaller and more precise target volumes.[28]

In the present study, seven patients developed grade 2 radiation pneumonitis and were managed conservatively. Some degree of increased lung dose is inevitable with thoracic RT; however, this can be mitigated through advanced techniques, such as tomotherapy and VMAT,[29-31] which allow for more conformal dose distribution and better sparing of normal lung tissue. In our cohort, these techniques were used in all our patients (Figures 3-5).

The most commonly utilized first-line chemotherapy regimen for thymomas in the present study was the combination of cisplatin, doxorubicin, and CAP, which has an overall response rate (ORR) of approximately 50%.[32] Data from the RYTHMIC prospective cohort study indicate that CAP-based chemotherapy yields superior ORR compared to non-anthracycline regimens in patients with advanced thymoma or thymic carcinoma (44% vs. 17%).[33] Second-line systemic therapies for relapsed or refractory thymoma are typically selected based on clinical context and histologic subtype and include everolimus, gemcitabine (with or without capecitabine), pemetrexed, 5-fluorouracil with leucovorin, and single-agent paclitaxel.[2] In the present study, one patient with relapsed thymoma, previously treated with CAP as NACT, received single-agent gemcitabine in the second-line setting.

The use of immune checkpoint inhibitors, particularly programmed cell death protein-1 (PD-1)/programmed death ligand-1 (PD-L1) inhibitors, is not routinely recommended in thymoma due to a high incidence of severe immune-related adverse events.[34,35] These findings highlight the unique immune milieu in thymoma, often associated with paraneoplastic autoimmune syndromes, necessitating caution with immunotherapeutic approaches.

For thymic carcinoma, systemic therapy remains the cornerstone of treatment for unresectable, metastatic, or recurrent disease.[2] The present preferred first-line regimen is the combination of carboplatin and paclitaxel, which has demonstrated an ORR of approximately 36%.[36] In our study, this combination was utilized in all three patients who received NACT for thymic carcinoma. Two patients with upfront metastatic disease received paclitaxel with carboplatin, while another two received a cisplatin-etoposide regimen.

In the second-line setting, several therapeutic options have demonstrated clinical activity, including lenvatinib (ORR of 38%),[37] sunitinib (partial response rate of 26%),[38,39] gemcitabine with or without capecitabine,[40] and pembrolizumab,[41-43] an anti–PD-1 immune checkpoint inhibitor (response rate of 22.5%). However, its use is associated with a notable incidence of severe immune-related adverse events, including grade 3–4 myocarditis reported in 5–9% of patients.[34,35]

Other second-line systemic therapies for subsequent lines include gemcitabine, 5-fluorouracil with leucovorin, pemetrexed, paclitaxel, single-agent etoposide or ifosfamide, avelumab with axitinib, and everolimus.[44-46] In our study, three patients with relapsed thymic carcinoma received multiple lines of chemotherapy, with two patients receiving up to the fifth line of systemic therapy. Although two patients had PD-L1 expression levels of 20% and 40%, respectively, and were planned for immunotherapy with pembrolizumab, neither was able to initiate treatment due to disease-related mortality before starting immunotherapy.

The 5-year OS of 70% observed in the thymoma subset of our study is comparable to the findings by Rea *et al.*[24] in an Italian cohort, where the majority also presented with advanced thymomas. However, the largest study from India reported a higher 5-year OS of 75.7%,[10] likely attributable to the predominance of early-stage disease (59.1% in stage I and II), in contrast to our cohort, in which the majority presented with stage IIIB or more advanced disease. In the largest database study of PORT for thymic tumors, Jackson *et al.*[1] reported outcomes for 4,056 patients. PORT was associated with improved OS, with the greatest relative benefit observed in patients with stage IIB to III and those with positive surgical margins. Other studies have also reported higher 5-year OS (88–91%).[47-49] The lower OS rates observed in our study may be attributed to the larger sizes and the predominance of advanced-stage disease at

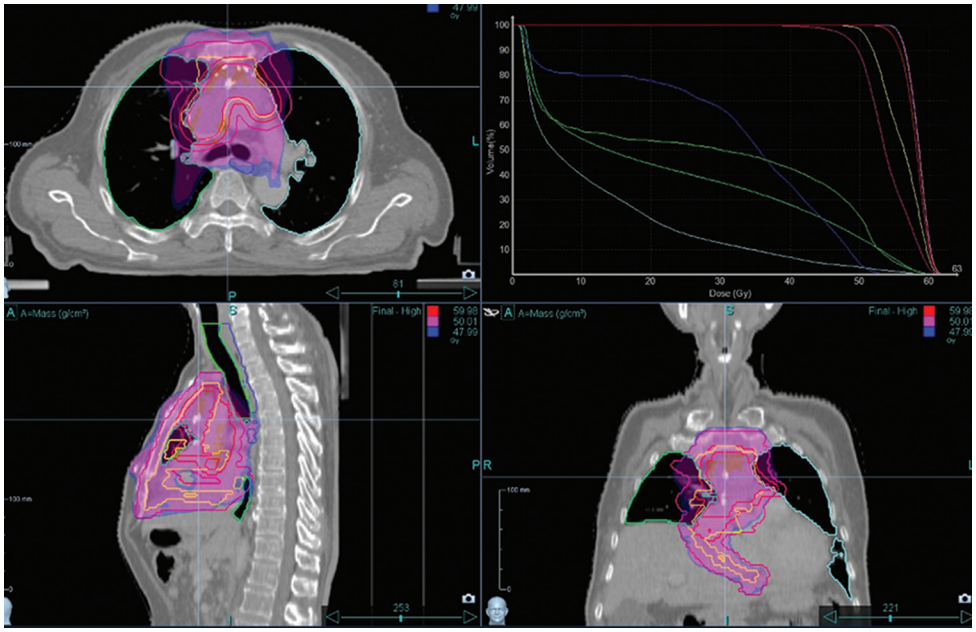

Figure 3. Thoracic radiotherapy image for a patient with stage IIIA thymoma

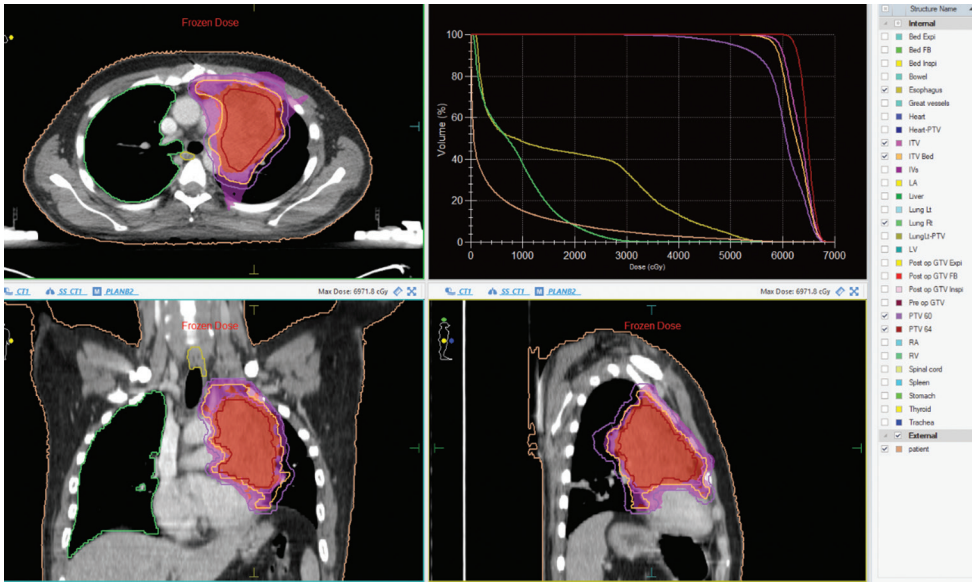

Figure 4. Post-operative radiotherapy target volumes for a patient with thymoma and macroscopic residual disease (R2) following debulking surgery

presentation, both of which are well-established adverse prognostic factors.[2,13,50]

The 5-year OS for thymic carcinoma patients in our study was 30.7%. Although this is much lower than the 65% 5-year OS reported by Rimner *et al.*[51] in the International Thymic Malignancy Group study with the use of PORT, it falls within the 30–50% range documented in literature.[52] Our thymic carcinoma subset was characterized by aggressive disease, with most patients in advanced stages, experiencing multi-site relapse. The 5-year PFS in our cohort was 26%, which is lower than the 36% reported in literature, likely due to a higher rate of distant relapses in our patients (64% vs. 31%).[53]

4.1. Impact of recurrence on survival

Recurrence emerged as the strongest determinant of mortality in our cohort. Among patients with thymic carcinoma, seven out of eight patients (87.5%) experienced recurrence, and all seven subsequently died, highlighting

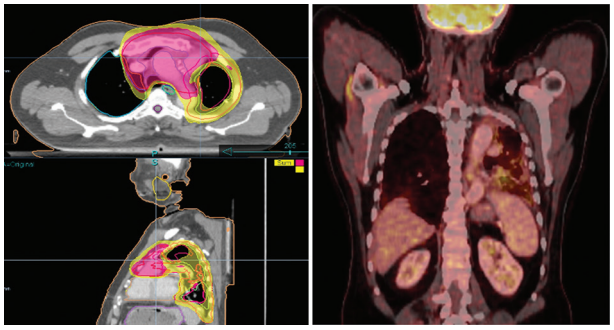

Figure 5. Hemi-thoracic radiotherapy for a patient with stage IVA thymoma, with corresponding post-treatment fibrotic changes observed on follow-up positron emission tomography-computed tomography scan

the aggressive nature of relapsed disease. In contrast, thymoma demonstrated a lower recurrence rate overall; however, six of the seven patients (85.7%) who relapsed also died. Taken together, these findings indicate that once recurrence occurs, the likelihood of disease-related mortality is extremely high. In this small cohort, recurrence status was more strongly associated with mortality than any individual treatment modality or clinical variable. Although the sample size limited the feasibility of robust multivariable modeling, the consistent pattern across both histologies suggests that disease recurrence is the principal prognostic factor, with substantially poorer survival following relapse.

5. Limitations, strengths, and future directions

This single-center, retrospective study is limited by the relatively small cohort and the absence of formal multivariable analyses, which restricts statistical power. The heterogeneity of treatment approaches and the limited sample size, particularly for thymic carcinoma, further limit the generalizability of the findings.

Nonetheless, the present study provides real-world data from one of the largest single-center series of TETs in India, with aggressive multimodal management, including surgery, systemic therapy, and advanced post-operative RT techniques (e.g., VMAT, tomotherapy), as well as HITHOC in select cases. Collaborative contouring of clinical target volumes and comprehensive documentation of systemic therapy across multiple lines further enhances clinical applicability.

Future research should explore complementary approaches, such as radiosensitizers, including ginsenoside Rg5, which have shown potential to enhance RT efficacy in thoracic tumors.[54] Prospective, multicenter studies with larger cohorts are needed to confirm these findings, define optimal stage-specific multimodality strategies, and identify interventions to reduce recurrence and improve long-term outcomes in TETs.

6. Conclusion

Recurrence is the strongest predictor of mortality in both thymoma and thymic carcinoma, irrespective of initial treatment. Despite advanced disease at presentation, aggressive multimodality therapy achieved high R0 resection rates and effective disease control in patients without recurrence.

Acknowledgments

We thank the technical and nursing staff of the Division of Radiation Oncology, Medanta, the Medicity, for the support and assistance in the care of all our patients.

Funding

None.

Conflict of interest

The authors declare that they have no competing interests.

Author contributions

Conceptualization: Sorun Shishak, Tejinder Kataria, Shyam Singh Bisht
Formal analysis: Sorun Shishak, Tejinder Kataria, Subham Pal, Shyam Singh Bisht
Investigation: Sorun Shishak, Tejinder Kataria, Susovan Banerjee, Deepak Gupta, Kushal Narang, Mayur Mayank, Shyam Singh Bisht
Methodology: Sorun Shishak, Tejinder Kataria, Shyam Singh Bisht
Writing – original draft: All authors
Writing – review & editing: Sorun Shishak, Tejinder Kataria, Subham Pal, Shyam Singh Bisht

Ethics approval and consent to participate

This study was conducted in accordance with the ethical principles outlined in the Declaration of Helsinki, Good Clinical Practice guidelines, and the Indian Council of Medical Research guidelines. Institutional ethics committee approval was obtained before study initiation (MICR: 1532/2023). The requirement for informed consent was waived due to the retrospective nature of the study.

Consent for publication

Informed consent was waived by the Institutional Review Board due to the retrospective nature of the study and the use of anonymized patient data.

Availability of data

Not applicable.

References

1. Jackson MW, Palma DA, Camidge DR, *et al*. The impact of postoperative radiotherapy for thymoma and thymic carcinoma. *J Thorac Oncol*. 2017;12(4):734-744.

doi: 10.1016/j.jtho.2017.01.002

2. Riely GJ, Wood DE, Loo BW, *et al*. Thymomas and thymic carcinomas, version 2.2025, NCCN clinical practice guidelines in oncology. *J Natl Compr Canc Netw*. 2025;23(6):255-269.

doi: 10.6004/jnccn.2025.0027

3. Chen L, Li Y, Dong X, *et al*. The value of postoperative radiotherapy in thymoma patients with myasthenia gravis. *Radiother Oncol*. 2023;183:109644.

doi: 10.1016/j.radonc.2023.109644

4. Rich AL. Epidemiology of thymoma. *J Thorac Dis*. 2020;12(12):7531-7535.

doi: 10.21037/jtd-2019-thym-02

5. Roden AC, Ahmad U, Cardillo G, *et al*. Thymic carcinomas-a concise multidisciplinary update on recent developments from the thymic carcinoma working group of the international thymic malignancy interest group. *J Thorac Oncol*. 2022;17(5):637-650.

doi: 10.1016/j.jtho.2022.01.021

6. Marx A, Chan JKC, Chalabreysse L, *et al*. The 2021 WHO classification of tumors of the thymus and mediastinum: What is new in thymic epithelial, germ cell, and mesenchymal tumors? *J Thorac Oncol*. 2022;17(2):200-213.

doi: 10.1016/j.jtho.2021.10.010

7. Zhang Y, Lin D, Aramini B, *et al*. Thymoma and thymic carcinoma: Surgical resection and multidisciplinary treatment. *Cancers (Basel)*. 2023;15(7):1953.

doi: 10.3390/cancers15071953

8. Girard N, Ruffini E, Marx A, Faivre-Finn C, Peters S; ESMO Guidelines Committee. Thymic epithelial tumours: ESMO clinical practice guidelines for diagnosis, treatment and follow-up. *Ann Oncol*. 2015;26(Suppl 5):v40-v55.

doi: 10.1093/annonc/mdv277

9. Rathod S, Munshi A, Paul S, Ganesh B, Prabhash K, Agarwal JP. Thymoma: First large Indian experience. *Indian J Cancer*. 2014;51:109-112.

doi: 10.4103/0019-509X.138144

10. Chowdhary RL, Chufal KS, Ismail M, *et al*. Intuitive evaluation of contemporary management strategies in thymoma - the largest Indian experience. *Rep Pract Oncol Radiother*. 2023;28(4):454-464.

doi: 10.5603/RPOR.a2023.0050

11. Gerber TS, Strobl S, Marx A, Roth W, Porubsky S. Epidemiology of thymomas and thymic carcinomas in the United States and Germany, 1999-2019. *Front Oncol*. 2024;13:130889.

doi: 10.3389/fonc.2023.1308989

12. Nakajima J, Okumura M, Yano M, *et al*. Myasthenia gravis with thymic epithelial tumour: A retrospective analysis of a Japanese database. *Eur J Cardiothorac Surg*. 2016;49:1510-1515.

doi: 10.1093/ejcts/ezv380

13. Lin L, Li Y, Huang Y, *et al*. Investigating the impact of tumor size on survival outcomes in thymoma and thymic carcinoma patients using the SEER database. *Sci Rep*. 2024;14(1):27680.

doi: 10.1038/s41598-024-79186-5

14. Kumar N, Kumar R, Bera A, *et al*. Thymoma: Clinical experience from a tertiary care institute from North India. *J Cancer Res Ther*. 2013;9:235-239.

doi: 10.4103/0973-1482.113364

15. Khandelwal A, Sholl LM, Araki T, Ramaiya NH, Hatabu H, Nishino M. Patterns of metastasis and recurrence in thymic epithelial tumours: Longitudinal imaging review in correlation with histologic subtypes. *Clin Radiol*. 2016;71(10):1010-1017.

doi: 10.1016/j.crad.2016.05.007

16. Vladislav T, Jain RK, Alvarez R, *et al*. Extrathoracic metastases of thymic origin: A review of 35 cases. *Mod Pathol*. 2012;25:370-377.

doi: 10.1038/modpathol.2011.178

17. Weis CA, Yao X, Deng Y, *et al*. The impact of thymoma histotype on prognosis in a worldwide database. *J Thorac Oncol*. 2015;10(2):367-372.

doi: 10.1097/JTO.0000000000000393

18. Guleria P, Parshad R, Malik PS, Ray R, Panday RM, Jain D. Histotyping of Indian thymomas: A clinicopathologic study from North India. *Indian J Med Res*. 2019;150(2):153-160.

doi: 10.4103/ijmr.IJMR_530_18

19. Liou DZ, Berry MF, Brown LM, *et al*. The society of thoracic surgeons expert consensus document on the surgical management of thymomas. *J Thorac Dis*. 2019;11(7):2695-2699.

doi: 10.1016/j.athoracsur.2024.04.013

20. Du X, Cui J, Yu X, Yu L. Risk factor analysis of thymoma resection and its value in guiding clinical treatment. *Cancer Med*. 2023;12(12):13408-13414.

doi: 10.1002/cam4.6043

21. Brascia D, De Palma A, Schiavone M, *et al*. Lymph nodes involvement and lymphadenectomy in thymic tumors: Tentative answers for unsolved questions. *Cancers (Basel)*. 2021;13(20):5085.

doi: 10.3390/cancers13205085

22. Da Nobrega Oliveira REN, De Andrade Pontual Peres C, Oliveira AC, *et al*. Efficacy of cytoreductive surgery and hyperthermic intrathoracic chemotherapy (HITHOC) in thymic neoplasia: A systematic review and single-arm meta-analysis. *Ann Surg Oncol.* 2025;32(3):1670-1678.

doi: 10.1245/s10434-024-16547-4

23. Tateishi Y, Horita N, Namkoong H, Enomoto T, Takeda A, Kaneko T. Postoperative radiotherapy for completely resected Masaoka/Masaoka-Koga stage II/III thymoma improves overall survival: An updated meta-analysis of 4746 patients. *J Thorac Oncol.* 2021;16(4):677-685.

doi: 10.1016/j.jtho.2020.12.023

24. Rea F, Marulli G, Di Chiara F, *et al*. Multidisciplinary approach for advanced stage thymic tumors: Long-term outcome. *Lung Cancer.* 2011;75:68-72.

doi: 10.1016/j.lungcan.2010.07.006

25. Lu CF, Yu L, Jing Y, Zhang YF, Ke J. Value of adjuvant radiotherapy for thymoma with myasthenia gravis after extended thymectomy. *Chin Med J (Engl).* 2018;131:927-932.

doi: 10.4103/0366-6999.229894

26. Lin L, Li Y, Huang Y, *et al*. Evaluation of the role of postoperative radiotherapy in locally invasive thymoma: A propensity-matched study based on the SEER database. *PLoS One.* 2023;18(4):e0283192.

doi: 10.1371/journal.pone.0283192

27. Rico M, Flamarique S, Casares C, *et al*. GOECP/SEOR radiotherapy guidelines for thymic epithelial tumours. *World J Clin Oncol.* 2021;12(4):195-216.

doi: 10.5306/wjco.v12.i4.195

28. Marcuse F, Peeters S, Herman K, *et al*. Optimal delineation of the clinical target volume for thymomas in the post-resection setting: A multicenter study. *Radiother Oncol.* 2021;165:8-13.

doi: 10.1016/j.radonc.2021.10.007

29. Rahi MS, Parekh J, Pednekar P, *et al*. Radiation-induced lung injury-current perspectives and management. *Clin Pract.* 2021;11(3):410-429.

doi: 10.3390/clinpract11030056

30. Moiseenko V, Craig T, Bezjak A, Van Dyk J. Dose-volume analysis of lung complications in the radiation treatment of malignant thymoma: A retrospective review. *Radiother Oncol.* 2003;67(3):265-274.

doi: 10.1016/S0167-8140(03)00003-3

31. Gomez D, Komaki R. Technical advances of radiation for thymic malignancies. *J Thorac Oncol.* 2010;5(Suppl 4):S336-S343.

doi: 10.1097/JTO.0b013e3181f20ea2

32. Loehrer PJ Sr., Kim K, Aisner SC, *et al*. Cisplatin plus doxorubicin plus cyclophosphamide in metastatic or recurrent thymoma: Final results of an intergroup trial. *J Clin Oncol*. 1994;12:1164-1168.

doi: 10.1200/JCO.1994.12.6.1164

33. Merveilleux Du Vignaux C, Dansin E, Mhanna L, *et al*. Systemic therapy in advanced thymic epithelial tumors: Insights from the RYTHMIC prospective cohort. *J Thorac Oncol*. 2018;13:1762-1770.

doi: 10.1016/j.tho.2018.08.005

34. Theochari K, Rapti K, Kotteas E, *et al*. Fatal adverse events in two thymoma patients treated with anti-PD-1 immune checkpoint inhibitor and literature review. *Lung Cancer*. 2019;135:29-32.

doi: 10.1016/j.lungcan.2019.06.015

35. Argentiero A, Solimando AG, Ungaro V, *et al*. Case report: Lymphocytosis associated with fatal hepatitis in a thymoma patient treated with anti-PD1: New insight into the immune-related storm. *Front Oncol*. 2020;10:583781.

doi: 10.3389/fonc.2020.583781

36. Hirai F, Yamanaka T, Taguchi K, *et al*. A multicenter phase II study of carboplatin and paclitaxel for advanced thymic carcinoma: WJOG4207L. *Ann Oncol*. 2015;26:363-368.

doi: 10.1093/annonc/mdu541

37. Sato J, Satouchi M, Itoh S, *et al*. Lenvatinib in patients with advanced or metastatic thymic carcinoma (REMORA): A multicentre, phase 2 trial. *Lancet Oncol*. 2020;21:843-850.

doi: 10.1016/S1470-2045(20)30162-5

38. Thomas A, Rajan A, Berman A, *et al*. Sunitinib in patients with chemotherapy-refractory thymoma and thymic carcinoma: An open-label phase 2 trial. *Lancet Oncol*. 2015;16:177-186.

doi: 10.1016/S1470-2045(14)71181-7

39. Proto C, Manglaviti S, Lo Russo G, *et al*. STYLE (NCT03449173): A phase 2 trial of sunitinib in patients with type B3 thymoma or thymic carcinoma in second and further lines. *J Thorac Oncol*. 2023;18:1070-1081.

doi: 10.1016/j.jtho.2023.04.009

40. Palmieri G, Buonerba C, Ottaviano M, *et al*. Capecitabine plus gemcitabine in thymic epithelial tumors: final analysis of a phase II trial. *Future Oncol*. 2014;10:2141-2147.

doi: 10.2217/fon.14.144

41. Giaccone G, Kim C, Thompson J, *et al*. Pembrolizumab in patients with thymic carcinoma: A single-arm, single-centre, phase 2 study. *Lancet Oncol*. 2018;19:347-355.

doi: 10.1016/S1470-2045(18)30062-7

42. Giaccone G, Kim C. Durable response in patients with thymic carcinoma treated with pembrolizumab after

prolonged follow-up. *J Thorac Oncol*. 2021;16:483-485.

doi: 10.1016/j.jtho.2020.11.003

43. Cho J, Kim HS, Ku BM, *et al*. Pembrolizumab for patients with refractory or relapsed thymic epithelial tumor: An open-label phase II trial. *J Clin Oncol*. 2019;37:2162-2170.

doi: 10.1200/JCO.2017.77.3184

44. Conforti F, Zucali PA, Pala L, *et al*. Avelumab plus axitinib in unresectable or metastatic type B3 thymomas and thymic carcinomas (CAVEATT): A single-arm, multicentre, phase 2 trial. *Lancet Oncol*. 2022;23:1287-1296.

doi: 10.1016/S1470-2045(22)00542-3

45. Conforti F, Pala L, Vivanet G, *et al*. High-dose continuous-infusion ifosfamide in advanced thymic epithelial tumors: A TYME network study. *Lung Cancer*. 2023;176:98-102.

doi: 10.1016/S1470-2045(22)00542-3.

46. Hellyer JA, Ouseph MM, Padda SK, Wakelee HA. Everolimus in the treatment of metastatic thymic epithelial tumors. *Lung Cancer*. 2020;149:97-102.

doi: 10.1016/j.lungcan.2020.09.006

47. Alothaimeen HS, Memon MA. Treatment outcomes and prognostic factors of malignant thymoma: A single institution experience. *Asian Pac J Cancer Prev*. 2020;21(3):653-661.

doi: 10.31557/APJCP.2020.21.3.653

48. Bruni A, Stefani A, Perna M, *et al*. The role of postoperative radiotherapy for thymomas: A multicentric retrospective evaluation from three Italian centers and review of literature. *J Thorac Dis*. 2020;12(12):7518-7530.

doi: 10.21037/jtd-2019-thym-09

49. Yuan ZY, Gao SG, Mu JW, *et al*. Long-term outcomes of 307 patients after complete thymoma resection. *Chin J Cancer*. 2017;36:46.

doi: 10.1186/s40880-017-0213-8

50. Liou DZ, Ramakrishnan D, Lui NS, Shrager JB, Backhus LM, Berry MF. Does size matter? A national analysis of the utility of induction therapy for large thymomas. *J Thorac Dis*. 2020;12(4):1329-1341.

doi: 10.21037/jtd.2020.02.63

51. Rimner A, Ahmad U, Lobaugh SM, *et al*. Postoperative radiation therapy for thymic carcinoma: an analysis of the international thymic malignancy interest group/european society of thoracic surgeons database. *J Thorac Oncol*. 2024;19(2):233-242.

doi: 10.1016/j.jtho.2023.12.011

52. Tseng YL. Thymic carcinoma: A rare cancer requiring special attention. *Formos J Surg*. 2011;44(5):169-175.

doi: 10.1016/j.fjs.2011.08.007

53. Cheng G, Gu C, Song Z. Impact of metastasis site for survival of patients with advanced thymic epithelial tumors. *Transl Cancer Res*. 2016;5(5):546-551.

doi: 10.21037/tcr.2016.09.35

54. Bai H, Lyu J, Nie X, *et al*. Ginsenoside Rg5 enhances the radiosensitivity of lung adenocarcinoma via reducing HSP90-CDC37 interaction and promoting client protein degradation. *J Pharm Anal*. 2023;13(11):1296-1308.

doi: 10.1016/j.jpha.2023.06.004

ACCSCIENCE PUBLISHING

Advances in Radiotherapy & Nuclear Medicine

MINI-REVIEW

Mini neutron tubes for boron neutron capture therapy and neutron imaging applications

Ka-Ngo Leung*

Department of Nuclear Engineering, University of California, Berkeley, California, United States of America

(This article belongs to the *Special Issue: Boron Neutron Capture Therapy: A Renaissance*)

Abstract

Recent advancements in negative deuterium and negative hydrogen ion source technology, as well as the commercial availability of high-frequency alternating-current high-voltage power supplies, have enabled the development of mini neutron generators using low-energy nuclear reactions. By operating these neutron tubes near the threshold energy of the p-^{7}Li reaction, a useful flux of epithermal energy neutrons can be obtained. The new epithermal neutron sources can be configured for the treatment of deep-seeded tumors through boron neutron capture therapy (BNCT), for performing BNCT-brachytherapy or for the determination of ^{10}B distribution in the tumor using the neutron transmission imaging technique. The new epithermal neutron tube is very compact and requires very low power for operation. It can easily combine BNCT with intraoperative radiotherapy or fast neutron therapy to enhance cancer treatment.

Keywords: Neutron tube; Epithermal neutrons; Boron neutron capture therapy; Intraoperative radiotherapy; Brachytherapy; Fast neutron therapy; Neutron transmission imaging

***Corresponding author:**
Ka-Ngo Leung
(kangoleung@pacbell.net)

Citation: Leung K. Mini neutron tubes for boron neutron capture therapy and neutron imaging applications. *Adv Radiother Nucl Med*. 2026;4(1):93-98. doi: 10.36922/ARNM025290035

Received: July 18, 2025

Revised: September 10, 2025

Accepted: September 17, 2025

Published online: September 30, 2025

1. Introduction

Compact and high-flux neutron generators are useful for many applications, such as cancer therapy, medical isotope production, material analysis, carbon and well logging, and cargo screening. Recent experimental investigations demonstrated that substantial amount of negative hydrogen (H^-) or negative deuterium (D^-) ions can be produced by thermal desorption processes.[1] Based on these new findings, mini neutron tubes are now being developed which can eliminate most issues from the larger positive hydrogen (H^+) or positive deuterium (D^+) ion-based neutron generators. Using a high-frequency alternating-current (AC) high-voltage power supply, short pulses of high intensity neutron beams can be generated using the d-d, d-^{10}B, d-^{7}Li, or p-^{7}Li nuclear reactions.[2] The p-^{7}Li reaction is particularly useful because it can provide neutrons with epithermal energy (0.5 eV–20 keV) by operating near the threshold energy of 1.88 MeV.[3,4] These epithermal neutrons have found important applications in medical isotope production,[2,5] in boron neutron capture therapy (BNCT),[2,6] and in material analysis by neutron resonance capture spectroscopy.[7-9] This article describes the design and development of compact epithermal neutron generators and their potential applications in cancer therapy.

2. Mini neutron tube for BNCT and fast neutron therapy

Based on the high probability of the stable isotope ^{10}B capturing a thermal neutron, BNCT relies on the resulting release of two high-energy ions ($^4He^{2+}$ and $^7Li^+$). Due to the high linear energy transfer and relative biological effectiveness of these ions, only cells near the reaction $^{10}B(n,\alpha)^7Li$ are damaged, leaving adjacent cells unaffected. The enhanced uptake of the boron-labeled agent in tumor cells versus normal cells results in selective killing of tumor cells. The neutrons for this BNCT treatment can come from a fission reactor, a high energy accelerator system (such as cyclotrons or linear accelerators), a compact neutron generator or a mini neutron tube. A comparison of these neutron sources for BNCT application is summarized in Table 1.

Throughout the last two decades, radio frequency-driven, positive-ion-based d-d neutron generators have been developed to treat cancer tumors using BNCT.[6] The 2.54 MeV d-d neutrons, however, need to be moderated to the epithermal energy range before entering the patient's body. The MCNP Monte Carlo computation code has been used for the moderator design study. It has been shown that a moderator with dimensions of 100 cm × 100 cm × 100 cm can provide the proper epithermal neutron energy spectrum for BNCT treatment.[6] Such a massive moderator design can be eliminated if an epithermal neutron generator is employed.

Figure 1 is a schematic diagram showing the design of an axial-type epithermal neutron tube. This neutron tube is made of Pyrex-glass, which is 2.5 cm in diameter and 8 cm in length. A slotted thin titanium (Ti) foil (0.1 mm in thickness and 2 cm in diameter), used as a H^- ion emitter, is located at one end of the tube, while a lithium (Li) target electrode is located at the opposite end. The Li target electrode (~2-cm-diam) is biased at +1.9 MV with respect to the emitter foil. To produce H^- ions by thermal desorption processes, hydrogen gas and cesium vapor are initially introduced into the glass tube. The temperature of the Ti foil can be varied by adjusting the heating current. When the temperature of the Ti foil reaches 250°C, copious amount of H^- ions are emitted.[1] These H^- ions are accelerated to the Li target electrode where epithermal neutrons will be produced by the p-^{7}Li reaction.[2,3] Today, commercial high frequency AC high voltage supplies are readily available. These compact AC high voltage power sources are commonly found in portable dental X-ray machines. A peak voltage between 500 kV and 2 MV (with peak current in tens of mA) can be obtained with these power supplies. Using these high-voltage power sources, the neutron tube can produce a high peak flux of epithermal neutrons suitable for cancer therapy and neutron transmission imaging. Since the air-cooled target electrode is completely enclosed inside a glass tube, the patient is electrically insulated from the applied high voltage pulses.

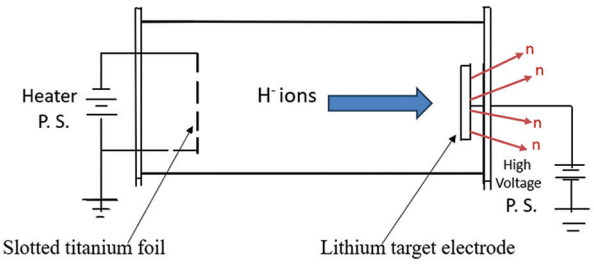

Figure 1. The axial-type epithermal neutron tube based on thermally emitted H^- ions. Schematic created by the author.
Abbreviation: P.S.: Power supply.

Using the axial p-^{7}Li neutron tube, a high flux of epithermal neutrons can be directly produced by operating the generator near the threshold interaction energy.[3,4] On entering the patient's body, these epithermal neutrons are moderated to thermal neutrons when they arrive at the tumor site. With an H^- ion beam of 1.9 MV, 70 mA, and a beam diameter of 5 cm, the average epithermal neutron yield for 1% duty factor operation is approximately 1×10^{10} n/s,[3] or an epithermal neutron flux of 5×10^8 n/cm^2/s, which is the recommended value for BNCT treatment.[10] The average ion beam power density on the target electrode is only 68 W/cm^2 for 1% duty factor operation. The treatment time is estimated to be about 30 min.[6]

If a higher epithermal neutron flux is needed, one can employ a cluster of mini neutron tubes each operated

Table 1. Comparison of different neutron sources for BNCT application

	Fission reactor	Accelerator system	Neutron generator	Mini neutron tubes
Moderator required	Yes	Yes	Yes	No
Shielding requirement	Yes	Yes	Yes	Much smaller
Neutron yield	High	Moderate	Moderate	Moderate
System operation	Complicated	Complicated	Simpler	Simpler
System cost	High	High	Low	Very low
Clinical feasibility	Yes	Yes	Yes	Yes

Abbreviation: BNCT: Boron neutron capture therapy.

with a 2-cm diameter target, as shown in Figure 2. These neutron tubes are focused on the tumor, providing the highest flux of thermal neutrons at the tumor site. As a result, the treatment time can be greatly reduced. The p-^{7}Li neutron tube should be the most compact and versatile tool for the treatment of cancer through BNCT. This approach of performing BNCT is much simpler than employing a fission reactor or a large accelerator system. The cost is much lower, and the total footprint of the system is small, making it suitable for operation inside a hospital or a clinical facility.

The mini neutron tube can also be used to produce higher energy 10 and 13 MeV d-^{7}Li neutrons for fast neutron therapy.[11] The cluster mini-tube arrangement (Figure 3) can then be used to combine fast neutron therapy with BNCT for deep-seeded tumor treatment. In a cluster of seven mini neutron tubes, the center one is a d-^{7}Li neutron tube for fast neutron therapy. The surrounding six are p-^{7}Li neutron tubes operating at 1.9 MV to produce epithermal neutrons for BNCT. The advantage of this combine cancer treatment method has been reported by Sauerwein *et al.*[6] With the recent development of the new mini neutron tubes, one should be able to perform the combined BNCT and fast neutron therapy treatment much easier than a large and expensive accelerator system.

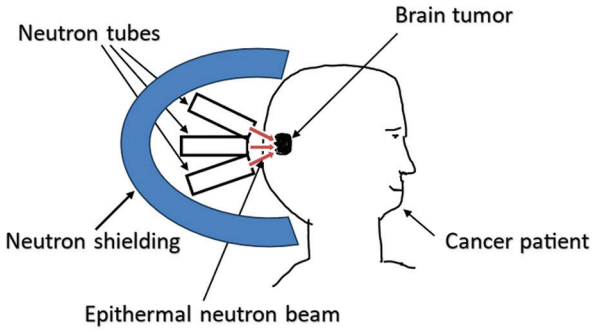

Figure 2. BNCT treatment of brain tumor with multiple epithermal neutron tubes. Schematic created by the author.
Abbreviation: BNCT: Boron neutron capture therapy.

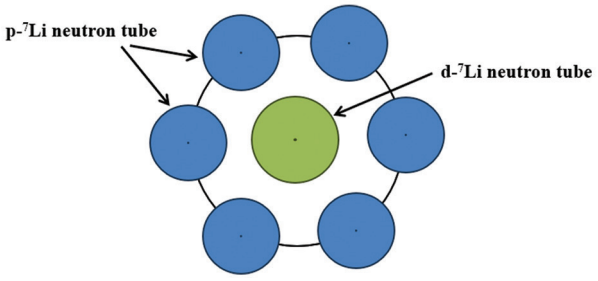

Figure 3. A cluster of p-^{7}Li and d-^{7}Li mini neutron tubes for BNCT and fast neutron therapy. Schematic created by the author.
Abbreviation: BNCT: Boron neutron capture therapy.

3. Mini neutron tube for brachytherapy and intraoperative radiotherapy (IORT)

The surgical removal of a solid cancer tumor is sometimes followed by IORT.[2] Isotropic neutron emission will permit the irradiation or "sterilization" of the surrounding side walls of the of the cavity, thereby reducing the chance of cancer recurrences. One can also populate the tumor cells in the cavity with ^{10}B and then perform BNCT-brachytherapy[12] by irradiating the cavity walls with epithermal neutrons. In this procedure, a mini p-^{7}Li neutron tube can be employed. Since the reaction produces directional epithermal neutrons when operated near the threshold energy, a coaxial-type neutron tube should be used.[2] Figure 4 shows the arrangement of the coaxial-type p-^{7}Li neutron tube. Figure 5 is a picture of a prototype mini coaxial-type neutron tube. The dimension of the glass tube is about 20 mm in diameter by about 25 mm long. The Li target electrode is located at the center of the glass tube. It is surrounded by the Ti heater foil where H^- ions are

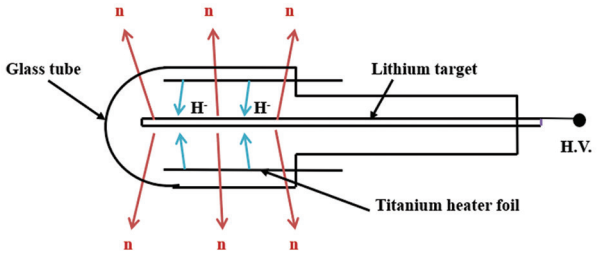

Figure 4. The coaxial type p-^{7}Li epithermal neutron tube for brachytherapy application. Schematic created by the author.
Abbreviation: H.V.: High voltage.

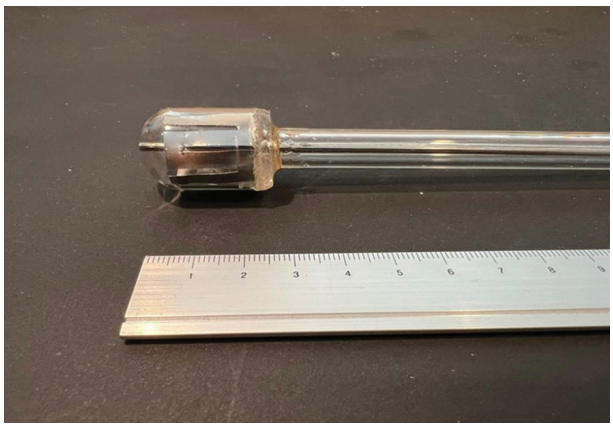

Figure 5. A prototype mini coaxial-type neutron tube. Photo captured by the author.

emitted. When a high positive voltage is applied to the Li target, H^- ions will be accelerated toward it. Epithermal neutrons will be produced by the p-^{7}Li reaction at the target electrode. These neutrons will be emitted uniformly in all directions inside the tumor cavity. If the mini p-^{7}Li neutron tube is operated at 1.9 MeV, 10 mA at 100% duty factor, the epithermal neutron yield is estimated to be 1.5×10^{11} n/s[3]. For 1% duty factor pulsed operation, the average epithermal neutron yield becomes 1.5×10^9 n/s. The average neutron flux at the surface of the neutron tube is approximately 1×10^8 n/cm^2/s. A detailed study will be performed to evaluate the treatment time required for this BNCT-brachytherapy operation.

For an IORT procedure, radiation in the form of photons, electrons, protons, or neutrons can be applied. It is essential to allow these radiation particles to reach all corners of the surrounding walls. In addition, the irradiation should be uniform on the cavity walls. To meet these requirements, a mini axial-type d-d neutron tube and applicator arrangement has been developed.[13] Figure 6 is a schematic diagram of a mini d-d neutron tube equipped with a conical shaped Ti target electrode. With this conical target arrangement, the d-d neutron flux on the spherical surface of the applicator will be uniform.[13] Besides performing IORT, this mini d-d neutron tube can be modified to generate both epithermal and 2.45 MeV d-d neutrons. This will enable one to carry out not only IORT but also BNCT in the presence of a ^{10}B agent.

Figure 6 shows a mini axial-type d-d neutron tube operated with a spherical applicator which also serves as a neutron moderator. The 2.45 MeV d-d neutrons produced at the Ti target will be moderated to form epithermal neutrons. With a 1-cm thick D_2O moderator, the MCNP simulation shows that about 10% of the d-d neutrons can be converted to epithermal neutrons.[13] If this mini d-d neutron tube is operated with 500 kV and 10 mA beam power, the total neutron yield is either 5×10^9 n/s or 5×10^{10} n/s for 10% duty factor pulsed operation.[14] On the outer surface of a 4 cm diameter applicator, the flux of d-d and epithermal neutron is 1×10^8 and 1×10^7 n/cm^2/s, respectively. Combining IORT with BNCT is an effective approach in cancer treatment.[15]

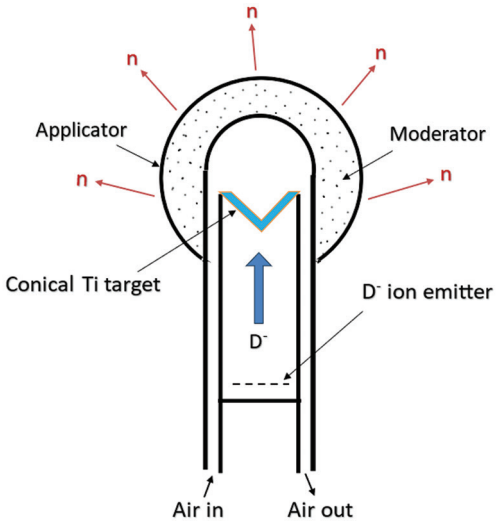

Figure 6. Schematic diagram of the mini axial-type d-d neutron tube and moderator arrangement for IORT and BNCT application. Schematic created by the author.
Abbreviations: BNCT: Boron neutron capture therapy; IORT: Intraoperative radiotherapy.

4. Epithermal neutron generator for neutron transmission imaging

Neutron imaging can be performed using high-energy, epithermal, or thermal neutrons. To achieve a high image resolution, the source size for neutron emission must be small.[2] For high-energy neutron imaging (using 10 and 13 MeV d-^{7}Li neutrons), one can use the coaxial neutron generator arrangement[2]. In this case, the neutron emission source size is equal to the dimension of the target tube. For thermal and epithermal neutron imaging, generating a small-point neutron source is technically challenging. These neutrons are normally produced using a large accelerator system (Figure 7). High-energy neutrons are first generated at the target by bombarding it with a multi-MeV proton beam. Subsequently, they are moderated to form thermal or epithermal neutrons. As they pass through the moderator, the thermal or epithermal neutrons are scattered in all direction. Some of these neutrons will exit through the collimator opening. The diameter (D) of this opening defines the size of the thermal or epithermal neutron source. The sample to be imaged is in front of the neutron detector. If L is the distance between the collimator and the detector, as shown in Figure 7, the quality of the sample image will depend on the L/D ratio. In general, L/D must exceed 100 to produce good-quality images.[7]

When a moderator is used to convert high-energy neutrons to thermal or epithermal neutrons, it will randomize the direction of the neutrons. It will also increase the distance of the collimator aperture from the beam target where high-energy neutrons are produced. As a result, the flux of the thermal or epithermal neutron at the collimator will be reduced, resulting in a longer exposure time for the imaging process. For this reason, the direct production of thermal or epithermal neutrons without a moderator has a significant advantage for neutron imaging applications. There is no direct production process for thermal neutrons, but epithermal neutrons can be formed

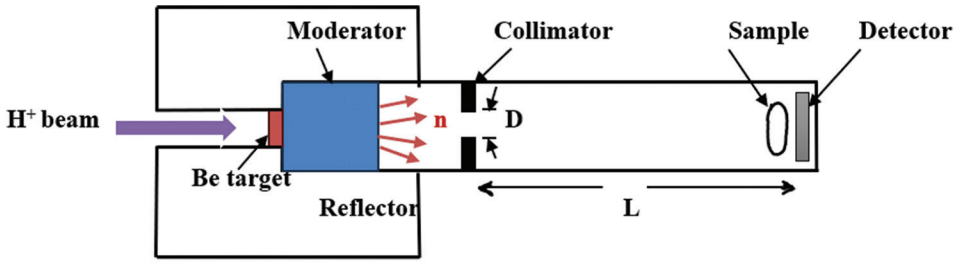

Figure 7. A typical thermal or epithermal neutron transmission imaging system. Schematic created by the author.

directly by the p-^{7}Li reaction at near-threshold energy (that is 1.88 MeV).

A compact p-^{7}Li neutron tube is an ideal tool for epithermal neutron imaging, particularly for analyzing radioactive waste in borosilicate glass[8] and in non-destructive and isotope-sensitive material analysis.[9] It can also be used to image the distribution of a ^{10}B agent in a tumor. In the past, the presence of ^{10}B was detected by means of positron emission tomography or nuclear magnetic resonance before BNCT treatment processes.[6] However, these ^{10}B imaging techniques are complicated, and the imaging equipment is typically located separately from the BNCT treatment facility. On the other hand, the neutron tube for boron imaging has almost the same arrangement as the epithermal neutron tube for BNCT. They can be operated in tandem in the treatment room.

To increase the neutron output from the epithermal neutron tube, a large hemispherical H^- ion emitter can be employed. Figure 8 shows the design of an intense epithermal neutron source for boron imaging and analysis prior to BNCT treatment. H^- ions emitted from the Ti emitter will impinge on a small Li target electrode. Using a hemispherical Li beam target electrode, the target area is increased by a factor of two, thereby reducing the beam power density by the same factor while maintaining the neutron source size, which is the diameter (D) of the hemispherical target (Figure 8). Using forced-air cooling, the temperature of the hemispherical Li target electrode can be maintained below its melting temperature of 180°C.

If the epithermal neutron source size (D) is 3 mm, and L/D is 100, then the distance of the detector from the source (L) will be 300 mm. For a H^- ion beam of 1.9 MV, 10 mA, the total number of epithermal neutron emitted into an angle of 23° will be about 1.5×10^{11} n/s^3. The epithermal neutron flux falling on an area of 50 cm^2 is about 3×10^9 n/cm^2/s. For 1% duty factor of operation, the average epithermal neutron flux on the sample becomes 3×10^7 n/cm^2/s, which is about two orders of magnitude higher than that of a linear accelerator-based epithermal neutron source.[7] The cross-section for

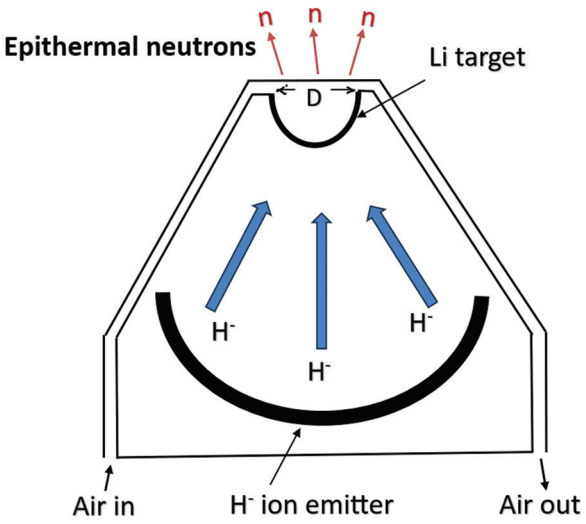

Figure 8. Schematic diagram of an epithermal neutron generator using H^- ions and a lithium target for use in neutron transmission imaging. "D" indicates the diameter of the hemispherical target. Schematic created by the author.

the ^{10}B(n,γ)^{11}B reaction is less than 1 mb for epithermal neutrons.[16] However, the cross-section for the ^{10}B(n,α)^{7}Li reaction is much higher (~10 b for epithermal neutrons[16]) and a reasonable contrast should be obtainable as the epithermal neutron beam passes through the tumor when ^{10}B is present. This new ^{10}B imaging technique needs to be studied in detail to optimize the neutron emission source size (D), the L/D parameters, and the exposure time. If it is successful, then it will be useful for analyzing the distribution of ^{10}B in the tumor before BNCT is performed.

5. Conclusion

A compact p-^{7}Li neutron tube based on thermal emission of H^- ions can provide a high flux of epithermal neutrons in pulsed mode operation. The p-^{7}Li neutron tube can be operated at 1.9 MV to generate high-flux and directional neutrons with epithermal energies. These new neutron tubes can be used in BNCT for cancer tumors in combination with IORT or fast neutron therapy. Operated

with a small-size neutron emission source, the high-flux epithermal neutron generator can be used in non-destructive neutron transmission imaging for detecting ^{10}B or other materials.

Acknowledgments

Fruitful discussions with I-Chow Hsu, Ke Sheng and staff members of the Radiation Oncology Dept., UC San Francisco are deeply acknowledged.

Funding

None.

Conflict of interest

The author declares no conflict of interest.

Author contributions

This is a single-authored article.

Ethics approval and consent to participate

Not applicable.

Consent for publication

Not applicable.

Availability of data

Not applicable.

References

1. Leung KN. Production of H- ions by thermal desorption process. *AIP Adv*. 2023;13(7):075123.

   doi: 10.1063/5.0162487

2. Leung KN. New mini neutron tubes with multiple applications. *J Nucl Eng*. 2024;5:197-208.

   doi: 10.3390/jne5030014

3. Lee CL, Zhou XL. Thick target yields for the 7Li(p,n)7be reaction near threshold. *Nucl Instrum Meth Phys Res B*. 1999;152:1-11.

4. Tanaka K, Kobayashi T, Sakurai Y, Nakagawa Y, Ishikawa M, Hoshi M. Irradiation characteristics of BNCT using near-threshold 7Li(p,n)7be direct neutrons: Application to intra-operative BNCT for malignant brain tumours. *Phys Med Biol*. 2002;47:3011-3032.

   doi: 10.1088/0031-9155/47/16/315

5. Leung KN, Leung JK, Melville G. Feasibility study on medical isotope production using a compact neutron generator. *Appl Radiat Isot*. 2018;137C:23.

   doi: 10.1016/j.apradiso.2018.02.026

6. Sauerwein WAG, Wittig A, Moss RL, Nakagawa Y, Ono K, editors. *Neutron Capture Therapy*. 2nd ed. Switzerland AG: Springer Nature; 2025.

   doi: 10.1007/978-3-031-82591-0

7. Hasemi H, Kamiyama T, Kiyanagi Y. Studies on a pulsed thermal/epithermal neutron source with a compact accelerator for neutron imaging. *Phys Proced*. 2013;43:86-91.

   doi: 10.1016/j.phpro.2013.03.011

8. Oba Y, Motokawa R, Kaneko K, *et al*. Neutron resonance absorption imaging of simulated high-level radioactive waste in borosilicate glass. *Sci Rep.* 2023;13:10071.

   doi: 10.1038/s41598-023-37157-2

9. Zimmer M, Scheuren S, Kleinschmidt A, *et al*. Demonstration of non-destructive and isotope-sensitive material analysis using a short-pulsed laser-driven epi-thermal neutron source. *Nat Commun*. 2022;13:1173.

   doi: 10.1038/s41467-022-28756-0

10. Durisi E, Zanini A, Manfredotti C, *et al*. Design of an epithermal column for BNCT based on D-D fusion neutron facility. *Nucl Instrum Methods Phys Res A*. 2007;574:363-369.

11. Kononov VN, Bokhovko MV, Kononov OE, Soloviev NA, Chu WT, Nigg D, Accelerator-based fast neutron sources for neutron therapy. *Nucl Instrum Methods Phys Res A*. 2006;564:525.

    doi: 10.1016/j.nima.2006.03.043

12. Brandao SF, Campos TPR. Intracavitary moderator balloon combined with (252)Cf brachytherapy and boron neutron capture therapy, improving dosimetry in brain tumour and infiltrations. *Br J Radiol*. 2015;88(1051):20140829.

    doi: 10.1259/bjr.20140829

13. Leung KN, Leung JK. Cancer radiotherapy with mini neutron/gamma-ray generators. *Adv Radiother Nucl Med*. 2024;2(3):3920.

    doi: 10.36922/arnm.3920

14. Leung KN. New compact neutron generator system for multiple applications. *Nucl Technol*. 2020;206:1607-1614.

    doi: 10.1080/00295450.2020.1719800

15. Kageji T, Nakagawa Y, Kumada H. Clinical results of sodium borocaptate (BSH)-based intraoperative boron neutron capture therapy (IO-BNCT). In: Sauerwein WAG, Wittig A, Moss R, Nakagawa Y, editors. *Neutron Capture Therapy*. Berlin: Springer-Heidelberg; 2012.

16. Brookhaven National Laboratory (BNL). Available from: http://www.nndc.bnl.gov

ACCSCIENCE PUBLISHING

Advances in Radiotherapy & Nuclear Medicine

MINI-REVIEW

Emerging immunotherapeutic approaches in hemophagocytic lymphohistiocytosis: A mini-review of novel targeted therapies

Vasisht Karri[1], Marcus Yoakam[1], and Samir Dalia[2]*

[1]Department of Medical Education, College of Osteopathic Medicine, Kansas City University, Joplin, Missouri, United States of America

[2]Department of Medical Oncology, Mercy Hospital, Joplin, Missouri, United States of America

Abstract

Hemophagocytic lymphohistiocytosis (HLH) and macrophage activation syndrome are life-threatening hyperinflammatory conditions marked by uncontrolled immune activation, excessive cytokine release, and pathologic hemophagocytosis, causing multi-organ dysfunction. Traditionally classified as primary (genetic) or secondary (acquired), HLH is now understood as a spectrum of overlapping mechanisms extending to therapy-related immune toxicities such as immune effector cell-associated HLH-like syndrome. Despite diagnostic advances, HLH remains associated with high morbidity and mortality, especially in malignancy-associated cases. Standard-of-care regimens—HLH-94 and HLH-2004 protocols using dexamethasone, etoposide, and cyclosporine—remain essential but are limited by toxicity, relapse, and poor applicability to secondary forms. Over the past decade, immunotherapy has transformed HLH management. Targeted cytokine blockade with emapalumab (anti-interferon gamma), anakinra (anti-interleukin [IL]-1), and tocilizumab (anti–IL-6) shows encouraging efficacy in refractory or secondary disease. Emerging macrophage-directed therapies, including anti-CD163 and experimental strategies targeting the signal regulatory protein alpha-CD47 axis, may further modulate hemophagocytosis. Translational studies also highlight the potential of Janus kinase inhibition, checkpoint blockade, and chimeric antigen receptor T-cell modulation for refractory disease. This structured review of literature (2000–2025) across PubMed, Embase, and ClinicalTrials.gov synthesizes preclinical and clinical evidence. Our analysis indicates that while biologics offer unprecedented opportunities for personalized treatment, challenges persist due to infection risk, trigger heterogeneity, and limited randomized data. Precision medicine integrating cytokine profiling, genomic sequencing, and artificial intelligence may enable individualized therapy. Overall, immunotherapy is reshaping HLH management, but its safe, effective integration demands international collaboration, well-designed trials, and sustained translational research.

Keywords: Hemophagocytic lymphohistiocytosis; Macrophage activation syndrome; Immunotherapy; Emapalumab; Anakinra; Tocilizumab; CD163; Signal regulatory protein alpha-CD47

***Corresponding author:**
Samir Dalia
(samir.dalia@mercy.net)

Citation: Karri V, Yoakam M, Dalia S. Emerging immunotherapeutic approaches in hemophagocytic lymphohistiocytosis: A mini-review of novel targeted therapies. *Adv Radiother Nucl Med*. 2026; 4(1):99-107.
doi: 10.36922/ARNM025310039

Received: August 11, 2025

Revised: September 16, 2025

Accepted: October 11, 2025

Published online: October 31, 2025

1. Introduction

Hemophagocytic lymphohistiocytosis (HLH) is a severe, life-threatening hyperinflammatory syndrome caused by aberrant activation of immune cells, leading to uncontrolled cytokine release, hemophagocytosis, cytopenia, and multi-organ damage.[1,2] Despite its rarity, HLH is increasingly recognized in both pediatric and adult populations, particularly in association with hematologic malignancies, viral infections, autoimmune conditions, and immunotherapy-related toxicities.[3] Mortality rates remain alarmingly high, often exceeding 40–50% even with standard therapy.[4]

1.1. Classification of HLH

Generally, HLH is classified as primary (familial) and secondary (acquired) HLH. Primary HLH results from genetic mutations affecting cytotoxic lymphocyte pathways, including perforin 1 (*PRF1*), UNC-13 Homolog D (*UNC13D*), syntaxin 11 (*STX11*), and syntaxin binding protein 2, leading to impaired perforin-mediated functions.[5] Secondary HLH arises in the context of infections, malignancies, autoimmune diseases, or iatrogenic triggers. Malignancy-associated HLH, particularly lymphoma-associated, is the most challenging subtype due to overlapping symptoms and underlying oncologic disease burden.[6]

Macrophage activation syndrome (MAS), a clinically similar entity, occurs predominantly in systemic juvenile idiopathic arthritis and adult-onset Still's disease, with interleukin (IL)-1 and IL-18–driven inflammation as central features.[7] The recognition of MAS within the HLH spectrum underscores the shared pathogenic mechanisms of hyperinflammation.

1.2. Clinical presentation and diagnostic criteria

Clinically, HLH manifests with persistent high-grade fever, splenomegaly, pancytopenia, liver dysfunction, coagulopathy, hyperferritinemia, and elevated soluble cluster of differentiation 25 (CD25) levels.8 The Histiocyte Society's HLH-2004 criteria remain the standard diagnostic framework, requiring five of eight features: fever, splenomegaly, cytopenia, hypertriglyceridemia and/or hypofibrinogenemia, hemophagocytosis, low/absent natural-killer-cell activity, ferritin ≥500 μg/L, and elevated soluble CD25 level.[8] Genetic confirmation may substitute for clinical criteria. Diagnostic overlap with severe sepsis, malignancy-associated macrophage activation, and cytokine release syndrome (CRS) complicates recognition, particularly in critically ill adults,[9] making early diagnosis crucial for survival.

1.3. Emerging entities: Immune effector cell-associated HLH-like syndrome (IEC-HS)

Recently, an IEC-HS has been described following chimeric antigen receptor T-cell (CAR-T) therapy and bispecific T-cell engager infusions.10 Unlike classical HLH, IEC-HS overlaps with CRS but represents a distinct hyperinflammatory complication requiring specific grading and management algorithms. IEC-HS differs from classical HLH in both etiology and clinical context. Classical HLH arises from genetic defects in cytotoxic lymphocyte function or secondary triggers such as infections, malignancy, or autoimmunity and is traditionally managed with dexamethasone and etoposide as recommended by the HLH-94/2004 protocols.[6,8] Conversely, IEC-HS is an iatrogenic hyperinflammatory state triggered by CAR-T or immune checkpoint inhibitor therapies and often overlaps with or follows CRS, presenting with hyperferritinemia, cytopenia, liver dysfunction, and coagulopathy; however, it may not fully meet HLH-2004 diagnostic criteria.[10,11] Management of IEC-HS emphasizes high-dose corticosteroids and cytokine-directed therapies, such as tocilizumab, anakinra, or ruxolitinib, with etoposide reserved for refractory cases due to toxicity concerns in heavily pretreated oncology patients. Early recognition and multidisciplinary care remain critical in both syndromes to reduce morbidity and mortality.

1.4. Pathophysiology

At the molecular level, HLH results from defective cytotoxic lymphocyte function, leading to the persistence of activated antigen-presenting cells and uncontrolled macrophage activation. This cascade triggers massive release of interferon gamma (IFN-γ), tumor necrosis factor alpha, IL-1β, IL-6, IL-18, and granulocyte-macrophage colony-stimulating factor, driving the cytokine storm and multi-organ failure.[12] Biomarkers such as soluble CD163 and IL-18 have emerged as indicators of disease activity and treatment response.[13]

2. Materials and methods

2.1. Literature search strategy

A systematic search was conducted across PubMed, Embase, and ClinicalTrials.gov for studies published between January 2000 and March 2025. The keywords used included "hemophagocytic lymphohistiocytosis," "macrophage activation syndrome," "cytokine storm," "emapalumab," "anakinra," "tocilizumab," "CD163," and "SIRPα-CD47."

2.2. Eligibility criteria

Studies were included if they:
(i) Investigated HLH, MAS, or HLH-like syndromes in humans or animal models
(ii) Reported therapeutic strategies, with emphasis on immunotherapy
(iii) Were peer-reviewed clinical trials, case reports, observational studies, or pre-clinical mechanistic research.

Exclusion criteria included non-English publications, abstracts without full text, conference posters without peer-reviewed publication, and studies unrelated to therapeutic strategies.

2.3. Data extraction and synthesis

Two authors independently screened and extracted data on the patient population, therapeutic intervention, outcomes, and adverse effects. Data were synthesized into thematic categories: (i) standard therapies, (ii) cytokine-targeted therapies, (iii) macrophage-directed therapies, and (iv) novel/emerging hypotheses.

2.4. Statistical considerations

Risk of bias was qualitatively assessed using the Newcastle–Ottawa scale for observational studies and the Cochrane risk-of-bias tool for randomized trials. Case reports and small cohorts were included for completeness, but the results were interpreted cautiously.

2.5. Thematic categorization

Therapeutic strategies were categorized into four domains:
(i) Standard therapy (HLH-94/HLH-2004 protocols)
(ii) Cytokine-directed immunotherapy (IFN-γ, IL-1, IL-6 blockade)
(iii) Macrophage-directed therapy (anti-CD163)
(iv) Emerging hypotheses (signal regulatory protein alpha [SIRPα]-CD47, Janus kinase [JAK] inhibitors, checkpoint blockade, CAR-T modulation, and radiotherapy).

3. Results

3.1. Standard therapies in HLH

The HLH-94 protocol, introduced in the 1990s, remains foundational, consisting of dexamethasone, etoposide, and cyclosporine, followed by hematopoietic stem cell transplantation (HSCT) for definitive cure in familial cases.[14] The updated HLH-2004 protocol refined supportive care and diagnostic criteria.8 While lifesaving, these regimens are associated with significant toxicity, particularly in adults with comorbidities.[5] Mortality remains 30–40% in pediatric cohorts and even higher in adult populations.[4]

3.2. Cytokine-directed immunotherapy

3.2.1. Emapalumab (anti–IFN-γ)

The IFN-γ protein plays a central role in macrophage activation and cytokine storm propagation.2 Emapalumab, a monoclonal antibody neutralizing IFN-γ, was Food and Drug Administration (FDA)-approved in 2018 for refractory primary HLH. In a pivotal Phase II/III trial, emapalumab induced responses in 63% of patients, enabling 65% to proceed to HSCT.[15] Long-term follow-up demonstrated sustained disease control but highlighted a high rate of opportunistic infections.[16] In addition, a Phase III trial, NCT05001737, evaluating emapalumab in HLH/MAS associated with rheumatologic conditions, was recently accepted as a priority review by the FDA.[17] Pooled analysis data of 39 patients from two open-label, single-arm interventional studies—the Phase II NI-0501-06 study (NCT03311854) and the Phase III EMERALD trial (NCT05001737)—demonstrated that 85% of patients (n = 33) achieved a complete response (defined as the resolution of clinical signs and symptoms present at baseline and the normalization of laboratory parameters relevant to MAS) at any time during the studies.[18]

3.2.2. Anakinra (anti–IL-1)

The IL-1 protein is particularly implicated in MAS and autoimmune-triggered HLH.[7] Anakinra, an IL-1 receptor antagonist, has shown efficacy in systemic juvenile idiopathic arthritis-associated MAS19 and adult Still's disease.[20] Retrospective studies suggest that high-dose anakinra improves survival and reduces steroid dependence in refractory HLH.21 Its use has expanded during the COVID-19 pandemic to treat HLH-like hyperinflammation.[22]

3.2.3. Tocilizumab (anti–IL-6)

The IL-6 protein drives systemic inflammation in both HLH and CRS. Tocilizumab, an IL-6 receptor blocker, has been widely used in CAR-T-associated CRS and extrapolated to HLH. Case reports and small cohorts suggest benefit in malignancy-associated HLH, particularly when combined with corticosteroids.[23,24]

3.2.4. NCT03113760, NCT02780583 (IL-1, IL-18)

Genetic inflammasomopathies (*XIAP* or *NLRC4* mutations) predispose patients to HLH. Trials are testing recombinant IL-18 binding protein (tadekinig α) in these patients (NCT03113760) and IL-1 receptor antagonist (anakinra) in HLH/MAS associated with juvenile idiopathic arthritis (NCT02780583), representing precision approaches targeting specific inflammatory pathways.[25-27]

3.3. Macrophage-directed therapies

3.3.1. Anti-CD163

The CD163 protein is a scavenger receptor expressed on activated macrophages. Soluble CD163 correlates with disease severity and mortality.[13] Pre-clinical studies of anti-CD163 antibody-drug conjugates demonstrated selective depletion of activated macrophages and reversal of hyperinflammation.[28,29] While not yet in clinical trials, CD163 represents a promising macrophage-specific therapeutic target.

3.4. Emerging hypotheses and experimental therapies

3.4.1. SIRPα-CD47 axis blockade

Macrophage phagocytosis is regulated by the CD47-SIRPα "don't eat me" signal. Dysregulation may contribute to inappropriate hemophagocytosis in HLH. Pre-clinical oncology studies showed that blocking this axis not only enhances antitumor immunity but also protects normal hematopoietic cells from phagocytosis.[30-32] Its application in HLH remains hypothetical but conceptually attractive.

3.4.2. JAK inhibitors

Hypercytokinemia in HLH is mediated through the JAK-STAT signaling. Case reports of ruxolitinib, a JAK1/2 inhibitor, described a rapid resolution of fever and ferritin elevation in refractory HLH.[33] A single-center, Phase II trial evaluating ruxolitinib with dexamethasone in newly diagnosed adult HLH reported a 2-month overall survival of 83.3–85.7% and an overall response rate of 85.7% (complete response 17.9%). Mortality was primarily driven by underlying lymphoma, with no deaths directly attributable to HLH. The regimen was well tolerated, and lymphoma-associated HLH patients were successfully bridged to chemotherapy. In addition, an ongoing, two-arm, non-randomized trial (NCT04551131) is investigating a combination of ruxolitinib with etoposide and dexamethasone for both newly diagnosed and relapsed/refractory HLH.[35] Primary goals of this trial include assessing efficacy, tolerability, response rates, and immunologic biomarker correlations contributing to the evolution of frontline therapy and bridging approaches.[34,35]

3.4.3. Checkpoint inhibitors and CAR-T modulation

Checkpoint inhibitors, such as nivolumab (anti-programmed cell death protein 1) and ipilimumab (anti-cytotoxic T-lymphocyte-associated protein 4 [CTLA-4]), have paradoxical roles in HLH: they may exacerbate immune activation while also rebalancing tolerance in malignancy-associated HLH.10 NCT02472054 and NCT 02385110 have investigated the use of alemtuzumab (anti-CD52) in primary and malignancy-associated HLH.25,36 Retrospective data in 22 refractory HLH patients showed a partial response in two-thirds, with 77% surviving to HSCT. The therapy carries profound immunosuppressive risk but is being actively evaluated in primary HLH and in combination with conventional agents for malignancy-associated HLH. Similarly, CAR-T therapy can trigger HLH-like syndromes but may also eradicate the underlying malignancy fueling HLH. Fine-tuned immunomodulation remains experimental.

3.4.4. Radiotherapy

At present, there are no ongoing trials investigating the use of radiotherapy in the treatment of HLH. A case report in 2005 detailed the use of radiotherapy with corticosteroid therapy to treat a suspected isolated central nervous system (CNS) HLH in a 5-year-old girl who was diagnosed after a 2-month history of right hemiparesis.[37] The treatment led to complete resolution of CNS lesions; however, the remission was transitory and only lasted 3 months. The patient died secondary to the refractory progression of the CNS lesion. Although discouraging, this case underscores the need to continue investigating novel modalities to treat HLH.

4. Discussion

The therapeutic landscape of HLH is undergoing a profound shift as immunotherapy emerges as a cornerstone strategy. Historically, treatment has relied heavily on the HLH-94 and HLH-2004 protocols, which combined corticosteroids, etoposide, and cyclosporine with the intent of dampening immune hyperactivation and bridging patients toward HSCT.[8,14] While these regimens remain lifesaving, their efficacy is limited in adults and in cases of secondary or malignancy-associated HLH, where overlapping disease processes complicate management.[4,5] The high toxicity of etoposide-based regimens and the frequent relapses following initial remission underscore the need for new therapeutic approaches that target the underlying immunopathology more precisely.

In recent years, cytokine-directed therapies have transformed our conceptual framework for treating HLH. The approval of emapalumab, an IFN-γ–neutralizing antibody, represented the first targeted biologic therapy designed specifically for HLH.15 By directly interrupting one of the central drivers of macrophage activation, emapalumab has demonstrated the ability to induce remission and improve transplant eligibility in refractory primary HLH.[16] Similarly, anakinra, an IL-1 receptor antagonist, has shown remarkable success in MAS associated with systemic juvenile idiopathic arthritis and adult-onset Still's

disease.[19,20] High-dose intravenous anakinra has also been effective in HLH-like hyperinflammatory states, including severe COVID-19, broadening its utility in secondary HLH.[21,22] Tocilizumab, an IL-6 receptor antagonist widely used in CRS, has been extrapolated to HLH, where it can alleviate systemic inflammation and organ dysfunction in select cases.[23,24] Collectively, these cytokine inhibitors highlight the potential of precise immunomodulation in mitigating the catastrophic cytokine storm of HLH.

Beyond cytokine blockade, macrophage-directed therapies represent an exciting frontier. CD163, a hemoglobin scavenger receptor expressed on activated macrophages, has emerged as both a biomarker and therapeutic target.[13] Pre-clinical studies with CD163-targeted antibody-drug conjugates have demonstrated selective depletion of pathogenic macrophages, suggesting that direct cellular targeting may complement or surpass cytokine blockade.[28,29] The SIRPα-CD47 checkpoint axis, which governs phagocytosis by transmitting a "don't eat me" signal, represents another innovative approach. While originally investigated in oncology, the blockade of this pathway may theoretically suppress inappropriate hemophagocytosis in HLH while preserving hematopoiesis.[30-32] Although these concepts remain investigational, they underscore the expanding scope of macrophage-specific therapies in HLH.

Despite these advances, translating HLH treatments into routine practice remains challenging. The most immediate concern is the risk of profound immunosuppression due to cytokine blockade and broad anti-inflammatory agents. Inhibition of key inflammatory cytokines, such as IFN-γ and IL-6, dramatically increases susceptibility to severe opportunistic and reactivation bacterial, fungal, and viral infections, thereby complicating therapy.[15] This necessitates prophylactic antimicrobial strategies, vigilant monitoring, and the integration of infectious disease expertise into HLH management. These safety concerns compound additional barriers. HLH's rarity and heterogeneity render randomized controlled trials logistically challenging and often unfeasible.[3] Much of the evidence base for novel agents relies on small retrospective cohorts or case series, which, while valuable, limit the generalizability of findings. Multi-institutional collaboration, adaptive trial designs, and international registries are therefore essential to advance the field.[6,9] Given the high risk of infection, discussions of using these novel immune therapies should include strategies based on regulatory guidance, such as HLH and CRS management literature. Table 1 presents the evidence-informed prophylactic monitoring strategies to aid clinicians and researchers in mitigating infectious risks during cytokine-targeted or broad immunosuppressive HLH therapies.

Personalized and precision medicine represent the future of HLH treatment, shifting the framework of treatment from broad immunosuppression to precision therapies guided by individual patient profiles. Cytokine profiling and transcriptomic analyses may facilitate the stratification of patients into distinct inflammatory phenotypes, such as IFN-γ–dominant versus IL-18–dominant subsets, guiding rational selection of biologics.[43,44] In addition, combination regimens targeting multiple cytokines synergistically, such as emapalumab with ruxolitinib or anakinra with tocilizumab, represent another promising avenue, though balancing efficacy with cumulative immunosuppression remains critical.[21,45,46] The development and validation of biomarkers associated with HLH show promise in

Table 1. Prophylactic monitoring strategies to reduce the risk of infection in immunosuppressive hemophagocytic lymphohistiocytosis treatments

Domain	Recommended action
Baseline screening	Emapalumab/FDA-approved materials and JAK inhibitor labels require TB/HBV screening and caution.[38,39]
Antimicrobial prophylaxis	Consider PJP prophylaxis (TMP-SMX) for patients on high-dose steroids, prolonged lymphopenia, or combination immunosuppression; HSV/VZV prophylaxis (acyclovir/valacyclovir) for seropositive patients or those on JAK inhibitors.[40]
Viral reactivation surveillance	Twice-weekly to weekly EBV and CMV PCR during induction/early therapy, then spacing per stability; PCR triggered by fevers or cytopenias.[41]
Clinical and lab monitoring	Daily to twice-weekly CBC, CRP/ESR, ferritin, transaminases, triglycerides, and coagulation during induction; culture work-up for new fevers; low threshold for chest imaging/CTs if pulmonary symptoms.[42]
Vaccination and prevention	Update inactivated vaccines before immunosuppression when possible; avoid live vaccines while on biologics/JAK inhibitors and for defined periods after therapy per Infectious Disease Physician guidance.[40]
Infectious disease involvement	Infectious disease consultation before initiating certain agents (emapalumab, prolonged ruxolitinib, or combined modalities). Pre-planned criteria for stopping/withholding therapy for uncontrolled infection.[40]

Abbreviations: CBC: Complete blood count; CMV: Cytomegalovirus; CRP: C-reactive protein; CT: Computed tomography; EBV: Epstein–Barr Virus; ESR: Erythrocyte Sedimentation rate; FDA: Food and Drug Administration; HBV: Hepatitis B virus; HSV: Herpes simplex virus; JAK: Janus kinase; PCR: Polymerase chain reaction; PJP: Pneumocystis jirovecii pneumonia; TB: Tuberculosis; TMP-SMX: Trimethoprim-Sulfamethoxazole; VZV: Varicella-Zoster Virus.

ensuring early diagnosis, patient stratification, and real-time monitoring of treatment. Recently, a study investigating HLH following CAR-T therapy identified early cytokine changes, specifically spikes in IL-2R, CD80, CTLA-4, and IL-33R, that were absent in controls but pronounced in HLH cases, highlighting their potential as diagnostic biomarkers.[47] Advances in artificial intelligence and machine learning may further accelerate patient stratification by integrating complex clinical and molecular data to predict treatment responses and optimize therapy. Collectively, these strategies highlight the potential of personalized medicine to deliver safer, more tailored HLH therapies.

Finally, HLH increasingly occupies an important intersection with modern immuno-oncology. CAR-T therapy, checkpoint blockade, and bispecific antibodies can all induce HLH-like toxicities such as IEC-HS, challenging clinicians to differentiate between overlapping syndromes and tailor treatment accordingly.[10] The recognition of IEC-HS underscores the need for flexible diagnostic frameworks and therapeutic algorithms that can adapt to emerging contexts.

In summary, HLH treatment is rapidly evolving from broad, toxic immunosuppression to targeted immunotherapy. While biologics such as emapalumab, anakinra, and tocilizumab represent important advances, future therapies will likely integrate macrophage-directed strategies, checkpoint modulation, and precision medicine tools. The central challenge remains balancing efficacy against infection risk, all within the constraints of a rare and heterogeneous disease. By leveraging global collaboration, adaptive trials, and translational research, the promise of personalized, immunologically tailored HLH therapy is within reach.

5. Conclusion

HLH and MAS represent catastrophic hyperinflammatory conditions requiring urgent recognition and treatment. While historical regimens remain foundational, they are insufficient in refractory or secondary cases. The development of cytokine-targeted therapies (e.g., emapalumab, anakinra, and tocilizumab) and preclinical, hypothetical macrophage-focused strategies (e.g., anti-CD163 and SIRPα-CD47 blockade) signal a paradigm shift in treatment. Adjunctive approaches, including JAK inhibition, checkpoint modulation, and radiotherapy in selected malignancy-associated cases, further broaden therapeutic options. Future directions must prioritize precision, personalization, and global collaboration. Integrating cytokine profiling, genomic sequencing, and artificial intelligence will allow the stratification of patients for targeted therapy. Currently, studies on multiplex cytokine profiling have investigated its ability to enhance diagnostic accuracy, aid subtype classification, and even inform prognosis in both adult and pediatric HLH. For example, a retrospective study of 166 adults with confirmed HLH and 142 febrile controls used multiplex liquid-phase microarray assays to measure 33 cytokines, demonstrating excellent diagnostic performance with a combined cytokine panel.48 Similarly, a pediatric study conducted at Beijing Children's Hospital between 2017 and 2021 enrolled 101 newly diagnosed HLH patients and assessed 34 cytokines, identifying distinct cytokine patterns across HLH subtypes and correlations with prognosis.49 While larger, confirmatory studies are ongoing, these findings highlight the translational utility of cytokine-based biomarkers for diagnosis and risk stratification. In addition, genetic profiling approaches, including targeted gene panels and whole-exome sequencing, remain essential for distinguishing primary from secondary HLH, reinforcing the complementary role of immunogenetic and cytokine-based diagnostics in guiding patient management. International trial networks and adaptive study designs are essential to generate robust evidence. In summary, HLH treatment is transitioning from broad immunosuppression to tailored immunotherapy. This shift offers the potential to transform outcomes, provided that risks of infection, cost, and feasibility are carefully managed through multidisciplinary, collaborative care.

Acknowledgments

None.

Funding

None.

Conflict of interest

The authors declare that they have no competing interests.

Author contributions

Conceptualization: Vasisht Karri, Marcus Yoakam
Writing–original draft: Vasisht Karri, Marcus Yoakam
Writing–review & editing: All authors

Ethics approval and consent to participate

Not applicable.

Consent for publication

Not applicable.

Availability of data

Not applicable.

References

1. Janka GE, Lehmberg K. Hemophagocytic lymphohistiocytosis: Pathogenesis and treatment. *Hematology*. 2013;2013(1):605-611.

   doi: 10.1182/asheducation-2013.1.605

2. Jordan MB, Hildeman D, Kappler J, Marrack P. An animal model of hemophagocytic lymphohistiocytosis (HLH): CD8+ T cells and interferon gamma are essential for the disorder. *Blood*. 2004;104(3):735-743.

   doi: 10.1182/blood-2003-10-3413

3. Hayden A, Park S, Giustini D, Lee AY, Chen LY. Hemophagocytic syndromes (HPSs) including hemophagocytic lymphohistiocytosis (HLH) in adults: A systematic scoping review. *Blood Rev*. 2016;30(6):411-420.

   doi: 10.1016/j.blre.2016.05.001

4. Ramos-Casals M, Brito-Zerón P, López-Guillermo A, Khamashta MA, Bosch X. Adult haemophagocytic syndrome. *Lancet*. 2014;383(9927):1503-1516.

   doi: 10.1016/S0140-6736(13)61048-X

5. Janka G. Hemophagocytic lymphohistiocytosis: When the immune system runs amok. *Klin Padiatr*. 2009;221(5): 278-285.

   doi: 10.1055/s-0029-1237386

6. La Rosée P, Horne A, Hines M, *et al*. Recommendations for the management of hemophagocytic lymphohistiocytosis in adults. *Blood*. 2019;133(23):2465-2477.

   doi: 10.1182/blood.2018894618

7. Grom AA, Mellins ED. Macrophage activation syndrome: Advances towards understanding pathogenesis. Curr Opin Rheumatol. 2010;22(5):561-566.

   doi: 10.1097/01.bor.0000381996.69261.71

8. Henter J, Horne A, Aricó M, *et al*. HLH-2004: Diagnostic and therapeutic guidelines for hemophagocytic lymphohistiocytosis. *Pediatr Blood Cancer*. 2007;48(2):124-131.

   doi: 10.1002/pbc.21039

9. Zoref-Lorenz A, Ellis M, Jordan MB. Inpatient recognition and management of HLH. *Hematology Am Soc Hematol Educ Program*. 2023;2023(1):259-266.

   doi: 10.1182/hematology.2023000509

10. Hines MR, Knight TE, McNerney KO, *et al*. Immune effector cell-associated hemophagocytic lymphohistiocytosis-like syndrome. *Transplant Cell Ther*. 2023;29(7):438.e1-438.e16.

    doi: 10.1016/j.jtct.2023.03.006

11. Diaz L, Jauzelon B, Dillies AC, *et al*. Hemophagocytic lymphohistiocytosis associated with immunological checkpoint inhibitors: A pharmacovigilance study. *J Clin Med*. 2023;12(5):1985.

    doi: 10.3390/jcm12051985

12. Brisse E, Wouters CH, Matthys P. Advances in the pathogenesis of primary and secondary haemophagocytic lymphohistiocytosis: Differences and similarities. *Br J Haematol*. 2016;174(2):203-217.

    doi: 10.1111/bjh.14147

13. Büll C, Heise T, Adema GJ, Boltje TJ. Sialic acid mimetics to target the sialic acid-siglec axis. *Trends Biochem Sci*. 2016;41(6):519-531.

    doi: 10.1016/j.tibs.2016.03.007

14. Henter JI, Samuelsson-Horne A, Aricò M, *et al*. Treatment of hemophagocytic lymphohistiocytosis with HLH-94 immunochemotherapy and bone marrow transplantation. *Blood*. 2002;100(7):2367-2373.

    doi: 10.1182/blood-2002-01-0172

15. Locatelli F, Jordan MB, Allen C, *et al*. Emapalumab in children with primary hemophagocytic lymphohistiocytosis. N Engl J Med. 2020;382(19):1811-1822.

    doi: 10.1056/NEJMoa1911326

16. Chandrakasan S, Jordan MB, Baker A, *et al*. Real-world treatment patterns and outcomes in patients with primary hemophagocytic lymphohistiocytosis treated with emapalumab. *Blood Adv*. 2024;8(9):2248-2258.

    doi: 10.1182/bloodadvances.2023012217

17. Swedish Orphan Biovitrum. *A Two-Cohort, Open-Label, Single Arm, Multicenter Study to Evaluate Efficacy, Safety and Tolerability, PK and PD, of Emapalumab in Children and Adults With MAS in Still's Disease or With MAS in Systemic Lupus Erythematous*; 2025. Available from: https://www.co/clinicaltrials.gov/study/nct05001737 [Last accessed on 2025 Sep 06].

18. Ernst D, *RPh. Emapalumab Gets Priority Review for HLH/MAS in Still Disease*. Rheumatology Advisor; 2025. Available from: https://www.rheumatologyadvisor.com/news/emapalumab/gets-priority-review-for-hlh-mas-in-still-disease [Last accessed on 2025 Sep 06].

19. Quartier P, Allantaz F, Cimaz R, *et al*. A multicentre, randomised, double-blind, placebo-controlled trial with the interleukin-1 receptor antagonist anakinra in patients with systemic-onset juvenile idiopathic arthritis (ANAJIS trial). Ann Rheum Dis. 2011;70(5):747-754.

    doi: 10.1136/ard.2010.134254

20. Minoia F, Davì S, Horne A, *et al*. Clinical features, treatment, and outcome of macrophage activation syndrome complicating systemic juvenile idiopathic arthritis: A multinational, multicenter study of 362 patients. Arthritis Rheumatol. 2014;66(11):3160-3169.

    doi: 10.1002/art.38802

21. Mehta P, Cron RQ, Hartwell J, Manson JJ, Tattersall RS.

Silencing the cytokine storm: the use of intravenous anakinra in haemophagocytic lymphohistiocytosis or macrophage activation syndrome. *Lancet Rheumatol*. 2020;2(6):e358-e367.

doi: 10.1016/S2665-9913(20)30096-5

22. Cavalli G, De Luca G, Campochiaro C, *et al*. Interleukin-1 blockade with high-dose anakinra in patients with COVID-19, acute respiratory distress syndrome, and hyperinflammation: A retrospective cohort study. *Lancet Rheumatol*. 2020;2(6):e325-e331.

doi: 10.1016/S2665-9913(20)30127-2

23. Herman M, Lee A, Fawcett S, Deodhare S. A case report of immune checkpoint-related hemophagocytic lymphohistiocytosis and review of the literature. Case Rep Oncol. 2024;17(1):809-817.

doi: 10.1159/000539955

24. Walmsley CS, Schoepflin Z, De Brabandt C, Rangachari D, Berwick S, Patell R. Hemophagocytic lymphohistiocytosis associated with immune checkpoint inhibitor use: A review of the current knowledge and future directions. Blood Cells Mol Dis. 2025;110:102896.

doi: 10.1016/j.bcmd.2024.102896

25. Jordan MB. Emergence of targeted therapy for hemophagocytic lymphohistiocytosis. *Hematology Am Soc Hematol Educ Program*. 2018;15(2):481-489.

doi: 10.1182/hem.V15.2.8257

26. Eloseily EM, Weiser P, Crayne CB, *et al*. Benefit of anakinra in treating pediatric secondary hemophagocytic lymphohistiocytosis. *Arthritis Rheumatol*. 2020;72(2):326-334.

doi: 10.1002/art.41103

27. AB2 Bio Ltd. *Multicenter, Double-Blind, Placebo-Controlled, Randomized Withdrawal Trial With Tadekinig Alfa (r-hIL-18BP) in Patients With IL-18 Driven Monogenic Autoinflammatory Conditions: NLRC4 Mutation and XIAP Deficiency*; 2025. Available from: https://clinicaltrials.gov/study/nct03113760 [Last accessed on 2025 Sep 06].

28. Etzerodt A, Moulin M, Doktor TK, *et al*. Tissue-resident macrophages in omentum promote metastatic spread of ovarian cancer. J Exp Med. 2020;217(4):e20191869.

doi: 10.1084/jem.20191869

29. Skytthe MK, Graversen JH, Moestrup SK. Targeting of CD163+ macrophages in inflammatory and malignant diseases. Int J Mol Sci. 2020;21(15):5497.

doi: 10.3390/ijms21155497

30. Barclay AN, Van Den Berg TK. The interaction between signal regulatory protein alpha (SIRPα) and CD47: Structure, function, and therapeutic target. Annu Rev Immunol. 2014;32(1):25-50.

doi: 10.1146/annurev-immunol-032713-120142

31. Weiskopf K, Jahchan NS, Schnorr PJ, *et al*. CD47-blocking immunotherapies stimulate macrophage-mediated destruction of small-cell lung cancer. *J Clin Invest*. 2016;126(7):2610-2620.

doi: 10.1172/JCI81603

32. Liu J, Wang L, Zhao F, *et al*. Pre-clinical development of a humanized anti-CD47 antibody with anti-cancer therapeutic potential. *PLoS One*. 2015;10(9):e0137345.

doi: 10.1371/journal.pone.0137345

33. Wang J, Wang Y, Wu L, *et al*. Ruxolitinib for refractory/relapsed hemophagocytic lymphohistiocytosis. *Haematologica*. 2020;105(5):e210-e212.

doi: 10.3324/haematol.2019.222471

34. Zhou D, Huang X, Zhu L, *et al*. Ruxolitinib combined with dexamethasone for adult patients with newly diagnosed hemophagocytic lymphohistiocytosis in China. *Blood*. 2025;146(3):318-327.

doi: 10.1182/blood.2024026139

35. St. Jude Childrens Research Hospital. *Use Of A Response-Adapted Ruxolitinib-Containing Regimen For The Treatment Of Hemophagocytic Lymphohistiocytosis*; 2025. Available from: https://clinicaltrials.gov/study/nct04551131 [Last accessed on 2025 Sep 06].

36. Marsh RA, Allen CE, McClain KL, *et al*. Salvage therapy of refractory hemophagocytic lymphohistiocytosis with alemtuzumab. *Pediatr Blood Cancer*. 2013;60(1):101-109.

doi: 10.1002/pbc.24188

37. Shinoda J, Murase S, Takenaka K, Sakai N. Isolated central nervous system hemophagocytic lymphohistiocytosis: Case report. *Neurosurgery*. 2005;56(1):187.

38. Haag C, Alexis A, Aoki V, *et al*. A practical guide to using oral Janus kinase inhibitors for atopic dermatitis from the international eczema council. Br J Dermatol. 2024;192(1):135-143.

doi: 10.1093/bjd/ljae342

39. Cheloff AZ, Al-Samkari H. Emapalumab for the treatment of hemophagocytic lymphohistiocytosis. *Drugs Today (Barc)*. 2020;56(7):439-446.

doi: 10.1358/dot.2020.56.7.3145359

40. Kordzadeh-Kermani E, Khalili H, Karimzadeh I, Salehi M. Prevention strategies to minimize the infection risk associated with biologic and targeted immunomodulators. *Infect Drug Resist*. 2020;13:513-532.

doi: 10.2147/IDR.S233137

41. Ayuketang FA, Jäger U. *Management of Cytokine Release Syndrome (CRS) and HLH*. In: Kröger N, Gribben J, Chabannon C, Yakoub-Agha I, Einsele H, editors. *The EBMT/EHA CAR-T Cell Handbook*. Springer; 2022. Available from: https://www.ncbi.nlm.nih.gov/books/

nbk584171 [Last accessed on 2025 Sep 06].

42. Carter M. *GIRFT Leads Cross-Specialty Clinical Group to Develop Best Practice Pathway for the Rare Syndrome HLH. Getting It Right First Time GIRFT*; 2024. Available from: https://gettingitrightfirsttime.co.uk/girft-leads-cross-specialty-clinical-group-to-develop-best-practice-pathway-for-the-rare-syndrome-hlh [Last accessed on 2025 Sep 06].

43. Landy E, Carol H, Ring A, Canna S. Biological and clinical roles of IL-18 in inflammatory diseases. *Nat Rev Rheumatol*. 2024;20(1):33-47.

doi: 10.1038/s41584-023-01053-w

44. Norsker FN, Pedersen C, Armstrong GT, *et al*. Late effects in childhood cancer survivors: Early studies, survivor cohorts, and significant contributions to the field of late effects. *Pediatr Clin North Am*. 2020;67(6):1033-1049.

doi: 10.1016/j.pcl.2020.07.002

45. Wu Y, Sun X, Kang K, *et al*. Hemophagocytic lymphohistiocytosis: Current treatment advances, emerging targeted therapy and underlying mechanisms. *J Hematol Oncol*. 2024;17(1):106.

doi: 10.1186/s13045-024-01621-x

46. Johnson WT, Epstein-Peterson ZD, Ganesan N, *et al*. Emapalumab as salvage therapy for adults with malignancy-associated hemophagocytic lymphohistiocytosis. *Haematologica*. 2024;109:2998-3003.

doi: 10.3324/haematol.2023.284179

47. Campodonico E, Angelillo P, Doglio M, *et al*. Biomarkers for an early diagnosis of immune effector cell associated-hemophagocytic syndrome. *Front Immunol*. 2025;16:1635062.

doi: 10.3389/fimmu.2025.1635062

48. Jin Z, Suolitiken D, Wang Y, Wang Z. The diagnostic importance of multiple cytokines in adult hemophagocytic lymphohistiocytosis. *J Clin Lab Anal*. 2023;37(6):e24669.

doi: 10.1002/jcla.24669

49. Ou W, Zhao Y, Wei A, *et al*. Serum cytokine pattern in children with hemophagocytic lymphohistiocytosis. *Ann Hematol*. 2023;102(4):729-739.

doi: 10.1007/s00277-02AGE3

ACCSCIENCE PUBLISHING

Advances in Radiotherapy & Nuclear Medicine

LETTER TO EDITOR

Defining the optimal local treatment approach in stage III non-small cell lung cancer: Surgery versus concurrent chemoradiation after induction chemoimmunotherapy

Melek Yakar*

Department of Radiation Oncology, Faculty of Medicine, Eskişehir Osmangazi University, Eskişehir, Turkey

(This article belongs to the *Special Issue: Advances in Chemoradiotherapy in the Era of Precision Medicine*)

Dear Editor,

The optimal local treatment approach for locally advanced non-small cell lung cancer (NSCLC) is a controversial issue. Concurrent chemoradiotherapy (CRT) followed by consolidation with immunotherapy is currently the standard of care for this patient group. However, recent studies on the perioperative use of immunotherapy have demonstrated that adding immunotherapy to treatment improves oncological outcomes.

The PACIFIC trial was a key study in establishing immunotherapy as the standard of care for stage III lung cancer. Its 5-year results demonstrated the superiority of immunotherapy in both overall survival and progression-free survival, and this approach has become the standard approach.[1]

Recently initiated phase III trials, such as CheckMate-73L and PACIFIC-2, are investigating the use of immunotherapy with CRT. These studies investigated the role of immunotherapy not only in the consolidation phase but also in the concurrent phase of treatment. In both studies, with a median follow-up of 30.5 months, the addition of concurrent immunotherapy to CRT did not alter survival outcomes.[2,3]

The AEGEAN phase III randomized trial evaluated perioperative durvalumab + neoadjuvant chemotherapy versus perioperative placebo + neoadjuvant chemotherapy, followed by surgery, in patients with stage II and IIIB disease. The addition of perioperative durvalumab was associated with higher event-free survival and pathological complete response, with no difference in toxicity between the two arms.[4] In the phase III CheckMate-77T trial, patients with resectable stage IIA–IIIB disease were randomized to receive perioperative nivolumab + neoadjuvant chemotherapy versus perioperative placebo plus neoadjuvant chemotherapy, followed by surgery. Perioperative nivolumab provided significantly longer event-free survival and significantly increased pathologic response rates compared to chemotherapy alone in resectable NSCLC.[5] In the CheckMate-816 study, patients with resectable stage IB–IIIA disease received nivolumab plus three cycles of chemotherapy versus chemotherapy alone, followed by surgery. At a median follow-up of 43.8 months, event-free survival, overall survival, and pathologic complete response were found to be higher in the immunotherapy arm.[6]

Despite the favorable outcomes of perioperative immunotherapy and surgery, concurrent CRT followed by durvalumab consolidation remains the standard approach, particularly in patients with extensive mediastinal involvement or those unsuitable for surgery.

***Corresponding author:**
Melek Yakar
(myakar@ogu.edu.tr)

Citation: Yakar M. Defining the optimal local treatment approach in stage III non-small cell lung cancer: Surgery versus concurrent chemoradiation after induction chemoimmunotherapy. *Adv Radiother Nucl Med*. 2026; 4(1):108-109.
doi: 10.36922/ARNM025400052

Received: October 1, 2025

Accepted: November 3, 2025

Published online: November 17, 2025

Long-term overall survival data, biomarker-based patient selection, and the balance between surgical morbidity and immune-related toxicities remain unanswered questions.

Results from ongoing phase III trials will further clarify which patient subgroups derive greater benefit from surgery plus immunotherapy versus those who may be better suited for CRT plus immunotherapy. Randomized trials are evaluating surgery after immunotherapy and chemotherapy. There are no prospective phase III studies evaluating randomized CRT with surgery after immunotherapy and chemotherapy. Therefore, it would be inappropriate to dismiss CRT so easily in patients initiated with perioperative immunotherapy. In light of these uncertainties, the role of multidisciplinary tumor boards in personalized treatment selection is critical.

In summary, while numerous phase III trials evaluating perioperative immunotherapy plus surgery after neoadjuvant chemotherapy have yielded promising results, all randomized trials published to date have focused only on surgery after immunotherapy plus chemotherapy. To my knowledge, there are no prospective phase III trials directly comparing surgery with definitive CRT after induction immunotherapy and chemotherapy. Therefore, it is premature to assume universal superiority of surgery. In contrast, CRT plus durvalumab consolidation, demonstrated by the PACIFIC trial and demonstrating a long-term survival advantage, remains a strong standard, particularly in patients with extensive mediastinal disease or those not suitable for surgery. Future research should determine whether CRT after induction of immunotherapy and chemotherapy can provide similar or even superior outcomes to surgery in selected patient groups. Until then, multidisciplinary tumor boards remain essential for guiding personalized treatment decisions, considering the risk-benefit balance between surgery and chemotherapy.

Conflict of interest

The author declares no conflict of interest.

References

1. Spigel DR, Faivre-Finn C, Gray JE, *et al*. Five-year survival outcomes from the PACIFIC trial: Durvalumab after chemoradiotherapy in stage III non-small-cell lung cancer. *J Clin Oncol.* 2022;40(12):1301-1311.

   doi:10.1200/JCO.21.01308. Erratum in: *J Clin Oncol.* 2022;40(17):1965.

   doi: 10.1200/JCO.22.01023

2. Peters S, Tan DS, Gerber DE, *et al*. CheckMate 73L: Phase III study comparing nivolumab plus concurrent chemoradiotherapy followed by nivolumab ± ipilimumab versus chemoradiotherapy followed by durvalumab for previously untreated, locally advanced stage III NSCLC. *Immuno Oncol Technol.* 2024;24:100808.

   doi: 10.1016/j.iotech.2024.100808

3. Bradley JD, Sugawara S, Lee KH, *et al*. Durvalumab in combination with chemoradiotherapy for patients with unresectable stage III NSCLC: Final results from PACIFIC-2. *ESMO Open*. 2024;9:102986.

   doi: 10.1016/j.esmoop.2024.102986

4. Heymach JV, Harpole D, Mitsudomi T, *et al*. Perioperative durvalumab for resectable non-small-cell lung cancer. *N Engl J Med.* 2023;389(18):1672-1684.

   doi: 10.1056/NEJMoa2304875

5. Cascone T, Spicer JD, Pulla MP. Perioperative nivolumab in resectable lung cancer. Reply. *N Engl J Med.* 2024;391(6): 573-574.

   doi: 10.1056/NEJMc2407267

6. Forde PM, Spicer J, Provencio M, *et al*. Overall Survival with Neoadjuvant Nivolumab plus Chemotherapy in Lung Cancer. *N Engl J Med.* 2025;393(8):741-752.

   doi: 10.1056/NEJMoa2502931

https://accscience.com/journal/ARNM

Contact
www.accscience.com
2 Venture Drive, #07-06 Vision Exchange,Singapore 608526
Email: editorial@accscience.com
Phone: +65 8182 1586